

The effects of cholesterol lowering agents
on the proteome of primary human hepatocytes

Dissertation
zur Erlangung des Grades
des Doktors der Naturwissenschaften
der Naturwissenschaftlich-Technischen Fakultät III
Chemie, Pharmazie, Bio- und Werkstoffwissenschaften
der Universität des Saarlandes

von
Martin Wörner

Saarbrücken

2009

Tag des Kolloquiums:	12.07.2010
Dekan:	Prof. Dr. Stefan Diebels
Berichterstatter:	Prof. Dr. Rita Bernhardt Prof. Dr. Elmar Heinzle
Vorsitzender:	Prof. Dr. Uli Müller
Akademischer Mitarbeiter:	Dr. Klaus Hollemeyer

Index

ABBREVIATIONS **I**

SUMMARY **IV**

SUMMARY (GERMAN) **V**

1 INTRODUCTION **1****1.1 CHOLESTEROL** **1**1.1.1 PHYSIOLOGICAL ROLE 11.1.2 TRANSPORT 21.1.3 BIOSYNTHESIS AND DEGRADATION 31.1.4 REGULATION OF BIOSYNTHESIS, TRANSPORT AND DEGRADATION 61.1.5 INHIBITORS OF CHOLESTEROL BIOSYNTHESIS 8**1.2 PRIMARY HUMAN HEPATOCYTES** **11****1.3 PROTEOMICS** **12**1.3.1 SAMPLE PREPARATION 121.3.2 SAMPLE SEPARATION 131.3.3 PROTEIN IDENTIFICATION 171.3.4 QUANTITATION 19**1.4 AIM OF THE WORK** **22**

2 MATERIALS **23****2.1 CHEMICALS** **23****2.2 INSTRUMENTS / MATERIALS** **25****2.3 BUFFER / SOLUTIONS / WATER** **26**

3 METHODS **27****3.1 CELL CULTURE** **29**3.1.1 PRIMARY HUMAN HEPATOCYTES 293.1.2 HUMAN COLON CARCINOMA CELL LINE 116 30

3.1.3	<i>SCHIZOSACCHAROMYCES POMBE</i>	30
3.1.4	<i>ECHERICHIA COLI</i>	30
3.2	PROTEIN ISOLATION	31
3.2.1	CELL DISRUPTION	31
3.2.2	DIFFERENTIAL CENTRIFUGATION	32
3.2.3	CLEANING THE MICROSOMES	32
3.3	DETERMINING THE PROTEIN CONCENTRATION	33
3.3.1	PLUSONE™ 2D QUANT KIT	33
3.3.2	BICINCHONIC ACID ASSAY	33
3.4	TWO DIMENSIONAL GEL ELECTROPHORESIS (2D – PAGE)	34
3.4.1	ISOELECTRIC FOCUSSING	34
3.4.2	SODIUM DODECYLSULFATE–POLYACRYLAMIDE GEL ELECTROPHORESIS	36
3.4.3	STAINING	38
3.4.4	IMAGE DIGITALISATION	38
3.4.5	IN-GEL DIGESTION	39
3.4.6	SPOTTING	40
3.5	NANO HIGH-PRESSURE LIQUID CHROMATOGRAPHY (NHPLC)	41
3.5.1	SAMPLE PREPARATION	41
3.5.2	FIRST DIMENSION, BASIC ELUENT	42
3.5.3	SECOND DIMENSION, ACIDIC ELUENT, ION-PAIRING	42
3.5.4	MATRIX MIXING AND SPOTTING	43
3.6	MASS SPECTROMETRY BY MALDI-TOF/TOF	44
3.6.1	IN-GEL DIGESTS	44
3.6.2	nLC-MS SAMPLES	47
3.7	REAL-TIME POLYMERASE CHAIN REACTION	49
3.8	BIOINFORMATICS	50
3.8.1	IMAGE ANALYSIS	50
3.8.2	PROTEIN IDENTIFICATION	55
3.8.3	PROTEIN QUANTITATION	56
3.8.4	DATA HANDLING	57
3.8.5	DATABASES	59
4	RESULTS	61
4.1	GENERAL REMARKS	61

4.2	EVALUATION OF THE METHODOLOGICAL APPROACHES	62
4.2.1	TWO DIMENSIONAL GEL ELECTROPHORESIS	63
4.2.2	NANO HIGH PRESSURE LIQUID CHROMATOGRAPHY	71
4.2.3	SUMMARY	88
4.3	THE EFFECTS OF RSV AND LEK-935	89
4.3.1	CYTOSOLIC FRACTION / TWO-DIMENSIONAL GEL ELECTROPHORESIS	89
4.3.2	MICROSOMAL FRACTION / NANO HIGH PRESSURE LIQUID CHROMATOGRAPHY	99
4.3.3	VALIDATION OF THE RESULTS BY RT-PCR	103
4.3.4	SUMMARY OF REGULATIONS	103
4.4	BIOINFORMATIC ANALYSIS OF THE REGULATED PROTEINS	106
4.4.1	ROSUVASTATIN TREATMENT	106
4.4.2	LEK-935 TREATMENT	112
5	DISCUSSION	117
5.1	EXPERIMENTAL APPROACHES, THEIR QUIRKS AND RESULTS	117
5.1.1	PROTEOMICS	117
5.1.2	TWO-DIMENSIONAL GEL ELECTROPHORESIS	118
5.1.3	NANO LIQUID CHROMATOGRAPHY COUPLED TO MASS SPECTROMETRY	127
5.1.4	SUMMARY	132
5.2	THE EFFECTS OF CHOLESTEROL LOWERING AGENTS	133
5.2.1	THE EFFECTS OF ROSUVASTATIN ON THE PROTEOME OF PRIMARY HUMAN HEPATOCYTES	133
5.2.2	THE EFFECTS OF LEK-935 ON THE PROTEOME OF PRIMARY HUMAN HEPATOCYTES	142
5.3	SUMMARY AND OUTLOOK	145
6	REFERENCES	147
APPENDIX		165
APPENDIX I: PUBLICATIONS RESULTING FROM THIS WORK		165
CONTRIBUTIONS TO INTERNATIONAL MEETINGS		165
MANUSCRIPTS		165
APPENDIX II: DETAILS OF THE PROTEINS FOUND TO BE REGULATED		167

SAMPLE 1 2D SPOT DETAILS	167
SAMPLE 1 NLC-MS RESULTS	181
SAMPLE 2 2D SPOT DETAILS	184
SAMPLE 2 NLC-MS DETAILS	209
<u>APPENDIX III: SPOT IDENTIFICATIONS FROM 2D GELS</u>	<u>211</u>
SAMPLE 1	211
SAMPLE 2	216
<u>APPENDIX IV: ITRAQ™ EVALUATION</u>	<u>219</u>
<u>APPENDIX V COMPLETE LIST OF PROTEINS IDENTIFIED BY NLC-MS</u>	<u>228</u>
<u>APPENDIX VI: KEGG PATHWAYS AFFECTED</u>	<u>248</u>
SAMPLE 1	248
RSV TREATMENT	248
LEK-935 TREATMENT	249
SAMPLE 2	250
RSV TREATMENT	250
LEK-935 TREATMENT	252
<u>ACKNOWLEDGEMENTS</u>	<u>255</u>

Abbreviations

2D	Two dimensional
2D-PAGE	Two dimensional gel electrophoresis
ACN	Acetonitrile
ACTH	Adrenocorticotropic hormone
APS	Ammoniumpersulfate
BCA	Bicinchoninic acid
CHAPS	3-[(3-cholamidopropyl)dimethylammonium]-1-propansulfonate
CHCA	Alpha-cyano-4-hydroxy-cinnamic acid
CID	Collision induced dissociation
Cl	Chloride
CO ₂	Carbon dioxide
CoA	Coenzyme A
CoA	Coenzyme A
CYP	Cytochrome P450
DMSO	Dimethyl sulfoxide
DNA	Deoxyribonucleic acid
DTT	Dithiothreitol
DTT	Dithiothreitol
E.coli	Escherichia coli
EBSS	Earl's balanced salt solution
EDTA	Ethylene diamine tetraacetic acid
EGTA	Ethylene glycol tetraacetic acid
ER	Endoplasmic reticulum
ESI	Electrospray ionisation
Glu-fib ¹	(Glu ¹)-fibrinopeptide B
HCT-116	Human carcinoma cell line 116
HDL	High density lipoprotein
HEPES	4-(2-hydroxyethyl)-1-piperazineethanesulfonic acid
HFBA	Heptafluorobutyric acid
HMG-CoA	3-hydroxy-3-methyl-glutaryl-CoA
HPLC	High pressure liquid chromatography

IAA	Iodacetamide
ICAT	Isotope coded affinity tag
IDL	Intermediate density lipoprotein
IEF	Isoelectric focussing
IP	Ion paired
IPGstrips	Immobilised pH gradient gels
IPP	Isopentenyl-pyrophosphate
iTRAQ™	Isotope tags for relative and absolute quantification
KCl	Potassium chloride
LC	Liquid chromatography
LDL	Low density lipoprotein
LEK-935	2-((3,4-dichlorophenethyl)(propyl)amino)-1-(pyridin-3-yl)ethanol
MALDI	Matrix assisted laser desorption/ionisation
mRNA	Messenger RNA
MS	Mass spectrometry / spectrometer
MS/MS	Tandem mass spectrometry
Na ₂ HPO ₄	Disodium hydrogen phosphate
NaCl	Sodiumchloride
NaH ₂ PO ₄	Sodium dihydrogen phosphate
NaHCO ₃	Sodium hydrogen carbonate
nLC-MS	Nano liquid chromatography coupled to mass spectrometry
NO	Nitric oxide
PAGE	Polyacrylamide gel electrophoresis
PCR	Polymerase chain reaction
PFF	Peptide-fragment fingerprint
PMF	Peptide-mass fingerprint
PMSF	Phenylmethylsulfonylfluoride
PSD	Post-source decay
PS-DVB	Poly-(sterene-divenlybenzene)
RNA	Ribonucleic acid
RP	Reversed phase
RSV	Rosuvastatin
RT	Real time
S.pombe	Schizosaccharomyces pombe

S/N	Signal to noise
SCX	Strong cation exchange
SDS	Sodiumdodecylsulfate
SILAC	Stable isotope labelling by amino acids in cell culture
SREBP	Sterol regulatory element binding protein
TEMED	N,N,N',N'-tetraethylmethanedi-amine
TFA	Trifluoro acetic acid
TFE	Trifluoro ethanol
TOF	Time of flight
Tris	Tris(hydroxymethyl)aminomethane
UdS	Saarland university
VLDL	Very low density lipoprotein
ZChL	Central chemical repository

Standard abbreviations for amino acids

A	Ala	Alanine	L	Leu	Leucine
R	Arg	Arginine	K	Lys	Lysine
N	Asn	Asparagine	M	Met	Methionine
D	Asp	Aspartic acid	F	Phe	Phenylalanine
C	Cys	Cysteine	P	Pro	Proline
Q	Gln	Glutamine	S	Ser	Serine
E	Glu	Glutamic acid	T	Thr	Threonine
G	Gly	Glycine	V	Val	Valine
H	His	Histidine	W	Trp	Tryptophan
I	Ile	Isoleucine	Y	Tyr	Tyrosine

Summary

Cholesterol plays a crucial role for human life. It is a part of eukaryotic lipid bilayers, necessary for cell division and serves as a precursor for steroid hormones. The effects of cholesterol lowering agents are not yet fully understood. This study describes, for the first time, the effects of the HMG-CoA reductase inhibitor rosuvastatin and the new CYP51A1 inhibitor LEK-935 on the proteome of primary human hepatocytes.

Samples derived from two different human donors were analysed. They were sub-fractionated prior to the proteome analysis to enhance the resolution of the analysis. The cytosolic and microsomal fractions were analysed in a semi-quantitative manner by 2D-PAGE and nLC-MS respectively. A final set of 44 proteins was found to be differentially expressed. This set contains proteins already known to be affected and involved in the cholesterol biosynthesis. It also contains proteins that cannot be directly related to cholesterol metabolism and that have not yet been described to be affected by cholesterol lowering agents. The finding of the already known proteins validates the chosen experimental design while the other proteins provide new information and represent targets for further investigations. RT-PCR measurements performed at a chosen set of proteins validate the results. They furthermore underline the huge inter-individual differences observed during the proteome analysis.

Summary (german)

Cholesterin ist essentiell für das menschliche Leben. Es ist integraler Bestandteil eukaryotischer Membranen, notwendig für die Zellteilung und dient als Vorläufermolekül der Steroidhormone. Die Effekte von cholesterinsenkenden Medikamenten sind bis heute noch nicht vollständig aufgeklärt. Diese Arbeit beschreibt zum ersten Mal die Effekte des HMG-CoA Inhibitors Rosuvastatin und des neuen CYP51A1 Inhibitors LEK-935 auf das Proteom primärer humaner Hepatozyten.

Die cytosolische sowie die mikrosomale Fraktion von zwei menschlichen Spendern wurde mittels 2D-PAGE und nLC-MS semi-quantitativ analysiert. Insgesamt wurden 44 Proteine als differenziell exprimiert gefunden. Unter diesen finden sich Proteine von denen bereits bekannt ist, dass sie beeinflusst werden und die in die Cholesterinbiosynthese involviert sind. Es finden sich aber auch Proteine die nicht direkt mit dem Cholesterinmetabolismus in Verbindung gebracht werden können und deren Beeinflussung durch cholesterinsenkende Medikamente noch nicht bekannt ist. Die bereits bekannten Proteine belegen den experimentellen Ansatz. Gleichzeitig stellen die anderen Proteine neue Informationen und damit neue Ziele für weitergehende Untersuchungen dar. Die gewonnenen Ergebnisse wurden durch RT-PCR-Analysen eines ausgewählten Sets an Proteinen bestätigt. Diese Validierungsexperimente unterstreichen darüber hinaus die großen inter-individuellen Unterschiede, die auch schon in der Proteomanalyse gefunden wurden.

1 Introduction

1.1 Cholesterol

1.1.1 Physiological role

The basic structure of cholesterol is a voluminous steroidal skeleton, with a hydroxyl group at C 3 and a flexible carbon-hydrate tail at C 17 (see Figure 1-1).

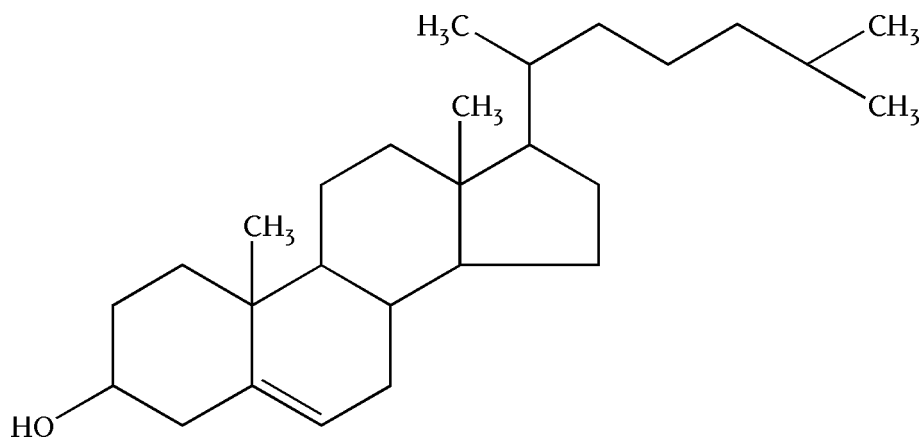


Figure 1-1 Structural formula of cholesterol

Cholesterol has a high impact on the life of eukaryotic organisms. It is an essential part of lipid bilayer membranes, where it constrains the crystallisation of the lipids fatty acids and thereby maintains the fluidity of the membrane. Its presence in the membrane leads to additional steric hindrance of the fatty acids which in turn limits the fluidity of the membrane (Yeagle et al. 1990).

Cholesterol serves as precursor molecule for the biosynthesis of the steroid hormones (Repa and Mangelsdorf 2000), indispensable for multiple regulation processes inside the human body. The steroid hormones are divided into three groups: the sexual hormones (estrogens and androgens) that are essential for the gender formation during the embryogenesis (Jacobs and Lewis 2002); the gestagens, mainly the progesterone, that are requisite for the reproduction (Bazer et al. 1979) and the mineralocorticoids, that control the salt- and water homeostasis (Rashid and Lewis 2005) and thereby the blood pressure (Fuller and Young 2005). The third group, the glucocorticoids, are known to be signal molecules of the stress response (Rashid et al. 2005).

Cholesterol and intermediate products of its biosynthetic pathway are involved in the regulation of signal molecules like Ras, Rab and Rho (Parhami et al. 2002) and essential for the replication and cell growth (Siperstein 1984).

Cholesterol is known to the public for its negative effects on the organism. Elevated ratios of normal cholesterol to high density lipoprotein cholesterol levels are known to be one of the risk factors of coronary heart disease (Castelli 1984). Cholesterol is described as a constitutive part of atherosclerotic plaques (Wissler 1991). Elevated plasma concentrations of cholesterol, foremost in form of LDL-cholesterol, foster the formation of these plaques. These effects are intensified in patients with familial hypercholesterolemia. In this case, the high plasma concentrations are caused by a mutation in the LDL receptor (Goldstein and Brown 1984). Besides the formation of atherosclerotic plaques, elevated levels of cholesterol can lead to osteoporosis (Parhami et al. 2000). Moreover, recent studies describe a positive influence of cholesterol on the surveillance of cells from leucemic tumours and a possible treatment by drugs that inhibit the biosynthesis of cholesterol (Li et al. 2003).

To summarise, cholesterol itself plays an important physiological role that is increased by the regulatory functions of some of its precursor and derivative molecules. Due to this important function it is also involved in several diseases.

1.1.2 Transport

Cholesterol is transported throughout the human body bound to lipoprotein particles. The lipoprotein particles are classified according to their density. For nutrient derived cholesterol, two particles exist. The chylomicrons consist of apolipoprotein B-48, C and E, triacylglycerides and esterified cholesterol. After the release of the triacylglycerides and the apolipoprotein C, so called chylomicron-remnants retain, that transport the bound esterified cholesterol to the liver (Sherrill and Dietschy 1978). Cholesterol and triacylglycerides that are not used by the liver are excreted to the blood in form of very low density lipoproteins (VLDL). The protein part of these particles consists of apolipoprotein B-100, C and E. After releasing the lipid part of the particles, intermediate density lipoproteins (IDL) retain that are rich in esterified cholesterol. The IDLs are either taken up by the liver again or transformed to low density lipoproteins (LDL) consisting of esterified cholesterol and one single apolipoprotein B-100 only. These are the most important cholesterol carriers

throughout the human body. They carry the cholesterol molecules to the periphery and thereby control the *de novo* cholesterol synthesis out there (Brown and Goldstein 1986). In contrast, high density lipoproteins (HDL) incorporate the cholesterol that is released to the plasma by apoptotic cells and degraded membranes. This cholesterol is esterified by an acyltransferase and then passed to LDL particles (Brown et al. 1981) or the HDL particles transport the esterified cholesterol from the peripheral tissues back to the liver (Mahley 1983).

The uptake of cholesterol from LDL-particles is performed via the LDL-receptor (Brown et al. 1981). This molecule is exposed to the outer surface of the cells and recognises the apoB-100 protein component of the LDL. The whole LDL-particle is ingested into the cells by endocytosis, the protein particles are hydrolysed to amino acids while the cholesteryl esters are hydrolysed to free cholesterol that is incorporated into membranes or re-esterified for storage purposes. In the case of familial hypercholesterolemia, the LDL receptor is mutated. This mutation leads to the accumulation of LDL particles, which in turn leads to an accumulation of cholesterol in different tissues with all the negative effects of elevated cholesterol levels described in 1.1.1. A level of about 150-200 mg/ml is regarded as “normal”, heterozygous patients of the familial hypercholesterolemia show a level of 300-500 mg/ml and homozygous patients one of about 500-1200 mg/ml (Hobbs et al. 1990)).

The cholesterol level in the hepatic cells is mainly controlled via the control of *de novo* synthesis followed by HDL/LDL uptake (Rudney and Sexton 1986), the extra-hepatic tissues obtain their cholesterol by *de novo* synthesis and via uptake of the cholesterol transported through the plasma by LDL particles (Dietschy 1984).

1.1.3 Biosynthesis and degradation

The daily need of cholesterol in the human body can be satisfied via two ways. Each day, 300-500 mg of cholesterol are absorbed from the nutrition while 700-900 mg are newly synthesised (Dietschy 1984). The nutrient derived cholesterol is transported by chylomicrons to the liver from which it is distributed through the whole body (see 1.1.2).

The biosynthesis starts from acetyl-CoA and acetoacetyl-CoA that are condensed to 3-hydroxy-3-methyl-glutaryl-CoA (HMG-CoA) by the cytosolic HMG-CoA synthase. The second step is rate-limiting and catalysed by the HMG-CoA reductase at the smooth

endoplasmic reticulum (ER). The HMG-CoA reductase reduces HMG-CoA to mevalonate that is later diphosphorylated and decarboxylated, leading to isopentenyl-pyrophosphate (IPP), as precursor for either isoprenoids or squalene synthesis. In the case of squalene synthesis, an equilibrium isomerisation takes place, resulting in dimethylallyl-pyrophosphate which condenses with a second molecule IPP to geranylpyrophosphate. The synthesised geranylpyrophosphate again condenses with a third molecule IPP to farnesyl-pyrophosphate. The farnesyl-pyrophosphate is the last position of the isoprenoidal part of the mevalonate pathway. With the formation of squalene, it enters the steroidal part. Two molecules of farnesyl-pyrophosphate condense to one molecule squalene, catalysed by the squalene synthase. In two steps, lanosterol is formed from squalene by the squalene monooxygenase and the lanosterol synthase. This step as well as all the following steps are carried out at the smooth ER. The first step of 19 steps leading from lanosterol to cholesterol is the C14 de-methylation, catalysed by the cytochrome P450 51A1 (CYP51, see Figure 1-2).

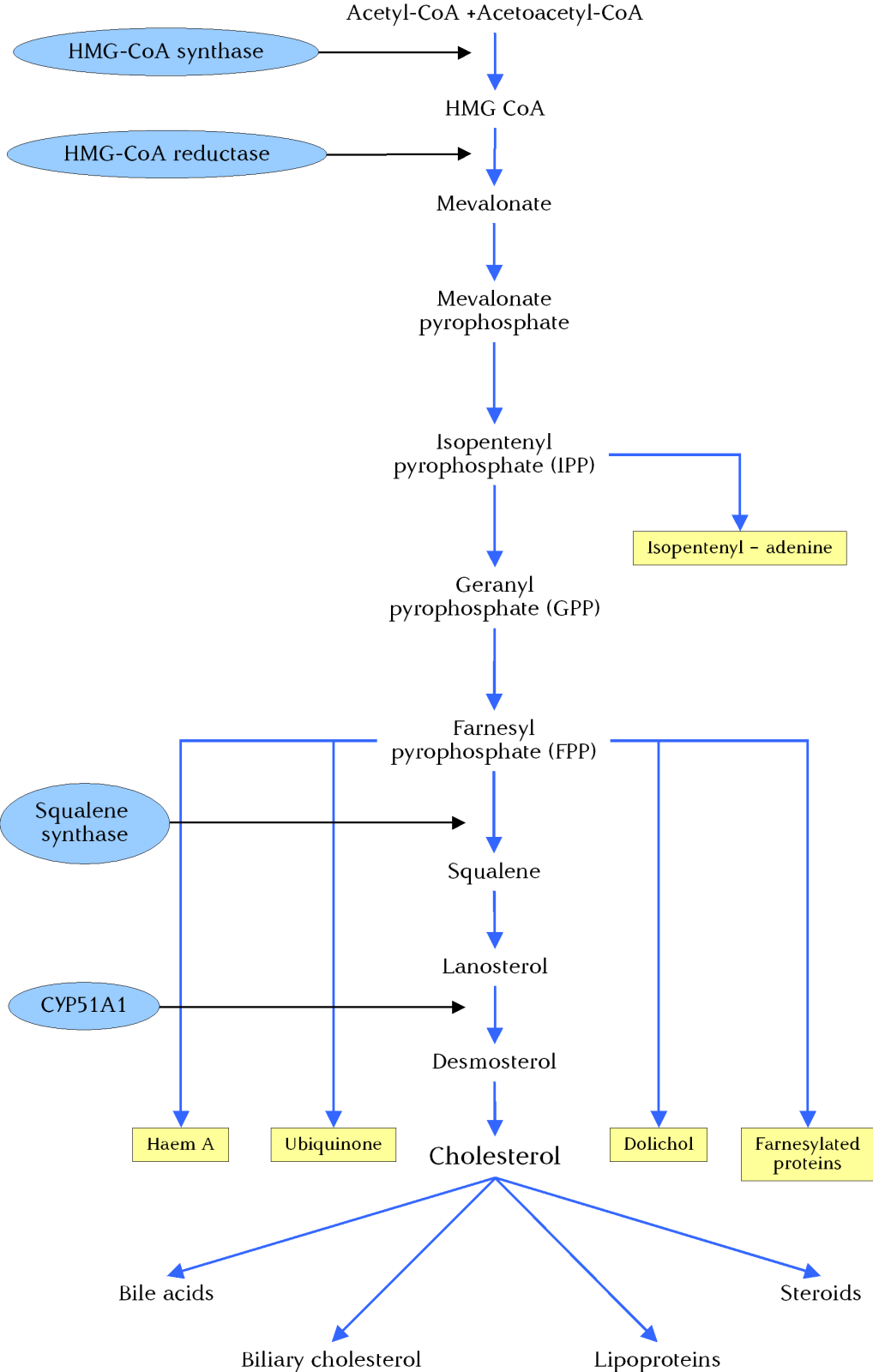


Figure 1-2 Simplified scheme of the isoprenoid and cholesterol biosynthetic pathway. Key enzymes of cholesterol biosynthesis are marked in blue, biosynthetic processes are marked by blue arrows.

The intermediates formed during the biosynthesis of cholesterol play an important role in other cellular processes, like the biosynthesis of dolichol, haem A, ubiquinone or posttranslational modifications of proteins by farnesylation (Goldstein and Brown 1990).

For the elimination, again, there are different pathways. Cholesterol can be excreted into the gastrointestinal tract (approximately 600 mg/day) or it is lost through the sloughing of skin (approximately 85 mg/day). Two other ways are its conversion to bile acids (approximately 400 mg/day) or steroid hormones (approximately 50 mg/day) which, in turn, are excreted from the body in bile or urine (Dietschy 1984).

The bile acids are essential molecules for the uptake of nutrients (Repa et al. 2000). Furthermore, they support the resorption of lipophilic substances from the intestine. Many steps of the cholesterol degradation, the steroid biosynthesis and the synthesis of vitamin D are catalysed by members of the cytochrome P450 family (Handschin et al. 2002).

1.1.4 Regulation of biosynthesis, transport and degradation

The biosynthesis of cholesterol is mediated by the mevalonate pathway and regulated in many ways (Goldstein et al. 1990; Russell 1992). The HMG-CoA reductase is the rate-limiting enzyme for cholesterol biosynthesis. Its transcriptional regulation is carried out by sterol regulatory element binding proteins (SREBP). These are membrane proteins that belong to the helix-loop-helix-leucine zipper family of transcription factors. In the case of cholesterol absence the cytosolic part of the SREBP is proteolytically released, representing the active transcription factor. These transcription factors bind to sterol-regulate-elements 5' to the promoter of key enzymes of the cholesterol biosynthesis (like HMG-CoA synthase, HMG-CoA reductase and squalene synthase)(Goldstein et al. 1990). In addition to this transcriptional regulation, the HMG-CoA reductase is also post-transcriptionally regulated (Goldstein et al. 1990).

The uptake and export of cholesterol also contributes to the overall cholesterol concentration inside the cell, so it is also regulated in a cholesterol dependent manner. The major regulatory element is the LDL-receptor. The amount of LDL-receptors on the surface of liver cells increases after blocking cholesterol biosynthesis

with a HMG-CoA reductase inhibitor. This is the underlying reason for the reduced plasma LDL concentration after statin treatment (see 1.1.5.1).

The regulation of cholesterol degradation is mainly carried out by regulating the rate-limiting enzyme, the cholesterol 7α -hydroxylase (CYP7A1). This enzyme is regulated at the mRNA and the protein level by mevalonate, diurnal rhythm and bile acid feedback (Sundseth and Waxman 1990). The transcriptional regulation is carried out by members of a family of nuclear receptors (Repa et al. 2000). Those with the highest impact are:

- Liver X Receptor (LXR): It forces the degradation to bile acids by activation of the transcription of CYP7A1 in the case of elevated cholesterol concentration.
- Farnesoid X Receptor (FXR): It lowers the transcription of CYP7A1 in the case of elevated bile acid concentrations.

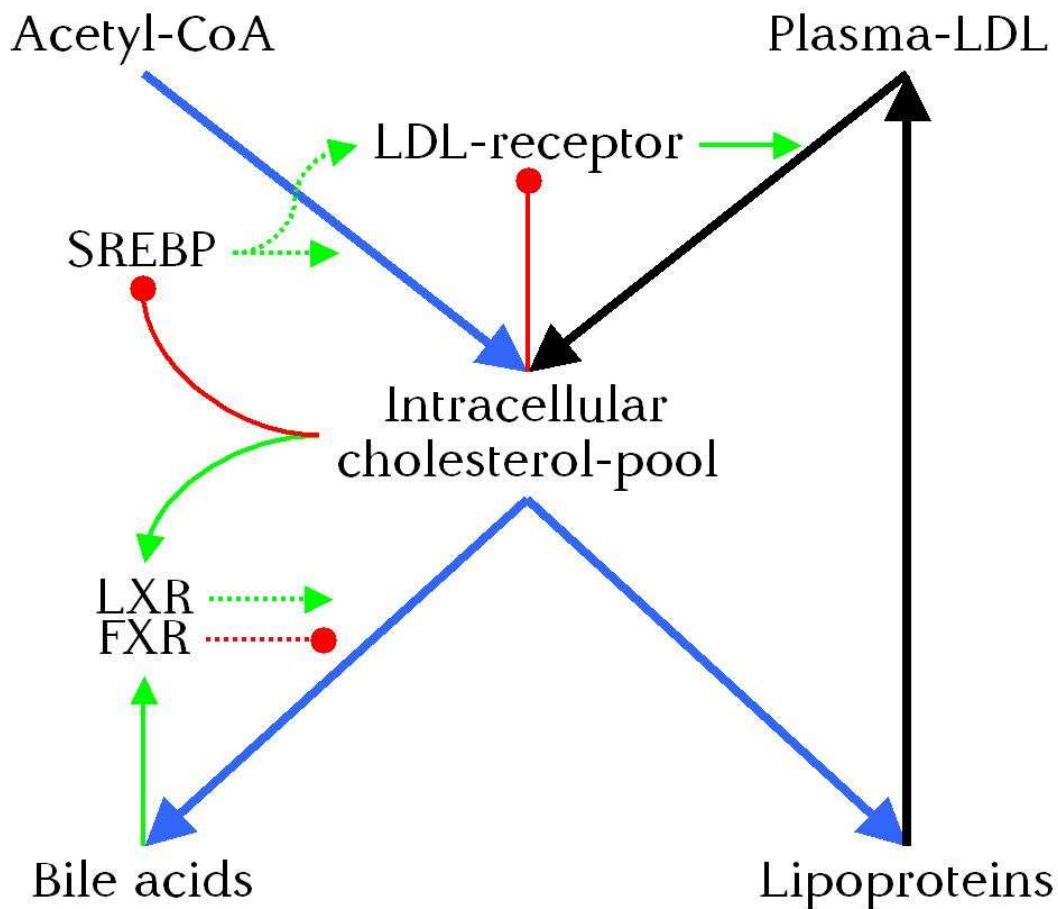


Figure 1-3 Simplified scheme of transcriptional control of the cholesterol homeostasis. Biosynthetic pathways are marked as blue arrows, positive regulations are marked as green arrows, negative regulations as red lines. Dotted lines represent transcriptional regulation.

1.1.5 Inhibitors of cholesterol biosynthesis

1.1.5.1 Statins

Competitive inhibition of the HMG-CoA reductase by two fungal metabolites was firstly described in 1976 (Endo et al. 1976). During the past thirty years, many HMG-CoA reductase inhibitors have been developed (Istvan and Deisenhofer 2001; Manzoni and Rollini 2002; Stark 2003). The amount of plasma cholesterol is regulated by the amount of lipoprotein receptors (Brown et al. 1981). The block of the hepatic cholesterol synthesis leads to an increase in the expression of LDL receptor, which in turn leads to a subsequent increase in the removal of plasma LDL (Brown et al. 1986). So statins are in clinical use to reduce the cholesterol plasma concentration of patients with elevated cholesterol levels to reduce the health risks coming along with these elevated levels. Statins also play a very important role in studies investigating the HMG-CoA reductase (Chin et al. 1982), the regulation of cholesterol biosynthesis by non-steroidal side products (Brown and Goldstein 1980), the influence of cholesterol and its intermediates onto the DNA synthesis (Siperstein 1984) and the role of isoprenylated proteins in cellular pathways and cholesterol biosynthesis (Russell 1992).

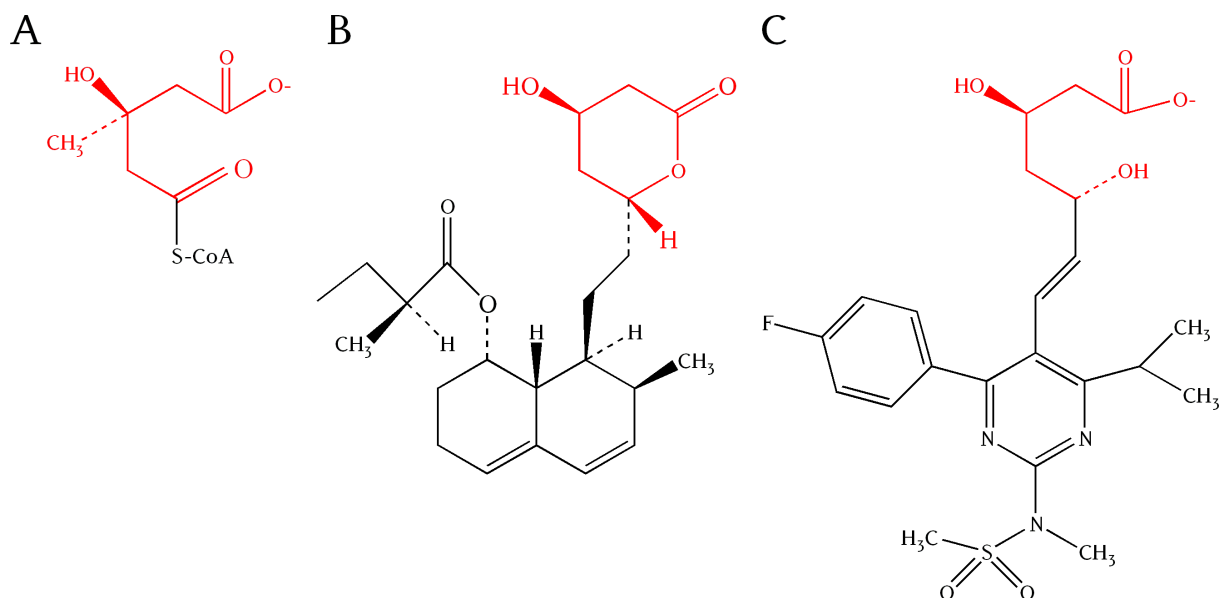


Figure 1-4 The chemical structures of HMG-CoA (A), mevastatin (B) and rosuvastatin (C). The HMG-like moiety is coloured in red.

All statins have a HMG-like moiety and the resulting competitive inhibitory effect is common (see Figure 1-4, (Istvan et al. 2001)). Starting from mevastatin (Endo et al. 1976) several naturally derived as well as synthetic statins have been developed, tested

and applied for clinical use (Manzoni et al. 2002; Stark 2003). Lipobay (cerivastatin) is a negative example for a statin. In 2001, it has been removed from the market worldwide, as a reaction to a multitude of rhabdomyoses (Information 2002; Yan et al. 2003).

Besides lowering cholesterol levels, several pleiotropic effects of statins are discussed in the literature (LaRosa 2001). They were shown to prevent plaque-rupture by inhibiting metalloproteases, increasing collagen and decreasing lipid content of carotid plaques (Crisby et al. 2001). The idea of pleiotropic effects of statins on plaques is further strengthened by reports about a decrease in adhesion of monocytes to the endothelium (Weber et al. 1997) and the inhibition of thromboxane biosynthesis and platelet function (Notarbartolo et al. 1995). In addition, an increase in fibrinolysis and a decrease of plasminogen activator inhibitor 1 has also been reported (Isaacsohn et al. 1994; Essig et al. 1998). Lovastatin was shown to suppress LDL oxidation and its uptake by macrophages (Aviram et al. 1992). As possibly atheroprotective effect, the up-regulation of the nitric oxide (NO) synthase, has been reported (Laufs et al. 1998). Most of the pleiotropic effects are not fully understood yet (Liao 2002; Liao and Laufs 2005; Corsini et al. 2007).

Among the younger generation of synthetic statins rosuvastatin (Smith et al. 2000) (RSV, see Figure 1-4 C) is one of the most promising ones. It is a potent inhibitor of the HMG-CoA reductase that is not metabolised by the major drug metabolising cytochromes P450 (McTaggart et al. 2001). In comparison to the other statins, it is relatively hydrophilic and has a high percentage of bioavailability that is not affected by food (Igel et al. 2002). Furthermore, it is taken up into liver cells by a high affinity active transport process (Nezasa et al. 2000). For RSV, an anti-inflammatory “pleiotropic” effect has already been described (Stalker et al. 2001).

1.1.5.2 Others

Due to the severe side-effects sometimes observed by the administration of statins and the high impact of intermediate products of the mevalonate pathway on cellular life, the inhibition of cholesterol biosynthesis downstream to the HMG-CoA synthase is under discussion. Thereby, three potential targets came into the focus. The squalene synthase, reviewed in (Charlton-Menys and Durrington 2007) seems to be the most promising one so far. The squalene epoxidase and the oxidosqualene cyclase are also

discussed as potential targets but with a minor impact on today's research as reviewed by (Seiki and Frishman 2009).

More recently, the 2-((3,4-dichlorophenethyl)(propyl)amino)-1-(pyridin-3-yl)ethanol (LEK-935) has been shown to be a potent inhibitor of the lanosterol 14 α -demethylase (see 1.1.3, (Korosec et al. 2008)). This enzyme is even more downstream towards the synthesis of cholesterol than all other targets studied before. The drug-interaction potential of LEK-935 has, in comparison to rosuvastatin, already been investigated (Monostory et al. 2009). It was shown to be a potent inducer of CYP3A4 transcription but also to be rapidly metabolised by primary human hepatocytes. RSV was shown to activate hCAR and thereby induce CYP3A4, CYP2C9 and CYP2B6 genes. So, both drugs show the potential for drug-drug interaction as side-effects of a co-administration with other drugs.

1.2 Primary human hepatocytes

Besides the brain, the liver represents the most complex organ of the human body (Malarkey et al. 2005). It has a high impact on physiological relevant homeostases. It serves as one of the major organs of energy homeostasis, as it stores glucose in form of glycogen and again releases the glucose (Gerich 1993) as a fast response to lowered blood sugar (Bondy et al. 1949). The liver is also the central organ for the gluconeogenesis (Exton 1972). It catalyses the major part of dietary amino acid catabolism (Brosnan 2000), is the major source of ketone bodies (Krebs 1966), important for fatty acid synthesis (Volpe and Vagelos 1973; Hellerstein et al. 1996) and triglyceride formation (Bell and Coleman 1980) as well as cholesterol synthesis (Russell 1992) and the production of coagulation factors and inflammatory mediators (Dhainaut et al. 2001). Besides these functions in the energy homeostasis, it plays a crucial role in the metabolism of endogenous and exogenous substances and their final excretion from the body.

These functions require a high rate of metabolite exchange between the liver and the blood. This necessity is mirrored in the complex morphology of the liver. Nearly all of the liver cells lay next to blood filled lacunas, so called liver capillaries or liver sinusoids. Thereby, a huge surface is formed that facilitates the exchange of metabolites between the cells and the blood. Most of the liver functions are carried out by hepatocytes, the main cell type in the liver (Malik et al. 2002). They are arranged as cell strings inside the liver lobes. At least 14 other cell types are also present in the liver, like Kuppfer-Cells (liver macrophages), dendritic cells and haematopoietic cells for example (Malarkey et al. 2005).

The high impact of the liver on total cholesterol-synthesis, uptake of exogenous cholesterol, cholesterol distribution throughout the body and the maintenance of plasma-cholesterol levels is of main interest of the present study. The cholesterol turnover is controlled by the hepatocytes, so these cells are the first choice trying to investigate effects on cholesterol homeostasis. As the liver displays big interindividual differences in its metabolic fluxes, the use of primary hepatocytes gained from different donors is superior to the use of hepatocytes of one donor or a pool of hepatocytes from different donors in cell culture. By the use of primary hepatocytes the experimental conditions are as near to an *in vivo* situation as possible.

1.3 Proteomics

The term proteome was firstly introduced by the Australian scientist Marc Wilkins in 1994 (Wasinger et al. 1995). The proteome is defined as the composition of the protein content of an organism, tissue or cell type at a specified point in time under specified conditions. The genome resembles a stable situation, while the other -omes, transcriptome, proteome and metabolome vary. Their composition is reliant on environmental circumstances, the composition of each other -ome, the time and so on. In contrast to genomic or transcriptomic analysis, the investigation of the proteome offers the advantage to analyse those molecules of the cell that exhibit the catalytic activities.

In principal, a proteomic analysis can be divided into three steps (see Figure 1-5). The majority of nowadays proteomic studies do not only analyse the status of a sample under defined conditions but are used to compare different conditions (like healthy and sick or treated and untreated samples). Comparison is usually made in a semi-quantitative manner, adding a fourth step, the quantification to the general experimental design (see Figure 1-5).

Sample preparation

Sample separation

Protein identification

Protein quantification

Figure 1-5 General scheme of the four parts of a semi-quantitative proteomic analysis

1.3.1 Sample preparation

The sample preparation is the most critical step of a proteomic analysis. Mistakes occurring at this stage of analysis are most often invisible and will only be detected at the end of the whole analysis. Therefore, special care has to be taken during sample preparation. The cells are lysed to release the proteins. Contaminant substances are removed that would disturb the analysis, like DNA or membrane fragments.

Mammalian cells display much higher complexity than those of more simple organisms. To cope with this complexity, the proteome is divided into sub proteomes by a fractionation into the cellular compartments. This fractionation is performed by differential centrifugation, whereby the different densities of the compartments are used to separate them from each other. The use of detergents to solve proteins has to be avoided prior to differential centrifugation, as this would disturb the fractionation process.

1.3.2 Sample separation

After sample preparation, the sample contains a mixture of several thousands of proteins. To efficiently analyse this mixture, it needs further separation. The final identification of the proteins inside this mixture is usually performed by a controlled proteolytic digestion of the proteins, followed by an analysis of the resulting peptide mixture by mass spectrometry (see 1.3.3). The way of proteome analysis is divided by two different strategies, depending on the level at which the separation is performed. In so called top-down approaches, the sample is separated prior to the proteolytic digestion at the protein level. In the bottom-up approaches, separation is performed after proteolytic digestion, at the peptide level. The 2D gel electrophoresis represents the classical top-down approach. Hereby, the proteins are separated according to their physico-chemical properties in two successive gel-based experimental designs. The two-dimensional gel electrophoresis was firstly described in the 70s of the last century (Klose 1975; O'Farrell 1975). It has further been developed and optimised and allows nowadays the reproducible resolution of up to 10000 proteins (Galeva et al. 2003). One of the major drawbacks of 2D-gel electrophoresis is its inability to separate membrane proteins (Santoni et al. 2000). The gel-free separation of the peptide mixtures by liquid chromatography (LC) has evolved as an equivalent and complementing bottom-up approach (Aebersold and Mann 2003) during the past years. The complexity of the peptide mixture is much larger than that of the protein mixture, therefore also combinations of LC separation modes are used to enhance the resolution of the analysis. Gel-based and gel-free methods nowadays turn out to be effective partners that may compensate for disadvantages of each other.

1.3.2.1 Two-dimensional gel electrophoresis (2D-PAGE)

In the classical approach, firstly described by O'Farrel and Klose independently in 1975, the proteins are separated according to their physico-chemical properties. At first, they are reduced and alkylated to expose as much of the primary structure to the buffer environment as possible. The proteins are separated in a pH gradient by applying an electric field to it. The net charge of the proteins is build by its carboxy and amino termini as well as the charged residues of its amino acids. In addition, it depends on the pH of the surrounding buffer. The pH at which the net charge equals zero is called the isoelectric point (pI) of the protein. By applying an electric field with the anode at the acidic end of the pH gradient and the cathode at the basic end the proteins migrate through the gel until they reach their pI or leave the gel, in the case their pI is out of the pH range (see Figure 1-6). At the end of the last and the beginning of this century, this technique was markedly improved by the development of so called immobilised pH gradients (IPG) which are commercially available and highly improve the reproducibility of the isoelectric focussing (Corbett 1994; Gorg et al. 2004).



Figure 1-6 Theoretical scheme of IEF after sample load by in-gel rehydration and after focussing. The P marks a phosphorylated protein.

After focussing the proteins at their pI, they are usually separated according to their molecular size by a denaturing polyacrylamid gel electrophoresis (PAGE). To enable this separation, they need to be fully denaturated and uniformly charged. The charge state should be in correlation to the size of the molecule, which is achieved by using the detergent sodiumdodeylsulfate (SDS). The complete event of denaturing and charging the proteins after IEF is called equilibration. The proteins are denaturated and negatively charged by incubation with a buffer containing SDS. The reductant dithiothreitol (DTT) reduces the proteins and reduces the disulfide bridges which further denaturates the protein and simplifies the attachment of SDS to the protein. In

a second step, the free -SH groups are blocked by incubation with iodacetamide (IAA) to inhibit the reassembly of the protein.

Separation is performed using a SDS polyacrylamide gel. By applying an electric field, the negatively charged proteins migrate towards the anode. During migration, they pass through the gel and are separated by the filtering effects of the cross-linked acrylamide monomers according to their molecular size. The smaller proteins pass more easily through the gel-matrix as the bigger ones. Applying a molecular weight standard as reference, this method also enables a rough estimation of the proteins molecular weight (Shapiro et al. 1967). To visualise the proteins on the gel, they are usually stained by silver (incompatible to mass spectrometry, high sensitivity) or a colloidal coomassie staining (compatible to mass spectrometry, lower sensitivity) (Miller et al. 2006). There are also high sensitive fluorescent stains available that are compatible to mass spectrometry but require additional equipment for analysis and spot picking.

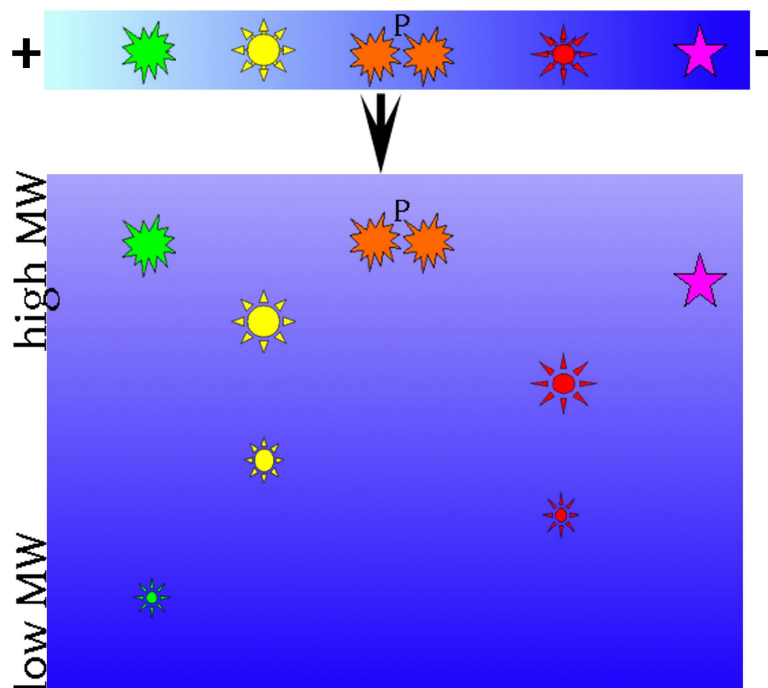


Figure 1-7 Theoretical scheme of a SDS-PAGE (2nd dimension) after IEF (1st dimension, see Figure 1-6)

In this study, the classical approach with IEF in the 1st and SDS-PAGE in the 2nd dimension was used. The proteins were stained by colloidal coomassie staining.

1.3.2.2 Nano High Pressure Liquid Chromatography – Mass Spectrometry (nLC-MS)

Strong cation-exchange (SCX) (Alpert and Andrews 1988) coupled with either reversed-phase (RP) (Molnar and Horvath 1977) or ion-pair reversed-phase (IP-RP) (Horvath et al. 1977) high-performance liquid chromatography (HPLC) turned out to be effective combinations of chromatographic separation modes, for both soluble and membrane-bound proteins. Using SCX, the proteins are separated according to electrostatic interactions with the stationary phase while the separation during RP occurs according to their hydrophobic properties. In the case of IP-RP additional electrostatic interactions are introduced into the separation process (see Figure 1-8).

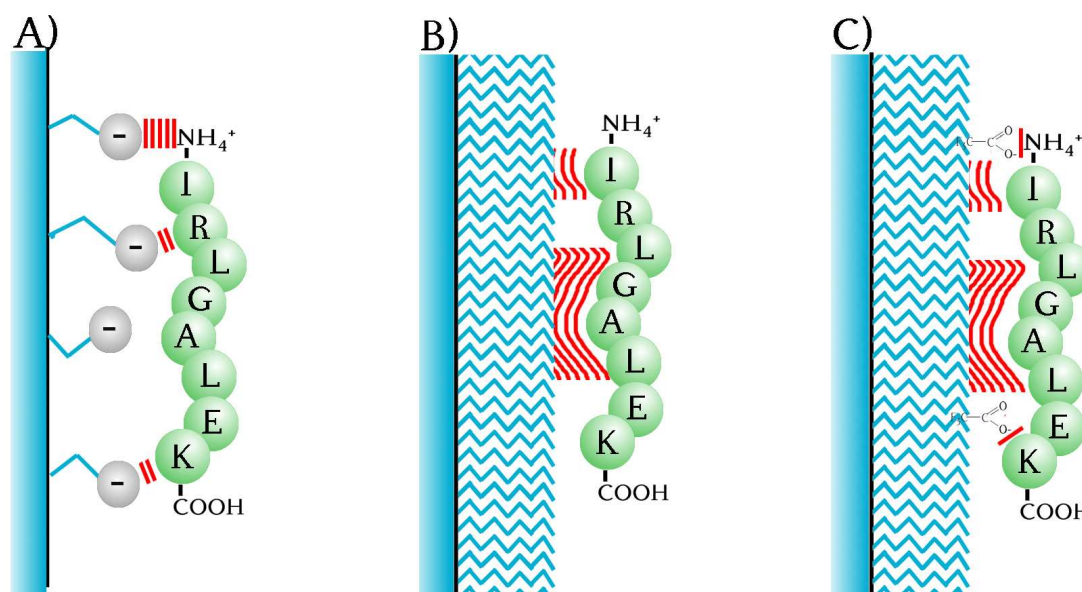


Figure 1-8 Schematic display of SCX (A), RP (B) and RP-IP (C) liquid chromatography separation modes.

Many efforts have been undertaken to improve the resolution of the gel free methodologies and their performance. Among others, nano scale experimental designs (Meiring et al. 2002) and monolithic columns (Premstaller et al. 2001) were introduced into this emerging field. The orthogonality of the combined separation is a prerequisite for an optimal result (Dugo et al. 2008). A new method of RP x IP-RP HPLC for shotgun proteomics (Delmotte et al. 2007) was recently set up and validated. It includes monolithic columns in a nano scale experimental design with a combination of chromatographic separation modes (RP x IP-RP) whose separation capacities have been shown before to be superior to that of the classical combinations (Gilar et al. 2005b, 2005a). This setup has been evaluated directly coupled to an electron spray ionisation mass spectrometer (ESI-MS) (Delmotte et al. 2007; Delmotte et al. 2009) as well as coupled to a matrix assisted laser desorption/ionisation time-of-

flight mass spectrometer (MALDI-TOF-MS) (Lasaosa et al. 2009). The latter has been shown to be superior with regard to the number of peptides and proteins identified (Lasaosa et al. 2009).

1.3.3 Protein identification

Regardless of the kind of separation, gel-based or gel-free, the proteins inside the sample are identified by mass spectrometry followed by computational database search. Mass spectrometry bases on the ionisation of the sample molecule followed by the determination of the mass to charge ratio (m/z). The general assembly of a mass spectrometer is depicted in Figure 1-9.

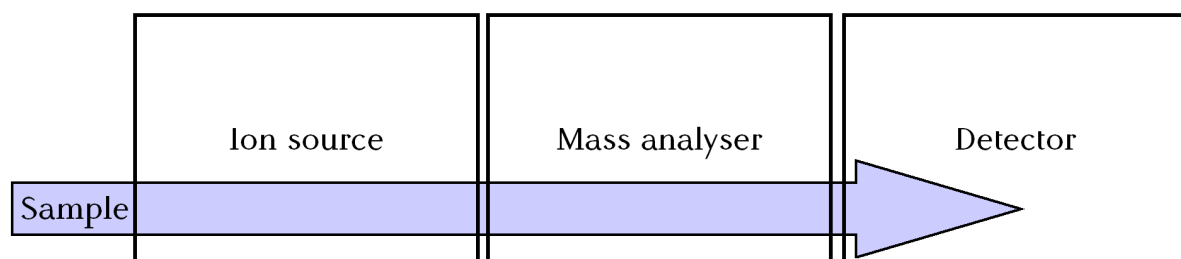


Figure 1-9 General scheme of a mass spectrometer, consisting of an ion source in which the analytes are ionised, followed by a mass analyser and an ion detector.

A mass spectrometer consists of an ion source, a mass analyser and a detector. Different ways to ionise samples for mass analysis are available. Proteins or peptides as analytes are in general non-volatile and quite instable under the influence of high temperatures. Therefore, the identification of proteins by mass spectrometry has evolved since the introduction of two soft ionisation techniques in the late 80s of the last century. The matrix assisted laser desorption/ionisation (Karas et al. 1987; Tanaka et al. 1988) is beside the electron spray ionisation (ESI) (Fenn et al. 1989) the most widely used ionisation technique in the field of proteomics.

1.3.3.1 MALDI-TOF/TOF

The general scheme of a MALDI-TOF analyser is illustrated in Figure 1-10. The sample is mixed with the matrix and this mixture is allowed to crystallise on a stainless steel target. To ionise the sample, the matrix sample mixture is subjected to a pulsed laser beam. The complete mechanism of ionisation is not yet fully understood. It is suggested that the laser heats the matrix and leads to small explosions in the frame of which the analytes enter the gaseous phase and are ionised by getting a proton from

the ionised matrix. In general, only singly charged ions are produced by MALDI (Karas et al. 2000).

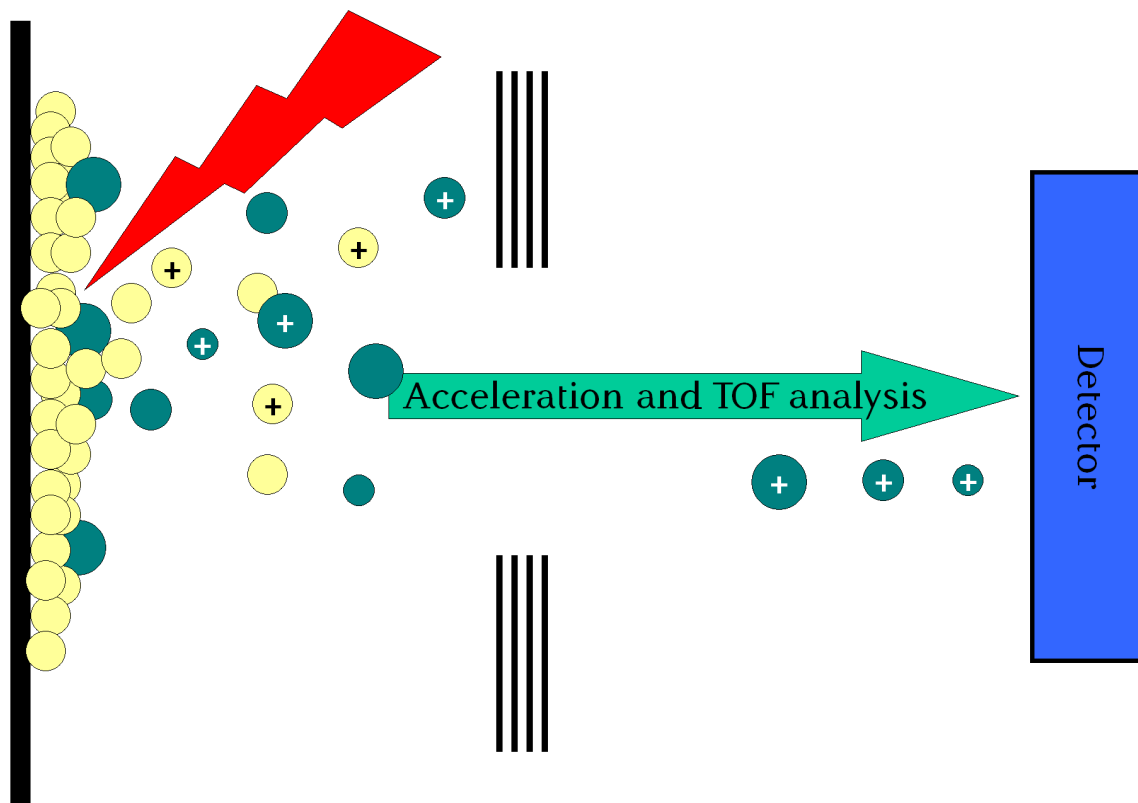


Figure 1-10 General scheme of a MALDI-TOF including a schematic view on the matrix assisted laser desorption/ionisation. The laser is shown as red lightning, matrix molecules and analyte molecules are shown in yellow and green respectively.

MALDI ionisation sources are usually coupled to a time-of-flight (TOF) mass analyser. The charged analytes are accelerated in a strong electric field followed by drifting in a field free flight tube. They are accelerated with the same kinetic energy but their velocities differ according to their different masses. So, they separate during the drift according to their velocities that depend on their masses. Therefore, their mass to charge ratio (m/z) can be determined according to the time they need to pass the specified flight path to the detector. The detector collects the m/z of all ionised analytes that enter the gaseous phase and summarises these information in a mass spectrum. In the case of tandem mass spectrometry (MS/MS), a defined number of m/z ratios of each spectrum is chosen for fragmentation. Fragmentation can be performed as post-source decay (PSD) or by colliding the analyte ions with gas molecules (CID) (Medzihradszky et al. 2000). The CID is favourable to PSD (Medzihradszky et al. 2000) and occurs in a collision chamber where the analytes slow

down and collide with gas molecules. After fragmentation, the fragments are accelerated and analysed as the unfragmented analytes.

1.3.3.2 Protein identification from mass spectra

The mass spectra collected from unfragmented peptides derived after the controlled proteolytic digestion of one protein are compared to the theoretical peptide masses obtained after “in-silico” digestion of all protein sequences in a database. To validate this comparative identification, different scoring algorithms can be applied. This method is called peptide-mass-fingerprint (PMF) (Pappin et al. 1993) and it is applicable for samples containing peptides derived from one protein only. In the case of bottom-up approaches, the sample peptides are derived from a mixture of proteins and some of them enter the mass spectrometer simultaneously. Therefore, a protein identification by PMF is not possible. In this case identification is performed by the use of the tandem mass spectra. This method is called peptide fragment fingerprint (PFF). Similar to PMF, experimental MS/MS spectra are compared and correlated to theoretical MS/MS spectra. This correlation is again statistically validated by calculating a matching score. Moreover, PFF are nowadays routinely used to validate PMF derived identifications.

1.3.4 Quantitation

The majority of proteomic analysis are not only used to catch the composition of the proteome of a sample under defined conditions. They are used to compare the proteomes under different conditions. Therefore, the individual proteins have to be quantitated, either in the absolute or, more often used, in a semi-quantitative manner. In the case of the gel-based approaches, quantitation is performed in a semi-quantitative manner by comparing the spot intensities of the gels. For this purpose, several software packages exist. Hereby, the quantitation is usually performed prior to protein identification.

In gel-free proteomic analysis, quantitation can be performed in an absolute or semi-quantitative manner (Lau et al. 2007). In semi-quantitative analyses, quantitation is either performed label free or by labelling the sample molecules (Lau et al. 2007). Methods for *in vivo* (SilAC (Ong et al. 2002) e.g.) or *in vitro* (ICAT (Gygi et al. 1999) or iTRAQ (Ross et al. 2004) e.g.) labelling exist.

In the case of iTRAQ™, the peptides are labelled with an isobaric tag (145 m/z). This tag consists of a reporter molecule, a balancer molecule and a protein reactive site (see Figure 1-11 A) and B)).

The masses of the different reporter groups are balanced by the balancer group, leading to a mass of 145 m/z for each label independently from the reporter group (see Figure 1-11B)). Therefore, the iTRAQ™ does not lead to an increase in complexity of either MS or MS/MS spectra. The MS spectra of all peptides are changed by the addition of 145 m/z while the MS/MS spectra are identical to those observed without labelling the peptides, except for the reporter ion signals in the mass range of 114 - 117 m/z (see Figure 1-11 C)). Semi-quantitation is performed by using the reporter ion signals.

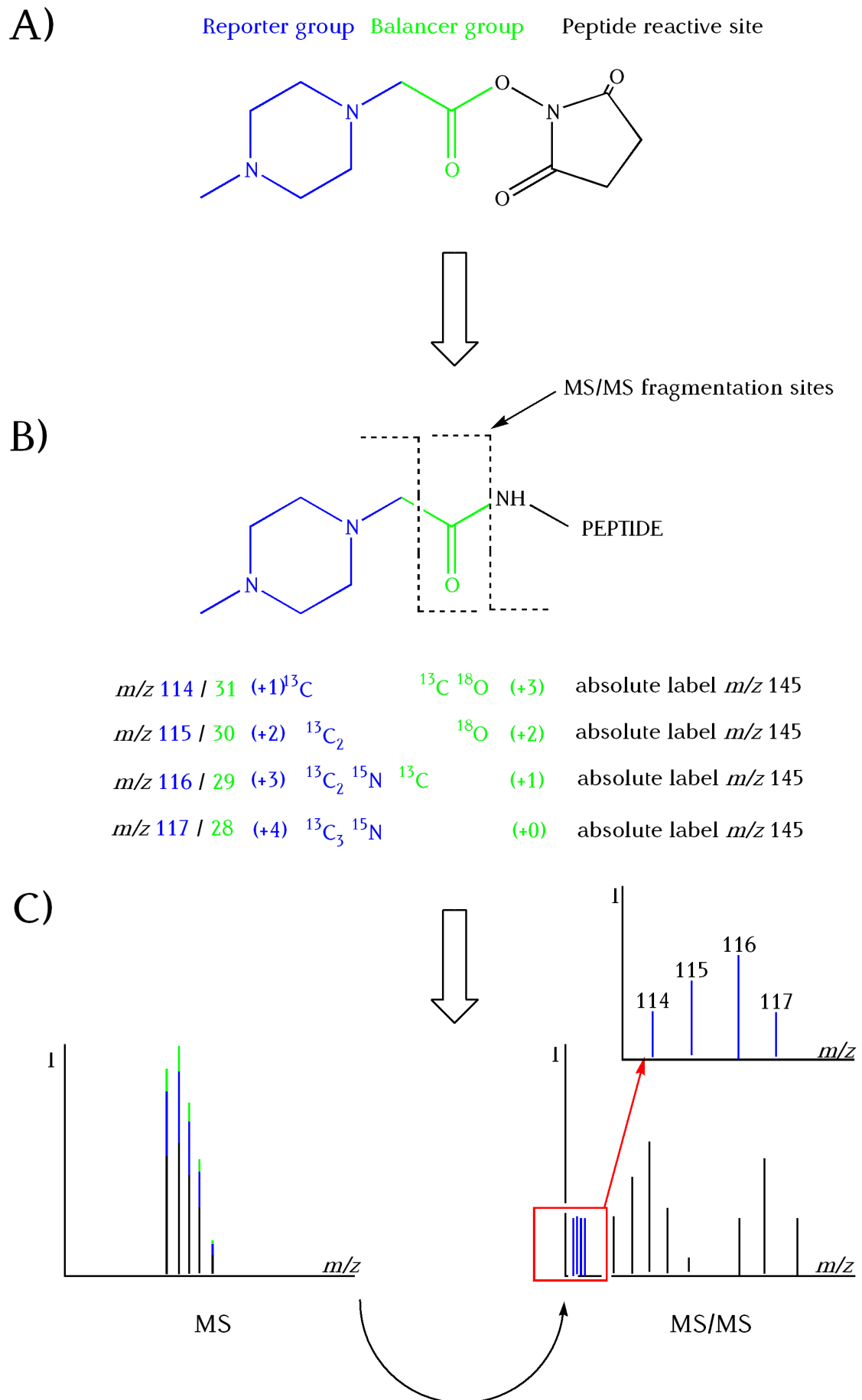


Figure 1-11 Schematic scheme of the iTRAQ method. Scheme developed according to (Ross et al. 2004).

1.4 Aim of the work

Cholesterol has a high impact on cardiovascular diseases in industrial countries. Elevated amounts of plasma cholesterol are treated by the administration of HMG-CoA reductase inhibitors that block *de novo* cholesterol biosynthesis. For these drugs, severe side-effects as well as pleiotropic effects have been described that are not yet fully understood. This study was carried out in order to get indications about proteins and thereby cellular pathways that are affected by treating primary human hepatocytes with rosuvastatin, one of the most promising new statins. In addition, the effects of the new CYP51A1 inhibitor LEK-935 were analysed to reveal indications about changes in the affected pathways by a block more downstream in the cholesterol biosynthesis. To get an impression about inter-individual differences that were supposed to be high, samples derived from two different human donors were analysed in parallel. The analysis should be carried out at the proteome of the cells. The cytosolic as well as the microsomal sub-proteomes were chosen as they contain many proteins involved in cholesterol biosynthesis as well as degradation.

The results should deliver information about the general reactions of the cells to the statin or the CYP51A1 inhibitor. Furthermore, information about differences of the effects of rosuvastatin and LEK-935 as well as inter-individual differences were expected. To further evaluate the gained results in a higher amount of individual samples, some of the found proteins should be validated by RT-PCR.

This study was performed to shed light into the biochemical pathways of primary human hepatocytes affected by the treatment with cholesterol lowering agents. The results should give indications for proteins or pathways that may be related to either some of the pleiotropic effects of the statins still unexplainable today or their more or less severe side-effects and thereby improve the understanding of statin action.

2 Materials

2.1 Chemicals

Chemical	Supplied by	Purity
2-iodo-acetamide	Merck	For synthesis
Acetonitrile	VWR	HPLC, gradient grade
Acetonitrile	Sigma-Aldrich	E Chromasolv
Acrylamide stock solution	National Diagnostics	Protein & sequencing grade
Ammoniumbicarbonate	Sigma-Aldrich	> 99.0 %
Ammoniumpersulfat	Sigma - Aldrich	Analytical grade
CHAPS	Fluka	> 98.0 %
DeStreak	GE Healthcare	---
Di-potassium-hydrogenphosphat	Roth	≥ 99.0 % p.a. free of water
Dithiotreitol	Diagnostic Chemicals Limited	High purity for molecular biology
EDTA	ZChL-UdS	≥ 99.9 % p.a.
Acetic acid	ZChL-UdS	99.5 - 99.8 %
Ethanol, embittered by 1%	ZChL-UdS	99.0 %
Petrolether		
Glycerol	ZChL-UdS	99.0 %
Urea	Roth	99.5 % p.a.
Potassium-di-hydrogenphosphate	Merck	p.a.
LE Agarose	Seakem®	For gelelectrophoresis
Methanol	ZChL-UdS	For synthesis
Mineral oil	GE Healthcare	---
Sodium deoxycholate	Serva	Purissime
Sodiumcarbonate, monohydrate	Sigma-Aldrich	99.5 %
Sodiumchloride	Grüssing	99.5 % p.a.
Sodiumdodecylsulfate	Serva	Research grade
Sodiumthiosulfate, pentahydrate	Merck	p.a.
Pharmalytes 3 - 10	GE Healthcare	---
Phenylmethylsulfonylfluoride (PMSF)	Serva	Research grade
Phosphoric acid	VWR	Analytical grade
Protease - inhibitor cocktail	Sigma - Aldrich	---
Protogel (30 % Acrylamide, 0.8 % Bisacrylamide)	Biozym	Ultra pure
Sucrose	Merck	Biochemical research
TEMED	Roth	99.0 % p.a., for electrophoresis

Chemical	Supplied by	Purity
Thio urea	GE Healthcare	
Triacetic acid	Merck	For synthesis
Trifluororic acid	Roth	For synthesis
Tris	Roth	Ultra Quality, $\geq 99.9\%$
Trypsin	Promega	Sequencing grade, modified

2.2 Instruments / Materials

Type of instrument / material	Company	Product
Autoclave	Zirrbus	LVSA 50/70
Water purifier, distilled water	Grünbeck	Ion separator GENO®-Sep
Water purifier, distilled water	Grünbeck	Weichwassermeister2 VFR14-1
Electrophoresis station SDS-PAGE	GE Healthcare	Ettan Dalt II separation unit
Electrophoresis station IEF	GE Healthcare	IPGphor
Liquid chromatography 1 st dimension	Self-made (Delmotte et al. 2007)	RP-HPLC - setup
Liquid chromatography 2 nd dimension	LCPackings	nanoHPLC Ultimate
Liquid chromatography column	Phenomenex	Gemini C18
Liquid chromatography column	Self-made (Premstaller et al. 2001)	Trap column (PS-DVB monolith)
Liquid chromatography column	Self-made (Premstaller et al. 2001)	Analytical column (PS-DVB monolith)
Gel caster	GE Healthcare	Dalt II Gelcaster
IPGstrips	GE Healthcare	IPGstrip pH 3-10 NL, 18 cm
Mass standard, internal	Sigma-Aldrich	ProteoMass™ ACTH Fragment 18-39
Mass standard, internal	Sigma-Aldrich	[Glu ¹]-Fibrinopeptide B human
Mass standard, external	Applied Biosystems	Mass Standards Kit for the 4700 Proteomics Analyzer
Mass spectrometer	Applied Biosystems	MALDI-TOF/TOF Proteomics Analyser 4800
MALDI targets in-gel	Applied Biosystems	OptiTOF® 384well MALDI plate insert
MALDI targets nLC-MS	Applied Biosystems	Opti-TOF® uLC MALDI Plate Inserts
Power supply	GE Healthcare	Ettan Dalt II power supply and control unit
Automated fractionation unit nLC-MS	Dionex	Probot
Protein concentration determination	GE Healthcare	2D Quant Kit
Protein concentration determination	Uptima	BC - Assay
Protein ladder	Fermentas	PageRuler unstained protein

Type of instrument / material	Company	Product
Protein ladder	Biolabs	ladder Prestained Protein Marker Broad Range
Rehydration tray	GE Healthcare	Reswellingtray
Water purifier, ultra pure water	Millipore	Milli-Q (biocel) Column 1: Quantum™ EX Column 2: Q-Gard®2
Photometer	Shimadzu	UV-Vis recording spectrophotometer UV2101
Sonication	Emich	USD 30
Sonication probe	Emich	6.4 mm in diameter
Ultra centrifuge	Hitachi	himac CP75B
ZipTips	Millipore	Zip-Tip pipette tips (0.6 µl C ₁₈ -resin)

2.3 Buffer / Solutions / Water

The 2D-PAGE as well as the nLC-MS are quite sensitive methods and thereby susceptible to impurities in any way. Therefore, all chemicals were of highest purity and all buffers and solutions were prepared using ultra pure water, unless otherwise stated.

3 Methods

The general experimental setup of this study is depicted in Figure 3-1. To enable the parallel analysis of different subcellular proteomes, the raw cell lysate was fractionated. Moreover, a relatively high resolution was achieved by reducing the predominance of high abundant proteins without the loss of information. The cytosolic fraction was applied to analysis by two dimensional gel electrophoresis followed by mass spectrometry. To analyse the membrane proteins contained in the microsomal fraction, it was applied to two dimensional liquid chromatography followed by mass spectrometry. The nuclear and mitochondrial fractions that were also gained during sample preparation were stored at -80 °C until further use. The present study was performed in the frame of an international research project (European Commission project number: 512096, www.steroltalk.net). Therefore, some of the experiments were performed in collaboration: Dr. Katalin Monostory (Hungarian academy of science, Chemical research centre, Budapest) isolated, cultivated and treated the primary human hepatocytes and Dr. Jean-Marc Pascussi (Institut de Génomique Fonctionnelle, Département d'Oncologie, CNRS UMR5203 - INSERM U661 - UFR de Médecine Montpellier-Nîmes) performed the RT-PCR experiments.

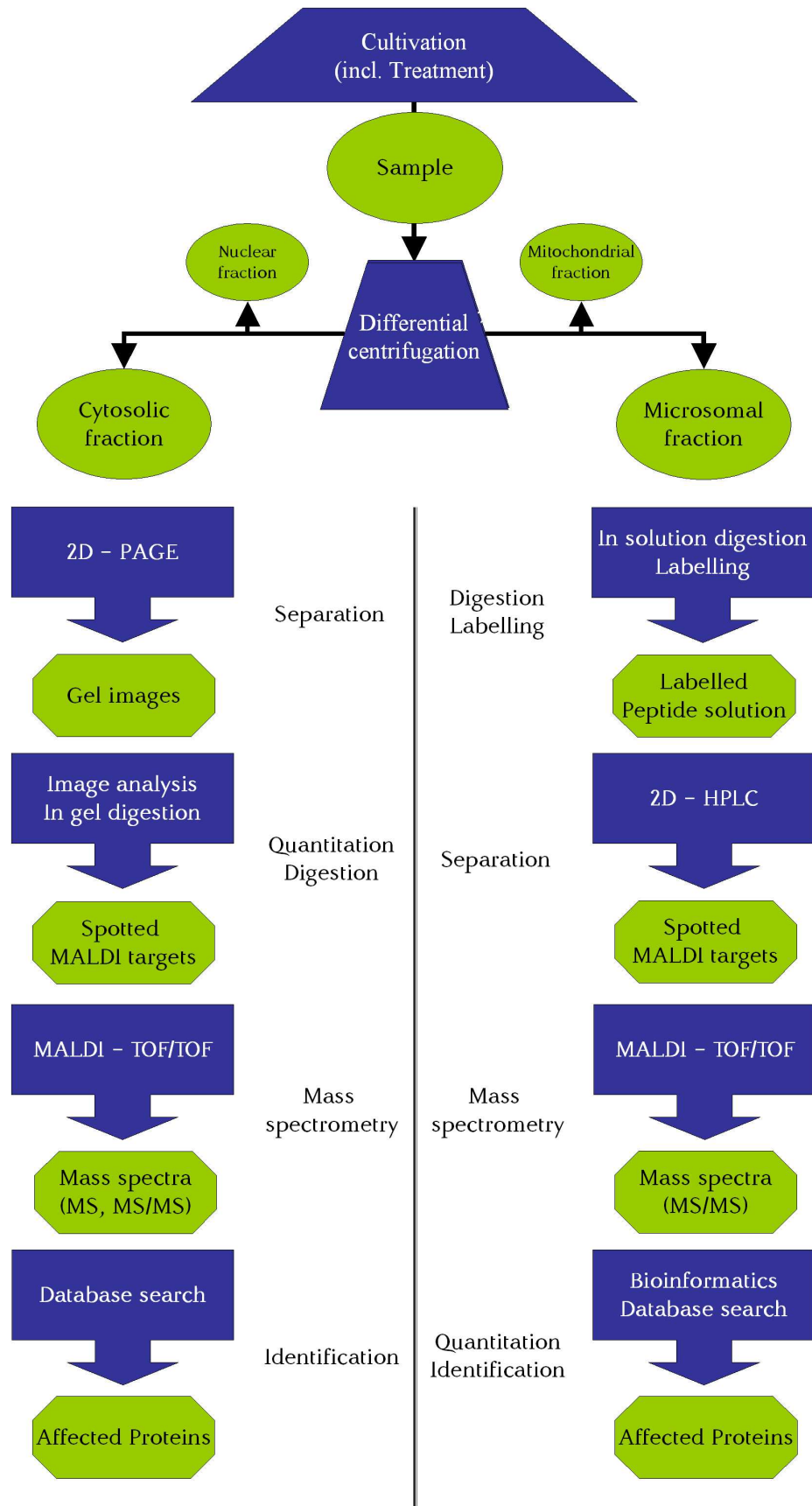


Figure 3-1 General experimental setup of the present study

3.1 Cell culture

3.1.1 Primary human hepatocytes

Isolation and cultivation of the primary human hepatocytes was performed by Dr. Katalin Monostory, Hungarian academy of science, Chemical research centre, Budapest.

The livers were obtained from kidney transplant donors resected from adult patients for medical reasons unrelated to this study (Transplantation and Surgical Clinic, Semmelweis University, Budapest, Hungary). Permission of the Hungarian and Regional Committee of Science and Research Ethics was obtained to use human tissues.

3.1.1.1 Liver perfusion and hepatocyte isolation

One of the branches of portal vein in the left lobe was cannulated and the tissue was perfused with Ca²⁺-free Earl's balanced salt solution (EBSS) containing ethylene glycol tetraacetic acid (EGTA, 0.5 mM) and then with Ca²⁺-free EBSS, finally with the perfusate containing collagenase (Type IV, 25 mg/100 ml) and Ca²⁺ (2 mM). Perfusion was carried out at pH 7.4 and at 37 °C. Softened tissue was gently minced and suspended in ice-cold hepatocyte dispersal buffer. Hepatocytes were filtered and isolated by low-speed centrifugation (50 x *g*) and washed three times in hepatocyte dispersal buffer and once in culture medium.

3.1.1.2 Plating and culture of hepatocytes

The yield and the percentage of cell viability according to the trypan blue exclusion test were determined. Hepatocytes were suspended to 1.3 x 10⁶ cells/ml concentration in culture medium with foetal calf serum (5 %). Liver cells were plated (150,000 cells/cm²) in culture dishes coated with collagen and maintained in a humid atmosphere of air containing 5 % CO₂ at 37 °C. Cell culture and treatment were performed as described in (Monostory et al. 2009). The samples used for proteome analysis were treated for 48 hrs with 10 μM of rosuvastatin (RSV), LEK-935 or 0.1 % dimethyl sulfoxide (DMSO, control). After harvesting, the cells were stored at - 80 °C and received on dry ice. Each vial obtained from Dr. Monostory contained 1 x 10⁷ cells.

Sample 1 and 2 were derived from cells of donor HH-129 and HH-114, respectively, see (Monostory et al. 2009).

3.1.1.3 Buffer / Solutions

<u>Earl's balanced salt solution pH 7.4</u> (Ca ²⁺ -free)		<u>Culture medium</u> <u>Williams' medium E : Ham's F12 medium 1:1 (v/v)</u>	
NaCl	117 mM	Gentamicin	50 mg/ml
KCl	5.4 mM	Amphotericin B	1.2 M
NaH ₂ PO ₄	0.9 mM	(or 0.75 mg/l fungizone)	
NaHCO ₃	26.16 mM	Glucose	6.9 mM
Glucose	5.56 mM	Pyruvate	0.4 mM
		Ethanolamine	66.8 mM
<u>Hepatocyte dispersal buffer pH 7.4</u>		Linoleic acid	40 nM
HEPES	10 mM	Vitamin C	142 M
NaCl	142 mM	Insulin	0.6 mg/ml
KCl	7 mM	Dexamethasone	0.1 M
		Glucagon	57.4 nM
		Transferrin	50 g/ml

3.1.2 Human colon carcinoma cell line 116

The cells of the human colon carcinoma cell line 116 (HCT 116), used for protein stability testing during this study, were obtained by courtesy of Dipl. Biol. Britta Wilzewski.

3.1.3 *Schizosaccharomyces pombe*

The wild-type strain MB163 was used for the tests of protein stability. The cells used were a gift of Dipl. Biol. Ming-Kwai Tin.

3.1.4 *Echerichia coli*

E. coli strain JM109 was used for stability tests, the cells were a courtesy of Dipl. Chem. Berna Mersinli.

3.2 Protein isolation

3.2.1 Cell disruption

Cells were thawed on ice, centrifuged for 3 min at 74 *g* and resuspended in 400 μ l potassium phosphate buffer (0.1 M, pH 7.4). To avoid any kind of protein degradation caused by intracellular proteases, they were blocked by the addition of 10 μ l of protease inhibitor cocktail, containing inhibitors for cystein and serin proteases, amino peptidases and acidic proteases.

The use of lysis buffer during cell lysis, as usually performed, was avoided during this study. It would cause a solubilisation of membrane attached or integral membrane proteins prior to the fractionation by differential centrifugation, which would counteract the fractionation process.

The samples derived from human cell lines and *E. coli* cultures were lysed by sonication, while the yeast cells were disrupted by shaking with glass beads.

3.2.1.1 Sonication

Cell lysis was performed using an Emich USD 30 sonicator equipped with a 6.4 mm sonication probe, which was dipped 6 - 8 mm into the cell solution. Parameters are shown in Table 3-1

Table 3-1 Parameters applied for cell lysis by sonication

Sonication parameters	
Pulse duration	10 seconds
Repeats	7
Pulse amplitude	20 μ m
Break between pulses	1.5 minutes
Temperature	4 °C

3.2.1.2 Cell lysis using glass beads

As the fission yeast cells are surrounded by a thick cell wall nearly unbreakable by sonication without lysis buffer, yeast samples were disrupted by shaking in an equal volume of glass beads, as previously described (Boehmer et al. 2006; Hwang et al. 2006).

3.2.2 Differential Centrifugation

The following steps were performed at 4 °C. The resulting pellets were stored at -20 °C while the supernatant was used for the following centrifugation step. The supernatant of step three was defined as the cytosolic fraction.

- 1) Centrifugation of the cell lysate for 10 minutes at 3 000 *g*.
→ pellet = nuclei, cell debris
- 2) Centrifugation of the supernatant from step 1) for 20 minutes at 20 000 *g*.
→ pellet = mitochondria
- 3) Centrifugation of the supernatant from step 2) for 60 minutes at 117 000 *g*.
→ pellet = microsomes, supernatant = cytosol

3.2.3 Cleaning the microsomes

The membrane attached proteins and parts of the proteins enclosed in the vesicle lumen during the vesicle formation were removed by washing with 0.15 % sodiumcholate and a sucrose step.

Removal was performed, with minimal changes, as described by (Zgoda et al. 2006). Briefly, the microsomal pellet was washed in 1 ml 1.15 % potassium chloride solution (117 000 *g*, 4 °C, 60 minutes). The resulting pellet was resuspended in 1 ml potassium phosphate buffer (0,1 M, pH 7,4), diluted 1:2 in solution 1 and incubated on a platform shaker for 60 minutes, 4 °C. It was than applied onto a 0.4 M sucrose step and centrifuged at 117 000 *g*, 90 minutes, 4 °C. The pellet was washed in 1 ml solution 2 (117 000 *g*, 4 °C, 60 minutes). The final pellet was stored at -20 °C.

3.2.3.1 Buffer / Solutions

<u>Solution 1</u>		<u>Solution 2</u>	
Sodium cholate	0.15 % (w/v)	EDTA	1 mM
EDTA	1mM		
In potassium phosphate buffer (0.1 M, pH 7.4)			

3.3 Determining the protein concentration

3.3.1 PlusOne™ 2D Quant Kit

The protein concentration of the cytosolic fraction was determined, using the „PlusOne™ 2D Quant Kit“ (GEHealthcare). This kit includes a precipitation step to remove contaminants. The whole procedure was performed according to the supplied instructions with slight modifications. Two times 5 µl of protein solution were subjected to protein determination. The resulting values were averaged to get the final protein concentration. The centrifugation step after precipitation was performed for 20 minutes at 20000 *g*, 4 °C.

3.3.2 Bicinchoninic acid assay

The protein concentration of the microsomal fraction was determined, using the bicinchoninic acid assay (Pierce, Uptima) following the suppliers instructions.

3.4 Two dimensional gel electrophoresis (2D - PAGE)

The protocol used in this study follows the classical setup. At first, the proteins were separated according to their isoelectric point, then according to their physical size in the second dimension.

The isoelectric focussing (IEF) was performed on immobilised pH gradient gels (IPGstrips), with a non-linear pH gradient from 3 - 10 and 18 cm in length. The strips were then applied to a 12.5 % sodium dodecyl sulfate (SDS) gel in the dimensions of 20 x 26 cm (see Table 3-2). IEF was performed using the IPGphor (Amersham), the sodium dodecyl sulfate polyacrylamide gel electrophoresis (SDS-PAGE) was performed in the EttanDALT II system. A maximum of 12 gels were run in parallel.

Table 3-2 Characteristics of the 2D-PAGE

	Dimension (cm)	Duration (h)
	Length x Breadth x Thickness	
IEF	18 x 0.5 x 0.1	8
SDS-PAGE	20 x 26 x 0.1	5 to 6
Coomassie staining	-	132 to 140

3.4.1 Isoelectric focussing

3.4.1.1 Sample preparation

In general, 100 µg of protein was applied per gel. The sample was loaded by in-gel rehydration. For this purpose the volume of sample solution corresponding to 100 µg protein was mixed with the same volume of lysis buffer. To further improve the solubilisation of the proteins, this mixture was incubated for 15 minutes at room temperature. The solution was adjusted to a volume of 340 µl with rehydration solution and Phenylmethylsulfonylfluoride (PMSF) was added to a final concentration of 3 ng/µl.

3.4.1.2 Rehydration

Rehydration was performed in the rehydration tray, over night and at room temperature. To avoid evaporation, the strips were covered with mineral oil.

3.4.1.3 IEF - Performance

The strips were transferred to the IPGphor and again covered with mineral oil. Filter paper wetted with 150 μ l of double-distilled water was placed on top of both strip-endings. The electrodes were placed on top of the filter paper but still above the gel. Parameters were the following: the temperature was set to 20 °C, a maximum current of 50 μ A was applied per strip and the program shown in Table 3-3 was used. After focussing, the IPGstrips were stored at -20 °C until further use.

Table 3-3 Program IPGphor

Step	Duration [h]	Voltage [V]	Volthours [Vhrs]
S1	1	150	150
S2	2	300	600
S3	1	600	600
S4	1	600- 8000	4300 (Gradient)
S5	3	8000	24000
Total: 29650 Vhrs			

3.4.1.4 Buffer / Solutions IEF

<u>Lysisbuffer</u>		<u>Rehydration solution</u>	
Urea	7 M	Urea	7 M
Thio-urea	2 M	Thiourea	2 M
CHAPS	65 mM	CHAPS	1 % (w/v)
DTT	60 mM	DTT	0.4 % (w/v)
Pharmalytes 3-10	2 % (v/v)	Pharmalytes 3-10	0.5 % (v/v)
		Bromphenolblue	≤ 0.002 % (w/v)
		DeStreak - reagent	1.2 % (v/v)
Stored in aliquots at -20 °C		Stored in aliquots at -20 °C	

3.4.2 Sodium dodecylsulfate–polyacrylamide gel electrophoresis

3.4.2.1 Casting the gels

To cast the gels, the Ettan DALT gel caster was used. As overlay solution, either a butanol : water mixture (10:1) or 0.1 % SDS was used. Gels were cast over night, prior to use.

3.4.2.2 Equilibration

Strips were incubated in reducing equilibration solution followed by incubation in alcyating equilibration solution. Both steps were performed at room temperature by shaking for fifteen minutes on an orbital shaker.

3.4.2.3 Gel electrophoresis

The IPGstrips were washed in 1 x electrophoresis buffer directly after equilibration to lubricate them and improve their application onto the second dimension. Two different protein ladders were used (see 2.2) to enable an approximation of the molecular weight range. To prevent floating of the strips, they were covered with 2 - 3 ml of sealing solution. The upper buffer chamber was filled with 2 x electrophoresis buffer while the lower chamber was filled with 1 x electrophoresis buffer. The SDS-PAGE was run according to the settings shown in Table 3-4.

Table 3-4 SDS-PAGE Program

Step	Duration	Power
S1	30-60 Min	5 W/Gel
S2	5 h	15 W/Gel
In total: 5 - 6 h		

Once the running dye reached the end of the gel, the experiment was stopped and the gels applied to fixation over night.

3.4.2.4 Buffer / Solutions SDS-PAGE

<u>Acrylamidsolution:</u>		<u>Displacing solution</u>	
Acryl-/Bisacrylamid	12 % (v/v)	TrisCl (pH 8.8)	375 mM
TrisCl (pH 8.8)	375 mM	Glycerol	50 % (v/v)
SDS	0.1 % (w/v)	Bromphenolblue	≈0.002 %
APS	0.1 % (w/v)		
TEMED	0.05 % (v/v)		
Always prepared ready-to-use		Always prepared ready-to-use	
<u>Equilibration solution, reducing</u>		<u>Equilibration solution, alkylating</u>	
Urea	6 M	Urea	6 M
SDS	2 % (w/v)	SDS	2 % (w/v)
TrisCl (pH 8.8)	50 mM, pH 8.8	TrisCl (pH 8.8)	50 mM, pH 8.8
Glycerol	30 % (v/v)	Glycerol	30 % (v/v)
DTT	1 % (w/v)	IAA	4 % (w/v)
Stored in aliquots at -20 °C, addition of reducing or alcyating reagent prior to use			
<u>Electrophoresis buffer (1X)</u>		<u>Sealing solution</u>	
Tris-Base	25 mM	Agarose	0.5 % (w/v)
SDS	0.1 %	Bromphenolblue	≈0.002 %
Glycin	0.19 M	In 1 X electrophoresis buffer	
Storage at room temperature		Heated in the microwave, stored at 60 °C	

3.4.3 Staining

Gels were stained by colloidal coomassie staining. All steps were performed at room temperature by gentle shaking on an orbital shaker. The volume was set to 0.5 l per gel. The solutions were prepared ready-to-use and the Coomassie brilliant blue was directly added to the shaking pre-incubation solution. The general procedure is shown in Table 3-5

Table 3-5 Procedure of colloidal coomassie staining

Step	Duration
Fixation	Overnight
Washing	2 x 15 minutes
Pre-incubation	1.5 h
Incubation	5 days
Destaining	2 - 3 times washing

3.4.3.1 Buffer / Solutions

<u>Fixativ</u>		<u>Wash / Destaining solution</u>	
Ethanol	50 % (v/v)	Water	
Phosphoric acid	2.55 % (v/v)		
<u>Pre-incubation</u>		<u>Incubation</u>	
Ammoniumsulfate	17 % (w/v)	Ammoniumsulfate	17 % (w/v)
Methanol	34 % (v/v)	Methanol	34 % (v/v)
Phosphoric acid	2.55 % (v/v)	Phosphoric acid	2.55 % (v/v)
		Coomassie brilliant blue G	1 % (w/v)
		250	

3.4.4 Image digitalisation

The stained gels were digitalised to enable their bioinformatical analysis. Scanning was performed at the Image Scanner controlled via Image Master Labscan v.3.0.1. (Amersham).

Parameters were the same for every gel (see Table 3-6). As the contrast/brightness parameters were set to auto, they changed according to the detail chosen to be

scanned in the scanner preview window. Therefore, a manual control of these values was done, to assure a final comparability of the gel images.

Table 3-6 Scanning parameters

Parameter	Settings
Object type	Transmissive
Colours	Grey, red channel
Resolution	300 dpi
Filter	No filter
Contrast/brightness	Auto

The pictures were stored as 16 bit greyscale .tiff images. The software PDQuest was applied to rotate or flip the images prior to semi-quantitative bioinformatical analysis.

3.4.5 In-Gel digestion

Gel pieces, approximately 1 x 1 mm in size, were excised from the gels and stored at -20 °C prior to their enzymatic digestion. Until otherwise stated, all steps of the excision and digestion process were performed at room temperature.

The tubes containing the gel pieces were placed in a Thermomixer comfort (Eppendorf). First, the gel plugs were washed for 10 minutes in 50 µl water. This step was followed by incubation for 15 minutes in 50 µl of an 50 % acetonitrile (ACN) solution; while they were shaken at 1 200 rpm, in intervals of 1 minute shaking followed by 1 minute break. Thereafter, the gel plugs were destained by incubation in 50 µl ACN for 1 minute, followed by 5 minutes incubation in 20 µl bicarbonate buffer (40 mM) at 450 rpm. After adding 20 µl ACN, the solution was further incubated for 15 minutes at 450 rpm. The destaining procedure was repeated until the dye was completely washed out of the plug.

After destaining, the plugs were dried in a speed vac and digestion was started by adding 15 µl of a trypsin solution (27 ng/µl in bicarbonate buffer (40 mM)). Digestion was performed at 37 °C over night and stopped by freezing the peptide solution in liquid nitrogen. The final peptide solution was stored at - 80 °C until matrix mixing and spotting onto a stainless steel target for matrix assisted laser desorption/ionisation (MALDI) mass spectrometry.

3.4.6 Spotting

3.4.6.1 Concentration using ZipTip™

Prior to matrix mixing, the peptide solution was concentrated using ZipTips™. A volume of 0.5 µl of a 5 % trifluoro acetic acid (TFA) solution was spiked to each vial to adjust the pH of the peptide solution to a value below 4 and reach a TFA concentration of at least 0.1 %.

The C18 resin was wetted and equilibrated by two times pipetting 10 µl ACN and 10 µl 0.1 % TFA, respectively. Sample was loaded onto the C18 material by ten times aspirating/dispensing 5 - 8 µl sample solution. This step was followed by three times washing in 5 µl 0.1 % TFA.

3.4.6.2 Matrix mixing

After washing, the sample was directly eluted in 5 µl of matrix (3 % alpha-cyano-4-hydroxy-cinnamic acid (CHCA) in 50 % ACN, 0.1 % TFA) by three times aspirating/dispensing.

3.4.6.3 Spotting

Of the eluate, 1 µl was spotted onto the MALDI target. Each sample solution was spotted twice to minimise the influence of mistakes occurring during matrix mixing or pipetting. Remaining eluate was stored at 4 °C in a 99-well plate, covered with plastic lid.

3.5 Nano high-pressure liquid chromatography (nHPLC)

This part of the project was performed in cooperation with Dr. Katja Melchior, member of the group of Prof. Dr. Huber, Department of Chemistry, Instrumental Analysis and Bioanalysis, Saarland University, Saarbruecken.

3.5.1 Sample preparation

As separation by two dimensional liquid chromatography is quite sensitive to impurities like for example salt, the samples needed to be further prepared after cleaning the microsomes. The 2D-Quant Kit was found to be incompatible with the iTRAQ™ 4-plex kit, so the BCA-assay was used to determine the protein concentration. The sample preparation was developed according to the iTRAQ™ chemical reference guide. Except for the BCA-assay, the solutions were provided with the iTRAQ™ 4-plex kit. After cleaning the microsomal fraction (see 3.2.3), the final pellet was resuspended in 100 µL dissolution buffer (pH 8.5, 500 mmol l⁻¹). To denature the sample, 5 µl of denaturant were added. The solution was then mixed and sonicated (15 seconds, 4 °C) to strengthen the denaturing process. After determining the protein concentration by BCA-assay, the disulfide bridges were reduced by adding an appropriate volume of reducing agent (60 minutes incubation at 60 °C) followed by adding cysteine blocking agent (10 minutes incubation at room temperature) to block the cysteines. Digestion was performed over night as described in the iTRAQ™ chemical reference guide. To label the samples, they were evaporated in a vacuum centrifuge to a volume of about 20 µl and adjusted with dissolution buffer to a volume of 120 µl (sample 1) and 60 µl (sample 2). Control samples were labelled with label 114 and 116 while for RSV treated samples, label 115 and 117 were used. Labelling was performed at room temperature for 60 minutes. Thereafter, all four samples of each donor were pooled, centrifuged at 3000 *g* to remove remaining membranes which would disturb the nLC separation and stored at -80 °C. The correction values for the iTRAQ™ reporter signal are listed in Table 3-7

Table 3-7 iTRAQ™ reagent correction, as supplied with the iTRAQ™ 4-plex kit

Reagent	% of -2	% of -1	% of 0	% of +1	% of +2
iTRAQ114	0.00	1.00	92.90	5.90	0.20
iTRAQ115	0.00	2.00	92.30	5.60	0.10
iTRAQ116	0.00	3.00	92.40	4.50	0.10
iTRAQ117	0.10	4.00	92.30	3.50	0.10

3.5.2 First dimension, basic eluent

For sample 1, 280 µg protein was applied to separation by nHPLC. For sample 2, only 90 µg was applied to test the sensitivity of the approach.

The samples were injected into a 150 x 2.0 mm i.d. Gemini C18 column. Sample loading was performed at 200 µL min⁻¹ with Eluent A. Elution was performed with Eluent B. The gradient was 0 – 60 % B in A during 35 min, 60 – 100 % B in A during 10 min, followed by isocratic elution at 100 % B for 2 min.

Fractions were collected manually, evaporated to nearly dryness to eliminate ACN, and dissolved in a final volume of 100 µL 0.10 % aqueous heptafluorobutyric acid (HFBA). After dissolution, the samples were stored at -80 °C until further separation in the second dimension. For the application onto the second dimension, eleven 3-min fractions were collected from minute twelve.

3.5.3 Second dimension, acidic eluent, ion-pairing

The second dimension separation setup consisted of a 2D capillary/nHPLC system, equipped with a low-pressure gradient micro-pump, a micro-column 10-port switching unit with loading pump, and a micro-autoinjector. Capillary preconcentration (10 x 0.2 mm i.d.) and capillary separation columns (60 x 0.1 mm i.d.) were PS-DVB monoliths. The chromatographic setup was coupled to an automatic fractionation unit, for matrix mixing prior to MALDI-MS/MS. Each fraction was analysed in triplicate. Of each fraction collected during the first dimension, 10 µL were injected into the second-dimension ion-pair reversed-phase nano-flow HPLC system described above. After injection, the peptides were isocratically concentrated and desalted on the precolumn for 3 min. The flow rate of 0.1 % aqueous HFBA solvent, delivered by the loading pump, was set to 10 µL min⁻¹. After switching the

valve, the peptides were eluted in back-flush mode onto the separation column. A 50-min gradient of 0-30 % ACN in 0.05 % aqueous TFA was applied followed by ramping to 100 % ACN in 10 min for fractions 1 to 5 of the samples. For fractions 6 to 11, a 5-min gradient of 0-10 % ACN followed by a 50-min gradient of 10-40 % ACN and ramping to 100 % ACN in 10 min was applied. The flow rate was set to $0.7 \mu\text{L min}^{-1}$.

3.5.4 Matrix mixing and spotting

The fractions collected after the second dimension were mixed with matrix, prior to mass measurement using the MALDI-TOF/TOF mass analyser. Mixing and parallel spotting onto a stainless steel target was realised using a spotting unit, directly coupled to the HPLC setup. The matrix flow was set to $3.1 \mu\text{L min}^{-1}$ with a spotting time of 5 s per spot (258 nL per spot). The samples of the HPLC run from min 8 to 75 were spotted to obtain fractions one to five, and from min 13 to 75 to obtain fractions six to eleven.

The spotted targets were stored for a maximum of two weeks at 20°C until their application to mass analysis by MALDI-TOF/TOF.

3.5.4.1 Buffer / Solutions nLC

<u>Eluent A</u>		<u>Eluent B</u>	
Triethylamine	72 mM	Triethylamine	72 mM
		Acetic acid	52 mM
Titrated to pH 10 with acetic acid		In ACN	
<u>Matrix</u>			
CHCA	3 mg/mL		
Glu-fib	15 fmol/ μL		
ACTH ¹⁸⁻³⁹	20 fmol/ μL		
TFA	0.1 %(v/v)		
ACN	70 %(v/v)		

3.6 Mass spectrometry by MALDI-TOF/TOF

Mass spectrometry was performed at a MALDI-TOF/TOF mass spectrometer (ProteomicsAnalyzer 4800™, Applied Biosystems). As different settings were used to measure the in-gel digests and the samples of the nLC-MS experiments, they are described in different sections.

3.6.1 In-Gel digests

3.6.1.1 MS data acquisition and processing

In MS mode, mass spectra were acquired in a mass range of 800 to 4000 m/z , with the focus mass set to 2100 m/z . Laser intensity was adapted for each measurement separately to get an optimal relation of signal intensity to resolution. Per sub-spectrum acquired, 50 laser shots were summarised. In total, eight sub-spectra were accumulated to the final MS-spectrum (400 shots). For data processing, the following parameters were set for peak filtering: raw spectrum filtering: subtract baseline; peak width: 50; smooth: no. Peak detection was performed according to the following settings: minimal S/N: 5; local noise window width (m/z): 50; minimal peak width at full width half max (bins): 2.9. The expected mass to resolution relations were: 1200 m/z , resolution of 17,000; 2400 m/z resolution of 22,000 and 3600 m/z resolution of 17,000. The monoisotopic peaks were flagged (adduct was set to H) and the cluster area S/N optimisation was enabled with a S/N threshold of 10.

3.6.1.2 Precursor selection for MS/MS

An interpretation method was written for precursor selection for MS/MS measurements containing the following parameters: minimal S/N: 35; adduct exclusion (Da): 21.982 and 37.956; adduct tolerance (m/z): ± 0.03 ; exclude precursors within: 200. The list of masses excluded from precursor selection is shown in Table 3-8. The tolerance at 850 Da was set to 50 to exclude all precursors in the range of 800-1000 as in this range also matrix clusters appear. A maximum of five precursors was chosen per spot.

Table 3-8 Mass exclusion list for precursor selection

Mass (Da)	Tolerance
850	50
996.5	0.1
1051.6	0.1
1165.7	0.1
1940	1
2082.9	0.2
2211	0.5
2222.1	0.2
2225.1	0.1
2239.1	0.1
2283	0.5
2407.9	0.1

3.6.1.3 MS/MS data acquisition and processing

In MS/MS mode fragmentation was realised using the CID chamber with air as collision gas. The precursor mass window was set to a resolution of 200,000 and the metastable suppressor was turned on. Here again, laser intensity was manually adjusted prior to each measurement. In total, 40 sub-spectra with 50 shots per sub-spectrum were acquired and accumulated to the final MS/MS-spectrum (2000 shots). The data processing settings were the same as for MS measurements, except for the parameters of peak detection. Changes were: the minimal S/N was set to 3, the local noise window width to 250 m/z and the expected mass to resolution relations were: 100 m/z , resolution of 4000; 500 m/z resolution of 4500, 1000 m/z resolution of 7000 and 1500 m/z resolution of 6000.

3.6.1.4 Mass calibration

To achieve an optimal mass accuracy, the instrument was calibrated in MS and MS/MS mode using a six-peptide calibration mix provided by Applied Biosystems spread over thirteen calibration spots on the MALDI target. The peak matching settings for the internal MS calibration were as follows: minimal S/N: 20; mass tolerance (m/z): 0.5; minimum number of peaks to match: 4; maximal outlier error (ppm): 5; use

monoisotopic peaks only: yes. The weighted fit was set to “equal”. The peptides and corresponding reference masses used are shown in Table 3-9.

Table 3-9 Peptides used for mass calibration in MS mode

Peptide	Mass (Da)
Des-Arg1-bradykinin	904.468
Angiotensin 1	1296.685
Glu1-Fibrino peptide B	1570.677
ACTH (1-17)	2093.087
ACTH (18-39)	2465.199

The peak matching settings for the internal calibration in MS/MS mode were as follows: minimal S/N: 10; mass tolerance (m/z): ± 1 ; minimum number of peaks to match: 5; maximal outlier error (ppm): 25; use monoisotopic peaks only: yes. The weighted fit was set to “equal”. Fragments for the glu-fib¹ peptide (1560.677 m/z) of the calibration mix were used for calibration. The masses of those fragments used for calibration are shown in Table 3-10. A plate model and default calibration in MS mode was performed for each target, at first. This was followed by the calibration of the default calibration in MS/MS mode and a final calibration of the default calibration in MS mode.

Table 3-10 Fragments of the glu-fib¹ peptide used for calibration in MS/MS mode

Fragment	Sequence	Mass (Da)
γ_1	R	175.199
γ_6	RASFFG	684.346
γ_7	RASFFGE	813.389
γ_9	RASFFGEEN	1056.475
γ_{13}	RASFFGEENDNVG	1441.634

3.6.2 nLC-MS samples

3.6.2.1 MS data acquisition and processing

The settings of data acquisition and processing were the same as in 3.6.1.1, except for the number of shots and spectra acquired. Here, 50 shots were acquired per sub-spectrum and 20 sub-spectra accumulated to the final MS-spectrum (1000 shots).

3.6.2.2 Precursor selection for MS/MS

A job-wide interpretation method was used in contrast to the per spot precursor selection performed during the in-gel measurements. The settings were the same as in 3.6.1.2, except for the additional adduct exclusion mass of -1.00 Da and the different masses on the exclusion list shown in Table 3-11. By these settings the masses between 800 Da and 1000 Da were excluded to avoid fragmentation of matrix clusters that may appear here. In addition, the mass range of 3000 Da to 4000 Da was excluded molecules of this size tend to fragment insufficiently.

Table 3-11 Mass exclusion list for precursor selection during nLC-MS mass measurements

<u>Mass (Da)</u>	<u>Tolerance</u>
850.00	50.0
1570.677	0.10
2465.199	0.10
3500.00	500.00

3.6.2.3 MS/MS data acquisition and processing

The settings of data acquisition and processing were the same as described in 3.6.1.3. Only two changes were made: the precursor selection window was set to 280 and additional stop conditions were set to achieve optimal quality of the MS/MS spectra: after 3000 shots (60 sub-spectra, 50 shots each) or a signal to noise ratio of 35 for at least 10 peaks, the fragment ion data acquisition was stopped.

3.6.2.4 Mass calibration

The same settings as described in 3.6.1.4 were used here, resulting in a mass accuracy of 50 ppm (= default calibration). For optimised mass accuracy (5 ppm), an internal calibration of the m/z using glu¹-fib (m/z 1570.677) and ACTH¹⁸⁻³⁹ (m/z 2465.198) was

performed during sample acquisition. In the case of a calibration failure due to signal suppression caused by high intensities of sample peptides, the default calibration was automatically used (50 ppm). The mass-to-charge ratio of glu¹-fib and ACTH¹⁸⁻³⁹ was set on the precursor selection exclusion list to circumvent fragmentation of it (see Table 3-11).

3.7 Real-time polymerase chain reaction

To validate differential protein expression, the results of some proteins found in altered amounts after the treatment with cholesterol lowering agents were also checked by real-time polymerase chain reaction (RT-PCR). These experiments were performed by Dr. Jean-Marc Pascussi (Institut de Génomique Fonctionnelle, Département d'Oncologie, CNRS UMR5203 - INSERM U661 - UFR de Médecine Montpellier-Nîmes).

The primers used were designed on or spanning exon boundaries using www.primer3. They are listed in Table 3-12. Total RNA samples (0.5 g/ml) from four different primary cultures of human hepatocytes were used. The cells were treated for 48 hours with rosuvastatin (10 μ M) or LK-935 (10 μ M). cDNAs were synthesized from 0.5 g of total RNA using the MMLV (Invitrogen) at 37 °C for 60 min, in the presence of random hexamers (GE HealthCare Sciences), and then diluted 10-fold in water. RT-PCR amplifications were performed using a SYBR Green mix and a Mx3000P apparatus from Stratagene. Cts were corrected according to GAPDH Cts and expressed as fold induction compared to control for each donor.

Table 3-12 Primer designed for RT-PCR

Protein	Primer	Sequence
PDIA3_HUMAN	F1	TCACGGACGACAACCTCGAGA
	R1	GGCAGTGCAATCAACCTTTC
	F2	GGATGCTGGGCACAACTCA
	R2	CCATCACGCGAGAACTCCT
ATPB_HUMAN	F1	GCCGAATCCCTCTGCTGTG
	R1	AGCATCCAAATGGGCAAACG
	F2	AGGACCCGTGAAGGCAATGA
	R2	AGCCACAGTCAGCCCAGTCA
NNMT_HUMAN	F1	TGCTGATGACATCGGCTCTG
	R1	TCACCACTGGGACCAGTC
	F2	CAGGCTTACCTCCAAGGACA
	R2	GGCCAGAGCCGATGTCAATC
PGM1_HUMAN	F1	CGCCAACACTACGCGGAGAACT
	R1	CAGGGGTGGAGAGGATCCA
	F2	TGGGCAAGCATGGGTTCIT
	R2	TCCAGCCAGTGGGGTCTC
HMCS1_HUMAN	F1	TCGTGGCTCACTCCCTTCC
	R1	GGCCAGCAAGTCTCTGCAT
	F2	CATGCCAGTGGCAGAAAGA
	R2	AACATCCCCAAAGGCTTCCA

3.8 Bioinformatics

The use of computational aid is essential for proteomic approaches. Personal computers equipped with the appropriate software are involved in nearly every step, from the control of the instruments to the digitalisation, storage and handling of the data and finally their interpretation.

The programs used for analysis and data interpretation are listed below. Those programs with a high impact on quantitation and/or identification are described in detail.

3.8.1 Image analysis

3.8.1.1 PDQuest

PDQuest is a commercially available software (BioRad) used for the quantitative analysis of the 2D gels. For each analysis six to twelve gels were run (two to four per treatment), as the biggest difficulty in 2D-PAGE is the reproducibility of single gels. The differences between the gels are small in themselves but the sum of differences may significantly disturb semi-quantitative expression studies. PDQuest is able to cope with small differences in the protein pattern and staining intensities. Furthermore, it allows to collect replicate gels in groups and thereby enables a statistical test of significance. Finally, the quantitative comparison of gels in different replicate groups is possible. In these studies, PDQuest version 8.0.1 build 055 was used.

3.8.1.1.1 Image preparation

The gel-images, scanned as described in 3.4.4, were opened and manipulated exclusively by using PDQuest prior to quantitative analysis.

In general, up to twelve gels were run in each experiment, four gels of the control, four gels of RSV treated samples and four gels of LEK-935 treated samples. Prior to their analysis by PDQuest, the gels were checked visually and, if necessary, removed from further analysis. Possible reasons for their elimination were pattern distortions obviously caused by experimental mistakes, failed staining, excess of dust or bubbles etc.

To ease and speed up the analysis, only that area of the gels that contains the spots was cropped of the whole picture. An example is shown in Figure 3-2. For each analysis, the same area was cropped of all the gels.

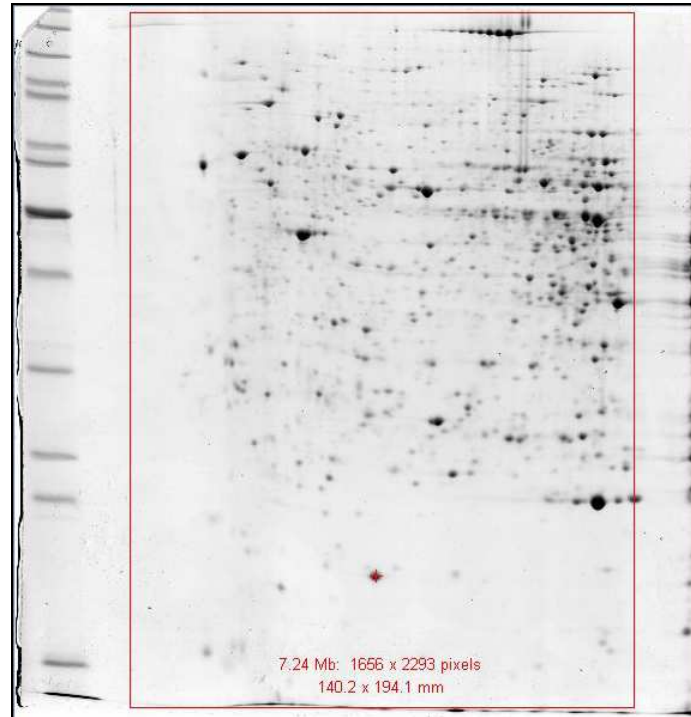


Figure 3-2 Example for the chosen crop area. Those regions of the gels, where no spots or only smear are visible, were excluded from bioinformatical analysis to ease and speed up the analytical process.

3.8.1.1.2 Spot detection

Either three or four gels of each sample were merged per replicate group. To enable spot detection, the faint, the smallest and the biggest spot cluster were marked in one of the gels. The chosen parameters were tested and, in the case of suboptimal spot detection, adapted until a good relation between detected spots, false positives and false negatives was reached. After automatic spot detection, all spots were manually checked and corrected, if necessary.

3.8.1.1.3 Matching

During the matching process, the signals detected as spots are summarised in a so-called master gel. With the use of this master gel the corresponding spots can be identified throughout each individual gel. The master gel is a virtual image, build of the signals of one exemplary gel and those signals which do not appear in this gel but in all gels that are members of one replicate group. The automated matching resulted

in a compliance of about 50 %. To further improve the analysis a manual control of all spots was performed. Thereby, the matching was corrected and possibly missing spots or false positive detections were corrected. The final matching rates and correlation coefficients are shown in Table 3-13.

Table 3-13 Final matching rates and correlation coefficients. Matching rate 1 is the percentage of matched spots relative to the total number of spots on the gel. Matching rate 2 is the percentage of matched spots relative to the total number of spots on the master gel.

Analysis	Matching rate 1	Matching rate 2	Correlation coefficient
Sample 1 I	> 96 %	> 86 %	> 0.847
Sample 1 II	> 98 %	> 89 %	> 0.855
Sample 2 I	> 95 %	> 84 %	> 0.766
Sample 2 II	> 96 %	> 90 %	> 0.815

3.8.1.1.4 Quantitative Analysis

PDQuest provides different analysis sets to perform a quantitative analysis. All of the analysis sets used in this study were written on the level of replicate groups. The analysis sets are shortly described below. In Figure 3-3 to Figure 3-5, the created sets are depicted.

Qualitative analysis set

Displays those spots present in one replicate group but not in another.

Qualitative analysis sets

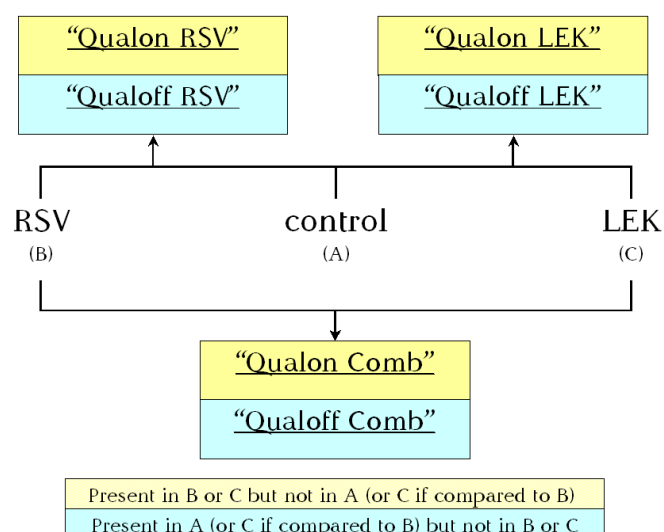


Figure 3-3 Qualitative analysis sets used in this study

Quantitative analysis set

Allows the comparison of spot quantities and displays those spots whose quantity is “Y” times higher or lower in one replicate group compared to another. Throughout the analysis “Y” was set to be two.

Quantitative analysis sets
(Two times changed quantity)

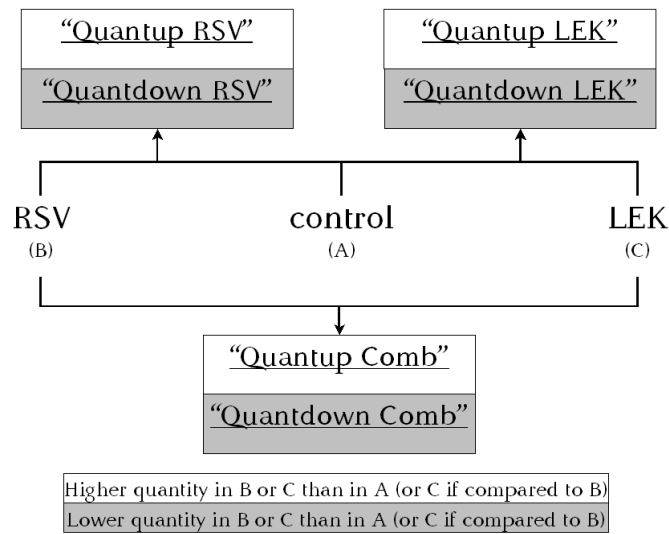


Figure 3-4 Quantitative analysis sets used in this study

Statistical analysis set

Allows the use of different statistical test to determine those spots that are significantly changed according to the corresponding test. Students t-test was used with a significance level of 99 %.

Statistical analysis sets
(99 % students t-test)

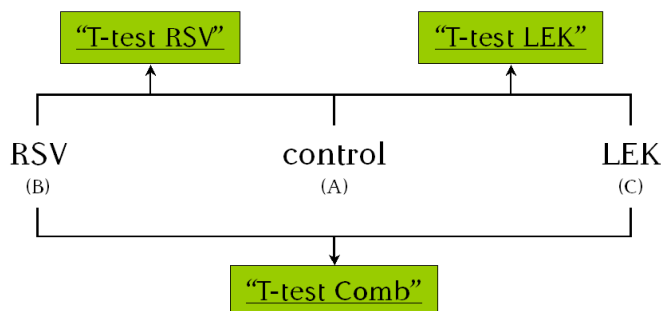
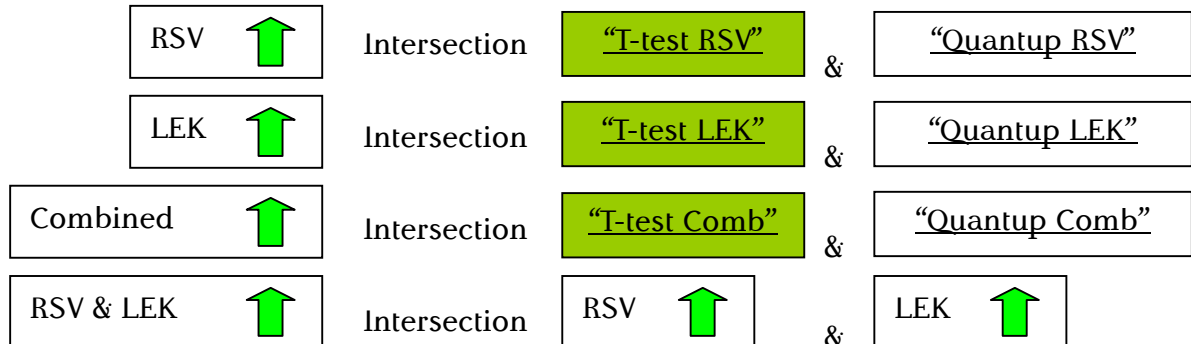


Figure 3-5 Statistical analysis sets used in this study

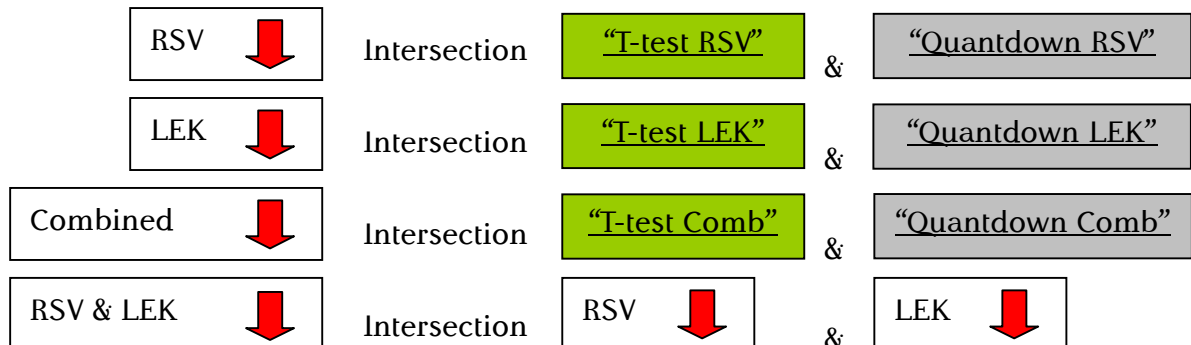
Boolean analysis set

Enables the comparison of two or more analysis sets. The scheme of boolean analysis sets used in the present study is shown below.

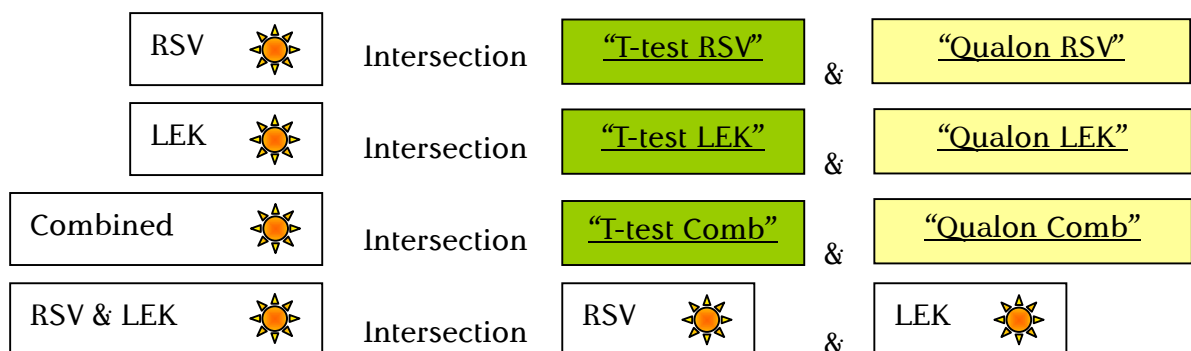
UPREGULATED



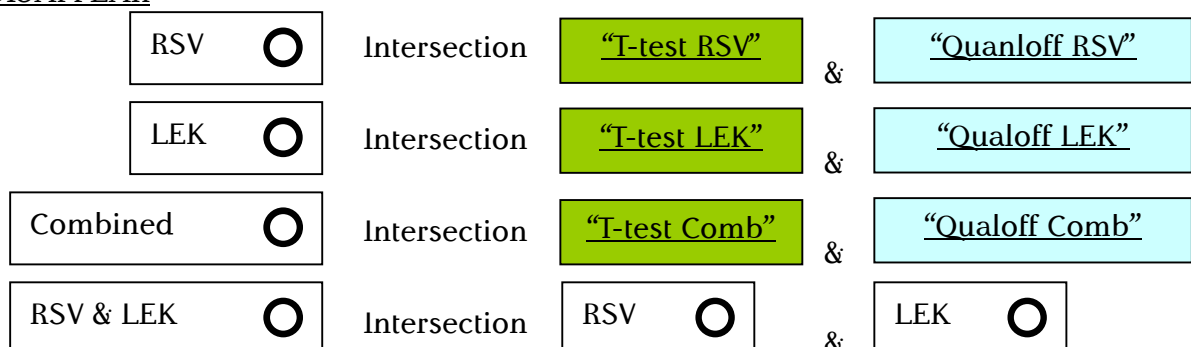
DOWNREGULATED



APPEAR



DISAPPEAR



3.8.1.1.5 Higher level experiments

To cope with the critical point of reproducibility, groups of three to four gels were used for analysis and the experiment was run in duplicate. Higher level experiments were created to compare the individual experiments with each other.

The basic steps were as follows:

- The individual simple experiments were matched on each other

- The matching was checked manually

- Analysis sets were written to create intersections of the Boolean analysis sets of the individual experiments

Only those spots that were found to be differentially represented on the gels in both experiments were regarded as true positive hits. They were cut from one gel of each treatment in every experiment. This yielded a set of two to six gel pieces per spot, depending on its presence on the gels. The gel pieces were stored at -20°C until they were applied to in-gel digestion, as described in 3.4.5.

3.8.2 Protein identification

3.8.2.1 Protein identification with MASCOT

In general, the MASCOT search engine based on the MOWSE scoring algorithm (Perkins et al. 1999) was used for protein identification.

3.8.2.1.1 Identification after in-gel digestion

The GPS explorer (Applied Biosystems) equipped with a MASCOT server (version 2.1.03) was used. A combined MS and MS/MS search was performed in all the cases. The peak filtering parameter for MS data were as follows: mass range, 800 – 4000 Da; minimum S/N, 10; maximum peak density, 20 per 200 Da, maximum number of peaks, 65. The filtering parameter for MS/MS data were the same except for the mass range, which was set to 60 Da to precursor mass minus 35 Da.

For identification, the following parameters were applied: taxonomy: no restriction; fixed modifications: none; variable modifications: carbamidomethyl (C), oxidation (M);

enzyme: trypsin; maximum missed cleavages: 1; precursor tolerance: 50 ppm, MS/MS tolerance: 0.1 Da; maximum peptide rank: 10. Search was performed against swissprot database (version 56.0).

3.8.2.1.2 Identification after nLC-MS

Protein identification from nLC-MS samples was done on a stand-alone MASCOT server version 2.2.03.

To enable identification of the samples, measured on the MALDI-TOF/TOF, the obtained mass spectra were exported using the launch-peaks-to-MASCOT tool (3.8.4.1) of the 4000series instrument software. The following parameters were applied: taxonomy: *homo sapiens*; fixed modification: iTRAQ 4-plex (N-term), iTRAQ 4-plex (K); variable modification: iTRAQ 4-plex (Y), methylthio (C), methionine oxidation; enzyme: trypsin; peptide tolerance: 50 ppm; MS/MS tolerance: ± 0.2 Da.

The search was performed against swissprot database (version 54.7).

3.8.2.2 Protein identification with ProteinPilot

In addition to identification by MASCOT, the nLC-MS data were further analysed by the ProteinPilot software, version 2 (Applied Biosystems).

The parameters applied for protein identification by the paragon algorithm were as follows: sample type: iTRAQ 4-plex (peptide labelled); Cys alkylation: MMTS; digestion: trypsin; special factors: no; species: *homo sapiens*; ID focus: biological modifications; search effort: thorough ID; detected protein threshold: >2.0 (99 %).

Search was performed against the same swissprot database used in 3.8.2.1.2.

3.8.3 Protein quantitation

As the samples analysed by nLC-MS were labelled with iTRAQ™, the recorded mass spectra were analysed in a semi-quantitative manner. Three different software packages were used to evaluate the quantitation data. ProteinPilot was chosen as quantitation and identification software available from Applied Biosystems, able to interact directly with the mass data stored in the instruments Oracle database. Mascot was chosen as the most prominent identification tool. It also allows to quantify proteins, but the mass data had to be exported from the instruments database. At the last Quant, a freely available software package for quantitation was chosen (Boehm et

al. 2007). It uses Mascot result files as a starting point, as it does not contain an algorithm for identification.

3.8.3.1 Protein quantitation with ProteinPilot

There are not many parameters that can be set, so only quantitation was enabled in addition to the parameters described in 3.8.2.2.

3.8.3.2 Protein quantitation with MASCOT

To obtain reliable quantitation results, the TS2MASCOT – tool (see 3.8.4.2) was used for data export from the MALDI-TOF/TOF. The parameters for the quantitation of iTRAQ™ reporter signals were as follows: Constrain search: no; protein ratio type: weighted; protein score type: mudpit; report detail: yes; show subsets: two; require bold red: yes; minimum peptides: two; significance threshold: 0.05; modification groups: iTRAQ (Y) variable, iTRAQ4plex; protocol: reporter; integration method: none. Quality settings were: minimum precursor charge: 1; isolated precursor: no; minimum a(1): 0.0; peptide threshold: at least identity; exclusion: iTRAQ (Y) variable. No outlier removal was performed and normalisation method was set to median.

3.8.3.3 Protein quantitation with Quant

Here again, the TS2MASCOT – tool (see 3.8.4.2) was used for data export from the MALDI-TOF/TOF. Protein identification was performed by MASCOT, as described in 3.8.2.1.2. Quant uses the data stored in the raw MASCOT result files as starting point for quantitation. Prior to data application to Quant the files had to be modified as described in 3.8.4.3. For quantitation, the following parameters were set: reporter tolerance: ± 0.5 Da; intensity range: no settings; absolute intensity error: 0.5 cts; experimental error: 0 %; only unique peptide: yes; Mascot significance threshold: p 0.05. The “mresx_1265.exe” application was used to handle the MASCOT result files.

3.8.4 Data handling

3.8.4.1 Data export by Launch peaks to Mascot

To export the acquired mass data to .mgf files, the following settings were used: the mass range was set from 60 *m/z* to precursor mass minus 35 Da; the peak density was

set to a maximum of 20 peaks per 200 Da; a minimal S/N of 10 and a minimal area of 200 was required. At maximum 65 peaks were exported per precursor.

3.8.4.2 Data export by TS2MASCOT

It turned out that the “launch peaks to mascot” function does not export the peak area information in a way suitable for quantitation by external software packages. So, for quantitation purposes, the TS2MASCOT tool available at www.matrixscience.com was used. It enables an “error-free” export of the stored data in order to allow quantitation beside the commercial software packages supplied by Applied Biosystems. Default parameters were used during peak exporting.

3.8.4.3 File modification

The “mres2x_1265.exe” part of the quant executable was not able to handle Mascot result files generated by a Mascot version 2.2 or higher. Therefore, the Mascot result files obtained from the stand-alone server were modified to enable their processing by Quant. Only those parts of the result files not recognized by Quant (“undeterminable variable”) were removed during modification. The text editor “Textpad” was used for this purpose. Modification only occurs as deletion of complete variable parts, no value changes or similar actions took place. Thereby, a “manipulation” of data, driving results into a possibly favoured direction was avoided.

3.8.4.4 Data validation by Peptide- and Proteinprophet (TransProteomicPipeline)

To check the amount of proteins identified by at least two unique peptides for quantitative experiments and validate the data gained by the nLC-MS approach, peptideprophet (Keller et al. 2002) and proteinprophet (Nesvizhskii et al. 2003) were used. Minimum peptide and protein probability were set to 0.95 and 0.99 respectively, forming of protein groups using protein prophet was excluded.

Peptide- and Proteinprophet were used as parts of the TransProteomicsPipeline, available at <http://tools.proteomecenter.org>.

3.8.5 Databases

The found proteins were further analysed according to their function, cellular localisation or possibly known interactions. For this purpose, the following databases were searched:

3.8.5.1 SwissProt /TrEMBL

To survey the cellular localisations described in the Expasy database the one written at first position was considered in the case of multiple descriptions. To get an overview about the cellular functions of those proteins identified during the nLC-MS experiments, they were summarised as follows: energy metabolism: proteins involved in glycolysis, mitochondrial respiratory chain etc.; protein biosynthesis and degradation: proteins involved in ribosomal complexes, translation, t-RNA synthesis, protein folding, post translational modifications and proteolysis; transcription: proteins involved in mRNA processing, DNA folding and histone complexes; cellular organisation: proteins involved in cell adhesion, signalling pathways, transmembrane and intracellular transport processes, vesicle forming, cell cycle and apoptosis, xenobiotic-lipid-cholesterol (XLC): proteins involved in xenobiotic/drug metabolism, fatty acid synthesis/degradation or cholesterol homeostasis.

SwissProt / TrEMBL is available at www.expasy.org.

3.8.5.2 Kyoto Encyclopaedia of Genes and Genomes (KEGG)

The KEGG database provides pathways all over the cell and enables the targeted search for pathways in which a distinct protein is involved. It thereby allows to check for pathway coverages by searching with lists of proteins, as done for the proteins identified during the nLC-MS experiments.

The KEGG database is available at www.genome.jp/kegg.

3.8.5.3 Gene Ontology database

To determine GO terms statistically overrepresented in the sample compared to the whole genome Cytoscape 2.6.0 (www.cytoscape.org) equipped with the BiNGO plug in (Maere et al. 2005) was used to search the Gene Ontology database. Except for species settings (*H. sapiens* or *S. pombe*) default parameters were used.

The GO is available at www.geneontology.org.

4 Results

4.1 General remarks

Starting point of this study was a general experimental setup for two dimensional gel electrophoresis, from sample preparation to staining, previously established with mouse protein and optimised for human liver proteins by the author (Woerner 2006). This setup was applied to the analysis of samples derived from primary human hepatocytes treated with cholesterol lowering agents.

There are three issues using this sample material. First, a big part of the proteins possibly affected by the treatment are integral or at least attached to membranes and are therefore difficult to analyse by 2D gel electrophoresis. Secondly, primary human hepatocytes are rare material so only a low amount of sample material was available. Third, the human liver is not only one of the most complex organs in the human body but also displays big inter-individual differences. And finally, issue four in this study was the sample stability with respect to freeze-thawing cycles.

First, methodical work was performed to cope with the issues one, two and four before the final proteomic analysis was started. Furthermore, samples derived from two different human donors were analysed to get an idea about the third issue, the inter-individual differences.

Therefore, the results are divided into three parts. In the first one, the methodical work is described, that was performed to create and validate the analytical setup used for the semi-quantitative analysis described in the second part. Finally, the proteins found to be significantly altered were searched against databases containing information about their cellular functions in order to get an overview about the pathways affected. This information is summarised in the third part.

4.2 Evaluation of the methodical approaches

The primary human hepatocytes were isolated, cultured and treated by Dr. K. Monostory. They were received as frozen cell pellets and stored at -80°C , until use. After cell lysis, the samples were fractionated by differential centrifugation to gain the cytosolic and microsomal sub-proteomes. The cytosolic fraction, containing almost exclusively soluble proteins, was applied to analysis by 2D gel electrophoresis, while for the analysis of the microsomal fraction, nLC-MS was chosen as promising and innovative analytical approach (see Figure 4-1).

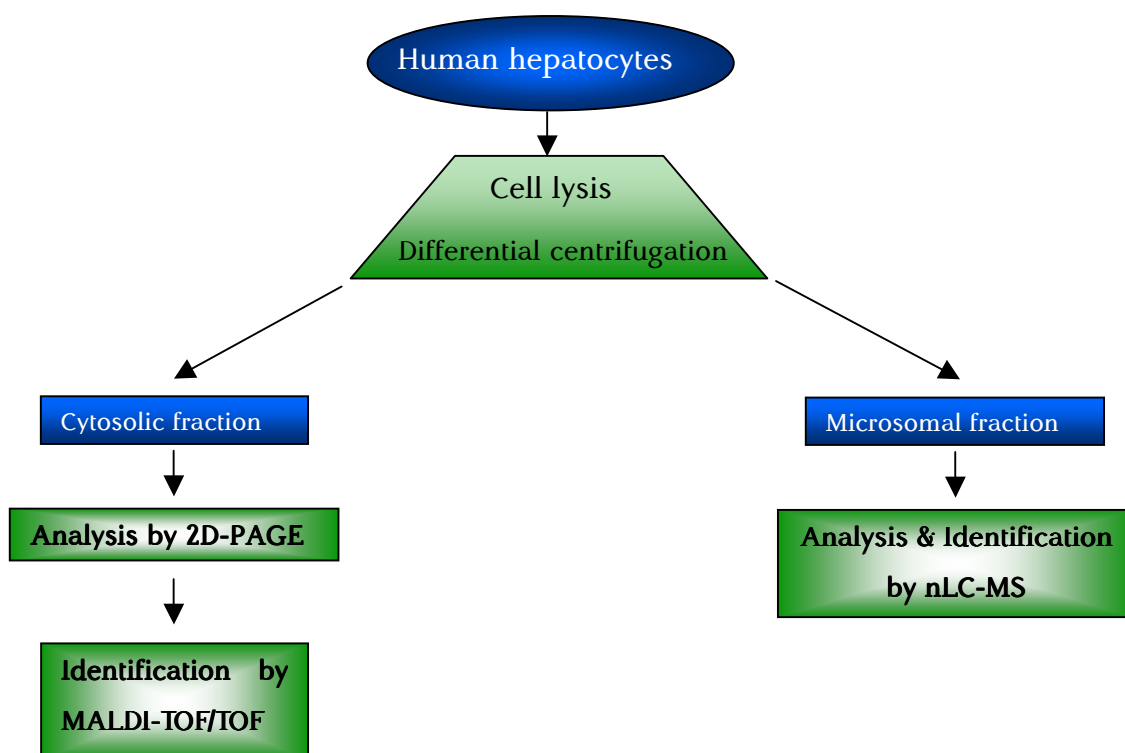


Figure 4-1 General scheme of sample preparation and analysis

In addition to some smaller adaptations of the 2D-PAGE setup to the low amount of sample material, the problem of protein stability during freeze-thawing cycles was faced and solved. During the nLC-MS analysis a new combination of separation modes was used for liquid chromatography; a RP x IP-RP setup with a basic eluent in the first and an acidic eluent in the second dimension. This had already been shown to be at least equivalent if not superior to the widely used SCX x RP setup (Gilar et al. 2005b, 2005a; Delmotte et al. 2007). Now its application to eukaryotic subcellular proteomes and its compatibility with the iTRAQ™-label, either with respect to the label itself but also with respect to the bioinformatical analysis of the reporter ion signals were proven.

4.2.1 Two dimensional gel electrophoresis

4.2.1.1 Protocol adaptation

As only a small amount of sample material was available, the experimental protocol for two-dimensional gel electrophoresis had to cope with this fact. All experimental steps were tested and, if necessary, optimised for this purpose. The adapted steps are briefly described below.

To avoid loosing sample material, the same 2D gels were used for semi-quantitative analysis as well as for spot excision. This also had the advantage that mistakes possibly occurring by the comparison of analytical and preparative gels were avoided. For protein visualisation colloidal coomassie staining was chosen, as the staining method had to be highly sensitive and, at the same time, compatible to mass spectrometry. Further optimisation steps were performed for the in-gel digestion. The basic protocol was developed and tested by Dr. S. Böhmer. It worked well with spots showing a high staining intensity, but it did not deliver satisfying identification results of those spots with low intensities. Therefore, accumulation/concentration of the peptides prior to matrix mixing and spotting was added to the protocol. Using ZipTips™ the amount of spots with identified proteins increased from 28 and 15 without ZipTips™ to 64 and 27 for donor 1 and donor 2, respectively. The final optimised versions of the experimental protocols as used for the semi-quantitative analysis are described in the material and methods chapter.

4.2.1.2 Effects of sample freezing on the gel quality

Trying to reproduce preliminary results gained during a proof-of-principle experiment with donor 0 (HH-089) nearly no correlation of the spots that were found to be significantly altered after treatment was observed between three individual experiments. By retracing every experimental step, the freezing-thawing cycles of the samples turned out to be the reason of this low correlation.

The decrease in overall quality of the gels by parallel increase in freezing-thawing cycles of the samples is obvious by looking at Figure 4-1 A-E. The presented gels were performed according to the same protocol. They only differ in an increasing number of freeze/thawing cycles of the samples prior to IEF. Even freezing the samples only once resulted in a worse picture (see Figure 4-2 A/B & C). In contrast, storing the IPGstrips after focussing for more than 2 weeks (see Figure 4-2 B) did not change the

spot pattern compared to short time freezing (see Figure 4-2 A). Freezing and thawing of the samples lead to an increase in horizontal smearing (see Figure 4-2), vanishing of spots and dispersing of single spots to a horizontal string of distinct spots. Until this observation was made, all protein samples were stored at -20°C after protein isolation, prior to their application to IEF.

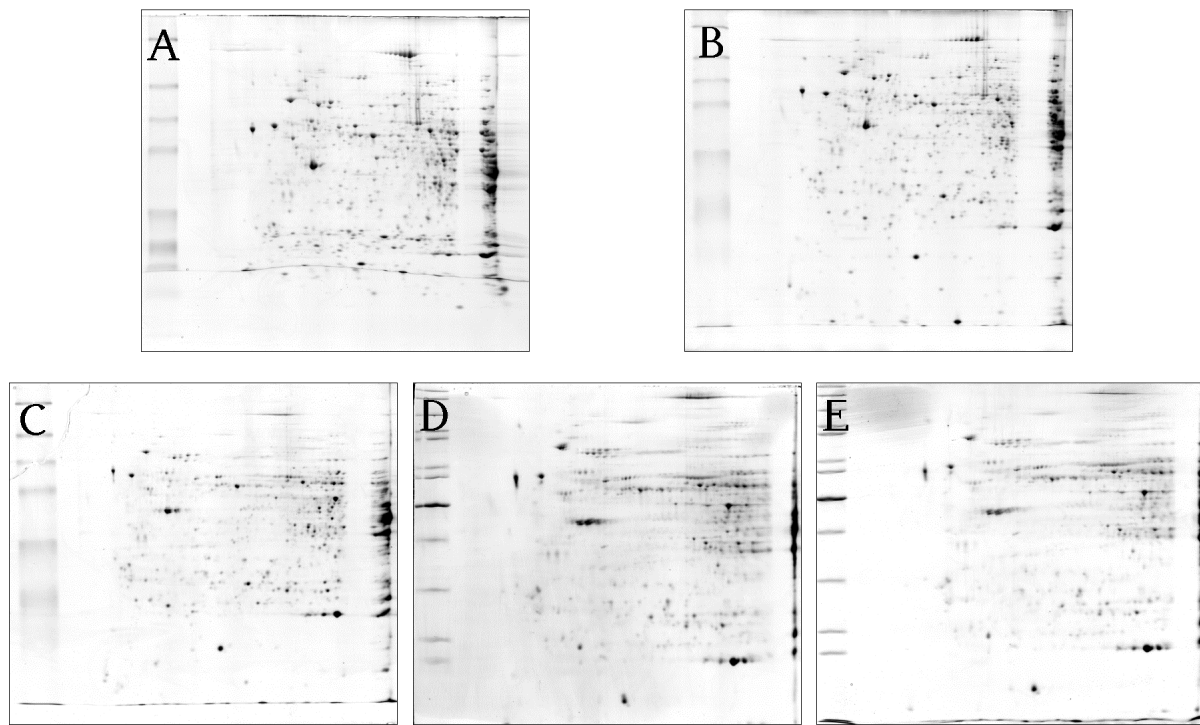


Figure 4-2 Effect of freeze/thawing cycles on the protein pattern. All pictures: SDS-PAGE (12.5 %) cytosolic fraction of HH-089 RSV treated cells, IPG strips (pH 3-10NL, 18 cm), 100 μg protein loaded per strip. IPG strip stored at -20°C after IEF. Visualisation by coomassie-staining. A) Sample application to IEF directly after protein isolation, no freezing; IPGstrip stored for 8 days. B) Sample application to IEF directly after protein isolation, no freezing; IPGstrip stored for 17 days. C) Sample application to IEF after 1 time freezing at -20°C . D) Sample application to IEF after 2 times freezing at -20°C . E) Sample application to IEF after 3 times freezing at -20°C .

According to experiences with 2D gel electrophoretic analysis of protein samples derived from *S.pombe*, the severe effects observed were not expected at all. This led to the suggestion that the severity of the effect may be related to the origin of the sample. To evaluate this assumption, additional experiments were performed with protein isolated from *Escherichia coli*, *Schizosaccharomyces pombe* and a human carcinoma cell line (HCT 116). Protein isolation, differential centrifugation and sample handling were performed in the same way as for the samples derived from primary human hepatocytes. The samples were untreated and frozen (-20°C) one and two times prior to IEF.

Two areas of each gel were cropped for a detailed analysis. One of the areas was located in a molecular weight range of 40 to 80 kDa and a more acidic range of the pH gradient (called high molecular weight detail), the second area was located in a molecular weight range of 15 to 40 kDa and in a more neutral to basic range of the pH gradient (called low molecular weight detail, see Figure 4-3). These areas were manually checked for spot appearance, fading and disappearance (see Figure 4-4 and Table 4-1).

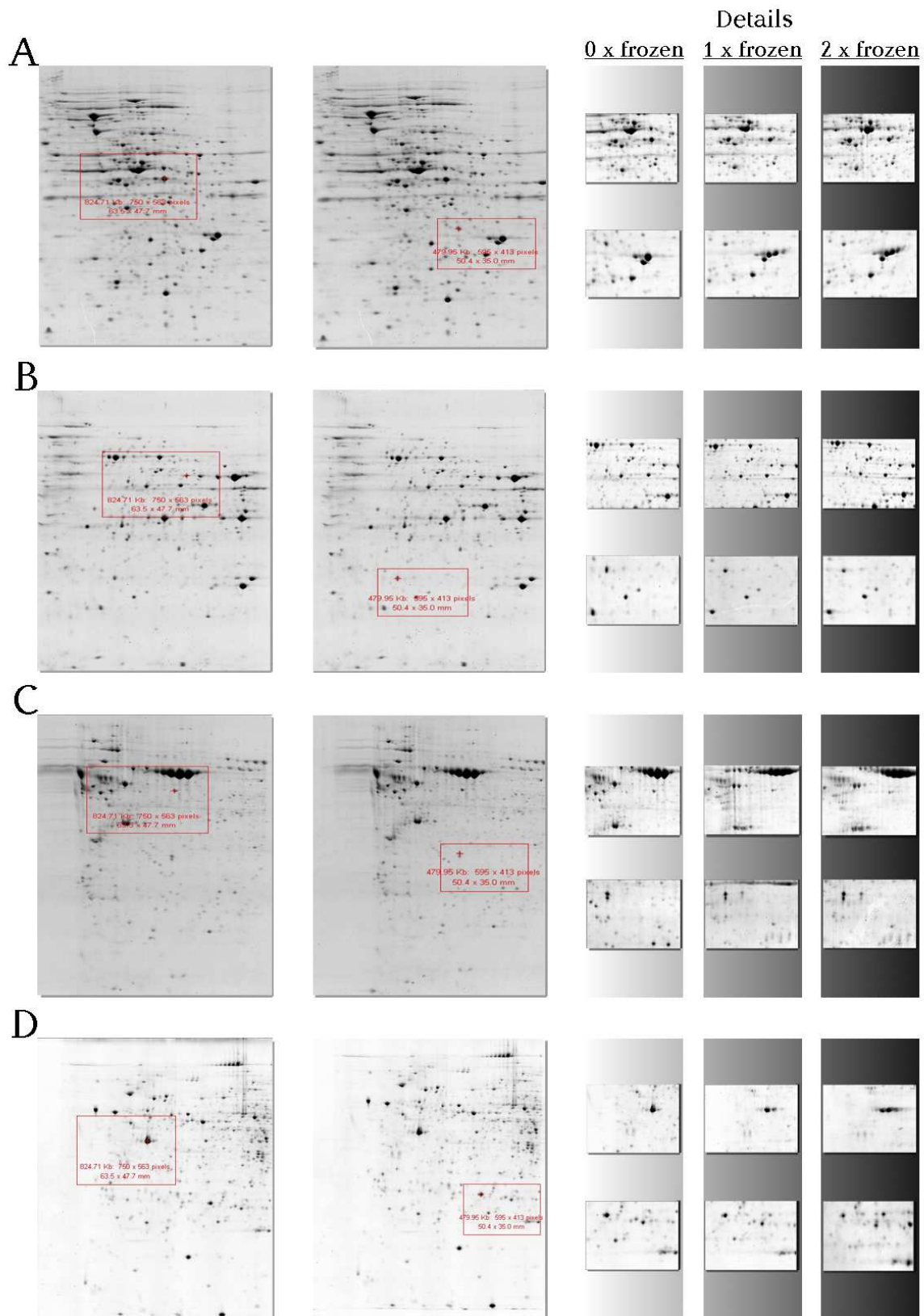


Figure 4-3 2D gels (IEF, 18 cm, pH 3-10 NL; SDS-PAGE, 12.5 %) of the cytosolic fraction of protein derived from *E. coli* (A), *S. pombe* (B), HCT 116 cells (C) and primary human hepatocytes (D). On the left side, the gels without freezing the sample prior to IEF are shown. The red rectangles mark those regions in the higher and lower molecular weight range cropped for a detailed analysis of the spot pattern (see Figure 4-4). Examples of cropped details after zero times, one time and two times freezing are shown on the right side.

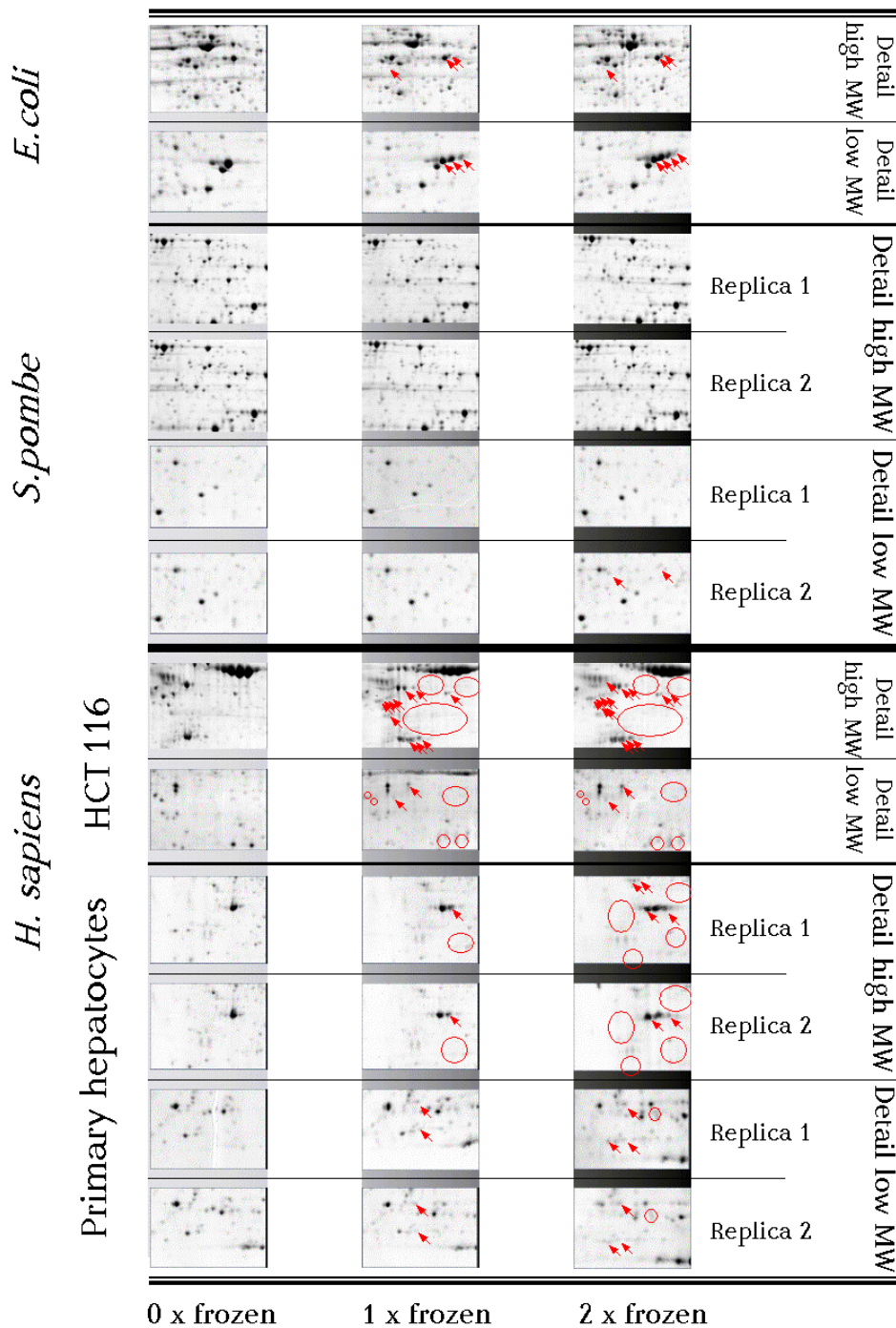


Figure 4-4 Analysis of the effect of freeze-thawing cycles on the spot pattern of 2D gels. Shown are the details cropped according to Figure 4-3. Spots, appearing or fading after freezing are marked by red arrows. Red circles mark spots disappearing after freezing. For yeast and primary human hepatocyte samples two replicas are shown to demonstrate the consistency of the effects.

For the *E. coli* sample, the analysis revealed two spots appearing in the high molecular weight area as well as in the low molecular weight area. These spots are part of the horizontal strings of spots mentioned above. Their origin seemed to lay in a spot fading away at the same time. For the yeast sample no changes were observed, that

are present in both replica. For both *E.coli* as well as *S.pombe* samples no disappearing of spots was found as it was observed in the human samples.

Table 4-1 Number of spots appearing, fading or disappearing after one or two freezing cycles. Only those spots changed additionally to the first freezing cycle are mentioned for the second one. For yeast and primary human hepatocytes, only those reactions observed in two replicate experiments are mentioned.

Sample	Detail	Freezing	Spots			
			Appearing	Fading	Disappearing	
<i>E.coli</i>	High MW	1	2	1	--	
		2	--	--	--	
	Low MW	1	2	1	--	
		2	--	--	--	
	Combined			4	2	--
	<i>S.pombe</i>	High MW	1	--	--	--
2			--	--	--	
Low MW		1	--	--	--	
		2	--	--	--	
Combined			--	--	--	
<i>H.sapiens</i> HCT 116		High MW	1	8	5	12
	2		3	--	--	
	Low MW	1	2	--	8	
		2	--	--	--	
	Combined			13	5	20
	<i>H.sapiens</i> Primary Hepatocytes	High MW	1	1	--	7
2			1	--	9	
Low MW		1	2	--	--	
		2	--	1	1	
Combined			4	1	17	

In contrast, just by looking over all the gels of the human samples severe effects on the protein pattern can be seen. Looking onto the details, the most severe effects were observed in the high molecular weight range. Freezing for only one time resulted in the loss of twelve and seven spots of the high molecular weight areas of HCT 116 and hepatocyte samples respectively. In addition, thirteen spots appeared and five spots

faded in the HCT 116 sample, while four spots appeared and one faded in the hepatocyte sample (see Figure 4-4 and Table 4-1).

In total, 38 and 22 spots were changed after freezing and thawing of the human samples, compared to six spots in the bacterial samples and no spot in the yeast samples. The consistency of the effect was proven by one time replicating the experiments with yeast and primary human hepatocyte samples.

Summarising, the spot pattern analysis revealed a high sensitivity of the samples derived from human cell culture to freeze-thawing prior to isoelectric focussing. Meanwhile samples derived from yeast seemed to be nearly unaffected and samples derived from bacteria showed only little effects. So, it was clearly demonstrated that the origin of the sample dramatically affects its stability against freeze-thawing cycles. To compensate the effects of freezing the samples prior to isoelectric focussing, the experimental protocol was further optimised.

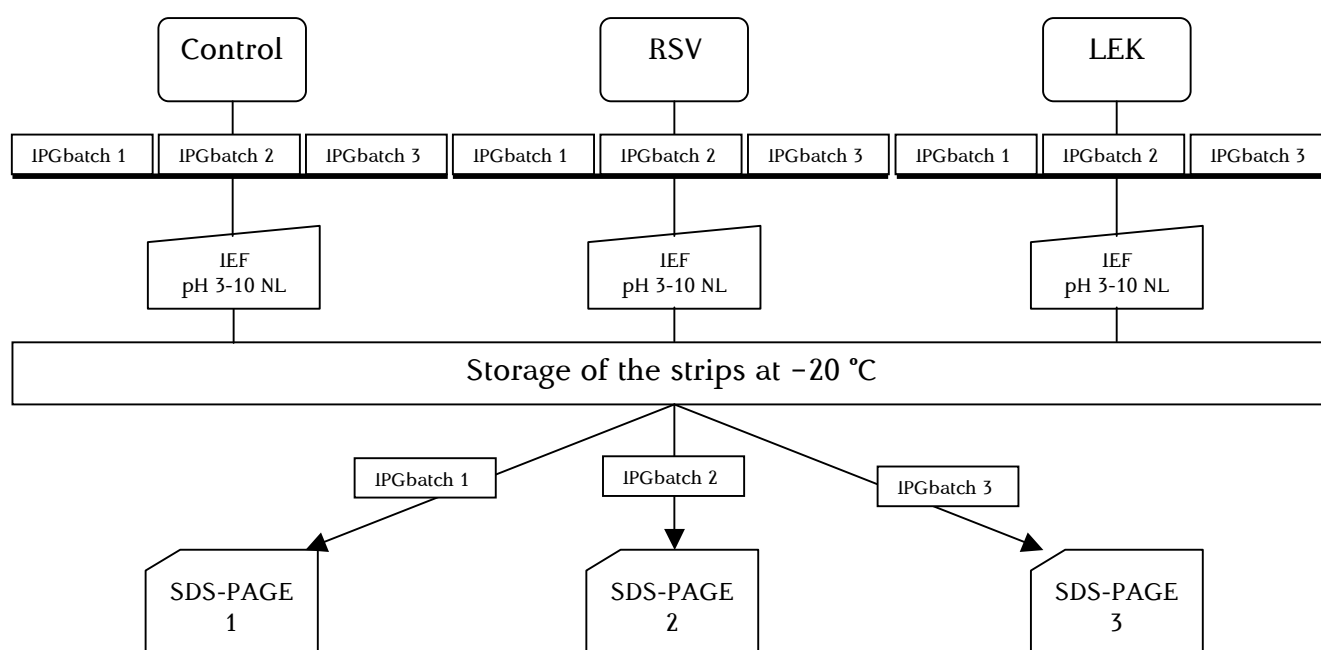


Figure 4-5 Final workflow, 2D-Gelelectrophoresis avoiding freezing before first dimensional separation

The resulting workflow is depicted in Figure 4-5. According to the effects seen in Figure 4-2 and Figure 4-4 the best gel images were expected by avoiding any freezing prior to sample application to the first dimension (see also Table 4-1). To realise this way of sample application the parallel workflow of the different samples and the unchanged sample status were compromised. Since freeze-thawing of the IPGstrips did not show such significant changes of the protein pattern on 2D gels (see Figure 4-2), every sample (control, RSV, LEK-935) was run individually in the first dimension. The focussed IPG strips were stored at -20°C . After focussing all three samples the

strips were mixed together in the 2nd dimension. The average protein amount of the cytosolic fraction isolated from 10^7 cells was about 1200 to 1400 μg . This allowed to run up to twelve IPGstrips per sample in parallel (using 100 μg sample load per strip). Four of these twelve strips were used in one SDS-PAGE. This led to a maximum of three final experiments, each consisting of twelve gels, four per sample.

To avoid changes in the protein pattern due to differences in the pre-cast IPGstrips, the different batches of strips were portioned before sample application. Every final experiment (twelve SDS-PAGES) contained IPGstrips of one batch.

Finally, the experimental setup allowed to run a maximum of three experiments per donor in “parallel”, without freezing the samples prior to the first dimension, ideally resulting in 36 gels for analysis (see Figure 4-5).

4.2.2 Nano high pressure liquid chromatography

4.2.2.1 Proof of applicability to eucaryotic proteomes with fission yeast

This experiment was done in cooperation with Dr. N. Delmotte and Dr. K. H. Hwang. The combination of separation modes used in this study was developed by Dr. N. Delmotte and he demonstrated its applicability to real proteome samples on the prokaryote *Chorynebacterium glutamicum* (Delmotte et al. 2007).

First of all, the applicability of this combination of separation modes to sub-fractionated eukaryotic proteomes needed to be proven. This was done using the fission yeast *Schizosaccharomyces pombe* as model organism. The data and their interpretation were recently published (Woerner et al. 2009). Summarising the applicability of the protocol for the analysis of sub-fractionated eukaryotic proteomes was proven, even if no real sub-proteome was observed in case of *S.pombe*. This was possibly due to the harsh conditions applied to disrupt the thick cell wall of the yeast (shaking with glass beads for 60 minutes). This experiment is not described in detail here, as its impact on the results of this study is low, except for the fact that the applicability was proven. For details of the experiment performed with yeast see (Woerner et al. 2009).

4.2.2.2 Application to human microsomal samples

Following the successful application of the approach to the fission yeast proteome, the microsomal fraction of the primary human hepatocytes was analysed. From sample 2, only one third of the sample load was applied to check the ability of the approach to analyse also rare sample material, where only low amounts of protein are available (Sample 1: 280 µg vs. Sample 2: 90 µg). The comparison between the samples was made with respect to the amount of identified proteins, their identity, localisation and biological function. The UV-chromatograms of the first separation dimension as well as the UV-chromatograms of fraction 4 of the two samples are illustrated in Figure 4-6.

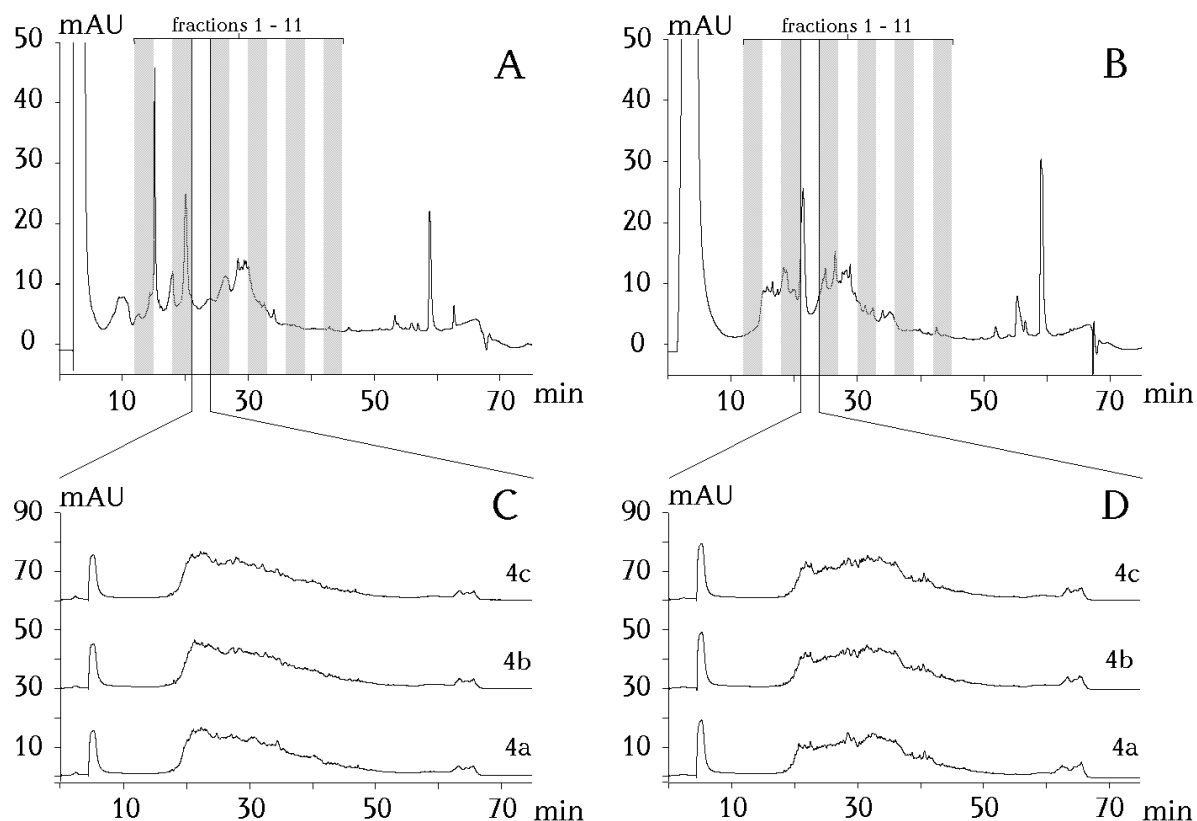


Figure 4-6 UV-chromatograms of the human samples. Chromatograms were recorded at 214 nm during first (A, B) and second (C, D) dimensional separation of the samples. Sample 1 is represented by A and C whereas B and D belong to Sample 2. The fractions collected in the first dimension are marked by alternating grey and white bars in A and B. Exemplary triplicate chromatograms of the second dimension are displayed in C and D, corresponding to fraction 4 collected in the first dimension.

For Sample 1, 690 proteins were identified using the MASCOT search algorithm. Those proteins identified by only one peptide (23 %) were rejected from further analysis. The remaining proteins (534) showed an average sequence coverage of 10.8 (Table 4-2, Figure 4-7). Manual search using the ExPASy database revealed some proteins where no information is available about the cellular localisation and/or the cellular function (approximately 30 %). A high percentage of the proteins where information is present are localised in the ER/microsomes (24 %), mitochondria (32 %) and cytoplasm (20 %, Figure 4-8). The majority of the proteins is involved in protein-biosynthesis/-degradation (29 %), related to xenobiotic metabolism and/or sterol/lipid metabolism (23 %) or is involved in cellular organisation including transport processes (27 %, Figure 4-9). Searching the Gene Ontology ‘biological process’ for overrepresented GO terms the translational elongation (GO-ID 6455), the oxidation reduction (GO-ID 55114) and the metabolic process (GO-ID 8152) were found among the five most overrepresented GO terms (Table 4-3).

Table 4-2 Comparison of the experimental conditions and number of proteins identified during the different nLC-MS experiments.

	<i>C. glutamicum</i>	<i>S. pombe</i>	<i>H. sapiens</i> Sample 1	<i>H. sapiens</i> Sample 2
Experimental conditions				
Sample	Cytosolic fraction	Microsomal fraction	Microsomal fraction	Microsomal fraction
Sample load [µg]	280	280	280	90
Collected fractions	30 x 1-minute	42 x 1 minute	11 x 3-minute	11 x 3-minute
Mass spectrometry	ESI - MS/MS	ESI - MS/MS	MALDI - MS/MS	MALDI - MS/MS
Results				
Proteins identified	745 ^{a)}	501	690	545
Proteins (at least 2 peptides)	594	367	534	426
<i>Average sequence coverage [%]</i> ^{b)}	<i>19.0</i>	<i>18.2</i>	<i>10.8</i>	<i>11.3</i>
Proteins identified by unique peptides ^{c)}	456	271	375	298
Proteins (at least 2 unique peptides ^{c)})	427	255	318	256
<i>Average sequence coverage [%]</i> ^{d)}	<i>22.1</i>	<i>27.7</i>	<i>15.8</i>	<i>16.3</i>

a) Data from (Delmotte et al. 2007)

b) Calculated from those proteins identified by at least two peptides

c) Peptideprophet probability: 0.95, Proteinprophet probability: 0.99

d) Calculated from those proteins identified by at least two unique peptides

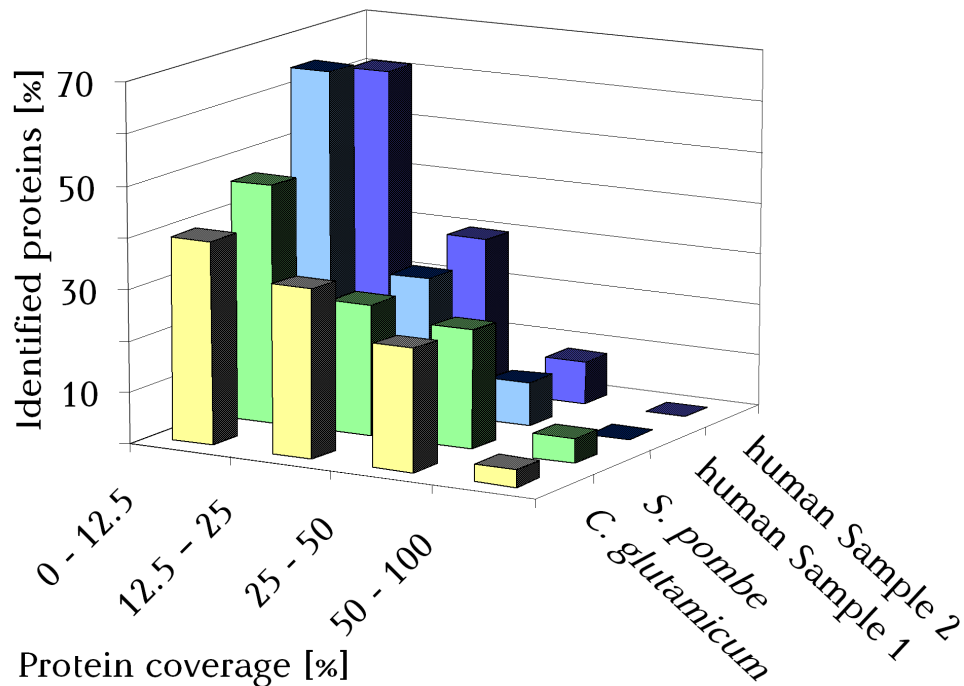


Figure 4-7 Distribution of the protein sequence coverage among the different samples. Data were collected from the MASCOT-results files; only those proteins identified by at least two peptides are included. Sequence coverage was split into four groups: 0-12.5 %, 12.5-25 %, 25-50 %, 50-100 % and plotted against the amount of proteins in the samples belonging to the corresponding group.

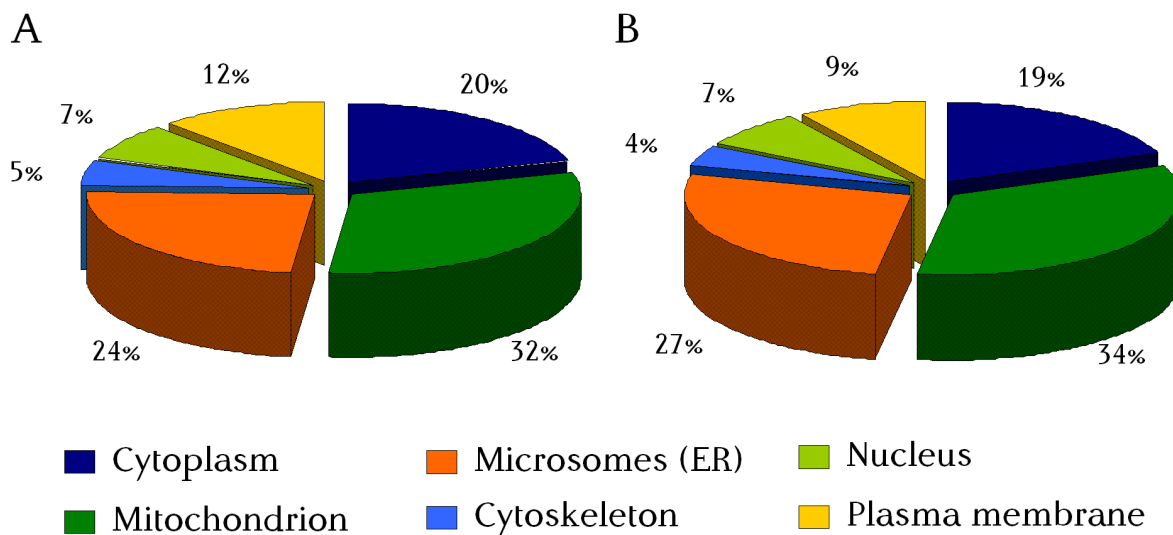


Figure 4-8 Proportional distribution of the cellular localisation, of the proteins identified in the samples, as described in the ExPASy database. Only those proteins identified by at least two peptides and with information available in the database are included. A and B display the distribution in the human sample 1 and sample 2, respectively. ER, Endoplasmic reticulum.

Using MASCOT search algorithm 545 proteins were identified in Sample 2. Those proteins identified by only one peptide (22 %) were rejected from further analysis. The remaining proteins (426) showed an average sequence coverage of 11.3 % (Table 4-2,

Figure 4-7). For some proteins no information is available in the ExPasy database about their cellular localisation and/or cellular function (approximately 20 %). A high percentage of the proteins where information is present are localised in the ER/microsomes (27 %), mitochondria (34 %) and cytoplasm (19 %, Figure 4-8). As for Sample 1, the majority of the proteins is involved in protein-biosynthesis/-degradation (32 %), related to xenobiotic metabolism and/or sterol/lipid metabolism (24 %) or is involved in cellular organisation including transport processes (20 %, Figure 4-9). Searching the Gene Ontology 'biological process' for overrepresented GO terms, among the five most overrepresented terms again the translational elongation (GO-ID 6455), the oxidation reduction (GO-ID 55114) and the metabolic process (GO-ID 8152) were found (Table 4-3).

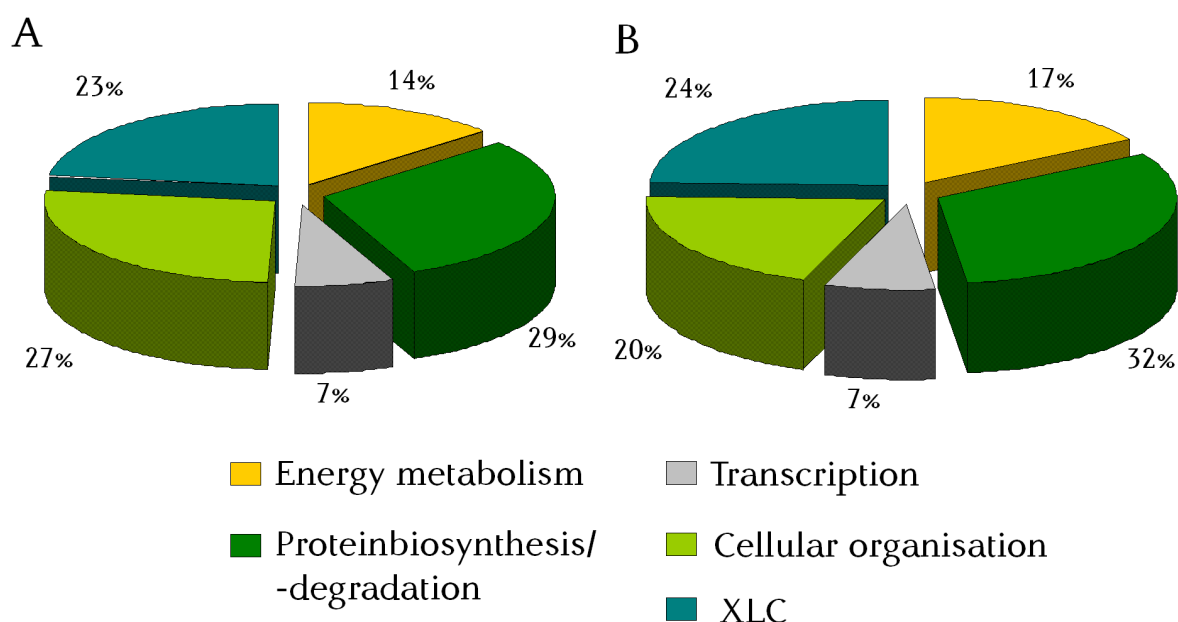


Figure 4-9 Proportional distribution of the cellular functions of the proteins identified in the samples, as described in the ExPasy database. Only those proteins identified by at least two peptides and with information available in the database are included. A and B represent the human sample 1 and sample 2 respectively. XLC (xenobiotic-lipid-cholesterol), proteins involved in the xenobiotic/drug metabolism, fatty acid synthesis/degradation or cholesterol homeostasis.

Assuming that the origin of the samples from two different donors had no or only little effect, the reduction of the amount of sample loaded into the first dimension by 66 % decreased the number of identified proteins by 20 %. The percentage of proteins identified by only one peptide (Sample 1: 23 %, Sample 2: 22 %) and the average sequence coverage (about 11 %) remained similar in both samples.

Taking both donors together, 588 proteins were identified by at least 2 peptides with an average sequence coverage of 11 %. Among these proteins 372 (63 %) were

identified in both samples, while 162 proteins (27.6 %) were found only in Sample 1 and 54 proteins (9.2 %) only in Sample 2 (Figure 5). The overall sample composition with regard to the cellular localisation and biological function correlated very well (compare Figure 4-8 and Figure 4-9). The five most over-represented GO terms were identical in both samples, only the order of positions four and five was exchanged (Table 4-3). Metabolism of the xenobiotics naphthalene, 1-nitronaphthalene, bromobenzene, 1,1-dichloroethylene and 1,2-dibromoethane as well as the metabolism of the drugs methadone and lidocaine, as described in the KEGG database were fully covered. Furthermore, the biosynthetic pathway from farnesyl-pyrophosphate to zymosterol, the central part of the sterol biosynthesis was covered in 5 out of 9 positions (data not shown).

To sum up these experiments, the applicability of the analytical approach to the analysis of human microsomal sub proteome was proven. In addition, it was shown that also low amounts of sample material can be applied. A complete list of the proteins identified is shown in Appendix V.

Table 4-3 The five most over-represented GO terms in the ontology biological process of the two human samples compared to terms in the whole genome of the corresponding organism. x = number of annotations found in the sample set, n = number of annotated proteins in the whole GO dataset, X = number of proteins in the sample set, N = number of proteins in the whole GO dataset

GO-ID	corr <i>p</i> -value	x	n	X	N	Description
Human Sample 1						
6455	4,72E-51	54	102	458	14528	Translational elongation
55114	2,87E-33	87	569	458	14528	Oxidation reduction
8152	1,51E-30	348	7116	458	14528	Metabolic process
6091	2,27E-23	49	243	458	14528	Generation of precursor metabolites and energy
6416	1,93E-21	64	465	458	14528	Translation
Human Sample 2						
6455	4,03E-64	59	102	383	14528	Translational elongation
55114	3,01E-35	82	569	383	14528	Oxidation reduction
8152	5,32E-34	306	7116	383	14528	Metabolic process
6416	7,30E-26	64	465	383	14528	Translation
6091	3,84E-22	44	243	383	14528	Generation of precursor metabolites and energy

4.2.2.3 Proof of compatibility with iTRAQ™ label

The aim of the whole analysis was a semi-quantitative comparison of untreated with treated samples. To allow semi-quantitation in gel-free proteomic approaches several

methods have been applied (see 1.3.4). For this study iTRAQ™ labelling was chosen. As the LC-separation method contained a new combination of separation modes, the stability of the label under these conditions, especially the alkaline ones, was tested. A random examination of 2,000 MS/MS spectra was checked for the presence of the reporter ion signals. In 95 % - 99 % of this random examination all four (114, 115, 116, 117) iTRAQ™ reporter ion signals were detectable, applying a mass tolerance of 0.05 Da (an example is shown in Figure 4-10). Furthermore, peptideprophet and proteinprophet were used to identify those proteins for which at least two unique peptides were present in the sample. This resulted in a final set of 318 and 256 proteins with an average sequence coverage of 16 % for Sample 1 and Sample 2 respectively (Table 4-2).

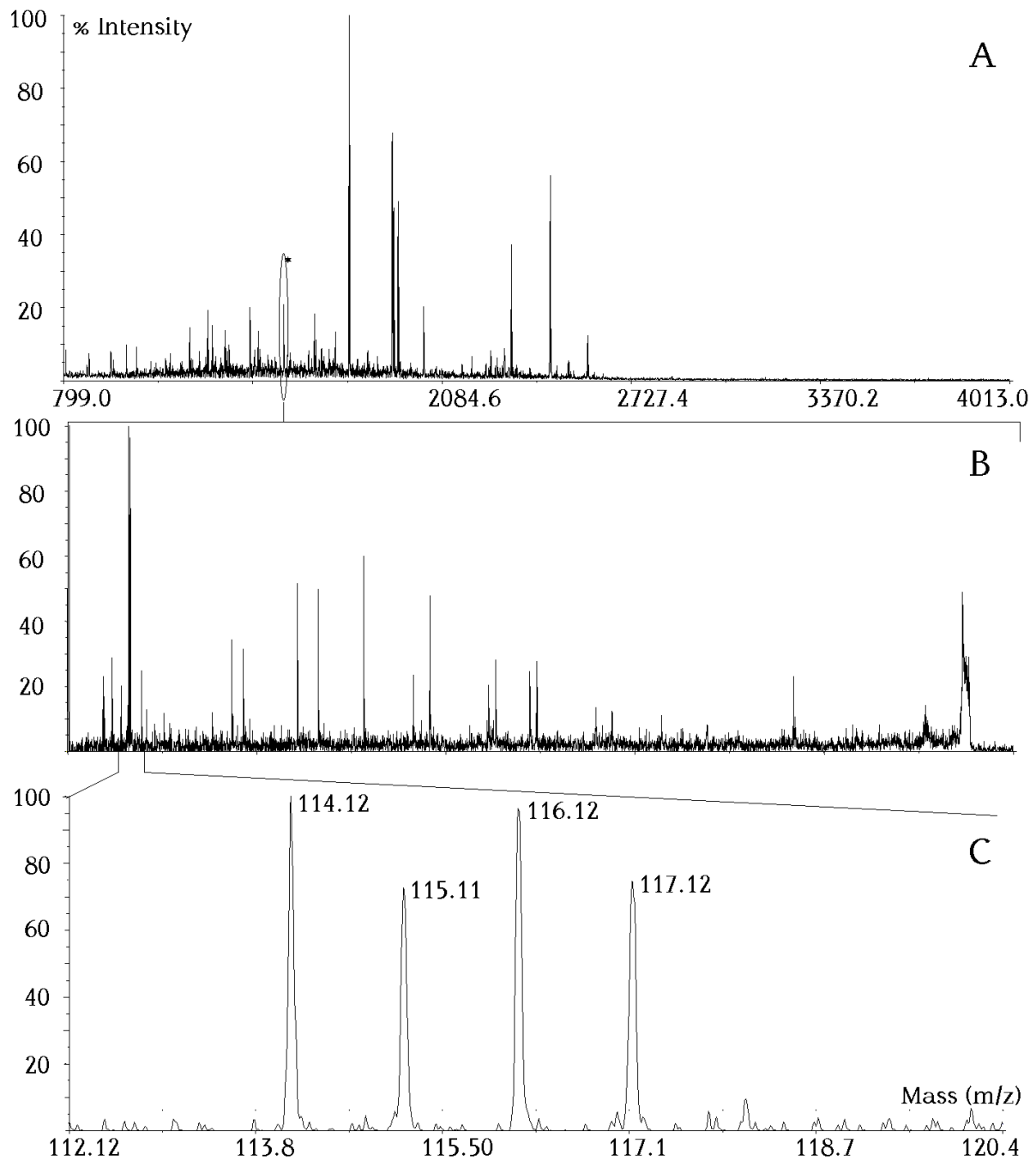


Figure 4-10 Example for mass spectra recorded by the ProteomeAnalyzer 4800. In A, a standard MS spectrum is depicted. The MS/MS spectrum recorded after CID fragmentation of the precursor ion circled and marked with asterisk in A is shown in B. To prove the presence of the iTRAQ™ reporter ions, the area from 112.1 m/z to 120.4 m/z is enlarged in C. The signal of all four reporter ions was detectable in 95 % - 99 % of a random examination of about 2,000 MS/MS spectra.

Accurate quantitative measurements are only possible if the labelling procedure for the control and the treated samples does not cause huge differences. The quality of the procedure was examined by labelling the control and the RSV treated samples with two different iTRAQ™ reporter labels each. The control samples were divided and labelled with the reporter 114 and 116 while the RSV samples were divided and

labelled with the reporter 115 and 117. Finally, the samples were mixed in a ratio of 1:1:1:1.

Subsequently after finishing the mass measurements and prior to any quantitative analysis, the reporter ion ratios of 114/116 and 115/117 were checked. The data were not examined as ratios but converted into a factor/divisor form. So, a ratio of 2.0 is regarded as a factor 2.0 as well as a ratio of 0.5 is regarded as a divisor of 2.0, reflecting the factors of up- or down-regulation of the underlying proteins. This way of data design was used for Figure 4-11 and Appendix IV. The factor/divisor should ideally be one for the internal controls (114/116 and 115/117), as the samples were mixed in a ratio of one to one.

The majority of values was found in a range of 0.8 to 1.2, but some of them also laid beyond these bounds. The average was approximately one (see Table 4-4), with a standard deviations of about 10 %. An exemplary plot of the average of the internal control from sample 1 analysed by ProteinPilot is depicted in Figure 4-11, the figures of all other values including those about the overall factor/divisor distribution are shown in Appendix IV.

Table 4-4 Ratios of the internal controls and the corresponding standard deviations.

Internalcontrol									
	CTRL114/116				RSV 115/117				
	Sample 1		Sample 2		Sample 1		Sample 2		
	Ratio	<i>Error</i>	Ratio	<i>Error</i>	Ratio	<i>Error</i>	Ratio	<i>Error</i>	
ProteinPilot	1.0042	<i>0.0955</i>	1.0041	<i>0.1095</i>	1.0095	<i>0.1057</i>	1.0056	<i>0.0960</i>	
Mascot	0.9984	<i>0.1082</i>	0.9983	<i>0.1154</i>	1.0020	<i>0.1042</i>	0.9926	<i>0.1037</i>	
Quant	0.9860	<i>0.1072</i>	0.9801	<i>0.1284</i>	0.9874	<i>0.1147</i>	0.9885	<i>0.0968</i>	

An experimental mistake by differences in the mixing ratios was excluded with these results.

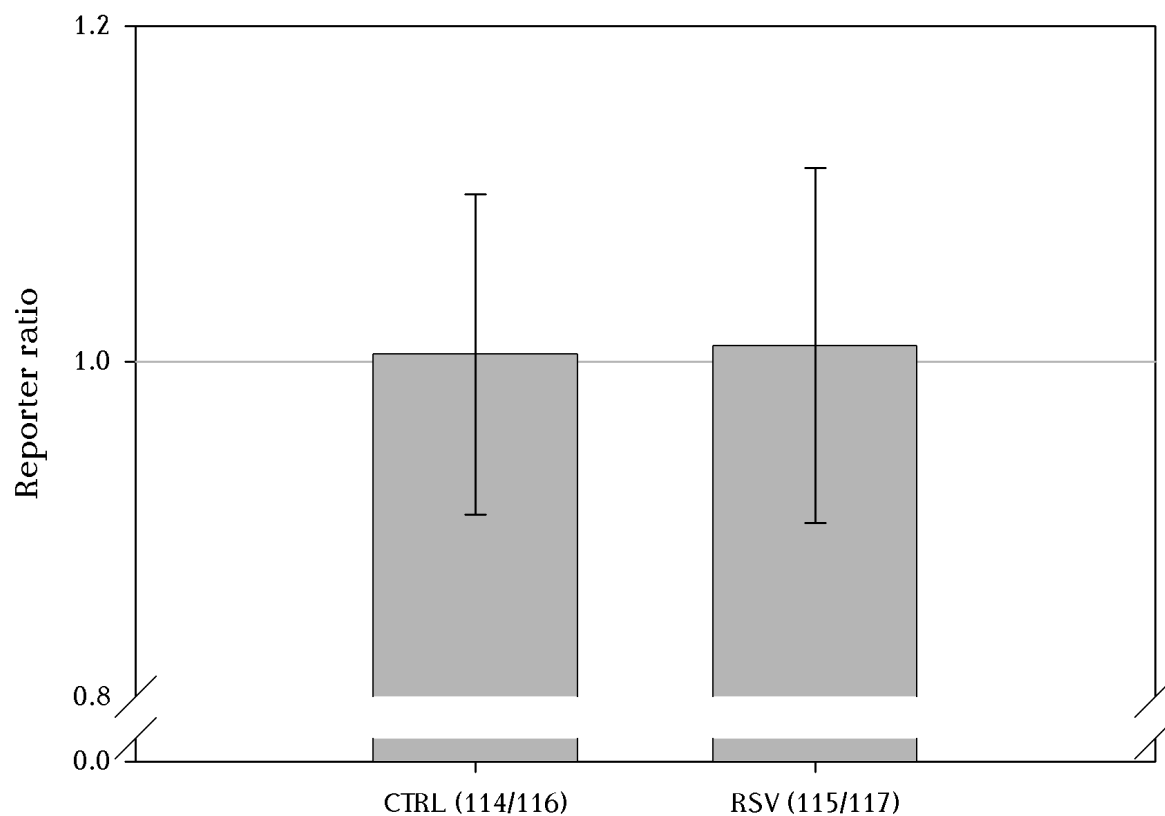


Figure 4-11 Diagramm showing the averaged reporter ion ratio and corresponding standard deviations of the internal controls of sample 1, as calculated by ProteinPilot.

To summarise, the stability of the label with respect to the separation conditions as well as appropriate labelling and mixing of the control and treated samples was proven.

4.2.2.4 Bioinformatics for quantification

After proving the presence of the iTRAQ™ label as well as the presence of proteins identified by unique peptides (see chapter 4.2.2.3), the quantitative analysis of the reporter ion signals came into the focus.

4.2.2.4.1 Data handling

The ProteomicsAnalyser 4800 stores the measured data in an oracle database. On one hand, this allows the parallel use of the raw data from different workstations, on the other hand every software used for data interpretation has to be able to handle oracle databases. It turned out that both, the oracle database as well as the instrument itself, are quite sensitive to improvident use, so the choice of software used for data analysis was generally restricted to firmware to assure the stability of the system.

Previous to this study, no quantitation of iTRAQ™ reporter signals out of real proteomic data had been performed at Saarland University. So, different software packages were compared to evaluate the quantification results. To make the data accessible to quantification by two of the three software packages chosen, they had to be exported from the oracle database in a suitable way. The “launch peaks to Mascot” function provided with the instruments software is reported to misinterpret the peak areas used for quantitation (see www.matrixscience.com). Matrix sciences offers the free-of-charge TS2MASCOT – tool (www.matrixscience.com) which allows the export of peak areas in the same way as the firmwares ProteinPilot™ and GPSexplorer™. To evaluate the difference between both exporting tools, a random examination of ten MS/MS spectra was exported by the TS2MASCOT as well as the “launch peaks to Mascot” tool. The exported peaks were compared with regard to their area specified in the export files. This comparison lead to an averaged difference in the peak area of 22.4 % (Table 4-5). Meaning the area of one peak exported by TS2MASCOT differed in average by 22.4 % from the area of the same peak exported by “launch peaks to Mascot”. Taking only the area of the iTRAQ™ reporter ion signal into account, this difference was reduced to 3.1 to 5.9 % (see Table 4-5).

Table 4-5 Relative peak area difference of a random examination of ten MS/MS spectra exported by TS2MASCOT and “launch peaks to Mascot”, respectively

Mass signals	Averaged peak area difference [%]
All	22.4
ITRAQ 114 (114.1 m/z)	5.9
ITRAQ 115 (115.1 m/z)	4.2
ITRAQ 116 (116.1 m/z)	3.1
ITRAQ 117 (117.1 m/z)	3.8

To evaluate the influence of data export on protein identification, comparison was made with respect to the number of proteins identified, the number of proteins identified by at least two peptides and the sequence coverage (see Table 4-6). In both samples a higher number of proteins was identified using the data exported via “launch peaks to mascot”. Nevertheless, the number of proteins identified was drastically reduced by looking only for proteins identified by at least two peptides. This finally lead to a lower number of identified proteins for those data exported by “launch peaks to mascot” compared to the number of proteins identified after

TS2Mascot export. The sequence coverage was slightly increased for the proteins identified after data export by TS2Mascot. At last, the correlation between the sets of proteins identified by at least two peptides was examined. A correlation of about 95 % was found for both samples (see Table 4-6).

Table 4-6 Differences in protein identification caused by the choice of data exporting software and the corresponding parameters. The Mascot server as well as the settings and the database were the same in all the cases.

	Donor 1		Donor 2	
	Launch peaks to mascot	TS2 Mascot	Launch peaks to mascot	TS2 Mascot
Proteins identified	690	670	545	543
Proteins identified by at least two peptides	534	526	426	420
<i>Sequence coverage [%]^{a)}</i>	<i>10.8</i>	<i>11.4</i>	<i>11.3</i>	<i>11.7</i>
Correlation^{a)}	507 (94.9 %)		406 (95.3 %)	

a) of/between those proteins identified by at least two peptides

The use of generalised data formats is strongly recommended among the proteomic society, to ease-up comparisons between different laboratories and data evaluation. Mass data conversion to this kind of files was tested several times. Unfortunately, no suitable conversion tool could be found.

The identification results obtained by using TS2MASCOT are comparable to those gained with the “launch peaks to mascot tool”, it is recommended by matrix science to export data of quantitative experiments and the general difference of the exported peak areas between the two tools was proven. Therefore, TS2MASCOT was chosen for peak export to enable the further quantitative analysis by Mascot or Quant.

4.2.2.4.2 Eligibility criteria

During 2D-PAGE a spot found to be significantly altered according to students *t*-test (99 %) and changed in its intensity by a factor of at least 2 was regarded as regulated if

it was found in two out of two individual experiments. For the proteins identified during nLC-MS the eligibility criteria needed to be set, too.

At first, borderlines had to be defined beyond which a reporter ion ratio can be regarded as significant for a difference between the treated and the control sample. To determine this range, several possibilities exist. On one hand, some of the quantification software provides information about values deviating from the average. On the other hand, in the literature, the use of 1.2 and 0.8 is often found. These values correspond to the doubled standard deviation, estimated according to internal standards as presented above (about 10 % representing a value of 0.1, see 4.2.2.3).

In this study, the double of the real standard deviation was used, calculated as the average of the standard deviations found in the four ratios examined. An individual threshold was determined for each software, as already the averaged internal controls differed from one software to another (see Table 4-4). The resulting thresholds are summarised in Table 4-7.

Table 4-7 Thresholds calculated as the doubled standard deviation of all ratios per sample.

	Sample 1		Sample 2	
	Up-regulated	Down-regulated	Up-regulated	Down-regulated
ProteinPilot	1.37	0.63	1.96	0.04
Mascot	1.43	0.57	2.04	0.00
Quant	1.39	0.61	2.04	0.00

These thresholds are obviously higher than the expected values of 0.8 and 1.2. Especially in the case of donor 2 a high standard deviation was observed. This observation is in line with the impression of complete deregulation by plotting the factor/divisors of all proteins quantified in sample 2 (see Appendix IV). The high standard deviation led to a threshold of 0.04 to lower than zero for down-regulation. These values could not be matched by any protein factor/divisor. Therefore, only up-regulation was detectable in sample 2. It has to be kept in mind that a huge deregulation was observed in sample 2, for which the criteria set may be wrong due to their theoretical assumption of a normal distribution of the values (see discussion).

The control as well as the RSV treated sample were labelled with two reporter molecules, so four ratios of reporter ion areas could be calculated after mass measurements: 115/114 – 115/116 – 117/114 – 117/116. In theory all of them should

show the same value. This was not true, so criteria were set in a way that the protein values need to cross the threshold in at least three out of the four values.

The third and last parameter is that the protein needed to match the first and second criterion in at least two of the three software packages used (see 4.2.2.4.3 and Table 4-7). The parameters of significance a protein value had to match are summarised in Table 4-8.

Table 4-8 Summary of the parameters and criteria of significance

Parameter	Criteria
Ion reporter ratio	Match the determined threshold, see Table 4-7
Four different reporter ratios	Match the threshold in at least three out of the four ratios calculated
Three different software packages	Found in at least two of the three packages according to the above criteria

These criteria are quite restrictive, compared to those often found in the literature. The reason for their choice was to avoid any false positive results by accepting the loss of information by false negative results.

4.2.2.4.3 Quantification software

In the case of protein identification, a strong influence of algorithm choice is described in the literature (Chamrad et al. 2004; Elias et al. 2005; Kapp et al. 2005). To evaluate the influence of the software tools used for quantification, three different packages were chosen.

The GPSexplorer used for identification of the in-gel digests was not able to handle the huge amount of data produced during the nLC-MS experiments. In every case, when loading the twentieth spot set for identification and quantification it crashed down. So it was not used, despite of the fact that it is able to quantify the iTRAQ™ reporter signals.

ProteinPilot® as recommended firmware tool was the first choice for quantification. Along with its quantification abilities, ProteinPilot® provides the Paragon algorithm (Shilov et al. 2007) for identification. Quantification of a protein is performed by only using peptides unique to this protein, while the sequence coverage of the protein is “strengthened” by peptides shared with other proteins.

The second choice was a MASCOT stand alone server as a firmware independent tool and the third choice was Quant (Boehm et al. 2007). For both, MASCOT as well as Quant, data were exported by TS2MASCOT (see 4.2.2.4.1). Mascot was first used to identify the proteins that were later quantified. During quantification, Mascot did not differentiate between unique and shared peptides in the samples. In contrast, for quantification Quant only uses information about peptides unique to one protein in the sample. As the program does not offer an algorithm for identification, it was fed with the raw result files of the Mascot identification. For the final analysis, only those proteins were considered that were identified by at least two peptides.

Comparison of the three packages was made with respect to identification (proteins identified by the Paragon algorithm vs Mascot) and quantification (data either identified by Paragon and quantified by ProteinPilot or identified by the Mascot stand-alone server and quantified by Mascot or Quant).

Using the Paragon algorithm 769 proteins were identified in sample 1 and 612 proteins in sample 2. This led to a set of 668 and 533 proteins identified by at least two peptides for sample 1 and sample 2 respectively. The averaged sequence coverage was 16.3 % for sample 1 and 20.3 % for sample 2. Compared to Mascot, the total number of proteins identified as well as their sequence coverage was obviously higher (see Table 4-6) using another algorithm for identification with direct access to the raw data.

The proteins found to be differentially present after RSV treatment differed between the software packages used. Using ProteinPilot in sample 1 nineteen proteins were found in higher amounts and seven in lower amounts after RSV treatment, while the Mascot analysis resulted in fifteen up-regulated and two down-regulated proteins and Quant finally showed six up-regulated and four down-regulated proteins (see Table 4-9). A similar discrepancy was observed for up-regulation in sample 2, in which ProteinPilot analysis ejected twenty-one proteins, Mascot fourteen proteins and Quant eight proteins. No down-regulated protein were observed for sample 2 (see 4.2.2.4.2 and Table 4-7).

Table 4-9 Number of proteins found to be regulated in sample 1 and sample 2 by the use of three different software packages

No. of proteins found to be regulated				
	Sample 1		Sample 2	
	Up-regulated	Down-regulated	Up-regulated	Down-regulated
ProteinPilot	19	7	21	0
Mascot	15	2	14	0
Quant	6	4	8	0

The correlation between the proteins found in altered amounts is listed in detail in Table 4-10. The use of ProteinPilot revealed 47 regulated proteins, while Mascot ejected 31 and Quant 18 hits. In average, the results correlated by 36.8 %, meaning every third protein was found by at least two of the three packages. To further evaluate whether the observed differences are caused by the quantification or the identification algorithms, the proteins differing between the software packages were further analysed.

Table 4-10 Correlation of the proteins found to be regulated by ProteinPilot, Mascot or Quant.

	ProteinPilot	Mascot	Quant
Number of proteins found	47	31	18
Proteins not found by ProteinPilot	0	16	10
Proteins not found by ProteinPilot due to differences in identification	0	3	0
Proteins not found by ProteinPilot due to differences in quantification	0	13	10
Proteins not found by Mascot	32	0	9
Proteins not found by Mascot due to differences in identification	18	0	0
Proteins not found by Mascot due to differences in quantification	14	0	9
Proteins not found by Quant	39	22	0
Proteins not found by Quant due to differences in identification	33	17	0
Proteins not found by Quant due to differences in quantification	6	5	0

The majority of hits found by ProteinPilot but not by one of the other packages was caused by differences in identification (70.4 %) rather than differences in quantification (29.6 %). In contrast, the differences leading to proteins found by other packages but not ProteinPilot were mainly due to differences in quantification (80.3 %) and not identification (19.7 %).

For Mascot a balanced situation was found for those proteins detected by Mascot but not one of the others (48.0 % not identified/used by Mascot, 52.0 % differentially quantified). A diminished but comparable effect as observed with ProteinPilot was found for those hits not seen by Mascot (71.9 % due to quantification differences, 28.1 % not identified/used by Mascot).

The quantification results of all proteins found only with the Quant package did not meet the significance criteria when calculated by the other packages. Those hits detected by others but not Quant were to 80.9 % due to differences in the identification/use of peptides, while only 19.1 % of them were differentially quantified. To summarise, 39.5 % of the differences observed were due to differences in identification processes, while the majority of 60.5 % were caused by a different performance of the used software package with respect to quantification.

The borderlines between these two criteria blur as the number of peptides identified of course affected the number of peptides used for quantification. Nevertheless, the results demonstrate a dramatic impact of the software used for quantification on the outcome of semi-quantitative nLC-MS experiments. In addition to the differences in protein identification, here again, the choice of software affected the out-coming result.

To incorporate this knowledge into this study, only proteins were considered to be regulated if they appear in at least two of the three packages as true positive hits.

4.2.3 Summary

For both analytical approaches, 2D-PAGE as well as nLC-MS, some problems of either the experimental performance or the data handling and interpretation were faced during this study. In order to improve the approaches with the knowledge about these problems some methodical work was performed as described above.

Summarising, the protocol for 2D-PAGE was adapted and optimised, to provide an experimental procedure, capable of handling low amounts of sample material nonetheless able to identify 68 to 84 % of the spots subjected to mass spectrometry. At the same time, the experimental setup avoids sample freezing prior to IEF and allows to run a maximum of three experiments per donor in “parallel”, ideally resulting in 36 gels for analysis.

On the other hand, the general applicability of the nLC-MS setup to eukaryotic sub-proteomes was proven. The data export and file handling was optimised in a way that enables accurate semi-quantification by different software packages. The differences observed by using three different programs for semi-quantification could be used to reduce the amount of false-positive hits during the analysis. This finally led to an improvement of the quality of the semi-quantitative data.

4.3 The effects of RSV and LEK-935

The methodical approaches evaluated in 4.2 were now applied to analyse the effects of the cholesterol lowering agents RSV and LEK-935 on the proteome of primary human hepatocytes. The cytosolic fraction of the samples was applied to two-dimensional gel electrophoresis. In addition, the microsomal fraction of the RSV treated cells was analysed by nLC-MS. Two individual experiments were performed with samples derived from two different donors.

4.3.1 Cytosolic fraction / two-dimensional gel electrophoresis

The analysis of donor 1 was performed according to the optimised sample application procedure (Figure 4-5), while the cytosolic fraction of donor 2 has been frozen two times at -20°C prior to analysis. A detailed view on each spot found to be differentially present, its regulation, identification and cellular function is shown in Appendix II and Appendix III.

4.3.1.1 Semi-quantification

Two experiments were performed with samples derived from donor 1. These resulted in two bioinformatical analyses consisting of twelve (4 x ctrl, 4 x RSV, 4 x LEK 935) and eleven (4 x ctrl, 4 x RSV, 3 x LEK) gels respectively.

For sample 2, a first analysis failed due to troubles occurring at the scanning process. So the remaining samples had to be used again in a second experiment. As the samples were already prepared prior to the knowledge about the effects of freezing-thawing, the experiments were now run with samples frozen two times at -20°C . The experiments of sample 2 also resulted in two bioinformatical analyses consisting of twelve (4 x ctrl, 4 x RSV, 4 x LEK 935) and eight (2 x ctrl, 2 x RSV, 4 x LEK) gels respectively.

For sample 1 as well as for sample 2, the two simple bioinformatical analyses were matched and compared in one higher level experiment per sample. The results obtained in these analyses are summarised in Table 4-11.

The averaged consistency between the two basic experiments was found to be 49.5 % and 41.1 % for sample 1 and sample 2 respectively. So, about every second spot found to be regulated per individual experiment was, with respect to the applied rules, a true positive hit (see Table 4-11).

A comparison between both samples at the level of gel image analysis was not possible due to the different freeze-thawing states of the samples when entering the experiment, leading to different gel images.

After RSV treatment the intensity of 20 spots was found to be significantly increased in sample 1 while 31 spots seemed to appear in comparison to the control samples. The signal intensity of two spots was decreased and five spots completely disappeared, compared to the control. In sample 2, RSV treatment led to the appearance and disappearance of ten and four spots, respectively. In addition, the increase in signal intensity of five spots and decrease in signal intensity of one spot was detected (see Table 4-11).

After LEK-935 treatment the intensity of 33 spots increased significantly in sample 1, while the appearance and disappearance of fourteen and three spots as well as a significant down-regulation of five spots was observed. Sample 2 treated with LEK-935 showed appearance of eight as well as disappearance of nine spots, while an increase and decrease in signal intensity was observed for four and five spots respectively (see Table 4-11).

Of the spots found to be altered in sample 1, thirteen increased in signal intensity and eight appeared after both treatments while no correlation was found regarding the decrease in intensity or disappearance of spots. In sample 2, the increase in signal intensity of four spots, decrease of intensity of one spot, appearance of seven and disappearance of three spots was observed to be similar after both treatments (see Table 4-11).

For sample 1, a direct comparison of the gels made with the treated samples, led to the detection of ten spots in the RSV treated samples showing more than two-fold intensity compared to the ones found in the LEK-935 treated samples as well as ten spots showing less than two-fold intensity. Appearance of 18 spots was observed, in parallel to disappearance of twelve spots. In sample 2, only one spot was found to be diminished and 1 spot appeared after RSV treatment compared to LEK-935 treatment (see Table 4-11).

Table 4-11 Comparison of the spots found to be regulated in two experiments with the number of spots found to be regulated in the same way in both experiments

	Sample I				Sample II			
	No. of spots found in experiment I	No. of spots found in experiment II	No. of spots found in both experiments	Averaged consistency [%]	No. of spots found in experiment I	No. of spots found in experiment II	No. of spots found in both experiments	Averaged consistency [%]
UP								
RSV	29	26	20	72.7	18	6	5	41.7
LEK	44	42	33	76.7	8	12	4	40.0
REGULATED								
RSV & LEK	16	20	13	72.2	6	6	4	66.7
RSV vs LEK	24	16	10	50.0	0	0	0	100.0
DOWN -								
RSV	11	9	2	20.0	16	4	1	10.0
LEK	30	13	5	23.3	13	7	5	50.0
REGULATED								
RSV & LEK	5	2	0	0.0	6	2	1	25.0
RSV vs LEK	15	13	10	71.4	1	2	1	66.7
APPEAR								
RSV	40	34	31	83.8	27	15	10	47.6
LEK	27	21	14	58.3	20	14	8	47.1
REGULATED								
RSV & LEK	13	13	8	61.5	19	12	7	45.2
RSV vs LEK	27	19	18	78.3	4	1	1	40.0
DISAPPEAR								
RSV	18	9	5	37.0	33	6	4	20.5
LEK	18	3	3	28.6	35	10	9	40.0
REGULATED								
RSV & LEK	4	0	0	0.0	31	3	3	17.6
RSV vs LEK	24	17	12	58.5	1	3	0	0.0

4.3.1.2 Identification

All of the spots found to be regulated, as described above, were again checked and some with doubts about their regulation were excluded from further investigations. A final set of 94 and 32 spots was subjected to identification for sample 1 and sample 2 respectively (see Figure 4-12). These spots were excised from one control, RSV as well as LEK-935 gel of each experiment, resulting in a set of two to six gel slices per spot. The spots were applied to in-gel digestions followed by MALDI-TOF/TOF mass spectrometry and a database search for identification.

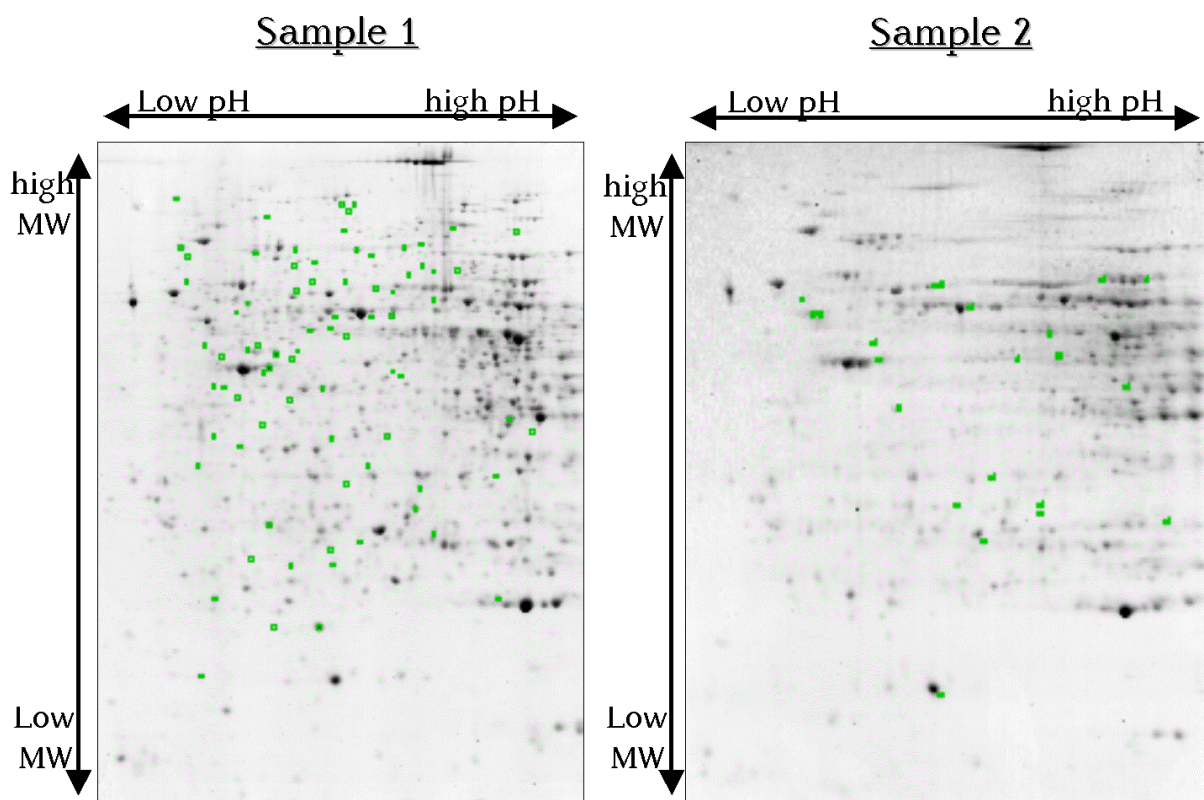


Figure 4-12 Gels of sample 1 and sample 2 showing the spots found to be differentially present and cut for in-gel digestions followed by mass spectrometry and database search.

The proteins were identified by a combination of peptide mass fingerprinting with peptide fragment mass fingerprinting (MS & MS/MS) and a GPS score of 100 %. For sample 1, they were identified out of one up to five individual gels, with an average sequence coverage of 37.5 % while for sample 2, identification was performed out of one up to six individual gels, with an average sequence coverage of 42.2 %.

In both samples, the practically estimated pIs and molecular weights of the identified proteins correlated very well with the theoretically calculated values (see Appendix II).

4.3.1.2.1 Sample 1

In sample 1, 94 differentially present spots were subjected to mass spectrometry followed by database search. For 60 of these spots proteins could be identified (see Appendix III). In 46 of the 60 spots, the identified protein originated from *E.coli*. This dramatically high number (76.6 %) excludes a random event, leading to the assumption of a systematic mistake. Contamination of the samples by *E.coli* during the sonication step was assumed to be most probably the underlying reason (see discussion). All of the *E.coli* proteins were either up-regulated or appear in the treated samples, suggesting a stronger contamination in these than in the control. The spots with identified *E.coli* proteins were excluded from further analysis, the remaining fourteen spots were further checked to exclude false positive hits. In general, the contamination does not disrupt the analysis but restricts the results to the top-hits, as the increased amount of strange proteins in the treated samples reduces the amount of human proteins and thereby shifts the averaged relations of intensities below one. The spots down-regulated by the treatment needed a detailed view on their regulation (see Appendix II). The spots up-regulated or even appearing in treated samples were regarded as top hits as the bacterial contamination did not diminish their regulations below the threshold.

Except for two spots, only one protein was identified per spot in sample 1 (see Table 4-12). Spot 35 contained a heat-shock protein but differentiation to one specific enzyme was not possible, leading to the exclusion of this spot from further analysis. In spot 89 radixin, ezrin and moesin were identified. Here a relative differentiation to radixin was possible (see Appendix II).

After manual control a set of eleven proteins identified out of nine spots was subjected to further analysis regarding their molecular and biological function. This set of proteins including their regulations is listed in Table 4-14.

Table 4-12 Proteins identified from spots found to be altered after treatment with cholesterol lowering agents in sample 1, including their theoretically calculated molecular weight, pI and the number of gels they were identified from.

Spot Number	Identified as	SwissProt - ID	MW [kDa]	pI	Sequence coverage [%]	Number of individual gels identified from
2	Proteasome subunit alpha type 5	PSA5_HUMAN	26.39	4.74	41.5	2
3	Annexin A5	ANXA5_HUMAN	35.91	4.94	71.6	4
8	Endoplasmic	ENPL_HUMAN	92.41	4.76	34.5	2
20	HMG-CoA synthase	HMCS1_HUMAN	57.26	5.22	38.5	3
23	Nicotinamid N-methyltransferase	NNMT_HUMAN	29.56	5.56	38.3	5
35	Heatshock cognate 71kDa protein	HSP7C_HUMAN	70.85	5.37	53.9	5
49	Isocitrate dehydrogenase [NADP]. mitochondrial	IDHP_HUMAN	50.88	8.88	33.0	1
71	Serum Albumin	ALBU_HUMAN	69.32	5.92	52.5	5
83	Phosphoglucosyltransferase 1	PGM1_HUMAN	61.41	6.3	37.2	5
86	Serum Albumin	ALBU_HUMAN	69.32	5.92	44.3	3
88	Phosphoglucosyltransferase 1	PGM1_HUMAN	61.41	6.3	29.2	3
	Radixin	RADI_HUMAN	68.52	6.03	31.4	2
89	Ezrin	EZRI_HUMAN	69.37	5.94	21.3	2
	Moesin	MOES_HUMAN	67.78	6.08	14.9	2
93	Glyceraldehyde-3 dehydrogenase	G3P_HUMAN	36.03	8.57	23.0	1
94	Serotransferrin	TRFE_HUMAN	77.00	6.81	40.4	2

4.3.1.2.2 Sample 2

For sample 2, identification succeeded for the proteins in 24 of the 32 spots found to be regulated. Two or more different protein species were identified out of three spots (spots 14, 17 and 24) while the specification of one distinct protein out of proteins with high sequence similarity was not possible in three other spots (spot 2, 11 and 26, see Table 4-13, Appendix II and Appendix III). The spots without clearly identified protein were excluded from further analysis. This led to a set of 16 proteins (see Table 4-14) subjected to further bioinformatical analysis to set them and their regulation into the cellular context.

Table 4-13 Proteins identified from spots found to be altered after treatment with cholesterol lowering agents in sample 2, including their theoretically calculated molecular weight, pI and the number of gels they were identified from.

Spot No	Identified as	Swiss-Prot ID	MW [kDa]	pI	Sequence coverage [%]	Number of individual gels, identified from
2	Tubulin beta chain	TBB2C_HUMAN (TBB2A_HUMAN, TBB2B_HUMAN, TBB5_HUMAN)	49.799	4.79	35.5	3
3	78kDa-glucose regulated protein precursor	GRP78_HUMAN	72.288	5.07	37.9	1
4	N(G),N(G)-1dimethylarginine dimethylaminohydrolyase 1	DDAH1_HUMAN	31.102	5.53	54.0	4
7	ATP synthase subunit beta, mitochondrial precursor	ATPB_HUMAN	56.525	5.26	49.5	5
8	ATP synthase subunit beta, mitochondrial precursor	ATPB_HUMAN	56.525	5.26	44.2	4
11	Actin cytoplasmic	ACTG_HUMAN (ACTB_HUMAN)	41.766	5.31	47.2	3
12	Eukaryotic initiation factor 4A-1	IF4A1_HUMAN	46.125	5.32	33.3	1
13	Superoxide dismutase [Cu-Zn]	SODC_HUMAN	15.926	5.7	44.2	1
14	Heat shock protein beta 1	HSPB1_HUMAN	22.768	5.98	37.6	1
	5-Hydroxyisobutyrate-dehydrogenase, mitochondrial precursor	3HIDH_HUMAN	35.306	8.38	32.1	2
15	3-hydroxyanthranilate 3,4-dioxygenase	3HAO_HUMAN	32.522	5.62	38.1	1
	Glutathione transferase omega 1	GSTO1_HUMAN	27.548	6.23	47.7	3
16	Retinal-dehydrogenase 1	AL1A1_HUMAN	54.862	6.3	29.7	2
17	Selenium binding protein 1	SBP1_HUMAN	52.358	5.93	54.4	5
	Aldehyde-dehydrogenase, mitochondrial	ALDH2_HUMAN	56.346	6.63	44.3	4
18	Protein-disulfid-isomerase A3	PDIA3_HUMAN	56.747	5.98	59.4	3

Table 4-13 continued Proteins identified from spots found to be altered after treatment with cholesterol lowering agents in sample 2, including their theoretically calculated molecular weight, pI and the number of gels they were identified from.

Spot No	Identified as	Swiss-Prot ID	MW [kDa]	pI	Sequence coverage [%]	Number of individual gels, identified from
19	Protein-disulfid-isomerase A3	PDIA3_HUMAN	56.747	5.98	44.0	3
20	Ketohexokinase	KHK_HUMAN	32.71	5.64	33.6	2
22	3,2-trans-enoyl-CoA isomerase	D3D2_HUMAN	32.795	8.8	21.5	3
23	Isopentenyl-diphosphate delta isomerase	IDI1_HUMAN	26.319	5.93	35.4	1
24	Beta-ureidopropionase	BUP1_HUMAN	43.139	6.09	40.9	3
	Aminoacylase 1	ACY1_HUMAN	45.856	5.77	39.2	2
25	Glutathione transferase omega 1	GSTO1_HUMAN	27.548	6.23	45.6	4
26	Enolase	ENOA_HUMAN	47.139	7.01	34.3	4
		(ENOB_HUMAN, ENOG_HUMAN)				3
27	Isocitrate dehydrogenase	IDHC_HUMAN	46.63	6.53	44.0	3
29	Catalase	CATA_HUMAN	59.719	6.90	48.8	5
30	Carbonic anhydrase 2	CAH2_HUMAN	29.228	6.87	33.8	2
31	Fructose-bisphosphat-aldolase B	ALDOB_HUMAN	39.448	8.00	35.2	5
32	Catalase	CATA_HUMAN	59.719	6.90	59.4	6

Table 4-14 Those proteins verified and used for further bioinformatical studies of their cellular function.

Regulations	Sample 1	Sample 2	
UP-REGULATED	RSV	HMCS1_HUMAN	ATPB_HUMAN, PDIA3_HUMAN
	LEK	ANXA5_HUMAN, G3P_HUMAN	ATPB_HUMAN, PDIA3_HUMAN
	RSV & LEK		ATPB_HUMAN, PDIA3_HUMAN
	RSV vs LEK	HMCS1_HUMAN, NNMT_HUMAN, ALBU_HUMAN, TRFE_HUMAN	
	RSV	PGM1_HUMAN	ALDOB_HUMAN
	LEK	NNMT_HUMAN, ALBU_HUMAN, RADL_HUMAN,	ACTB_HUMAN, ALDOB_HUMAN
DOWN - REGULATED	RSV & LEK		
	RSV vs LEK	PSA5_HUMAN, ANXA5_HUMAN, ALBU_HUMAN	
APPEAR	RSV		TBB2C_HUMAN, DDAH1_HUMAN, GSTO1_HUMAN, PDIA3_HUMAN, KHK_HUMAN, D3D2_HUMAN, IDHC_HUMAN, CAH2_HUMAN
	LEK	IDHP_HUMAN	TBB2C_HUMAN, DDAH1_HUMAN, GSTO1_HUMAN, PDIA3_HUMAN, KHK_HUMAN, D3D2_HUMAN, IDHC_HUMAN, CAH2_HUMAN
	RSV & LEK		TBB2C_HUMAN, DDAH1_HUMAN, GSTO1_HUMAN, PDIA3_HUMAN, KHK_HUMAN, D3D2_HUMAN, IDHC_HUMAN, CAH2_HUMAN
	RSV vs LEK		IDHC_HUMAN, CAH2_HUMAN
	RSV		GRP78_HUMAN, IF4A1_HUMAN, SODC_HUMAN, AL1A1_HUMAN
	LEK	ENPL_HUMAN	GRP78_HUMAN, SODC_HUMAN, AL1A1_HUMAN
DISAPPEAR	RSV & LEK		
	RSV vs LEK		

4.3.1.3 Comparison of sample 1 and sample 2

The consistency between the single experiments was similar in both donors with slightly lower values for sample 2 than for sample 1 (see Table 4-11). For both donors, a better consistency was observed in those analyses targeting the up-regulation or appearance of spots, compared to those which target a down-regulation or disappearance (see Table 4-11). The overall consistency was 40.1 to 49.5 % for donor 1 and donor 2 respectively.

With respect to protein identification, both samples correlate well. In both cases it was possible to identify a high percentage of the differentially present spots. In sample 1 63.8 % (60 out of 94) and in sample 2 75 % (24 out of 32) of the spots could be identified. The average sequence coverage is also similar with 37.5 % and 42.2 % for sample 1 and 2, respectively.

A comparison of “regulated spots” between sample 1 and 2 was not possible due to the different freezing-thawing status of the samples when applied to IEF. So, comparison was made on the level of identified proteins but none of the proteins found to be regulated in sample 1 was also found in sample 2, and vice versa (see 4.3.1.2 and Table 4-14).

4.3.2 Microsomal fraction / nano high pressure liquid chromatography

In addition to analysing the effects of RSV and LEK-935 on the cytosol of primary human hepatocytes by 2D gel electrophoresis, the microsomal fractions of the samples treated with RSV were analysed by nLC-MS.

4.3.2.1 Semi-quantitation

In addition to the semi-quantitative analysis, the control as well as the treated samples were double-labelled. The samples were aliquoted, labelled with the iTRAQ™ labels 114,116 and 115,117 for the control and treated samples respectively and finally mixed in a ratio of 1:1:1:1. By this, the experimental procedure was checked for technical variances as the ratios 114/116 and 115/117 were examined. Ideally the resulting values should be one. In reality, the values were about one with a standard deviation of about 10 %, see 4.2.2.3 and Figure 4-13 A and B. The factor/divisor distribution of

the internal controls was near to a normal distribution and a clear difference was observed between the factor/divisor distribution of the internal controls (see Figure 4-13 A and B) and the factor/divisor distribution of the comparisons between RSV and control (see C and D). These results prove a low technical variance of the experimental setup.

In general, the factor/divisor distributions of the comparisons between RSV and control were considerably broader than that of the internal controls (see Figure 4-13). No proteins were found to appear or disappear after RSV treatment, only increases and decreases in the amount of proteins compared to the control samples were observed. For sample 1, the shape of factor/divisor distribution was similar to a normal distribution while sample 2 showed a distribution spread over the whole range of values (see Figure 4-13).

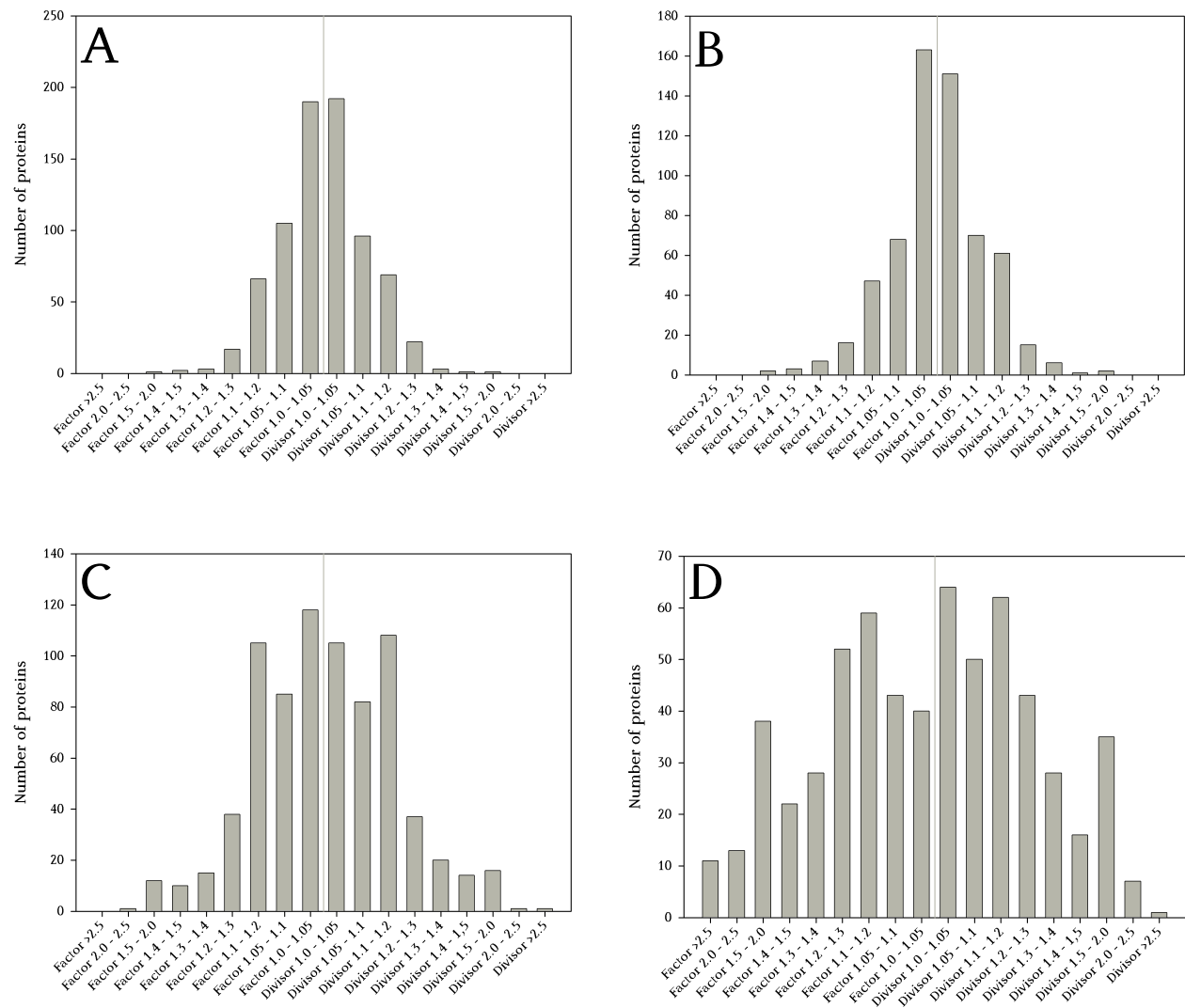


Figure 4-13 Exemplary comparison of the factor/divisor distributions of the internal control 114/116 (A, B) and the RSV to control comparison of 117/114 (C, D) for sample 1 (A, C) and sample 2 (B, D). The data were taken from the analysis by ProteinPilot, a comparable picture was observed with every quantitation software applied. A much stronger de-regulation can be seen in sample 2 compared to sample 1, leading to a shape of the diagram no more similar to that observed by a normally distributed set of values.

In sample 1, twelve proteins were found to be significantly altered after RSV treatment. Among them, ten were found to be up-regulated while two were down-regulated.

In sample 2, a set of nine proteins shows increased amounts after RSV treatment. Because of the high standard deviation, no protein could be found in decreased amounts.

The detected proteins and their regulation are summarised in Table 4-15.

Table 4-15 Proteins found in the microsomal fraction of primary human hepatocytes by nLC-MS to be regulated after treatment with rosuvastatin

	Proteins found by nLC-MS		
	Sample 1	Sample 2	
UP REGULATED	Long chain fatty acid CoA ligase		
	Apolipoprotein C1		
	Apolipoprotein C3	Mitochondrial dicarboxylate carrier	
	Succinate-dehydrogenase	Glyceraldehyde-3-phosphate dehydrogenase	
	cytochrome b560 subunit, mitochondrial	Hydroxy-methyl-glutaryl-CoA synthetase, cytoplasmic	
	Lanosterol 14-alpha demethylase (CYP 51A1)	Peroxiredoxin 6	
	Estradiol-17-beta-dehydrogenase 12	Radixin	
	Transmembrane protein 56	Fibrinogen alpha	
	ATP-citrate synthase	Fibrinogen beta	
	Squalene synthetase	GTP-binding protein SAR1b	
	Mannose-P-dolichol utilisation defect 4 protein	Voltage-dependent anion-selective channel protein 2	
	DOWN - REGULATED	Actin	
		60 S ribosomal protein L9	

4.3.2.2 Comparison of sample 1 and sample 2

As already shown during the analysis of the cytosolic fraction (0), no correlation between sample 1 and sample 2 was observed. None of the proteins found to be regulated in the microsomal fraction of donor 1 were also found to be regulated in the microsomal fraction of donor 2 and vice versa.

However, some correlations between sample 1 and sample 2 were found by comparing the proteins detected during 2D gel electrophoresis and those detected during nLC-MS, as discussed in 4.3.4.

4.3.3 Validation of the results by RT-PCR

To validate the results from the proteomic analysis, the effects of the treatments were also checked by RT-PCR on the level of transcription. These experiments were performed by Dr. Jean-Marc Pascussi (Institut de Génomique Fonctionnelle, Département d'Oncologie, CNRS UMR5203 - INSERM U661 - UFR de Médecine Montpellier-Nîmes).

A set of five proteins was checked on samples derived from four different human donors (see Table 4-16). RT-PCR measurements were performed on cells treated for 24 hours compared to the 48 hours treated samples used for proteomic analysis. The results are summarised in Table 4-16. Only for HMG-CoA synthase 1, the measurements were absolutely consistent between the six donors analysed. While the fold-changes of the proteome analysis correlate well, the values obtained by RT-PCR of four samples differed a lot (see Table 4-16). For two other proteins, ATPB and PDIA3 changes correlating to those measured on the proteome were also observed by measuring the mRNA levels. Even if the regulations were not observed in all four samples. For NNMT as well as PGM1, values even opposite to those observed by the proteomic analysis were seen in the RT-PCR. Nevertheless, the majority of RT-PCR measurements underline the effects observed by the proteome analysis.

Table 4-16 Validation of five of the proteins found in altered amounts after RSV and/or LEK-935 treatment by RT-PCR. Values above a threshold of 2.0 are marked in green and values below a threshold of 0.5 are marked in orange.

	ATPB		HMGCS1		NNMT		PDIA3		PGM1	
	RSV	LEK-935	RSV	LEK-935	RSV	LEK-935	RSV	LEK-935	RSV	LEK-935
Sample1			3.4	1.0	1.0	0.4			0.4	0.7
Sample2	2.7	2.3	3.0*				2.2	2.3		
HH-269	2.3	1.7	18.7	1.5	3.5	3.5	3.6	2.6	2.9	1.7
HH-270	2.5	0.9	20.5	0.9	4.4	1.0	2.4	1.1	5.5	0.9
HH-271	1.6	0.9	7.6	0.8	2.6	1.8	1.4	1.1	1.7	0.7
HH-272	1.1	0.6	3.1	1.2	1.0	0.6	1.3	0.6	1.1	0.6

4.3.4 Summary of regulations

A set of 44 different proteins was found to be altered by treating primary human hepatocytes with the cholesterol lowering agents rosuvastatin and LEK-935. The

correlation between the two donors was relatively low. Only one protein was found to be regulated by the same drug into the same direction in both donors. This protein was identified as the cytoplasmic hydroxy-methyl-glutaryl CoA synthase, responsible for the formation of HMG-CoA from acetyl-CoA and acetoacetyl-CoA. Two other proteins were found to be regulated in the same direction but by different drugs. For glyceraldehydes-3-phosphat dehydrogenase, up-regulation by LEK-935 was observed in donor 1 while it was up-regulated by RSV in donor 2. For radixin, an up-regulation by RSV was observed in donor 2, while it was down-regulated by LEK-935 in donor 1. In general, much more proteins were found to be up-regulated (41) than down-regulated (17) either reflecting the real situation inside the cell or the limitations of the analytical approaches used (see discussion).

The majority of the results obtained by the validation experiments were in accordance to the proteome data. Nevertheless, changes in the opposite directions were also observed. The analysis of four donors during the validation experiments underline the big inter-individual differences as observed with two donors in the proteomic study. The whole set of proteins is depicted in Table 4-17. The table was simplified, only differentiating between up- and down-regulation and the proteins are named by their Swiss-Prot identifier. The HMG-CoA synthetase is marked in green while Glyceraldehyde-3-phosphate dehydrogenase is marked in blue and radixin is marked in red. A detailed view on the proteins can be found in Appendix II.

Table 4-17 Summary of the proteins found in the cytosolic or microsomal fraction of primary human hepatocytes, by 2D gel electrophoresis and nLC-MS, respectively, to be regulated by rosuvastatin and/or LEK-935.

Regulations		Proteins identified to be regulated and used for further analysis	
		Sample 1	Sample 2
UP	RSV	ACLY_HUMAN, APOC3_HUMAN, CP51A_HUMAN, DHB12_HUMAN, FDFT_HUMAN, HMCS1_HUMAN, MPU1_HUMAN, TMM56_HUMAN	ATPB_HUMAN, CAH2_HUMAN, D3D2_HUMAN, DDAH1_HUMAN, DIC_HUMAN, FIBA_HUMAN, FIBB_HUMAN, G3P_HUMAN, GSTO1_HUMAN, HMCS1_HUMAN, IDHC_HUMAN, KHK_HUMAN, PDIA3_HUMAN, PRDX6_HUMAN, RADL_HUMAN, SAR1B_HUMAN, TBB2C_HUMAN, VDAC2_HUMAN
	LEK	ANXA5_HUMAN, G3P_HUMAN, IDHP_HUMAN	ATPB_HUMAN, CAH2_HUMAN, D3D2_HUMAN, DDAH1_HUMAN, GSTO1_HUMAN, IDHC_HUMAN, KHK_HUMAN, PDIA3_HUMAN, TBB2C_HUMAN,
	RSV & LEK		ATPB_HUMAN, CAH2_HUMAN, D3D2_HUMAN, DDAH1_HUMAN, GSTO1_HUMAN, IDHC_HUMAN, KHK_HUMAN, PDIA3_HUMAN, TBB2C_HUMAN,
DOWN	RSV vs LEK	ALBU_HUMAN, HMCS1_HUMAN, NNMT_HUMAN, TRFE_HUMAN	
	RSV	ACTH_HUMAN, PGM1_HUMAN, RL9_HUMAN	AL1A1_HUMAN, ALDOB_HUMAN, GRP78_HUMAN, IF4A1_HUMAN, SODC_HUMAN
	LEK	ACTB_HUMAN, ALBU_HUMAN, ENPL_HUMAN, NNMT_HUMAN, RADL_HUMAN	AL1A1_HUMAN, ALDOB_HUMAN, GRP78_HUMAN, IF4A1_HUMAN, SODC_HUMAN
RSV & LEK		AL1A1_HUMAN, ALDOB_HUMAN, GRP78_HUMAN, SODC_HUMAN	
RSV vs LEK	ALBU_HUMAN, ANXA5_HUMAN, PSA5_HUMAN		

4.4 Bioinformatic analysis of the regulated proteins

To get an impression about the cellular pathways and biological processes affected, the set of differentially expressed proteins found in 4.3 was further analysed by database searches. For a general overview about the processes affected, the expasy database (www.expasy.org) and the gene ontology (www.geneontology.org) were screened manually or with computational aid. To additionally deepen the view on biological pathways affected by the regulated proteins, the KEGG database (www.genome.jp/kegg) was also used for screening. The focus was set on functions/pathways either over-represented in the set of 45 proteins or related to cholesterol synthesis and metabolism.

4.4.1 Rosuvastatin treatment

4.4.1.1 General overview

In sample 1 the amounts of eleven proteins were increased after RSV treatment opposed to only three proteins found in decreased amounts. Most of the proteins increased after RSV belong to the XLC group (8), related to either the metabolism of cholesterol (6) fatty acids or lipids (2). The remaining three proteins are involved in energy metabolism (1), protein-biosynthesis or -degradation (1) and cellular organisation (1). The down-regulated proteins are equally distributed to protein-biosynthesis and -degradation (1), cellular organisation inclusive transport processes (1) and energy metabolism (1, see Figure 4-14 A and B).

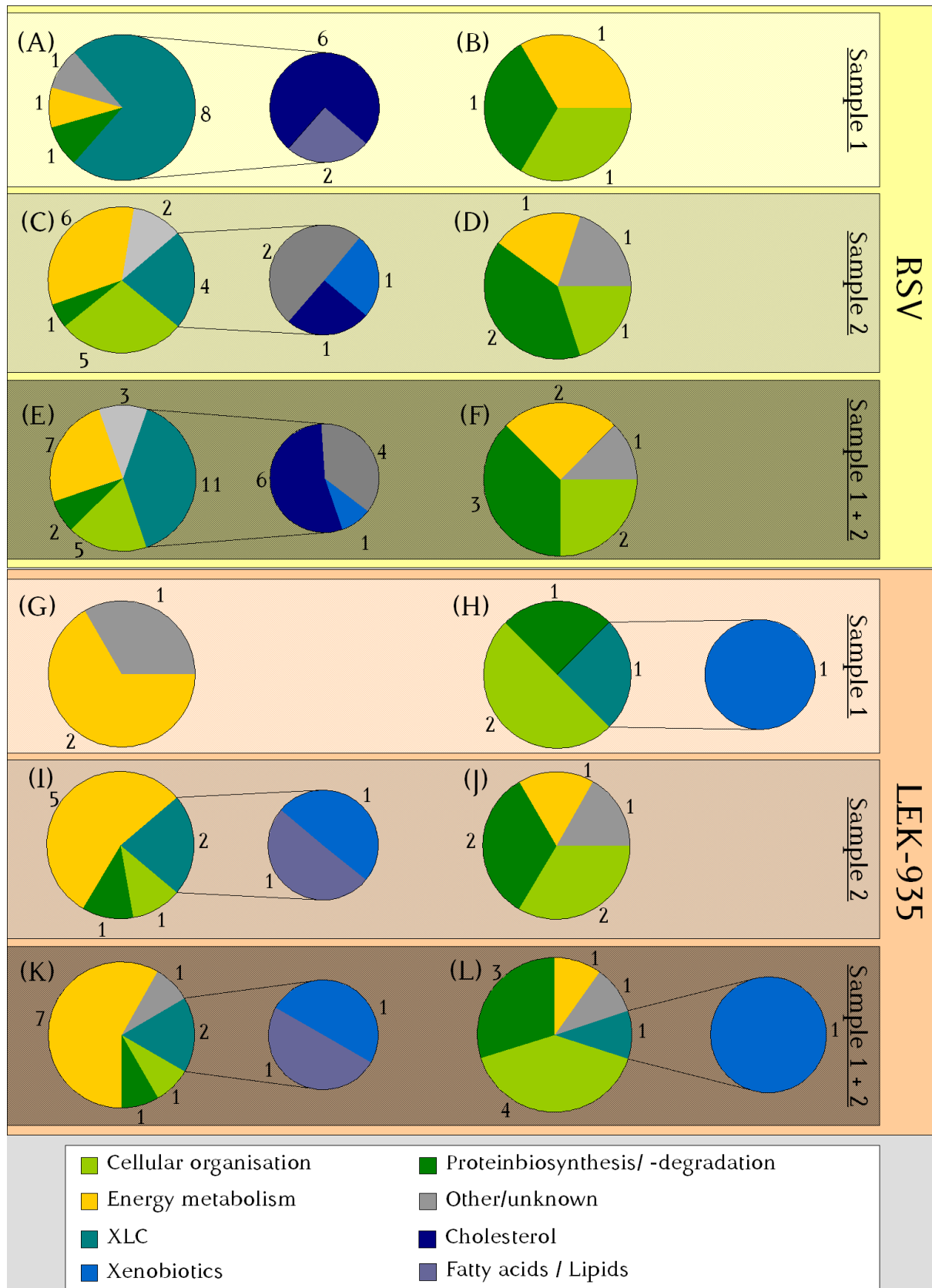


Figure 4-14 Proportional distribution of the cellular functions of the proteins found to be regulated by RSV (A-F) or LEK-935 (G-L) in sample 1 (A-B,G-H) and sample 2 (C-D,I-J), as described in the Expasy database. The first (A,C,E,G,I,K) and second (B,D,F,H,J,L) column of diagrams show the distributions of the upregulated and downregulated proteins respectively. In E-F and K-L a summary is displayed of all proteins found to be regulated by RSV or LEK-935. XLC (xenobiotic-lipid-cholesterol), proteins involved the xenobiotic/drug metabolism, fatty acid synthesis/degradation or cholesterol homeostasis.

Using Cytoscape equipped with the Bingo plug-in for a search of GO terms in the category biological process, over-represented in the set of regulated proteins in comparison to the whole set of annotations, no result was found for the three proteins down-regulated in sample 1. For the proteins up-regulated, among the ten most over-represented GO-terms, cholesterol biosynthetic process (GO-ID 6695), cholesterol transport (GO-ID 30301) and isoprenoid biosynthetic process (GO-ID 9241) were found. The remaining GO-terms were also related to either sterols or lipids (see Table 4-18).

Table 4-18 The ten most over-represented GO terms in the ontology biological process of the set of proteins found to be up-regulated after RSV treatment of sample 1 and sample 2, compared to terms in the whole genome. x = number of annotations found in the sample set, X = number of proteins in the sample set, N = number of proteins in the whole GO dataset

GO-ID	p-value	corr p-value	x	N	X	N	Description
Sample 1							
6629	3,64E-07	5,02E-05	6	717	8	14529	Lipid metabolic process
44255	4,92E-06	2,63E-04	5	577	8	14529	Cellular lipid metabolic process
6694	6,42E-06	2,63E-04	3	72	8	14529	Steroid biosynthetic process
8610	7,93E-06	2,63E-04	4	272	8	14529	Lipid biosynthetic process
33700	9,53E-06	2,63E-04	2	9	8	14529	Phospholipid efflux
33344	1,46E-05	3,35E-04	2	11	8	14529	Cholesterol efflux
9241	3,17E-05	6,25E-04	2	16	8	14529	Isoprenoid biosynthetic process
6695	5,54E-05	7,65E-04	2	21	8	14529	Cholesterol biosynthetic process
15918	5,54E-05	7,65E-04	2	21	8	14529	Sterol transport
30301	5,54E-05	7,65E-04	2	21	8	14529	Cholesterol transport
Sample 2							
51258	2,50E-05	7,28E-03	3	47	18	14529	Protein polymerisation

In sample 2, eighteen proteins were found to be up-regulated and five were found to be down-regulated by RSV treatment. Among the up-regulated proteins, the majority are involved in energy metabolism (6), followed by cellular organisation (5) and the XLC group (4), herein distributed among cholesterol (1), fatty acids or lipids (2) and xenobiotics (1). The majority of the down-regulated proteins are involved in protein-biosynthesis and -degradation (2) followed by energy metabolism (1), cellular organisation (1) and one protein has another or unknown function (see Figure 4-14 C and D).

Looking for GO terms over-represented in the set of regulated proteins compared to the whole set of annotations, only one GO term was found among the up-regulated

proteins, protein polymerisation (GO-ID 51258). This is a more general GO term, whose finding is caused by fibrinogen alpha, fibrinogen beta and tubulin, present in this set of proteins.

Table 4-19 The ten most over-represented GO terms in the ontology biological process of the set of proteins found to be down-regulated after RSV treatment of sample 1 and sample 2, compared to terms in the whole genome. x = number of annotations found in the sample set, n = number of annotated proteins in the whole GO dataset, X = number of proteins in the sample set, N = number of proteins in the whole GO dataset

GO-ID	p-value	corr p-value	x	n	X	N	Description
Sample 1							
No over-represented GO terms found							
Sample 2							
10033	1,57E-04	1,46E-02	2	75	4	14529	Response to organic substance
32287	2,75E-04	1,46E-02	1	1	4	14529	Myelin maintenance in the peripheral nervous system
43217	2,75E-04	1,46E-02	1	1	4	14529	Myelin maintenance
22011	5,51E-04	1,46E-02	1	2	4	14529	Myelination in the peripheral nervous system
50665	5,51E-04	1,46E-02	1	2	4	14529	Hydrogen peroxide biosynthetic process
2093	5,51E-04	1,46E-02	1	2	4	14529	Auditory receptor cell morphogenesis
45939	5,51E-04	1,46E-02	1	2	4	14529	Negative regulation of steroid metabolic process
32292	5,51E-04	1,46E-02	1	2	4	14529	Ensheathment of axons in the peripheral nervous system
45541	5,51E-04	1,46E-02	1	2	4	14529	Negative regulation of cholesterol biosynthetic process
60117	5,51E-04	1,46E-02	1	2	4	14529	Auditory receptor cell development

The terms negative regulation of steroid metabolic process (GO-ID 45939) and negative regulation of cholesterol biosynthetic process (GO-ID 45541) were found among the ten most over-represented terms in the set of down-regulated proteins of sample 2. Except for position one, all of the terms presented in Table 4-19 were related to only one protein, the superoxide-dismutase [Cu-Zn].

4.4.1.2 Cellular pathways affected

Searching the KEGG database with the proteins affected in sample 1, two of them were found in the citrate cycle (KEGG pathway hsa00020), the PPAR signalling

pathway (KEGG pathway hsa03320) and the biosynthesis of steroids (KEGG pathway hsa00100).

In the TCA cycle, the ATP citrate lyase (ACLY) and succinate dehydrogenase (SDHC) were found to be up-regulated. The ACLY is the enzyme responsible for the formation of acetyl-CoA in the cytoplasm, while the SDHC is a monoheme cytochrome b, part of the complex II of the respiratory chain, responsible for transferring electrons from succinate to ubiquinone.

In the PPAR signalling pathway, the apolipoprotein C-III (APOC3) and the long-chain-fatty-acid CoA ligase 3 (ACSL3) were found to be up-regulated. The APOC3 is a secreted protein and as a part of VLDLs and HDLs it plays a role in the systemic cholesterol transport. The ACSL3 activates long-chain fatty acids by the ligation of CoA. It thereby plays a key role in the synthesis of cellular lipids as well as the degradation of fatty acids.

The biosynthesis of steroids is affected at three different positions, which are directly linked to the synthesis of cholesterol from farnesyl-pyrophosphate. The squalene synthetase (FDFT1) as well as the lanosterol 14- α demethylase (CYP51A1) were found to be up-regulated. The FDFT1 catalyses the first specific step in the cholesterol biosynthetic pathway, the conversion of farnesyl-diphosphate to squalene. CYP51A1 catalyses the 14- α demethylation of lanosterol, a step essential for cholesterol biosynthesis.

In addition, several pathways were found in which only one of the regulated proteins is involved. In three of them, the HMG-CoA synthase 1 plays a role: the synthesis and degradation of ketone bodies (KEGG pathway 00072), the butanoate metabolism (KEGG pathway 00650) and the valine, leucine and isoleucine degradation (KEGG pathway 00280). Furthermore, five other pathways somehow related to cholesterol were present, terpenoid biosynthesis (KEGG pathway hsa00900), fatty acid metabolism (KEGG pathway hsa00071), biosynthesis of unsaturated fatty acids (KEGG pathway hsa01040), adipocytokine signalling pathway (KEGG pathway hsa04920) and androgen and estrogen metabolism (KEGG pathway hsa00150).

Searching the KEGG database with the proteins affected in sample 2 revealed one pathway in which three of the proteins are involved, seven pathways in which two of the proteins are involved and several others in which one of the proteins is involved. The pathway for Huntington's disease (KEGG pathway hsa05016) is covered in three

positions. The superoxide dismutase [Cu-Zn] (SOD1) was found to be down-regulated, while two positions in the mitochondria were up-regulated, the ATPsynthase subunit beta, mitochondrial (ATPB) and the voltage-dependent anion-selective channel protein 2 (VDAC2). The SOD1 is involved in the ROS defence of the cells and its inhibition has been shown to induce apoptosis (Huang et al. 2000). Besides its role in energy production, the ATPB was recently shown to act as high selective receptor for apolipoprotein A1, possibly playing a role in endocytosis of HDL particles (Martinez et al. 2003). VDAC2 is somehow involved in the connection between the general mitochondrial physiology and apoptosis, moreover, the VDAC are the sites of binding of the hexokinase and glycerol kinase to the mitochondria.

Not to loose focus on the effects on proteins somehow related to cholesterol synthesis or metabolism, the pathways of Parkinson's disease (KEGG pathway hsa05012), Alzheimer's disease (KEGG pathway hsa05010), the complement and coagulation cascades (KEGG pathway hsa04610) and antigen processing and presentation (KEGG pathway hsa04612) covered in two positions were not considered in detail.

Two positions of the glycolysis/gluconeogenesis (KEGG pathway hsa00010) were covered. The fructose-bisphosphate aldolase B (ALDOB) was found to be down-regulated and the glyceraldehyde-3-phosphate dehydrogenase (GAPDH) was up-regulated after RSV treatment. The reversible conversion of fructose-1,6 bisphosphate to glyceraldehydes-3-phosphate is catalysed by ALDOB, while GAPDH catalyses the reversible oxidative phosphorylation of glyceraldehydes-3-phosphate. Beside this role in energy metabolism, the GAPDH plays a crucial role in protecting the cells from caspase-independent cell-death (CICD, (Colell et al. 2007)).

In the glutathione metabolism (KEGG pathway hsa00480) two positions were covered and both were up-regulated. The isocitrate dehydrogenase 1 (IDH1) catalyses the NADP-dependent decarboxylation of iso-citrate to alpha-ketoglutarate while the glutathione S-transferase omega-1 (GSTO1) is involved in detoxification processes. The IDH1 was already shown to be up-regulated in sterol-deprived HegG2 cells and suggested to deliver the NADPH necessary for cholesterol and fatty acid synthesis (Shechter et al. 2003). So, it is also involved in glutathione metabolism, as a producer of NADPH, necessary for the formation of glutathione from glutathione-disulfide.

The fructose and mannose metabolism (KEGG pathway hsa00051) was covered in two positions, of which one, the ALDOB, also present in the Glycolysis/Gluconeogenesis, was down-regulated while the other, the Ketohexokinase (KHK) was up-regulated. The

KHK catalyses the conversion of fructose to fructose-1P, the first step in the fructose metabolism.

The synthesis and degradation of ketone bodies (KEGG pathway 00072), the butanoate metabolism (KEGG pathway 00650) and the valine, leucine and isoleucine degradation (KEGG pathway 00280) were again found, as the HMG-CoA synthase was also found in sample 2.

One more pathway related to cholesterol was covered in one position, the fatty acid metabolism (KEGG pathway hsa00071).

4.4.2 LEK-935 treatment

4.4.2.1 General overview

In sample 1, three proteins were found in elevated amounts after LEK-935 treatment. Two of them are involved in energy metabolism, while the remaining one was categorised into the group of other/unknown functions. In addition, four proteins were found to be down-regulated. Two are involved in cellular organisation including transport processes, one in the protein synthesis or degradation and one in detoxification processes (see Figure 4-14 G and H).

In sample 2, a higher number of proteins was found to be affected. In total, nine proteins were found to be up-regulated. The majority is involved in energy metabolism (5) while the remaining four proteins are equally distributed among protein biosynthesis or degradation (1), cellular organisation (1), fatty acids/lipids (1) and detoxification (1). Six proteins were found to be down-regulated, they were distributed among cellular organisation (2), protein-biosynthesis or -degradation (2), energy metabolism (1) and other functions (1, see Figure 4-14 I and J).

Searching for over-represented GO terms in the category biological process, a tendency to general metabolic processes as shown in Figure 4-14 was proven for sample 1. In addition, two of the terms were related to coagulation. For sample 2, no statistically over-represented terms were found (see Table 4-20).

Table 4-20 The ten most over-represented GO terms in the ontology biological process of the set of proteins found to be up-regulated after LEK-935 treatment in sample 1 and sample 2, compared to terms in the whole genome. x = number of annotations found in the sample set, n = number of annotated proteins in the whole GO dataset, X = number of proteins in the sample set, N = number of proteins in the whole GO dataset

GO-ID	p-value	corr p-value	x	n	X	N	Description
Sample 1							
6097	4,13E-04	1,49E-02	1	2	3	14529	Glyoxylate cycle
46487	6,19E-04	1,49E-02	1	3	3	14529	Glyoxylate metabolic process
6102	8,26E-04	1,49E-02	1	4	3	14529	Isocitrate metabolic process
6091	8,27E-04	1,49E-02	2	243	3	14529	Generation of precursor metabolites and energy
44262	1,12E-03	1,61E-02	2	283	3	14529	Cellular carbohydrate metabolic process
5975	2,75E-03	2,87E-02	2	445	3	14529	Carbohydrate metabolic process
6081	3,51E-03	2,87E-02	1	17	3	14529	Aldehyde metabolic process
50819	3,71E-03	2,87E-02	1	18	3	14529	Negative regulation of coagulation
50818	4,33E-03	2,87E-02	1	21	3	14529	Regulation of coagulation
55114	4,47E-03	2,87E-02	2	569	3	14529	Oxidation reduction
Sample 2							
No statistically over-represented GO terms found							

For both samples, GO terms could be found to be over-represented in the set of down-regulated proteins. In sample 1, mainly terms related to organelle localisation and cation homeostasis were found (see Table 4-21). Some of the terms over-represented among the proteins of sample 2 were related to negative regulations of cholesterol and sterol biosynthetic processes (see Table 4-21).

Table 4-21 The ten most over-represented GO terms in the ontology biological process of the set of proteins found to be down-regulated after LEK-935 treatment in sample 1 and sample 2, compared to terms in the whole genome. x = number of annotations found in the sample set, n = number of annotated proteins in the whole GO dataset, X = number of proteins in the sample set, N = number of proteins in the whole GO dataset

GO-ID	p-value	corr p-value	x	n	X	N	Description
Sample 1							
51235	3,20E-05	1,79E-03	2	48	3	14529	Maintenance of location
1666	4,21E-05	1,79E-03	2	55	3	14529	Response to hypoxia
51659	2,06E-04	1,79E-03	1	1	3	14529	Maintenance of mitochondrion location
51657	2,06E-04	1,79E-03	1	1	3	14529	Maintenance of organelle location
31643	2,06E-04	1,79E-03	1	1	3	14529	Positive regulation of myelination
15682	2,06E-04	1,79E-03	1	1	3	14529	Ferric iron transport
65008	2,32E-04	1,79E-03	3	894	3	14529	Regulation of biological quality
30005	3,07E-04	1,79E-03	2	148	3	14529	Cellular di-, tri-valent inorganic cation homeostasis
55066	3,20E-04	1,79E-03	2	151	3	14529	Di-, tri-valent inorganic cation homeostasis
30003	4,05E-04	1,79E-03	2	170	3	14529	Cellular cation homeostasis
Sample 2							
10033	2,60E-04	1,70E-02	2	75	5	14529	Response to organic substance
32287	3,44E-04	1,70E-02	1	1	5	14529	Myelin maintenance in the peripheral nervous system
43217	3,44E-04	1,70E-02	1	1	5	14529	Myelin maintenance
22011	6,88E-04	1,70E-02	1	2	5	14529	Myelination in the peripheral nervous system
50665	6,88E-04	1,70E-02	1	2	5	14529	Hydrogen peroxide biosynthetic process
2093	6,88E-04	1,70E-02	1	2	5	14529	Auditory receptor cell morphogenesis
45939	6,88E-04	1,70E-02	1	2	5	14529	Negative regulation of steroid metabolic process
32292	6,88E-04	1,70E-02	1	2	5	14529	Ensheathment of axons in the peripheral nervous system
45541	6,88E-04	1,70E-02	1	2	5	14529	Negative regulation of cholesterol biosynthetic process
60117	6,88E-04	1,70E-02	1	2	5	14529	Auditory receptor cell development

4.4.2.2 Cellular pathways affected

For sample 1, no pathways affected by more than one protein were found, searching the KEGG database. For a complete list of the pathways, see Appendix VI. Glycolysis/Gluconeogenesis was again covered by GAPDH (see 4.4.1.2). The Citrate cycle and glutathione metabolism were also found, both involving the isocitrate

dehydrogenase 2 (IDH2). The IDH2 is a mitochondrial protein that catalyses the oxidative decarboxylation of isocitrate to alpha-ketoglutarate.

For sample 2, five pathways were found to be covered in two positions, the Huntington's disease (KEGG pathway hsa05016), the pathogenic *E.coli* infection (KEGG pathway hsa05130), the glutathione metabolism (KEGG pathway hsa00480), the antigen processing and presentation (KEGG pathway hsa04612) and the fructose and mannose metabolism (KEGG pathway hsa00051). The proteins involved in these pathways were the same as described in 4.4.1.2, except for those not affected by LEK-935 but by RSV. The fatty acid metabolism (KEGG pathway hsa00071) was the only pathway somehow related to cholesterol affected by one of the proteins.

5 Discussion

The aim of this study was the analysis of the effects of cholesterol lowering agents on the proteome of primary human hepatocytes. In order to get information about low-abundant proteins, the samples were fractionated. The cytosolic fraction and the microsomal fraction were analysed by two-dimensional gel electrophoresis and a nLC-MS approach, respectively.

For reasons of clarity, the discussion has been divided into two chapters. The first comprises the analytical approaches used during this study, the results gained, the advantages as well as the major drawbacks observed. In the second chapter, the proteins found to be regulated and their possible relationship to cholesterol homeostasis is critically discussed.

5.1 Experimental approaches, their quirks and results

5.1.1 Proteomics

Usually, 2D-PAGE and nLC-MS are used to determine the proteome of a cell or cellular compartment at a distinct time point under distinct conditions. In a semi-quantitative analysis, there is an additional comparison of samples with different status, like health versus ill or untreated versus treated and so on.

Only determining the protein content of a cellular status provides information about proteins present in the cell under distinct conditions and builds the basis for further investigations. In addition, the semi-quantitative experiments are sought either to deliver information about cellular processes initiated by a treatment or to help finding biomarkers present in sick but not in healthy cells or tissues. Quantification occurs at the level of protein abundance, measured by either the spot intensity or the presence of peptides derived from a protein. The proteomics does not analyse some kind of precursor or product molecules like the other-omics (genomics, transcriptomics or metabolomics), but the real executing molecules of a cell.

The more and more evolving picture of high-complexity of cellular processes and regulations underlines the need for analytical approaches at the level of the proteome,

but at the same time clearly demonstrates the prospects and challenges of the approaches present today. To name a few, 2D gel electrophoresis provides a high resolution and enables the detection of post-translational modifications as well as the differentiation between protein-isoforms, both quite difficult to achieve with nLC-MS approaches. In contrast, it is quite difficult to display integral membrane proteins by 2D-PAGE due to their hydrophobic nature. The nLC-MS in turn is able to display membrane proteins and quite high separation capacities can be achieved by adding some more separation steps. But an increasing number of separation steps reduces the reproducibility of the experiments.

Both approaches should not be regarded as opponent players but as tools that may, in the frame of an experimental setup as used in this study, complement each other. The question arises as to whether the expression analysis alone is the method of choice to understand the effects of a drug or cellular behaviour. The final outcome of a proteomic study is a raw overview about the processes taking place inside the cell. Among the found proteins, some are specific for the treatment/cell status investigated but there are also a few that are related as unspecific reactions, caused by culturing, stress of the treatment and so on. So, each protein found during such a study needs a detailed further analysis to fully understand the processes inside the cells. The proteomic analysis thus leads to a starting point and gives some, of course important, impressions about where to go next, but its combination with other -omics, like transcriptomics and metabolomics is necessary to get a complete picture.

5.1.2 Two-dimensional gel electrophoresis

The general applicability of the approach for the analysis of different sub-cellular fractions derived from primary human hepatocytes has previously been proven (Woerner 2006). Nevertheless, strong effects of the sample handling on the protein pattern of the 2D-PAGE as well as a contamination with bacterial protein were observed. These issues will be discussed in the following sections in detail. An evaluation of the experimentally gained data as well as explanations and solutions for the observed effects will be given.

5.1.2.1 **Sample handling**

Freezing the protein only one time prior to its application to IEF led to dramatic changes in the spot pattern of the resulting gels (see 4.2.1.2). This is in accordance with studies in the literature that describe the effect of freeze-thawing cycles on the activity of some enzymes (see (Shikama and Yamazaki 1961; Seguro et al. 1989; Heinz et al. 1990; Seguro et al. 1990) for example). Several factors affect the severity of activity inhibition by freeze-thawing cycles, like the nature and condition of protective additives, the pH of the solution, the freeze-thawing rates and the protein concentrations (Tamiya et al. 1985).

Protective additives were not used during this study to not disturb the following proteomic analysis. The pH was the same for each sample (potassium phosphate buffer adjusted to pH 7.4). Freezing samples in sodium phosphate buffer, a method widely used in molecular biology, is known to be not ideal due to a drop of the pH during the freezing process. This is caused by precipitation of the disodium salt (Na_2HPO_4) at low temperatures (Murase and Franks 1989) which acidifies the sample solution. Drops of the pH from 7.5 to 4.5 are described, leading to the dissociation of at least quaternary structures (Anchordoquy and Carpenter 1996). In contrast, potassium phosphate buffer as used in this study does not exhibit such a drop in pH at $-20\text{ }^\circ\text{C}$. With a pH of 7.7 it remains more or less at the adjusted value (pH 7.5) (Anchordoquy et al. 1996). Moreover, (Cao et al. 2003) reported the recovery of lactate dehydrogenase activity stored (frozen and thawed) in potassium phosphate buffer that is at least equal if not superior to Tris or HEPES buffer, recommended for protein storage. To sum up, the buffer used during this study complied with the requirements of a system that provides a maximum of protein stability during storage.

For the freeze-thawing rate, studies describing different effects on different proteins have been published (Shikama et al. 1961; Jiang and Nail 1998; Cao et al. 2003). Here, additional experiments were performed to examine the observed effects of freezing-thawing rates on the spot pattern of 2D gels more closely. All samples of the experiments were handled in the same way, slowly freezing and fast thawing, as recommended by (Cao et al. 2003). The experiments were performed with proteins derived from primary human hepatocytes, HCT-116, *S.pombe* as well as *E.coli* cells, to validate the effect of the samples origin.

The obtained results clearly demonstrate an extreme effect of freezing-thawing in human samples. In contrast, the samples derived from the unicellular organisms seem to be more or less resistant (see 4.2.1.2).

Between the four samples examined, only the protein concentration differed. While the protein concentration of the samples derived from HCT-116 was relatively low (1.7 $\mu\text{g}/\mu\text{l}$), that of the samples derived from primary human hepatocytes, yeast and bacteria was a bit higher (3.3 $\mu\text{g}/\mu\text{l}$, 2.5 - 2.8 $\mu\text{g}/\mu\text{l}$ and 5.0 $\mu\text{g}/\mu\text{l}$ for hepatocytes yeast and bacteria respectively). One may argue that the low protein concentration of the HCT-116 sample is the reason for the disturbed spot pattern. In contrast, (Jiang et al. 1998) as well as (Cao et al. 2003) reported a recovery of nearly 100 % of enzymatic activity at a protein concentration of 0.5 - 1 $\mu\text{g}/\mu\text{l}$, which is considerably lower than that of the HCT-116 samples. While the concentrations reported belong to isolated single-proteins, the concentration used during this study is that of a mixture of proteins. Nevertheless, a cryoprotective effect of BSA or albumin has been reported that is related to the increase in total protein concentration (Tamiya et al. 1985; Heinz et al. 1990). In sum, the observed effect cannot be related to the protein concentration as the differences in the protein concentrations are too small to cause a detectable effect.

One reason for the obviously increased sensitivity of the human samples could be their high complexity compared to the samples derived from single-cellular organisms. In the human samples, the loss of low amounts of protein may already be visible due to the high amount of different protein species. The more simple samples of the single-cellular organisms may compensate for this loss by the high amount of each protein in relation to the mass of protein present in the sample. In contrast, the number of spots present per gel does not count for this explanation, as it is more or less equal between the four different samples. Interestingly, the effect is not specific for primary human hepatocytes, what may be speculated due to its characteristic as a primary cell culture. The effect was observed in a similar manner in samples derived from HCT-116 cells, too. HCT-116 is a widely used malignant tumorigenic cell-line.

To sum up, the proteins derived from human samples show a high sensitivity towards freeze-thawing cycles, while the bacterial and yeast samples do not. The reasons could not be determined. Nevertheless, the effect underlines the necessity, in particular in the case of human samples, to adapt the experimental conditions to each kind of sample for proteomic approaches separately. The effect of freeze-thawing

should be studied in detail, as its compensation may really ease up gel-based proteomic studies of human samples.

5.1.2.2 Sample contamination

After finishing all identifications (60 out of 94 spots were identified) a contamination of sample 1 was obvious as the protein in 46 (76 %) of the 60 spots identified originated from *E.coli*. Therefore, the further use of this sample was getting questionable as the contamination of the sample could also affect the proteome of the cells and thereby the result of the experiments.

Retracing every experimental step, two possible entries for the *E.coli* proteins were found. The first one is a contamination already during cell culture. This entry point can most probably be excluded as no contamination of other samples was observed and the *E.coli* cells would have been detected during the culturing process. After their reception from Dr. Monostory, the vials were opened during sample preparation and prior to their application to analysis only. Luckily, a contamination occurring during these processes would not affect the protein expression of the cells in a way that disturbs the proteomic analysis.

Furthermore, the first step after opening the vial is the addition of protease inhibitors to avoid the degradation of proteins by intracellular proteases. These inhibitors do not only target mammalian proteases but also prokaryotic proteases. Therefore, an effect of the *E.coli* contamination caused by degradation of the human proteins by bacterial proteases can also be excluded. In the second step, cell lysis is performed by sonication. Thereby, all cells are destroyed which prevents bacterial growth and any kind of large-scale bacterial protein expression. For these reasons an effect of the *E. coli* contamination on protein expression or degradation is quite implausible.

At the same time, the sonication step is suggested to be the most probable point of entrance of the *E. coli*. In our lab, *E. coli* are widely used for heterologous protein expression and cell lysis is usually performed at the same sonicator that was used during the sample preparation of this study. Although the sonotrode was cleaned two times with a bulk of 70 % ethanol prior to each sonication, 100 % purity cannot be guaranteed here. In addition, this is the only step in which the sample is in touch with material that was in contact with *E. coli* protein.

As mentioned above, an observable effect of the contamination on the synthesis or degradation of the human proteins is implausible to impossible. Nevertheless, there is

a general effect as the bacterial proteins replace or even squeeze out human proteins of the 100 µg protein load onto the IEF. Their detection occurred during the semi-quantitative analysis, therefore the strength of contamination has to differ between the three samples. This resulted in their detection as “regulated” proteins.

To evaluate the effect of squeezing on the results of the semi-quantitative analysis, a theoretical examination of a sample contamination was performed. It was assumed that each sample is divided into three vials and spiked with three different amounts of bacterial protein (high, middle and low amount). This would result in six different combinations of effects detectable at the level of regulation. The theoretical scheme is shown in Figure 5-1.

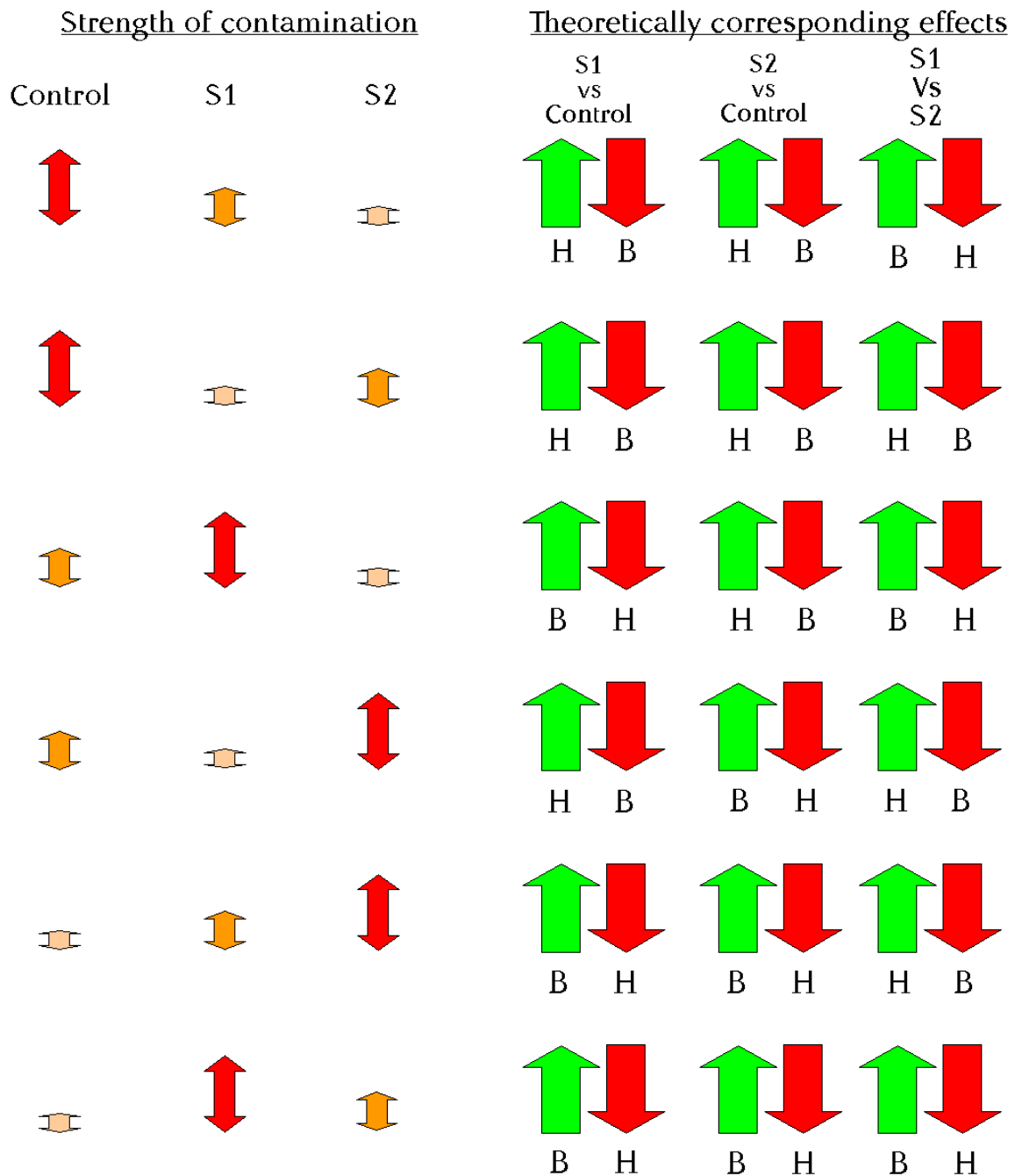


Figure 5-1 Theoretical examination of the effects observable at different strengths of relative sample contamination with protein derived from bacteria. On the left, the relative strength of contamination is depicted, where the strength correlates with the size of the arrows. The bigger the size of the arrow, the bigger is the contamination in this sample compared to the other. On the right, the theoretical effects are shown, green arrows mark up-regulated proteins, red arrows mark down-regulated proteins, B = bacterial protein identified, H = human protein identified.

According to the relative strength of contamination in the three samples, different “regulation-patterns” have to be expected. For example, the strongest contamination in sample 2 (S2) followed by sample 1 (S1) and the lowest amount of bacterial protein in the control sample, would result in bacterial proteins “up-regulated” in the two

treatments compared to the control and “down-regulated” in S1 compared to S2 (see Figure 5-1, line 4). At the same time, the tendencies of the human proteins would point towards a “down-regulation” in the two treatments compared to control as well as an “up-regulation” in S1 compared to S2.

All of the spots identified as *E.coli* protein in the LEK-935 treated sample were “up-regulated” compared to the control. The same was true for the majority of spots in the RSV treated sample. In addition, four spots “disappeared” after RSV treatment. Compared to the LEK-935 treated sample the RSV sample showed both up- as well as down-regulated spots, with a tendency towards down-regulation, see Figure 5-2.

For the human proteins, regulations into both directions were observed, with a stronger tendency towards down-regulations for RSV vs control and LEK-935 vs control. The comparison of RSV and LEK-935 pointed towards an up-regulation (see Figure 5-2).

Setting RSV treatment as S1 and LEK-935 treatment as S2, comparison was made to the ideal contamination depicted in Figure 5-1. The contamination observed in reality clearly resembles the effects shown in line four of Figure 5-1 and described in the text above. The LEK-935 sample (S2) showed the strongest contamination, followed by the RSV sample (S1) and the control. The four proteins found to be down-regulated after RSV treatment are contradictory to this kind of contamination, but have to be regarded as a concession to reality. The overall tendencies clearly point towards a contamination according to the pattern of line four of Figure 5-1.

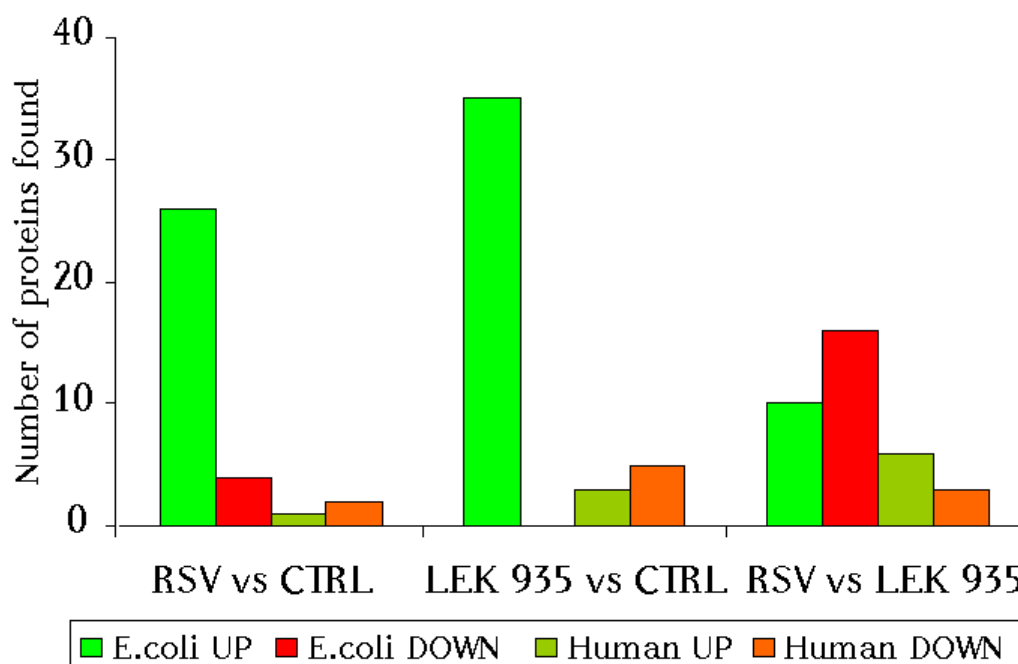


Figure 5-2 Summary of regulations as found in sample 1. Only those proteins that have been identified were concerned.

Following the explanations above, the human proteins found to be up-regulated can be regarded as real regulations. Those proteins found to be down-regulated need a detailed view on their regulation. The same is true for the comparison of RSV and LEK-935, the proteins down-regulated can be regarded as positive hits, while the up-regulated proteins also need a detailed view.

During the nLC-MS analysis, the *E.coli* contamination would not have been detected as the identification is usually restricted to a specific organism to shorten the analysis time. To exclude an effect of the contamination at the level of quantitation, the MS/MS spectra were also applied to a species open search after detection of the contamination during 2D gel electrophoresis. No such contamination was detectable in the microsomal fraction (see Table 5-1). Even if the number of *E.coli* proteins identified in sample 1 was a bit higher (47) than that observed in sample 2 (9), it does not count for an *E. coli* contamination as it was a number comparable to other false positive identifications of bacterial as well as eukaryotic proteins in the open-species search (data not shown). This kind of false positive identifications is usually found in database searches performed with huge amounts of mass spectra, as gained during nLC-MS experiments.

Table 5-1 Number of human and bacterial proteins identified in an open-species search of the MS/MS spectra gained by nLC-MS analysis of the microsomal fraction of primary human hepatocytes.

Number of proteins identified		
	Sample 1	Sample 2
<i>Homo sapiens</i>	755	629
<i>Escherichia coli</i>	47	9

In general, the contamination did not disrupt the analysis but restricted the results of the 2D-PAGE of sample 1 to the top hits. The increased amount of strange proteins in the treated samples reduced the amount of human proteins. So, those spots down-regulated by the treatment needed a detailed view on their regulation, mainly if their regulation was marginal, with a value near the cut-off of 0.5. The spots up-regulated or even appearing in treated samples are top hits as their regulation was not diminished below the threshold by the bacterial contamination.

5.1.3 Nano liquid chromatography coupled to mass spectrometry

5.1.3.1 General applicability

A total of 588 proteins were identified with an average sequence coverage of 11.0 % and an overlap of 63.3 % (372 proteins) between the two human donors investigated. This shows that the reproducibility and comparability of the method regarding different donors is quite high (cf. Figure 4-8 and Figure 4-9). It has to be mentioned that this high correlation was obtained despite the reduced amount of sample load in the case of Sample 2 (90 µg) compared to Sample 1 (280 µg), demonstrating the high sensitivity of the approach. On the other hand, these results reflect the limits of the approach concerning the resolution, since a three times higher sample load leads to an only 1.25 times higher number of proteins identified (Sample 1: 534 proteins, Sample 2: 426 proteins) with the same average sequence coverage. This observation may be explained by the predominance of high abundant peptides in the sample superposing the signals of lower abundant peptides. To overcome this limitation, several possibilities exist. One would be the adaptation of the rules for precursor ion selection in the MALDI-TOF/TOF, excluding those precursor masses already used once or twice for fragmentation from further experiments. Other possibilities are the use of more shallow gradients or the collection of more and smaller fractions in the first and/or second dimension, which could lead to an increase in the number of identified proteins. However, this would proportionally increase the time for analysis, while the adaptation of the rules for precursor ion selection keeps the analysis time as short as possible. It should be mentioned that even the lower (90 µg) amount of sample material lead to a number of proteins identified in the microsomal fraction of mammalian cells which is comparable to other iTRAQ™ related approaches presented in the literature (Glen et al. 2008) where much higher sample loads were used (280 proteins identified by unique peptides from 400 µg sample load compared to 298 proteins identified by unique peptides from 90 µg sample load in our study). As shown in a previously published study (Archakov et al. 2007) the relationship between the number of identified proteins / peptides and the sample concentration has a logarithmic dependence. Thus, it seems that the amount of sample usually loaded onto 2D LC-MS experiments might be located in the saturation region of the curve. Taken together, our results paved the way for further proteomic studies with human

hepatocytes and possibly other cell types which are missing until now due to the low amounts of available sample material.

To evaluate the usefulness of this experimental design for the analysis of the targeted microsomal fraction containing proteins involved in cholesterol homeostasis as well as drug metabolism, the identified proteins were analysed regarding cellular localisation and function.

To check the subcellular localisations of the identified proteins, a manual search of the ExPasy database, supported by bioinformatic analysis of the Gene Ontology database (data not shown), was performed. The high amount of mitochondrial and cytosolic proteins inside the microsomal fraction of a cell lysate as observed here is a common phenomenon, described several times in the literature (Filen et al. 2005; Stevens et al. 2008). Since microsomes are generated during cell lysis by fragmentation of intracellular membranes and their reassembly to smaller lipid-bilayer micelles, they contain many cytoplasmic proteins. The huge amount of ribosomal subunits is due to the ribosomes localised at the rough endoplasmic reticulum, which is part of the microsomal fraction. The composition of the two samples correlates very well with respect to the cellular localisation of the proteins (see Figure 4-8). Additionally, the samples contained a huge amount (50 %) of membrane proteins, which is impossible to obtain using gel-based proteomic approaches.

The proteins identified in the microsomal fraction (see Appendix V and 4.2.2.2) confirm the choice of nLC-MS for the analysis of this fraction. This high amount of membrane proteins would not be detectable by 2D gel electrophoresis.

To further explore which cellular pathways are accessible for biological studies using this experimental design, the function of the identified proteins and their participation in corresponding biological networks was analysed using the ExPasy (Figure 4-9), Gene Ontology (Table 4-3) and KEGG (data not shown) databases. The human samples contained many proteins involved in xenobiotic metabolism and/or lipid/cholesterol metabolism, reflecting the specialisation of hepatocytes. The quite interesting group of cytochromes P450 playing a central role in the xenobiotic and steroid metabolism (reviewed in (Bernhardt 2006) and (Schuster and Bernhardt 2007)) was covered by fourteen members, a number comparable to targeted approaches using SDS-PAGE – LC-MS combinations published during the last years (Galeva et al. 2003; Lane et al. 2004; Jia et al. 2007). Together with the high coverage of distinct xenobiotic/drug

metabolising pathways and the central part of the sterol biosynthesis in the human samples, this opens the possibility for a deeper analysis of these crucial pathways in further proteomic studies.

Finally, since a semi-quantitative proteomic approach was the aim of this study, the applicability of the method to iTRAQ™ labelling and further quantitation was checked. In 95 % - 99 % of a random examination of 2,000 MS/MS spectra the reporter masses were detected, proving the suitability of the approach for semi-quantitative experiments. Moreover, the identification of 60 % of the proteins by at least two unique peptides was proven. To get reliable quantitative data of single proteins in a LC-MS experimental design the use of unique peptides for quantification is strongly recommended (Boehm et al. 2007). So these results furthermore confirmed the practicability of the approach for quantitative studies and have recently been published (Woerner et al. 2009).

5.1.3.2 Bioinformatics

After proving the applicability of the approach for semi-quantitative experiments targeted towards the microsomal fraction of primary human hepatocytes, the semi-quantitative analysis of the MS/MS spectra was evaluated.

Almost no experience on semi-quantitative nLC-MS experiments using the iTRAQ™-label was present at Saarland University at the beginning of this study. But different results for protein identifications using the same data but different algorithms have already been described (Keller et al. 2005). Besides the identification, the quantitation is the second very important part of a proteomic study that is performed by computational aid.

For the software packages available for the analysis of 2D gel images, studies are available comparing their handling, performance and the gained results (Raman et al. 2002; Rosengren et al. 2003; Arora et al. 2005; Kang et al. 2009) as well as their impact on the experimental variance (Maurer et al. 2005; Wheelock and Buckpitt 2005).

The iTRAQ™ label belongs to a quite young generation of semi-quantitative approaches, so the situation is different here. Only a few algorithms are available for iTRAQ™ reporter ion quantitation. Comparison of these algorithms was usually described on defined protein mixtures mixed in defined ratios. The publication introducing iTRACKER (Shadforth et al. 2005) for quantitation of iTRAQ™ reporter ion signals describes a good correlation ($r^2=0.98$) between the results of iTracker and

ProQuant, the quantitation algorithm supplied by Applied Biosystems. The publication introducing Mult-Q (Lin et al. 2006) for iTRAQ™ quantitation did not show any comparison to another quantitation software. In the publication introducing Quant (Boehm et al. 2007), the authors compare ProteinPilot™ (ProQuant algorithm), Mascot 2.2 and Quant on quantitation of a six protein mixture. On this level (low amount of different proteins), they proved the consistency of their results with those gained by ProQuant™ and Mascot 2.2.

In contrast to the studies above, a more recently published study (Lacerda et al. 2008) reported dramatic differences between the results of Peaks and Mascot after the quantitation of a six-protein mixture and a real proteomic sample.

So far only one comparison of software packages available for iTRAQ quantitation has been performed on a real proteomic sample (Lacerda et al. 2008). This comparison revealed major differences in the results gained from these packages. Under defined conditions, most of the other packages finally come to consistent results according to the corresponding publications.

The general consistency of ProteinPilot, Mascot and Quant has been proven by a six protein-mixture (Boehm et al. 2007). So they were chosen for quantitation. This should allow an evaluation of the effect of algorithm choice on detectable regulations in the context of a real proteomic analysis.

ProteinPilot™ 2.0 incorporating the ProGroup™ algorithm is the recommended firmware. It allows identification (Shilov et al. 2007) as well as quantitation. Quantitation is performed on unique peptides only, while identification is “improved” by adding information about the shared peptides, too.

MASCOT 2.0 also allows identification as well as quantitation. In contrast to ProteinPilot, a restriction of the quantitation to unique peptides is not possible in Mascot.

The use of Quant should deliver data about the effect of the restriction to unique peptides as already described by (Boehm et al. 2007). It is a tool not able to identify proteins but to use the Mascot result file (.dat) as source for quantitation.

The consistency between the quantitation results of the three software packages used in this study was unexpectedly low, which led to the suggestion of the detection of false-positive as well as false-negative results. A discrepancy between Mascot and Quant compared to ProteinPilot™ may be likely to be expected due to the differences in data extraction (see 4.2.2.4) and in the identification algorithms. But no systematic

basis for the differences was observable. The parameters of quantitation that can be set in the packages differ from nearly no experimenter-influence for ProteinPilot™ to a variety of parameters that need to be set in Mascot 2.0 as well as Quant. These settings were made as similar as possible (see 3.8.3). Nevertheless, some of the differences observed may be related to different settings of the quantitation algorithms.

As reported by (Boehm et al. 2007), the three packages correlate well under defined conditions, like a 1:1 mix of a six-protein mixture. This was proven in this study, as no big differences were observed at the level of internal controls. The averaged values ranged from 0.99 to 1.01, the corresponding standard deviations from 0.10 to 0.13. Both values are absolutely consistent with those reported in the literature (Ross et al. 2004; Boehm et al. 2007; Wiese 2007).

The number of proteins found to be regulated varied between the three software packages. The averaged correlation between the results was about 36.8 %. It was shown that this difference is, to some extent, related to differences in identification (either not or only insufficiently identified in one of the packages). About 39.5 % of the differences observed were due to differences in identification processes while the majority of 60.5 % was caused by different quantitation results. In fact, the borderlines between these two criteria blur, as the number of identified peptides finally affects the number of peptides used for quantitation.

Another factor that has to be mentioned is the cut-off value set to detect regulated proteins. The criteria for the detection of regulated proteins developed and applied during this nLC-MS approach are highly stringent, which is true for those criteria used in the gel-based approach, too. This high stringency was chosen with the knowledge about the high risk of false negatives. Decision was made to accept a possibly high number of false negatives to avoid, if procurable, any false positive hit. False positives may dramatically interfere the following ranking of the hits into the biological background, while false negatives causes gaps which are, in the case of affected interesting pathways, easy to investigate by further studies using Western blots etc..

Nevertheless, this high stringency may further strengthen the differences between the software packages as the cut-off was set for each package separately.

To summarise, a dramatic effect was observed for the choice of software used for quantitation on the outcome of semi-quantitative nLC-MS experiments. These results underline the fundamental and indispensable role of bioinformatics in proteomic approaches.

5.1.4 Summary

Both approaches, nLC-MS and 2D-PAGE, were successfully applied for the proteomic analysis of primary human hepatocytes. The 2D-PAGE was used to analyse cytosolic proteins while the protein content of the microsomal fraction was determined by nLC-MS (see Appendix V). A set of 44 proteins was found to be regulated after treatment with one of the cholesterol lowering agents, rosuvastatin or LEK-935 by the combination of both approaches (see below).

Despite the problems which occurred during this study, both the general experimental setup as well as the choice of 2D-PAGE and nLC-MS were proven for the analysis of primary human hepatocytes. Through the addition of the nLC-MS to the analytical setup, the targeted cholesterol related pathways were covered, while the 2D-PAGE revealed information about the soluble proteins in the cytosol, providing metabolic precursors for cholesterol biosynthesis (see below).

Furthermore, the two dimensional gel electrophoresis delivered information about the sample status, like protein degradation and *E. coli* contamination, that are usually not visible during a nLC-MS approach.

5.2 The effects of cholesterol lowering agents

5.2.1 The effects of rosuvastatin on the proteome of primary human hepatocytes

This study describes for the first time the effects of rosuvastatin on the proteome of primary human hepatocytes. The examination of the cytosolic and microsomal fraction of sample 1 treated with rosuvastatin revealed eleven proteins present in higher amounts than in the untreated samples, while the amounts of three proteins were found to be reduced. For sample 2, the amounts of 24 proteins were found to be significantly altered. Of these 24 proteins again the majority (19) was found in increased amounts.

5.2.1.1 Cholesterol related proteins

For sample 1, five of the proteins present in higher amounts could be somehow related to a possible compensating mechanism of the cell to enhance the cholesterol synthesis.

The ATP citrate lyase (ACLY), found to be up-regulated, plays a crucial role for the synthesis of cytoplasmic acetyl-CoA (Wang et al. 2009) that is especially used by the cytoplasmic HMG-CoA synthase 1. This protein was found to be more than three times up-regulated and catalyses the synthesis of HMG-CoA.

The acetyl-CoA produced by ACLY could also be used for fatty acid synthesis. But the increased amount of long-chain fatty acid coA ligase (ACSL) points towards a down-regulation of this metabolic pathway. The ACSL produces long-chain fatty acyl CoAs that have an inhibitory effect on the acetyl-CoA carboxylase, catalysing the initiation step of *de novo* fatty acid synthesis (Goodridg.Ag 1973b, 1973a; Hardie 1989).

This inhibitory effect of the long-chain fatty acyl-CoAs may only be a side-effect of the beta-oxidation of fatty acids started by the ACSL (Schoonjans et al. 1995). The up-regulation of this pathway that leads to acetyl-CoA or acetoacetyl-CoA, has already been described for lovastatin (Singh et al. 1998). The finding of up-regulated ACSL may explain this previously described effect. A correlation between the expression level and the activity of all three proteins mentioned so far has previously been described (Spence and Pitot 1982; Mehrabian et al. 1986; Schoonjans et al. 1993).

Beside these enzymes delivering precursor molecules or acting at quite early steps of the mevalonate pathway, in sample 1, two more enzymes involved in the sterol-targeted branch of the pathway were found in higher amounts. The squalene synthase (FDFT), a key enzyme for the metabolite flow into the sterol branch of the mevalonate pathway (Do et al. 2009) was detected as well as the lanosterol 14-demethylase (CYP51).

For the estradiol 17-beta dehydrogenase 12 (DHB12), on the first sight, an effect is expected on the formation of estrogens. The 17-beta dehydrogenases catalyses the transformation of estrone to estradiol, which exhibits besides its function as sexual hormone also ROS protective functionality (Wang et al. 2001). Nevertheless, the (DHB12) was shown to be involved in fatty acid elongation, acting as a reductase of long-chain fatty acyl-CoA as well as 3-keto-acyl-CoA (Moon and Horton 2003). Furthermore, only a poor correlation of the enzyme to estradiol levels is reported (Nagasaki et al. 2009). So, in addition to the beta-oxidation of the fatty acids activated by ACSL, they may also be elongated, leading to a set of different long-chain fatty acyl-CoAs involved in different regulation mechanisms, reviewed in (Faergeman and Knudsen 1997).

As already shown for HMCS1, FDFT1, CYP51 and ACLY (Horton et al. 2002), the expression of DHB12 may also be regulated, at least in parts, by SREBP2, even if the regulation is not as strong as reported for the other enzymes (Moon et al. 2003). In contrast to SREBP1 that activates *de novo* fatty acid synthesis, SREBP2 is known to be mainly responsible for the regulation of cholesterologenic enzymes (Horton et al. 2002). In sample 2 two proteins related to cholesterol biosynthesis were found in increased amounts. The cytoplasmic isocitrate dehydrogenase plays a key role in lipogenesis by supplying the NADPH for fatty acid and cholesterol biosynthesis (Shechter et al. 2003) (Koh et al. 2004). Again, the HMG-CoA synthase 1 was found in increased amounts, necessary for the production of HMG from acetyl-CoA and acetoacetyl-CoA. An indication for activated beta-oxidation of fatty acids in sample 2 is given by the increased amounts of mitochondrial 3,2 trans-enoyl-CoA isomerase (D3D2). This enzyme catalyses a key-step of beta-oxidation of unsaturated fatty acids in both compartments peroxisomes (Hiltunen et al. 1996) as well as mitochondria (Janssen et al. 1994) (Stoffel et al. 1994). Another indication for an enhanced beta-oxidation may be the increased amount of carbonic anhydrase 2 (CAH2), catalysing the formation of

bicarbonate from carbon dioxide, which is a side-product of beta oxidation and has to be buffered in the bicarbonate system.

Thus, enzymes involved into the biosynthesis of cholesterol and acting at key positions of these pathways were found to be up-regulated in both samples. For sample 1, a regulation via the SRBP2 can be suggested but that was not found for sample 2. Furthermore, the findings of ACSL, D3D2 and CAH2 point towards an increased beta-oxidation in both samples.

In addition, proteins involved in cholesterol transport were found to be regulated in both samples. The members of the apolipoprotein C family (ApoC) are protein constituents of chylomicrons, VLDL and HDL particles (Jong et al. 1999). The increased amounts of Apo CIII and Apo CI in sample 1 may be related to their role as important modulators of lipoprotein metabolism, as reviewed in (Shachter 2001). They exhibit inhibitory effects on the clearance of plasma lipoprotein particles. This way, their presence in the plasma is elongated and the supply of cholesterol and fatty acids to extrahepatic tissues is guaranteed. Therefore, the increased expression may directly be related to a decrease in hepatic clearance of lipoprotein particles, securing the supply of triglycerides and cholesterol to extrahepatic tissues. On the other hand, (Ooi et al. 2008) reported a decreased production and increased catabolism of VLDL Apo-CIII in the metabolic syndrome after rosuvastatin treatment. So the question comes up as to whether the increased amount of Apo CI and Apo CIII is caused by an enhanced expression, a decreased exocytosis or an increased endocytosis leading to their accumulation in the ER. This question is further strengthened by the knowledge about the different actions of the two sub-types (CI and CIII) as well as their involvement in VLDL, chylomicrons but also HDL particles. For Apo CI for example (de Haan et al. 2008) suppose an elevating effect on plasma HDL levels in vivo, suggesting an enhanced reverse cholesterol transport.

In sample 2, the beta-chain of mitochondrial ATP synthase (ATPB) was found in increased amounts. This protein has recently been shown to be a high affinity receptor of apolipoprotein A1 and apolipoprotein E (Martinez et al. 2003). Thereby it triggers the endocytosis of HDL particles. The second protein of sample 2 involved into cholesterol transport processes is the GTP-binding protein SAR1b, required for the intracellular transport of chylomicrons and VLDL (Shoulders et al. 2004). Mutations of this protein are the reason for Anderson's disease that has recently been shown to be related to myolysis (Silvain et al. 2008). This protein may serve as a starting point for

investigations targeted towards the rare side-effect of rhabdomyolysis caused by statins. In sample 2, a protein among those found in reduced amounts is also involved in cholesterol transport processes. The 78 kDa glucose-regulated protein protects against oxidative stress and apoptosis (Yu et al. 1999) but beside this effect, it was also shown to catalyse the rate-limiting step in LDL maturation (Jorgensen et al. 2000).

5.2.1.2 Proteins related to side-products of the mevalonate pathway

The succinate dehydrogenase cytochrome b560 subunit (C560) is a mono-heme cytochrome b involved in complex II of the respiratory chain, responsible for the electron transfer from succinate to ubiquinone. In sample 1 it was found in increased amounts after RSV treatment. This may be a kind of compensation for a possibly reduced amount of ubiquinone, one of the end-products of the non-sterol branch of the mevalonate pathway (Goldstein et al. 1990). In addition, the enhanced beta-oxidation produces electrons that are normally directed into the ubiquinone pool of the respiratory chain.

The “side-products” of the mevalonate pathway seem to be even more affected by the treatment through the increased expression of the FDFT in sample 1, directing the produced farnesyl-pyrophosphate towards the sterol-branch.

Dolichol as another product of the non-sterol branch is normally used for glycosylation reactions, formation of GPI anchors and so on. The mannose-P-dolichol utilisation defect protein 1 is a key protein of glycosylation by catalysing the first step (Anand et al. 2001). Its increased amount may reflect the need of the cells for mannose-P-dolichol that is not present, due to the statin treatment and the increased FDFT. No proteins were found in sample 2 that could be related to the side-products of the mevalonate pathway.

5.2.1.3 Energy metabolism

In sample 1, energy metabolism may be affected by the increased amounts of C560 as well as the decreased amount of phosphoglucomutase 1 (PGM1). The PGM1 catalyses the conversion of glucose-1-phosphate to glucose-6-phosphate. This step is necessary to use the glucose-1-phosphate, gained during glycogen decomposition, for glycolysis. Its down-regulation leads to the impression of a reduced use of glycogen as energy source. This is in line with the enhanced beta-oxidation and the high amount of

acetyl-CoA and most probably also increased amount of keton bodies through the block of the HMG-CoA reductase but high amounts of HMG-CoA synthase.

In sample 2, four proteins were found to be involved in energy metabolism. The voltage-dependent anion-selective channel 2 (VDAC2) found in increased amounts mediates the flow of ATP through the mitochondrial membrane and thereby plays a crucial role in energy metabolism (Rostovtseva and Colombini 1997). In addition, the increased amount of ATPB may also point towards an increased need for ATP as energy source and the increased amount of glyceraldehyde-3-phosphate dehydrogenase (GAPDH) towards an increase in glycolysis. Another part of the energy metabolism was affected by the increased amounts of ketohexokinase involved in fructose metabolism (Heinz et al. 1968). A second enzyme of the fructose metabolism, the fructose-bisphosphate aldolase B (ALDOB), responsible for the metabolism of fructose 1-phosphate (Lebherz and Rutter 1969) was found in decreased amounts in sample 2.

5.2.1.4 ROS protection and inflammation

The effects towards cholesterol and fatty acids are in sample 2 superposed by increased amounts of proteins somehow involved in the protection against oxidative stress and inflammatory effects. Besides the glycolytic activity of GAPDH, different biological activities in apoptosis and proliferation of hepatocytes according to its subcellular localisation are described (Sirover 1999) (Barbini et al. 2007). Among others, it is involved in tubulin bundling (Sirover 1999), interacts with glutathione (Sirover 1999) and it shows a hepatoprotective effect against oxidative stress (Kuo and Slivka 1994).

Two of the proteins found in increased amounts are directly related to the protection against oxidative stress. The glutathione-S-transferase omega 1 is not involved in xenobiotic detoxification as other glutathione transferases. But it shows a functionality comparable to glutaredoxins and may play a critical role in protection against oxidative stress by restoring enzymatic activity formerly blocked by S-thiol formation (Board et al. 2000). Furthermore, it was shown to be somehow involved in cytokine signalling and apoptosis (Laliberte et al. 2003). The second enzyme is the peroxidoredoxin 6, which is reduced by glutathione and shows at the neutral pH of the cytosol a protective effect against oxidative stress (Manevich et al. 2009). In

addition the GRP78 was also shown to exhibit ROS protective effects, but found in decreased amounts in sample 2.

A possibly enhanced oxidative stress may be caused by the increased amount of Voltage-dependent anion-selective channel protein 2 (VDAC2_HUMAN) that controls the release of superoxide anion from mitochondria to the cytosol (Han et al. 2003). Moreover, the VDAC proteins affect the activity of the copper-zinc superoxide dismutase (SODC) (Budzinska et al. 2007). A deletion of the VADC was shown to decrease the SODC activity (Budzinska et al. 2007). This suggests an increased SODC activity after an increased amount of VDAC. This, in turn, may be part of the explanation of a decreased amount of SODC as a kind of compensation mechanism, after RSV treatment as observed for sample 2. Either, the increased activity of SODC leads to a decrease in its expression level or the increased amount of VDAC2 leads to increased import of SODC from the cytosol towards the mitochondrial inter-membrane space. Both reactions would reduce the amount of SODC that can be found in the cytoplasm.

The N(G),N(G)-dimethylarginine dimethylaminohydrolase 1 (DDAH1) increases basal levels of vascular NO and thereby protects against endothelial dysfunction induced by ADMA (Dayoub et al. 2008). ADMA was shown to be involved in the inflammatory effect of angiotensin II (Chen et al. 2007) and has negative effects on the cardiovascular system (Achan et al. 2003) counterbalanced by DDAH1. So the up-regulation of DDAH1 may point towards the so called pleiotropic effects of statins, acting beside the low levels of cholesterol, like mitigating the cardiovascular effect of angiotensin II as described for pravastatin (Straznický et al. 1995). Moreover, (Smirnova et al. 2004) reported an up-regulation of lectin-like oxidized low-density lipoprotein receptor by nitric oxide deficiency, caused by ADMA and (Atzler et al. 2009) showed a reduced plaque-formation in ApoE deficient mice by DDAH1 overexpression. So, the DDAH1 may play a critical role in the protective effects of statins towards the cardiovascular system.

Another protein discussed in the context of inflammatory processes in other proteomic studies (Vivanco et al. 2005) is the protein disulfide isomerase A3 (PDIA3) also found in increased amounts in this study. Its relation to inflammatory diseases could not be proven, as the enzyme used for the study in which it is shown to suppress the NF-kappaB, a proinflammatory signalling molecule (Higuchi et al. 2004) is the murine homologue to PDIA1, not PDIA3. So an inflammatory action of PDIA3 is

speculative. Nevertheless, its localisation was shown to be different from the ER and its function different from the “normal” action of disulfide isomerases (Turano Carlo et al. 2002). Furthermore, (Zhou et al. 2008) could correlate its downregulation in sepsis with increases in the cytokine expression and release.

The increased amounts of fibrinogen alpha and beta may also point towards a kind of inflammatory reaction as they belong to the group of acute phase proteins (Redman and Xia 2000). In contrast, the assembly of fibrin fibers takes place in the ER (Redman et al. 2000) so its finding may also point towards an retention mechanism, prohibiting the export of fibrin into the plasma. The fibrinogen gamma, coordinately expressed with the alpha and beta chain may not be found due to the restrictive conditions of the true positive criteria.

5.2.1.5 Cytoskeleton

In sample 1 actin was found to be down-regulated, which may be explained by a study of (Endres and Laufs 2004). They reported that statins block Rho which in turn leads to a disruption of the actin cytoskeleton. At the same time, two of the proteins found in increased amounts in sample 2 are related to the cytoskeleton. The first one is tubulin, as a part of the microtubules (Desai and Mitchison 1997). The second one is radixin as part of the anchor structures that connect the cytoskeleton to the plasma membrane (Sato et al. 1992).

5.2.1.6 Other / Unknown functions

Nothing is known about the functionality of the eleventh up-regulated protein found in sample 1, the transmembrane protein 56. The finding of a down-regulated ribosomal protein in sample 1 was quite surprising as ribosomal proteins are normally regarded as house-keeping genes, not or only little effected in their expression level.

In sample 2 the mitochondrial dicarboxylate carrier (DIC) was found in increased amounts. While (Lin et al. 2005) describes an increased ROS production and hyperpolarisation of the mitochondrial membrane after DIC overexpression, (Zhong et al. 2008) describes a ROS protective effect due to its partial involvement in glutathione transport into the rat liver mitochondria. The protein is also involved in gluceroneogenesis (Reshef et al. 2003), its mRNA is induced by fatty acids (Reshef et al. 2003) while its activity is inhibited by long-chain fatty acyl CoAs (Ventura et al. 2005) and the enzyme itself mediates the protonotrophic action of long chain fatty

acids (Wieckowski and Wojtczak 1997). Moreover, the over-expression of DIC also led to an increased up-take of succinate which is directly fed into complex II, the rate-limiting step of the respiratory chain (Lin et al. 2005). So a final conclusion about its role cannot be drawn but it remains a very interesting protein whose up-regulation should be kept in mind. The eukaryotic initiation factor 4A found to be down-regulated in sample 2 exhibits RNA helicase activity. At the last, the retinal dehydrogenase 1 metabolises 4-hydroxynonenal (Esterbauer et al. 1985) a product formed during lipid peroxidation.

5.2.1.7 Summary

At first sight, there was almost no correlation between the proteins found to be altered after RSV treatment in sample 1 and 2. Only HMG-CoA synthase 1 was found in both samples regulated similarly. This regulation was proven in four out of four samples of the RT-PCR validation experiments. The regulation is not surprising as this protein catalyses the first and thereby one of the most important steps of the mevalonate pathway, the formation of HMG-CoA. Its product is the substrate of the HMG-CoA reductase, catalysing the rate-limiting step of this pathway which is blocked by rosuvastatin. So its up-regulation is obviously a compensation mechanism of the hepatocytes for the block of the mevalonate pathway that has already been described. There was no correlation among the 35 remaining proteins. But by setting the proteins into the cellular context, the results switched to a higher degree of correlation as the proteins themselves differed but the cellular pathways and the direction of regulation correspond with each other.

In both samples indication is given for an up-regulation of the mevalonate pathway, accompanied by an enhanced beta-oxidation of fatty acids and changes in the cholesterol and lipid transport processes. The cellular metabolism seems to be driven towards a compensation of the blocked cholesterol synthesis.

The correlation of the samples may be even higher but in sample 2 a situation of nearly de-regulation in the protein content was observed in the microsomal samples. This may superpose the effects observed in sample 1. This effect of superposing could be forced by the criteria of evidence in the nLC-MS experiments chosen by the experimenter. The global changes in the protein amounts led to a high standard deviation that resulted in quite restrictive exclusion criteria. These led to the detection

of the top hits of changed proteins only. At the same time those proteins with minor changes remain undetectable below the threshold.

The reason for the massive de-regulation in sample 2 remains unknown, as no clear conclusion can be drawn from the proteins found in altered amounts. Indication is given for an increase in oxidative stress of the cells which is counterbalanced by an increased expression of protective enzymes. A quite interesting player is the DDAH1 involved in NO signaling and the maintenance of endothelial function. It may point towards the so called pleiotropic effects of statins that are discussed in the literature to work in addition to cholesterol lowering (LaRosa 2001; Liao 2002; Liao et al. 2005; Corsini et al. 2007).

The way of proteomic data interpretation needs to be discussed briefly by looking at the apolipoproteins as well as the fibrinogen alpha and beta found in increased amounts in the ER of sample 2 and sample 1, respectively. These proteins belong to the group of secreted proteins, processed in the ER and later released into the plasma. A semi-quantitative proteomic study analyses the amount of proteins. In general, this changed amount of proteins is correlated to gene expression or protein degradation as a reaction of the cell to changed circumstances. In the case of sub-cellular proteomes as well as secreted proteins, an additional fact needs to be kept in mind: retention or enhanced secretion could also take place, leading to increased/decreased amounts of the proteins in the cells (or compartments) while their plasma levels (or levels in other compartments) decreases/increases. This would explain the finding of fibrinogen but also of some of the apolipoproteins. Moreover, the finding of reduced amounts of 78GRP underlines this assumption as it is a protein catalysing the rate-limiting step of VLDL maturation. Here, one may argue that the down-regulation of this protein is energetically worthwhile for the cell by maintaining the normal expression levels of the other proteins involved.

To summarise, the effect of RSV is in sample 1 mainly focussed on cholesterol and fatty acid metabolism and transport, accompanied by effects on the cytoskeleton and some proteins about which not enough is known to draw a clear picture. In sample 2, the eye-catching effects are on the side of oxidative stress response and inflammatory reactions but there are obviously also effects on cholesterol and fatty acid metabolism and transport as well as the cytoskeleton.

The observed effects on the protein level are on one side easily ranked into already described effects of statins but also give some intentions about possibly starting points

for further investigations of not yet explainable effects (like the DDAH1 for endothelial function and the SAR1b for relations to myolysis, for example).

5.2.2 The effects of LEK-935 on the proteome of primary human hepatocytes

The treatment of sample 1 with LEK-935 led to the detection of eight proteins in significantly altered amounts. Among these proteins three were found in elevated amounts and five in reduced amounts compared to the control.

All of the proteins detected in altered amounts in sample 2 had also been found after RSV treatment of sample 2.

These proteins have already been discussed above, so they are not included in the detailed discussion presented below.

5.2.2.1 Cholesterol related proteins

No protein directly involved in the cholesterol biosynthetic pathway has been found in altered amounts after LEK-935 treatment of sample 1. Two of the found proteins are related to cholesterol transport processes. Serum-albumin, found in reduced amounts, is the major protein in the plasma and binds fatty acids (Spector 1975) as well as steroid hormones (Pardridge and Mietus 1979). It thereby serves as a transporter of these molecules. Its reduced amount in the cytoplasm may be an indication for an enhanced secretion rate to compensate for decreased amount of circulating VLDL particles.

Endoplasmin (ENPL) found in decreased amounts has been shown to be co-ordinately regulated with GRP78 (Chang et al. 1989). GRP78 has been found to be reduced after RSV treatment of sample 2 and is involved in VLDL maturation (see 5.2.1.1). Even if an involvement of the ENPL in VLDL maturation is not described yet in the literature, the co-ordinate expression of the two proteins may indicate a correlation between their functionality.

5.2.2.2 Energy metabolism

The only protein involved in energy metabolism found in altered amounts in sample 1 is the GAPDH. It has also been found in elevated amounts after RSV treatment in sample 2 (see 5.2.1.3). In general, GAPDH is often found by proteomic studies to be

regulated, as discussed in (Petрак et al. 2008). Its central role in the energy metabolism and the different other processes in which it is involved (see 5.2.1.4 and 5.2.2.3) may turn it into a favourable target for regulation processes.

5.2.2.3 ROS protection and inflammation

Three of the proteins found in altered amounts in sample 1 are related to ROS protection or inflammation. Annexin A5 (ANXA5) found in elevated amounts is used as an apoptosis analysis tool as it binds to phosphatidyl-serine, present at the outer cellular surface only during apoptosis (van Engeland et al. 1998). This binding may explain its anticoagulant (Thiagarajan and Tait 1990) and anti-inflammatory effects (Reutelingsperger and vanHeerde 1997). As already mentioned above, the GAPDH was found in elevated amounts. This finding could be related to its protective effect against oxidative stress (Kuo et al. 1994) but it also displays other functionalities in hepatocytes (Sirover 1999) (Barbini et al. 2007). The mitochondrial isocitrate dehydrogenase [NADP] (IDHP_HUMAN) was also found in elevated amounts and is a major NADPH producer in Mitochondria whose up-regulation has already been shown to enhance ROS protection (Jo et al. 2001).

5.2.2.4 Cytoskeleton

Both actin and radixin were found in reduced amounts. They are involved in the cytoskeleton (Bretscher 1991) (Sato et al. 1992) but also in some signalling processes (Tsukita and Yonemura 1997).

5.2.2.5 Other / Unknown functionalities

For the nicotinamide N-methyltransferase (NNMT) found in reduced amounts, a direct correlation between the amount of protein and its activity has been shown (Smith et al. 1998). A reduced activity of the NNMT could result in a decrease in nicotinamide excretion. This would lead to an increased NAD or NADP synthesis, the latter necessary for cholesterol biosynthesis. As a second product of the reaction catalysed by NNMT, homocysteine is formed. (Souto et al. 2005) suggested NNMT as the major source of plasma homocysteine. Elevated plasma levels of homocysteine are associated with an increased risk of cardiovascular diseases. For simvastatin a decrease in plasma homocysteine has already been described (Luftjohann et al. 2001). This may be an effect of a reduced amount of NNMT. In addition, an increase in NNMT

expression along with atherosclerosis was recently described (Mateuszuk et al. 2009) so the decreased amount found here may exhibit atheroprotective effects.

5.2.2.6 Summary

After LEK-935 treatment, the mevalonate pathway was not covered by any of the proteins found in altered amounts, neither in sample 1 nor sample 2. This can, in parts, be explained by the analysis of the cytosolic but not the microsomal fraction. Nevertheless, after RSV treatment, some of the proteins involved in the mevalonate pathway (like HMG-CoA synthase) were found in the cytosolic fraction. Thus, at least a hint is given that the mevalonate pathway itself may not be affected by blocking CYP51A1 as it is affected by a block of the HMG-CoA reductase.

The proteins found to be affected in sample 1 are involved in general energetic metabolism, oxidative stress response and inflammation, the cytoskeleton and some transport processes, also including fatty acids and steroids. Nevertheless, a clear picture cannot be drawn due to the microsomal fraction which has not been analysed and of which the main information about the cholesterol and fatty acid related pathways were gained after RSV treatment.

The proteins affected in sample 2 are also involved in general energetic metabolism, the cytoskeleton, oxidative stress protection and inflammation. In addition, the enhanced amounts of D3D2 indicate an increased beta-oxidation in sample 2.

To summarise, analysing the cytosolic fraction only led to results that cannot be ranked in the same way as it was possible for the results gained by the additional analysis of the microsomal fraction after RSV treatment. This underlines the necessity of a complete analysis, including all sub-proteomes to come to a clear picture.

5.3 Summary and outlook

This study describes for the first time the effects of RSV and LEK-935 on the proteome of primary human hepatocytes. The analysis was performed on two independent cultures of primary human hepatocytes. The focus was set on the proteome of the cytosolic and the microsomal fraction of these cells.

During the present study, more than 100 IEFs and SDS-PAGEs of the cytosolic fraction were run. About 500 spots were cut off the gels, applied to in-gel digestion and analysed by MALDI-TOF/TOF. Two runs of the RP x IP-RP HPLC setup were performed to analyse the microsomal fraction. These resulted in 33 MALDI targets with about 1570 spots each, that were measured by MALDI-TOF/TOF. Via bioinformatical analyses of the experiments a sum of 44 proteins was found to be altered in their amounts after the two treatments.

Treating the cells with RSV led to an increase in proteins involved in cholesterol biosynthesis, cholesterol transport and fatty acid beta-oxidation. In addition, some proteins involved in oxidative stress response and the cytoskeleton were found. Except for the elevated amounts of HMG-CoA synthase, no correlation was observed between the two samples. By ranking the proteins into the cellular pathways affected, the two samples reacted more similar to the RSV treatment. This observation may be a reflection of the big inter-individual differences of human beings in their response to administered drugs. At the same time it shows that, even if the proteins affected differ, the cellular pathways and thereby the real response of the cells does not differ that much.

The observed differences on the protein level could also be the result of different ways of analysis, as the samples were in a different freeze-thawing status prior to 2D gel electrophoresis and the amount of protein applied to nLC-MS also differed. This has to be kept in mind, also for the interpretation of the LEK-935 treated samples. Nevertheless, the RT-PCR validation of some of the proteins explicitly underlines the huge differences between samples derived from different donors.

The usefulness of the analysis of the microsomal fraction by nLC-MS to trigger the pathways in the focus of interest is getting obvious by looking at the results gained by 2D-PAGE of the cytosolic fraction only. The analysis of the cytosolic fraction gave impressions about the changes taking place that were complemented and strengthened by the analysis of the microsomal fraction. This fraction enabled a

deeper insight into the cholesterol biosynthesis and transport due to the important role of the ER in transport processes and the cholesterol biosynthesis. This insight would not have been possible in the way achieved by the use of 2D-PAGE but was strengthened by the choice of nLC-MS for the analysis of membrane proteins, too. This way, the sub-fractionation process, the use of appropriate analysis methods and merging of the gained results led to clearer results about the processes taking place. In accordance with these findings, the stored mitochondrial and nuclear fractions need to be analysed, too, to complement the picture. The mitochondria as second important compartment in cholesterol biosynthesis and degradation are a hot spot for an analysis of these pathways. The nuclear fraction could deliver information about changed amounts of transcription factors etc. that can be used for a discussion of the signalling pathways affected. In addition, it would be interesting to specifically analyse proteins that were missed during this study as they fall outside the frames given by the experimental setups but that are known to be regulated by one or another transcription factor.

6 References

- Achan, V., M. Broadhead, M. Malaki, G. Whitley, J. Leiper, R. MacAllister and P. Vallance (2003). "Asymmetric dimethylarginine causes hypertension and cardiac dysfunction in humans and is actively metabolized by dimethylarginine dimethylaminohydrolase." Arteriosclerosis Thrombosis and Vascular Biology **23**(8): 1455-1459.
- Aebersold, R. and M. Mann (2003). "Mass spectrometry-based proteomics." Nature **422**(6928): 198-207.
- Alpert, A. J. and P. C. Andrews (1988). "Cation-Exchange Chromatography of Peptides on Poly(2-Sulfoethyl Aspartamide)-Silica." Journal of Chromatography **443**: 85-96.
- Anand, M., J. S. Rush, S. Ray, M. A. Doucey, J. Weik, F. E. Ware, J. Hofsteenge, C. J. Waechter and M. A. Lehrman (2001). "Requirement of the Lec35 gene for all known classes of monosaccharide-P-dolichol-dependent glycosyltransferase reactions in mammals." Molecular Biology of the Cell **12**(2): 487-501.
- Anchordoquy, T. J. and J. F. Carpenter (1996). "Polymers protect lactate dehydrogenase during freeze-drying by inhibiting dissociation in the frozen state." Archives of Biochemistry and Biophysics **332**(2): 231-238.
- Archakov, A. I., Y. D. Ivanov, A. V. Lisitsa and V. G. Zgoda (2007). "AFM fishing nanotechnology is the way to reverse the Avogadro number in proteomics." Proteomics **7**(1): 4-9.
- Arora, P. S., H. Yamagiwa, A. Srivastava, M. E. Bolander and U. Sarkar (2005). "Comparative evaluation of two two-dimensional gel electrophoresis image analysis software applications using synovial fluids from patients with joint disease." Journal of Orthopaedic Science **10**(2): 160-166.
- Atzler, D., J. Jacobi, J. Strobel, N. Cordasic, M. Arend, E. Schwedhelm, R. H. Boger, K. F. Hilgers and R. Maas (2009). "Effect of enhanced monomethylarginine metabolism by human dimethylarginine dimethylaminohydrolase 1 on plaque formation in ApoE-deficient mice." Naunyn-Schmiedeberg's Archives of Pharmacology **379**: 493.
- Aviram, M., G. Dankner, U. Cogan, E. Hochgraf and J. G. Brook (1992). "Lovastatin Inhibits Low-Density-Lipoprotein Oxidation and Alters Its Fluidity and Uptake by Macrophages - Invitro and Invivo Studies." Metabolism-Clinical and Experimental **41**(3): 229-235.
- Barbini, L., J. Rodriguez, F. Dominguez and F. Vega (2007). "Glyceraldehyde-3-phosphate dehydrogenase exerts different biologic activities in apoptotic and proliferating hepatocytes according to its subcellular localization." Molecular and Cellular Biochemistry **300**(1-2): 19-28.

- Bazer, F. W., R. M. Roberts and W. W. Thatcher (1979). "Actions of hormones on the uterus and effect on conceptus development." J Anim Sci **49 Suppl 2**.
- Bell, R. M. and R. A. Coleman (1980). "Enzymes of Glycerolipid Synthesis in Eukaryotes." Annual Review of Biochemistry **49**: 459-487.
- Bernhardt, R. (2006). "Cytochromes P450 as versatile biocatalysts." Journal of Biotechnology **124**(1): 128-145.
- Board, P. G., M. Coggan, G. Chelvanayagam, S. Easteal, L. S. Jermiin, G. K. Schulte, D. E. Danley, L. R. Hoth, M. C. Griffor, A. V. Kamath, M. H. Rosner, B. A. Chrnyk, D. E. Perregaux, C. A. Gabel, K. F. Geoghegan and J. Pandit (2000). "Identification, characterization, and crystal structure of the omega class glutathione transferases." Journal of Biological Chemistry **275**(32): 24798-24806.
- Boehm, A. M., S. Putz, D. Altenhofer, A. Sickmann and M. Falk (2007). "Precise protein quantification based on peptide quantification using iTRAQ (TM)." Bmc Bioinformatics **8**.
- Boehmer, S., C. Carapito, B. Wilzewski, E. Leize, A. Van Dorsselaer and R. Bernhardt (2006). "Analysis of aldosterone-induced differential receptor-independent protein patterns using 2D-electrophoresis and mass spectrometry." Biological Chemistry **387**(7): 917-929.
- Bondy, P. K., D. F. James and B. W. Farrar (1949). "Studies of the Role of the Liver in Human Carbohydrate Metabolism by the Venous Catheter Technic .1. Normal Subjects under Fasting Conditions and Following the Injection of Glucose." Journal of Clinical Investigation **28**(2): 238-244.
- Bretscher, A. (1991). "Microfilament structure and function in the cortical cytoskeleton." Annu Rev Cell Biol **7**.
- Brosnan, J. T. (2000). "Glutamate, at the interface between amino acid and carbohydrate metabolism." J Nutr **130**(4S Suppl).
- Brown, M. S. and J. L. Goldstein (1980). "Multivalent Feedback-Regulation of Hmg Coa Reductase, a Control Mechanism Coordinating Isoprenoid Synthesis and Cell-Growth." Journal of Lipid Research **21**(5): 505-517.
- Brown, M. S. and J. L. Goldstein (1986). "A Receptor-Mediated Pathway for Cholesterol Homeostasis." Science **232**(4746): 34-47.
- Brown, M. S., P. T. Kovanen and J. L. Goldstein (1981). "Regulation of Plasma-Cholesterol by Lipoprotein Receptors." Science **212**(4495): 628-635.
- Budzinska, M., H. Galganska, M. Wojtkowska, O. Stobienia and H. Kmita (2007). "Effects of VDAC isoforms on CuZn-superoxide dismutase activity in the intermembrane space of Saccharomyces cerevisiae mitochondria." Biochemical and Biophysical Research Communications **357**(4): 1065-1070.

- Cao, E. H., Y. H. Chen, Z. F. Cui and P. R. Foster (2003). "Effect of freezing and thawing rates on denaturation of proteins in aqueous solutions." *Biotechnology and Bioengineering* **82**(6): 684-690.
- Castelli, W. P. (1984). "Epidemiology of Coronary Heart-Disease - the Framingham-Study." *American Journal of Medicine* **76**(2A): 4-12.
- Chamrad, D. C., G. Korting, K. Stuhler, H. E. Meyer, J. Klose and M. Bluggel (2004). "Evaluation of algorithms for protein identification from sequence databases using mass spectrometry data." *Proteomics* **4**(3): 619-628.
- Chang, S. C., A. E. Erwin and A. S. Lee (1989). "Glucose-Regulated Protein (Grp94 and Grp78) Genes Share Common Regulatory Domains and Are Coordinately Regulated by Common Trans-Acting Factors." *Molecular and Cellular Biology* **9**(5): 2153-2162.
- Charlton-Menys, V. and P. N. Durrington (2007). "Squalene synthase inhibitors: Clinical pharmacology and cholesterol-lowering potential." *Drugs* **67**(1): 11-16.
- Chen, M. F., X. M. Xie, T. L. Yang, Y. J. Wang, X. H. Zhang, B. L. Luo and Y. J. Li (2007). "Role of asymmetric dimethylarginine in inflammatory reactions by angiotensin II." *Journal of Vascular Research* **44**(5): 391-402.
- Chin, D. J., K. L. Luskey, J. R. Faust, R. J. Macdonald, M. S. Brown and J. L. Goldstein (1982). "Molecular-Cloning of 3-Hydroxy-3-Methylglutaryl Coenzyme-a Reductase and Evidence for Regulation of Its Messenger-Rna." *Proceedings of the National Academy of Sciences of the United States of America-Biological Sciences* **79**(24): 7704-7708.
- Colell, A., J. E. Ricci, S. Tait, S. Milasta, U. Maurer, L. Bouchier-Hayes, P. Fitzgerald, A. Guio-Carrion, N. J. Waterhouse, C. W. Li, B. Mari, P. Barbry, D. D. Newmeyer, H. M. Beere and D. R. Green (2007). "GAPDH and autophagy preserve survival after apoptotic cytochrome c release in the absence of caspase activation." *Cell* **129**(5): 983-997.
- Corbett, J. (1994). "Positional reproducibility of protein spots in two-dimensional polyacrylamide gel electrophoresis using immobilised pH gradient isoelectric focussing in the first dimension: an interlaboratory comparison." *Electrophoresis* **15**: 1205 - 1211.
- Corsini, A., N. Ferri and M. Cortellaro (2007). "Are pleiotropic effects of statins real?" *Vasc Health Risk Manag* **3**(5): 611-3.
- Crisby, M., G. Nordin-Fredriksson, P. K. Shah, J. Yano, J. Zhu and J. Nilsson (2001). "Pravastatin treatment increases collagen content and decreases lipid content, inflammation, metalloproteinases, and cell death in human carotid plaques - Implications for plaque stabilization." *Circulation* **103**(7): 926-933.
- Dayoub, H., R. Rodionov, C. Lynch, J. P. Cooke, E. Arning, T. Bottiglieri, S. R. Lentz and F. M. Faraci (2008). "Overexpression of dimethylarginine

- dimethylaminohydrolase inhibits asymmetric dimethylarginine-induced endothelial dysfunction in the cerebral circulation." Stroke **39**(1): 180-184.
- de Haan, W., R. Out, J. F. P. Berbee, C. C. van der Hoogt, K. W. van Dijk, T. J. C. van Berkel, J. A. Romijn, J. W. Jukema, L. M. Havekes and P. C. N. Rensen (2008). "Apolipoprotein CI inhibits scavenger receptor BI and increases plasma HDL levels in vivo." Biochemical and Biophysical Research Communications **377**(4): 1294-1298.
- Delmotte, N., M. Lasaosa, A. Tholey, E. Heinzle and C. G. Huber (2007). "Two-dimensional reversed-phase x ion-pair reversed-phase HPLC: An alternative approach to high-resolution peptide separation for shotgun proteome analysis." Journal of Proteome Research **6**: 4363-4373.
- Delmotte, N., M. Lasaosa, A. Tholey, E. Heinzle, A. van Dorsselaer and C. G. Huber (2009). "Repeatability of peptide identifications in shotgun proteome analysis employing off-line two-dimensional chromatographic separations and ion-trap MS." Journal of Separation Science **32**(8): 1156-1164.
- Desai, A. and T. J. Mitchison (1997). "Microtubule polymerization dynamics." Annual Review of Cell and Developmental Biology **13**: 83-117.
- Dhainaut, J. F., N. Marin, A. Mignon and C. Vinsonneau (2001). "Hepatic response to sepsis: Interaction between coagulation and inflammatory processes." Critical Care Medicine **29**(7): S42-S47.
- Dietschy, J. M. (1984). "Regulation of Cholesterol-Metabolism in Man and in Other Species." Klinische Wochenschrift **62**(8): 338-345.
- Do, R., R. S. Kiss, D. Gaudet and J. C. Engert (2009). "Squalene synthase: a critical enzyme in the cholesterol biosynthesis pathway." Clinical Genetics **75**(1): 19-29.
- Dugo, P., F. Cacciola, T. Kumm, G. Dugo and L. Mondello (2008). "Comprehensive multidimensional liquid chromatography: Theory and applications." Journal of Chromatography A **1184**(1-2): 353-368.
- Elias, J. E., W. Haas, B. K. Faherty and S. P. Gygi (2005). "Comparative evaluation of mass spectrometry platforms used in large-scale proteomics investigations." Nature Methods **2**(9): 667-675.
- Endo, A., M. Kuroda and K. Tanzawa (1976). "Competitive Inhibition of 3-Hydroxy-3-Methylglutaryl Coenzyme a Reductase by MI-236a and MI-236b Fungal Metabolites, Having Hypocholesterolemic Activity." Febs Letters **72**(2): 323-326.
- Endres, M. and U. Laufs (2004). "Effects of statins on endothelium and signaling mechanisms." Stroke **35**(11): 2708-2711.
- Essig, M., G. Nguyen, D. Prie, B. Escoubet, J. D. Sraer and G. Friedlander (1998). "3-hydroxy-3-methylglutaryl coenzyme A reductase inhibitors increase fibrinolytic activity in rat aortic endothelial cells - Role of geranylgeranylation and Rho proteins." Circulation Research **83**(7): 683-690.

- Esterbauer, H., H. Zollner and J. Lang (1985). "Metabolism of the Lipid-Peroxidation Product 4-Hydroxynonenal by Isolated Hepatocytes and by Liver Cytosolic Fractions." Biochemical Journal **228**(2): 363-373.
- Exton, J. H. (1972). "Gluconeogenesis." Metabolism-Clinical and Experimental **21**(10): 945-&.
- Faergeman, N. J. and J. Knudsen (1997). "Role of long-chain fatty acyl-CoA esters in the regulation of metabolism and in cell signalling." Biochemical Journal **323**: 1-12.
- Fenn, J. B., M. Mann, C. K. Meng, S. F. Wong and C. M. Whitehouse (1989). "Electrospray Ionization for Mass-Spectrometry of Large Biomolecules." Science **246**(4926): 64-71.
- Filen, J. J., T. A. Nyman, J. Korhonen, D. R. Goodlett and R. Laheesmaa (2005). "Characterization of microsomal fraction proteome in human lymphoblasts reveals the down-regulation of galectin-1 by interleukin-12." Proteomics **5**(18): 4719-4732.
- Fuller, P. J. and M. J. Young (2005). "Mechanisms of mineralocorticoid action." Hypertension **46**(6): 1227-1235.
- Galeva, N., D. Yakovlev, Y. Koen, T. Duzhak and M. Alterman (2003). "Direct identification of cytochrome P450 isozymes by matrix-assisted laser desorption/ionization time of flight-based proteomic approach." Drug Metabolism and Disposition **31**(4): 351-355.
- Gerich, J. E. (1993). "Control of Glycemia." Baillieres Clinical Endocrinology and Metabolism **7**(3): 551-586.
- Gilar, M., P. Olivova, A. E. Daly and J. C. Gebler (2005a). "Orthogonality of separation in two-dimensional liquid chromatography." Analytical Chemistry **77**(19): 6426-6434.
- Gilar, M., P. Olivova, A. E. Daly and J. C. Gebler (2005b). "Two-dimensional separation of peptides using RP-RP-HPLC system with different pH in first and second separation dimensions." Journal of Separation Science **28**(14): 1694-1703.
- Glen, A., C. S. Gan, F. C. Hamdy, C. L. Eaton, S. S. Cross, J. W. F. Catto, P. C. Wright and I. Rehman (2008). "iTRAQ - Facilitated proteomic analysis of human prostate cancer cells identifies proteins associated with progression." Journal of Proteome Research **7**(3): 897-907.
- Goldstein, J. L. and M. S. Brown (1984). "Progress in Understanding the Ldl Receptor and Hmg-Coa Reductase, 2 Membrane-Proteins That Regulate the Plasma-Cholesterol." Journal of Lipid Research **25**(13): 1450-1461.
- Goldstein, J. L. and M. S. Brown (1990). "Regulation of the Mevalonate Pathway." Nature **343**(6257): 425-430.

- Goodridg.Ag (1973a). "Regulation of Fatty-Acid Synthesis in Isolated Hepatocytes - Evidence for a Physiological Role for Long-Chain Fatty Acyl Coenzyme a and Citrate." Journal of Biological Chemistry **248**(12): 4318-4326.
- Goodridg.Ag (1973b). "Regulation of Fatty-Acid Synthesis in Isolated Hepatocytes Prepared from Livers of Neonatal Chicks." Journal of Biological Chemistry **248**(6): 1924-1931.
- Gorg, A., W. Weiss and M. J. Dunn (2004). "Current two-dimensional electrophoresis technology for proteomics." Proteomics **4**(12): 3665-3685.
- Gygi, S. P., B. Rist, S. A. Gerber, F. Turecek, M. H. Gelb and R. Aebersold (1999). "Quantitative analysis of complex protein mixtures using isotope-coded affinity tags." Nature Biotechnology **17**(10): 994-999.
- Han, D., F. Antunes, R. Canali, D. Rettori and E. Cadenas (2003). "Voltage-dependent anion channels control the release of the superoxide anion from mitochondria to cytosol." Journal of Biological Chemistry **278**(8): 5557-5563.
- Handschin, C., M. Podvinec, R. Amherd, R. Looser, J. C. Ourlin and U. A. Meyer (2002). "Cholesterol and bile acids regulate xenosensor signaling in drug-mediated induction of cytochromes P450." Journal of Biological Chemistry **277**(33): 29561-7.
- Hardie, D. G. (1989). "Regulation of Fatty-Acid Synthesis Via Phosphorylation of Acetyl-Coa Carboxylase." Progress in Lipid Research **28**(2): 117-146.
- Heinz, F., Lamprech.W and J. Kirsch (1968). "Enzymes of Fructose Metabolism in Human Liver." Journal of Clinical Investigation **47**(8): 1826-&.
- Heinz, K. A., D. J. Głofcheski, J. R. Lepock and J. Kruuv (1990). "Mechanism of Freeze Thaw Damage to Liver Alcohol-Dehydrogenase and Protection by Cryoprotectants and Amino-Acids." Cryobiology **27**(5): 521-538.
- Hellerstein, M. K., J. M. Schwarz and R. A. Neese (1996). "Regulation of hepatic de novo lipogenesis in humans." Annual Review of Nutrition **16**: 523-557.
- Higuchi, T., Y. Watanabe and I. Waga (2004). "Protein disulfide isomerase suppresses the transcriptional activity of NF-kB." Biochemical and Biophysical Research Communications **318**(1): 46-52.
- Hiltunen, J. K., S. A. Filppula, K. T. Koivuranta, K. Siivari, Y. M. Qin and H. M. Hayrinen (1996). "Peroxisomal beta-oxidation and polyunsaturated fatty acids." Peroxisomes: Biology and Role in Toxicology and Disease **804**: 116-128.
- Hobbs, H. H., D. W. Russell, M. S. Brown and J. L. Goldstein (1990). "The Ldl Receptor Locus in Familial Hypercholesterolemia - Mutational Analysis of a Membrane-Protein." Annual Review of Genetics **24**: 133-170.

- Horton, J. D., J. L. Goldstein and M. S. Brown (2002). "SREBPs: activators of the complete program of cholesterol and fatty acid synthesis in the liver." Journal of Clinical Investigation **109**(9): 1125-1131.
- Horvath, C., W. Melander, I. Molnar and P. Molnar (1977). "Enhancement of Retention by Ion-Pair Formation in Liquid-Chromatography with Nonpolar Stationary Phases." Analytical Chemistry **49**(14): 2295-2305.
- Huang, P., L. Feng, E. A. Oldham, M. J. Keating and W. Plunkett (2000). "Superoxide dismutase as a target for the selective killing of cancer cells." Nature **407**(6802): 390-395.
- Hwang, K. H., C. Carapito, S. Bohmer, E. Leize, A. Van Dorselaer and R. Bernhardt (2006). "Proteome analysis of *Schizosaccharomyces pombe* by two-dimensional gel electrophoresis and mass spectrometry." Proteomics **6**(14): 4115-4129.
- Igel, M., T. Sudhop and K. von Bergmann (2002). "Pharmacology of 3-hydroxy-3-methylglutaryl-coenzyme A reductase inhibitors (statins), including rosuvastatin and pitavastatin." Journal of Clinical Pharmacology **42**(8): 835-845.
- Information, S. (2002). "WHO international drug monitoring cerivastatin and gemfibrozil." WHO Drug information **16**: 8-11.
- Isaacsohn, J. L., J. F. Setaro, C. Nicholas, J. A. Davey, L. J. Diotallevi, D. S. Christianson, E. Liskov, E. A. Stein and H. R. Black (1994). "Effects of Lovastatin Therapy on Plasminogen-Activator Inhibitor-1 Antigen Levels." American Journal of Cardiology **74**(7): 735-737.
- Istvan, E. S. and J. Deisenhofer (2001). "Structural mechanism for statin inhibition of HMG-CoA reductase." Science **292**(5519): 1160-1164.
- Jacobs, M. N. and D. F. V. Lewis (2002). "Steroid hormone receptors and dietary ligands: a selected review." Proceedings of the Nutrition Society **61**(1): 105-122.
- Janssen, U., T. Fink, P. Lichter and W. Stoffel (1994). "Human Mitochondrial 3,2-Trans-Enoyl-Coa Isomerase (Dci) - Gene Structure and Localization to Chromosome 16p13.3." Genomics **23**(1): 223-228.
- Jia, N., X. Liu, J. Wen, L. Y. Qian, X. H. Qian, Y. T. Wu and G. R. Fan (2007). "A proteomic method for analysis of CYP450s protein expression changes in carbon tetrachloride induced male rat liver microsomes." Toxicology **237**(1-3): 1-11.
- Jiang, S. and S. L. Nail (1998). "Effect of process conditions on recovery of protein activity after freezing and freeze-drying." European Journal of Pharmaceutics and Biopharmaceutics **45**(3): 249-257.
- Jo, S. H., M. K. Son, H. J. Koh, S. M. Lee, I. H. Song, Y. O. Kim, Y. S. Lee, K. S. Jeong, W. B. Kim, J. W. Park, B. J. Song and T. L. Huhe (2001). "Control of mitochondrial redox balance and cellular defense against oxidative damage by

- mitochondrial NADP(+)-dependent isocitrate dehydrogenase." Journal of Biological Chemistry **276**(19): 16168-16176.
- Jong, M. C., M. H. Hofker and L. M. Havekes (1999). "Role of ApoCs in lipoprotein metabolism - Functional differences between ApoC1, ApoC2, and ApoC3." Arteriosclerosis Thrombosis and Vascular Biology **19**(3): 472-484.
- Jorgensen, M. M., O. N. Jensen, H. U. Holst, J. J. Hansen, T. J. Corydon, P. Bross, L. Bolund and N. Gregersen (2000). "Grp78 is involved in retention of mutant low density lipoprotein receptor protein in the endoplasmic reticulum." Journal of Biological Chemistry **275**(43): 33861-33868.
- Kang, Y. Y., T. Techanukul, A. Mantalaris and J. M. Nagy (2009). "Comparison of Three Commercially Available DIGE Analysis Software Packages: Minimal User Intervention in Gel-Based Proteomics." Journal of Proteome Research **8**(2): 1077-1084.
- Kapp, E. A., F. Schutz, L. M. Connolly, J. A. Chakel, J. E. Meza, C. A. Miller, D. Fenyo, J. K. Eng, J. N. Adkins, G. S. Omenn and R. J. Simpson (2005). "An evaluation, comparison, and accurate benchmarking of several publicly available MS/MS search algorithms: Sensitivity and specificity analysis." Proteomics **5**(13): 3475-3490.
- Karas, M., D. Bachmann, U. Bahr and F. Hillenkamp (1987). "Matrix-Assisted Ultraviolet-Laser Desorption of Nonvolatile Compounds." International Journal of Mass Spectrometry and Ion Processes **78**: 53-68.
- Karas, M., M. Gluckmann and J. Schafer (2000). "Ionization in matrix-assisted laser desorption/ionization: singly charged molecular ions are the lucky survivors." Journal of Mass Spectrometry **35**(1): 1-12.
- Keller, A., J. Eng, N. Zhang, X. J. Li and R. Aebersold (2005). "A uniform proteomics MS/MS analysis platform utilizing open XML file formats." Molecular Systems Biology **1**.
- Keller, A., A. I. Nesvizhskii, E. Kolker and R. Aebersold (2002). "Empirical statistical model to estimate the accuracy of peptide identifications made by MS/MS and database search." Analytical Chemistry **74**(20): 5383-5392.
- Klose, J. (1975). "Protein Mapping by Combined Isoelectric Focusing and Electrophoresis of Mouse Tissues - Novel Approach to Testing for Induced Point Mutations in Mammals." Humangenetik **26**(3): 231-243.
- Koh, H. J., S. M. Lee, B. G. Son, S. H. Lee, Z. Y. Ryoo, K. T. Chang, J. W. Park, D. C. Park, B. J. Song, R. L. Veech, H. B. Song and T. L. Huh (2004). "Cytosolic NADP(+)-dependent isocitrate dehydrogenase plays a key role in lipid metabolism." Journal of Biological Chemistry **279**(38): 39968-39974.
- Korosec, T., J. Acimovic, M. Seliskar, D. Kocjan, K. F. Tacer, D. Roman and U. Urleb (2008). "Novel cholesterol biosynthesis inhibitors targeting human lanosterol 14 alpha-demethylase (CYP51)." Bioorganic & Medicinal Chemistry **16**(1): 209-221.

- Krebs, H. (1966). "The regulation of the release of ketone bodies by the liver." Advances in Enzyme Regulation **4**: 339-353.
- Kuo, P. C. and A. Slivka (1994). "Nitric-Oxide Decreases Oxidant-Mediated Hepatocyte Injury." Journal of Surgical Research **56**(6): 594-600.
- Lacerda, C. M. R., L. Xin, I. Rogers and K. F. Reardon (2008). "Analysis of iTRAQ data using Mascot and Peaks quantification algorithms." Brief Funct Genomic Proteomic **7**(2).
- Laliberte, R. E., D. G. Perregaux, L. R. Hoth, P. J. Rosner, C. K. Jordan, K. M. Peese, J. F. Egglar, M. A. Dombroski, K. F. Geoghegan and C. A. Gabel (2003). "Glutathione S-transferase omega 1-1 is a target of cytokine release inhibitory drugs and may be responsible for their effect on interleukin-1 beta posttranslational processing." Journal of Biological Chemistry **278**(19): 16567-16578.
- Lane, C. S., S. Nisar, W. J. Griffiths, B. J. Fuller, B. R. Davidson, J. Hewes, K. J. Welham and L. H. Patterson (2004). "Identification of cytochrome P450 enzymes in human colorectal metastases and the surrounding liver: a proteomic approach." European Journal of Cancer **40**(14): 2127-2134.
- LaRosa, J. C. (2001). "Pleiotropic effects of statins and their clinical significance." American Journal of Cardiology **88**(3): 291-+.
- Lasaosa, M., N. Delmotte, C. G. Huber, K. Melchior, E. Heinzle and A. Tholey (2009). "A 2D reversed-phase x ion-pair reversed-phase HPLC-MALDI TOF/TOF-MS approach for shotgun proteome analysis." Analytical and Bioanalytical Chemistry **393**(4): 1245-1256.
- Lau, K. W., A. R. Jones, N. Swainston, J. A. Siepen and S. J. Hubbard (2007). "Capture and analysis of quantitative proteomic data." Proteomics **7**(16): 2787-2799.
- Laufs, U., V. La Fata, J. Plutzky and J. K. Liao (1998). "Upregulation of endothelial nitric oxide synthase by HMG CoA reductase inhibitors." Circulation **97**(12): 1129-1135.
- Lebherz, H. G. and W. J. Rutter (1969). "Distribution of Fructose Diphosphate Aldolase Variants in Biological Systems." Biochemistry **8**(1): 109-&.
- Li, H. Y., F. R. Appelbaum, C. L. Willman, R. A. Zager and D. E. Banker (2003). "Cholesterol-modulating agents kill acute myeloid leukemia cells and sensitize them to therapeutics by blocking adaptive cholesterol responses." Blood **101**(9): 3628-3634.
- Liao, J. K. (2002). "Beyond lipid lowering: the role of statins in vascular protection." International Journal of Cardiology **86**(1): PII S01675273(02)00195-X.
- Liao, J. K. and U. Laufs (2005). "Pleiotropic effects of statins." Annual Review of Pharmacology and Toxicology **45**: 89-118.

- Lin, W. T., W. N. Hung, Y. H. Yian, K. P. Wu, C. L. Han, Y. R. Chen, Y. J. Chen, T. Y. Sung and W. L. Hsu (2006). "Multi-Q: A fully automated tool for multiplexed protein quantitation." Journal of Proteome Research **5**(9): 2328-2338.
- Lin, Y., A. H. Berg, P. Iyengar, T. K. T. Lam, A. Giacca, T. P. Combs, M. W. Rajala, X. L. Du, B. Rollman, W. J. Li, M. Hawkins, N. Barzilai, C. J. Rhodes, I. G. Fantus, M. Brownlee and P. E. Scherer (2005). "The hyperglycemia-induced inflammatory response in adipocytes - The role of reactive oxygen species." Journal of Biological Chemistry **280**(6): 4617-4626.
- Luftjohann, D., J. I. Sigit, S. Locatelli, K. von Bergmann and H. H. A. Schmidt (2001). "High-dose simvastatin (80 mg/day) decreases plasma concentrations of total homocyst(e)ine in patients with hypercholesterolemia." Atherosclerosis **155**(1): 265-266.
- Maere, S., K. Heymans and M. Kuiper (2005). "BiNGO: a Cytoscape plugin to assess overrepresentation of Gene Ontology categories in Biological Networks." Bioinformatics **21**(16): 3448-3449.
- Mahley, R. W. (1983). "Apolipoprotein-E and Cholesterol-Metabolism." Klinische Wochenschrift **61**(5): 225-232.
- Malarkey, D. E., K. Johnson, L. Ryan, G. Boorman and R. R. Maronpot (2005). "New insights into functional aspects of liver morphology." Toxicologic Pathology **33**(1): 27-34.
- Malik, R., C. Selden and H. Hodgson (2002). "The role of non-parenchymal cells in liver growth." Seminars in Cell & Developmental Biology **13**(6): 425-431.
- Manevich, Y., T. Shuvaeva, C. Dodia, A. Kazi, S. I. Feinstein and A. B. Fisher (2009). "Binding of peroxiredoxin 6 to substrate determines differential phospholipid hydroperoxide peroxidase and phospholipase A(2) activities." Archives of Biochemistry and Biophysics **485**(2): 139-149.
- Manzoni, M. and N. Rollini (2002). "Biosynthesis and biotechnological production of statins by filamentous fungi and application of these cholesterol-lowering drugs." Applied Microbiology and Biotechnology **58**(5): 555-564.
- Martinez, L. O., S. Jacquet, J. P. Esteve, C. Rolland, E. Cabezon, E. Champagne, T. Pineau, V. Georgeaud, J. E. Walker, F. Terce, X. Collet, B. Perret and R. Barbaras (2003). "Ectopic beta-chain of ATP synthase is an apolipoprotein A-I receptor in hepatic HDL endocytosis." Nature **421**(6918): 75-79.
- Mateuszuk, L., T. I. Khomich, E. Slominska, M. Gajda, L. Wojcik, M. Lomnicka, P. Gwozdz and S. Chlopicki (2009). "Activation of nicotinamide N-methyltransferase and increased formation of 1-methylnicotinamide (MNA) in atherosclerosis." Pharmacological Reports **61**(1): 76-85.

- Maurer, M. H., R. E. Feldmann, J. O. Bromme and A. Kalenka (2005). "Comparison of statistical approaches for the analysis of proteome expression data of differentiating neural stem cells." Journal of Proteome Research **4**(1): 96-100.
- McTaggart, F., L. Buckett, R. Davidson, G. Holdgate, A. McCormick, D. Schneck, G. Smith and M. Warwick (2001). "Preclinical and clinical pharmacology of rosuvastatin, a new 3-hydroxy-3-methylglutaryl coenzyme A reductase inhibitor." American Journal of Cardiology **87**(5A): 28B-32B.
- Medzihradzky, K. F., J. M. Campbell, M. A. Baldwin, A. M. Falick, P. Juhasz, M. L. Vestal and A. L. Burlingame (2000). "The characteristics of peptide collision-induced dissociation using a high-performance MALDI-TOF/TOF tandem mass spectrometer." Analytical Chemistry **72**(3): 552-558.
- Mehrabian, M., K. A. Callaway, C. F. Clarke, R. D. Tanaka, M. Greenspan, A. J. Lusic, R. S. Sparkes, T. Mohandas, J. Edmond, A. M. Fogelman and P. A. Edwards (1986). "Regulation of Rat-Liver 3-Hydroxy-3-Methylglutaryl Coenzyme-a Synthase and the Chromosomal Localization of the Human-Gene." Journal of Biological Chemistry **261**(34): 6249-6255.
- Meiring, H. D., E. van der Heeft, G. J. ten Hove and A. de Jong (2002). "Nanoscale LC-MS(n): technical design and applications to peptide and protein analysis." Journal of Separation Science **25**(9): 557-568.
- Miller, I., J. Crawford and E. Gianazza (2006). "Protein stains for proteomic applications: Which, when, why?" Proteomics **6**(20): 5385-5408.
- Molnar, I. and C. Horvath (1977). "Separation of Amino-Acids and Peptides on Nonpolar Stationary Phases by High-Performance Liquid-Chromatography." Journal of Chromatography **142**(V): 623-640.
- Monostory, K., J. M. Pascussi, P. Szabo, M. Temesvari, K. Kohalmy, J. Acimovic, D. Kocjan, D. Kuzman, B. Wilzewski, R. Bernhardt, L. Kobori and D. Rozman (2009). "Drug Interaction Potential of 2-((3,4-Dichlorophenethyl)(propyl)amino)-1-(pyridin-3-yl)ethanol (LK-935), the Novel Nonstatin-Type Cholesterol-Lowering Agent." Drug Metabolism and Disposition **37**(2): 375-385.
- Moon, Y. A. and J. D. Horton (2003). "Identification of two mammalian reductases involved in the two-carbon fatty acyl elongation cascade." Journal of Biological Chemistry **278**(9): 7335-7343.
- Murase, N. and F. Franks (1989). "Salt Precipitation During the Freeze-Concentration of Phosphate Buffer Solutions." Biophysical Chemistry **34**(3): 293-300.
- Nagasaki, S., T. Suzuki, Y. Miki, J. I. Akahira, K. Kitada, T. Ishida, H. Handa, N. Ohuchi and H. Sasano (2009). "17 beta-Hydroxysteroid Dehydrogenase Type 12 in Human Breast Carcinoma: A Prognostic Factor via Potential Regulation of Fatty Acid Synthesis." Cancer Research **69**(4): 1392-1399.

- Nesvizhskii, A. I., A. Keller, E. Kolker and R. Aebersold (2003). "A statistical model for identifying proteins by tandem mass spectrometry." Analytical Chemistry **75**(17): 4646-4658.
- Nezasa, K., K. Higaki, H. Hasegawa, K. Inazawa, M. Takeuchi, T. Yukawa, F. McTaggart and M. Nakano (2000). "Uptake of HMG-CoA reductase inhibitor ZD4522 into hepatocytes and distribution into liver and other tissues of the rat." Atherosclerosis **151**(1): 39.
- Notarbartolo, A., G. Davi, M. Averna, C. M. Barbagallo, A. Ganci, C. Giammarresi, F. P. Laplaca and C. Patrono (1995). "Inhibition of Thromboxane Biosynthesis and Platelet-Function by Simvastatin in Type IIA Hypercholesterolemia." Arteriosclerosis Thrombosis and Vascular Biology **15**(2): 247-251.
- O'Farrell, P. H. (1975). "High-Resolution 2-Dimensional Electrophoresis of Proteins." Journal of Biological Chemistry **250**(10): 4007-4021.
- Ong, S. E., B. Blagoev, I. Kratchmarova, D. B. Kristensen, H. Steen, A. Pandey and M. Mann (2002). "Stable isotope labeling by amino acids in cell culture, SILAC, as a simple and accurate approach to expression proteomics." Molecular & Cellular Proteomics **1**(5): 376-386.
- Ooi, E. M. M., G. F. Watts, D. C. Chan, M. M. Chen, P. J. Nestel, D. Sviridov and P. H. Barrett (2008). "Dose-dependent effect of rosuvastatin on VLDL-apolipoprotein C-III kinetics in the metabolic syndrome." Diabetes Care **31**(8): 1656-1661.
- Pappin, D. J. C., P. Hojrup and A. J. Bleasby (1993). "Rapid Identification of Proteins by Peptide-Mass Fingerprinting." Current Biology **3**(6): 327-332.
- Pardridge, W. M. and L. J. Mietus (1979). "Transport of Steroid-Hormones through the Rat Blood-Brain-Barrier - Primary Role of Albumin-Bound Hormone." Journal of Clinical Investigation **64**(1): 145-154.
- Parhami, F., A. Garfinkel and L. L. Demer (2000). "Role of lipids in osteoporosis." Arteriosclerosis Thrombosis and Vascular Biology **20**(11): 2346-2348.
- Parhami, F., N. Mody, N. Gharavi, A. J. Ballard, Y. Tintut and L. L. Demer (2002). "Role of the cholesterol biosynthetic pathway in osteoblastic differentiation of marrow stromal cells." Journal of Bone and Mineral Research **17**(11): 1997-2003.
- Perkins, D. N., D. J. C. Pappin, D. M. Creasy and J. S. Cottrell (1999). "Probability-based protein identification by searching sequence databases using mass spectrometry data." Electrophoresis **20**(18): 3551-3567.
- Petrak, J., R. Ivanek, O. Toman, R. Cmejla, J. Cmejlova, D. Vyoral, J. Zivny and C. D. Vulpe (2008). "Déjà vu in proteomics. A hit parade of repeatedly identified differentially expressed proteins." PROTEOMICS **8**(9): 1744-1749.
- Premstaller, A., H. Oberacher, W. Walcher, A. M. Timperio, L. Zolla, J. P. Chervet, N. Cavusoglu, A. van Dorselaer and C. G. Huber (2001). "High-performance liquid

- chromatography-electrospray ionization mass spectrometry using monolithic capillary columns for proteomic studies." Analytical Chemistry **73**(11): 2390-+.
- Raman, B., A. Cheung and M. R. Marten (2002). "Quantitative comparison and evaluation of two commercially available, two-dimensional electrophoresis image analysis software packages, Z3 and Melanie." Electrophoresis **23**(14): 2194-2202.
- Rashid, S. and G. F. Lewis (2005). "The mechanisms of differential glucocorticoid and mineralocorticoid action in the brain and peripheral tissues." Clinical Biochemistry **38**(5): 401-409.
- Redman, C. M. and H. Xia (2000). "A review of the expression, assembly, secretion and intracellular degradation of fibrinogen." Fibrinolysis & Proteolysis **14**(2-3): 198-205.
- Repa, J. J. and D. J. Mangelsdorf (2000). "The role of orphan nuclear receptors in the regulation of cholesterol homeostasis." Annual Review of Cell and Developmental Biology **16**: 459-481.
- Reshef, L., Y. Olswang, H. Cassuto, B. Blum, C. M. Croniger, S. C. Kalhan, S. M. Tilghman and R. W. Hanson (2003). "Glyceroneogenesis and the triglyceride/fatty acid cycle." Journal of Biological Chemistry **278**(33): 30413-30416.
- Reutelingsperger, C. P. M. and W. L. vanHeerde (1997). "Annexin V, the regulator of phosphatidylserine-catalyzed inflammation and coagulation during apoptosis." Cellular and Molecular Life Sciences **53**(6): 527-532.
- Rosengren, A. T., J. M. Salmi, T. Aittokallio, J. Westerholm, R. Lahesmaa, T. A. Nyman and O. S. Nevalainen (2003). "Comparison of PDQuest and Progenesis software packages in the analysis of two-dimensional electrophoresis gels." Proteomics **3**(10): 1936-1946.
- Ross, P. L., Y. L. N. Huang, J. N. Marchese, B. Williamson, K. Parker, S. Hattan, N. Khainovski, S. Pillai, S. Dey, S. Daniels, S. Purkayastha, P. Juhasz, S. Martin, M. Bartlett-Jones, F. He, A. Jacobson and D. J. Pappin (2004). "Multiplexed protein quantitation in *Saccharomyces cerevisiae* using amine-reactive isobaric tagging reagents." Molecular & Cellular Proteomics **3**(12): 1154-1169.
- Rostovtseva, T. and M. Colombini (1997). "VDAC channels mediate and gate the flow of ATP: Implications for the regulation of mitochondrial function." Biophysical Journal **72**(5): 1954-1962.
- Rudney, H. and R. C. Sexton (1986). "Regulation of Cholesterol-Biosynthesis." Annual Review of Nutrition **6**: 245-272.
- Russell, D. W. (1992). "Cholesterol-Biosynthesis and Metabolism." Cardiovascular Drugs and Therapy **6**(2): 103-110.

- Santoni, V., M. Molloy and T. Rabilloud (2000). "Membrane proteins and proteomics: Un amour impossible?" Electrophoresis **21**(6): 1054-1070.
- Sato, N., N. Funayama, A. Nagafuchi, S. Yonemura and S. Tsukita (1992). "A Gene Family Consisting of Ezrin, Radixin and Moesin - Its Specific Localization at Actin Filament Plasma-Membrane Association Sites." Journal of Cell Science **103**: 131-143.
- Schoonjans, K., B. Staels, P. Grimaldi and J. Auwerx (1993). "Acyl-Coa Synthetase Messenger-Rna Expression Is Controlled by Fibric-Acid Derivatives, Feeding and Liver Proliferation." European Journal of Biochemistry **216**(2): 615-622.
- Schoonjans, K., M. Watanabe, H. Suzuki, A. Mahfoudi, G. Krey, W. Wahli, P. Grimaldi, B. Staels, T. Yamamoto and J. Auwerx (1995). "Induction of the Acyl-Coenzyme-a Synthetase Gene by Fibrates and Fatty-Acids Is Mediated by a Peroxisome Proliferator Response Element in the C-Promoter." Journal of Biological Chemistry **270**(33): 19269-19276.
- Schuster, I. and R. Bernhardt (2007). "Inhibition of cytochromes P450: Existing and new promising therapeutic targets." Drug Metabolism Reviews **39**(2-3): 481-499.
- Seguro, K., T. Tamiya, T. Tsuchiya and J. J. Matsumoto (1989). "Effect of Chemical Modifications on Freeze Denaturation of Lactate-Dehydrogenase." Cryobiology **26**(2): 154-161.
- Seguro, K., T. Tamiya, T. Tsuchiya and J. J. Matsumoto (1990). "Cryoprotective Effect of Sodium Glutamate and Lysine-Hcl on Freeze Denaturation of Lactate-Dehydrogenase." Cryobiology **27**(1): 70-79.
- Seiki, S. and W. H. Frishman (2009). "Pharmacologic Inhibition of Squalene Synthase and Other Downstream Enzymes of the Cholesterol Synthesis Pathway A New Therapeutic Approach to Treatment of Hypercholesterolemia." Cardiology in Review **17**(2): 70-76.
- Shachter, N. S. (2001). "Apolipoproteins C-I and C-III as important modulators of lipoprotein metabolism." Current Opinion in Lipidology **12**(3): 297-304.
- Shadforth, I. P., T. P. J. Dunkley, K. S. Lilley and C. Bessant (2005). "i-Tracker: For quantitative proteomics using iTRAQ (TM)." Bmc Genomics **6**.
- Shapiro, A. L., E. Vinuela and J. V. Maizel (1967). "Molecular Weight Estimation of Polypeptide Chains by Electrophoresis in Sds-Polyacrylamide Gels." Biochemical and Biophysical Research Communications **28**(5): 815-&.
- Shechter, I., P. H. Dai, L. A. Huo and G. M. Guan (2003). "IDH1 gene transcription is sterol regulated and activated by SREBP-1a and SREBP-2 in human hepatoma HepG2 cells: evidence that IDH1 may regulate lipogenesis in hepatic cells." Journal of Lipid Research **44**(11): 2169-2180.

- Sherrill, B. C. and J. M. Dietschy (1978). "Characterization of Sinusoidal Transport Process Responsible for Uptake of Chylomicrons by Liver." Journal of Biological Chemistry **253**(6): 1859-1867.
- Shikama, K. and I. Yamazaki (1961). "Denaturation of Catalase by Freezing Andthawing." Nature **190**(477): 83-&.
- Shilov, I. V., S. L. Seymour, A. A. Patel, A. Loboda, W. H. Tang, S. P. Keating, C. L. Hunter, L. M. Nuwaysir and D. A. Schaeffer (2007). "The paragon algorithm, a next generation search engine that uses sequence temperature values and feature probabilities to identify peptides from tandem mass spectra." Molecular & Cellular Proteomics **6**(9): 1638-1655.
- Shoulders, C. C., D. J. Stephens and B. Jones (2004). "The intracellular transport of chylomicrons requires the small GTPase, Sar1b." Current Opinion in Lipidology **15**(2): 191-197.
- Silvain, M., D. Bligny, T. Aparicio, P. Laforet, A. Grodet, N. Peretti, D. Menard, F. Djouadi, C. Jardel, J. M. Begue, F. Walker, J. Schmitz, A. Lachaux, L. P. Aggerbeck and M. E. Samson-Bouma (2008). "Anderson's disease (chylomicron retention disease): a new mutation in the SARA2 gene associated with muscular and cardiac abnormalities." Clinical Genetics **74**(6): 546-552.
- Singh, I., K. Pahan and M. Khan (1998). "Lovastatin and sodium phenylacetate normalize the levels of very long chain fatty acids in skin fibroblasts of X-adrenoleukodystrophy." Febs Letters **426**(3): 342-346.
- Siperstein, M. D. (1984). "Role of Cholesterologenesis and Isoprenoid Synthesis in DNA-Replication and Cell-Growth." Journal of Lipid Research **25**(13): 1462-1468.
- Sirover, M. A. (1999). "New insights into an old protein: the functional diversity of mammalian glyceraldehyde-3-phosphate dehydrogenase." Biochimica Et Biophysica Acta-Protein Structure and Molecular Enzymology **1432**(2): 159-184.
- Smirnova, I. V., T. Sawamura and M. S. Goligorsky (2004). "Upregulation of lectin-like oxidized low-density lipoprotein receptor-1 (LOX-1) in endothelial cells by nitric oxide deficiency." American Journal of Physiology-Renal Physiology **287**(1): F25-F32.
- Smith, G., R. Davidson, S. Bloor, K. Burns, C. Calnan, P. McAulay, N. Torr, W. Ward and F. McTaggart (2000). "Pharmacological properties of ZD4522 -- A new HMG-CoA reductase inhibitor." Atherosclerosis **151**(1): 39.
- Smith, M. L., D. Burnett, P. Bennett, R. H. Waring, H. M. Brown, A. C. Williams and D. B. Ramsden (1998). "A direct correlation between nicotinamide N-methyltransferase activity and protein levels in human liver cytosol." Biochimica Et Biophysica Acta-Gene Structure and Expression **1442**(2-3): 238-244.
- Souto, J. C., F. Blanco-Vaca, J. M. Soria, A. Buil, L. Almasy, J. Ordonez-Llanos, J. M. Martin-Campos, M. Lathrop, W. Stone, J. Blangero and J. Fontcuberta (2005). "A

- genomewide exploration suggests a new candidate gene at chromosome 11q23 as the major determinant of plasma homocysteine levels: Results from the GAIT project." American Journal of Human Genetics **76**(6): 925-933.
- Spector, A. A. (1975). "Fatty-Acid Binding to Plasma Albumin." Journal of Lipid Research **16**(3): 165-179.
- Spence, J. T. and H. C. Pitot (1982). "Induction of Lipogenic Enzymes in Primary Cultures of Rat Hepatocytes - Relationship between Lipogenesis and Carbohydrate-Metabolism." European Journal of Biochemistry **128**(1): 15-20.
- Stalker, T. J., A. M. Lefer and R. Scalia (2001). "A new HMG-CoA reductase inhibitor, rosuvastatin, exerts anti-inflammatory effects on the microvascular endothelium: the role of mevalonic acid." British Journal of Pharmacology **133**(3): 406-412.
- Stark, H. (2003). "Medizinisch-chemische Aspekte von Statinen." Pharmakologie Unserer Zeit **32**(6): 464-470.
- Stevens, S. M., R. S. Duncan, P. Koulen and L. Prokai (2008). "Proteomic analysis of mouse brain microsomes: Identification and bioinformatic characterization of endoplasmic reticulum proteins in the mammalian central nervous system." Journal of Proteome Research **7**(3): 1046-1054.
- Stoffel, W., G. Mullernewen and U. Jansen (1994). "Recombinant DNA-Techniques in the Study of Fatty-Acid Metabolism, Paradigma Demonstrated with 3,2trans-Enoyl-Coa-Isomerase." Fett Wissenschaft Technologie-Fat Science Technology **96**(1): 1-6.
- Straznicky, N. E., L. G. Howes, W. Lam and W. J. Lois (1995). "Effects of Pravastatin on Cardiovascular Reactivity to Norepinephrine and Angiotensin-II Patients with Hypercholesterolemia and Systemic Hypertension." American Journal of Cardiology **75**(8): 582-586.
- Sundseth, S. S. and D. J. Waxman (1990). "Hepatic-P-450 Cholesterol 7-Alpha-Hydroxylase - Regulation In Vivo at the Protein and Messenger-Rna Level in Response to Mevalonate, Diurnal Rhythm, and Bile-Acid Feedback." Journal of Biological Chemistry **265**(25): 15090-15095.
- Tamiya, T., N. Okahashi, R. Sakuma, T. Aoyama, T. Akahane and J. J. Matsumoto (1985). "Freeze Denaturation of Enzymes and Its Prevention with Additives." Cryobiology **22**(5): 446-456.
- Tanaka, T., H. Waki, Y. Ido, S. Akita, Y. Yoshida, T. Yoshida and T. Matsuo (1988). "Protein and polymer analysis up to m/z 100 000 by laser-ionisation time-of-flight mass spectrometry." Rapid Communications in Mass Spectrometry **2**(8): 151-153.
- Thiagarajan, P. and J. F. Tait (1990). "Binding of Annexin-V Placental Anticoagulant Protein I to Platelets - Evidence for Phosphatidylserine Exposure in the

- Procoagulant Response of Activated Platelets." Journal of Biological Chemistry **265**(29): 17420-17423.
- Tsukita, S. and S. Yonemura (1997). "ERM (ezrin/radixin/moesin) family: From cytoskeleton to signal transduction." Current Opinion in Cell Biology **9**(1): 70-75.
- Turano Carlo, Sabina Coppari, Fabio Altieri and Anna Ferraro (2002). "Proteins of the PDI family: Unpredicted non-ER locations and functions." Journal of Cellular Physiology **193**(2): 154-163.
- van Engeland, M., L. J. W. Nieland, F. C. S. Ramaekers, B. Schutte and C. P. M. Reutelingsperger (1998). "Annexin V-affinity assay: A review on an apoptosis detection system based on phosphatidylserine exposure." Cytometry **31**(1): 1-9.
- Ventura, F. V., J. Ruiten, L. Ijlst, I. T. de Almeida and R. J. A. Wanders (2005). "Differential inhibitory effect of long-chain acyl-CoA esters on succinate and glutamate transport into rat liver mitochondria and its possible implications for long-chain fatty acid oxidation defects." Molecular Genetics and Metabolism **86**(3): 344-352.
- Vivanco, F., J. L. Martin-Ventura, M. C. Duran, M. G. Barderas, L. Blanco-Colio, V. M. Darde, S. Mas, O. Meilhac, J. B. Michel, J. Tunon and J. Egido (2005). "Quest for novel cardiovascular biomarkers by proteomic analysis." Journal of Proteome Research **4**(4): 1181-1191.
- Volpe, J. J. and P. R. Vagelos (1973). "Saturated Fatty-Acid Biosynthesis and Its Regulation." Annual Review of Biochemistry **42**: 21-60.
- Wang, J., P. S. Green and J. W. Simpkins (2001). "Estradiol protects against ATP depletion, mitochondrial membrane potential decline and the generation of reactive oxygen species induced by 3-nitropropionic acid in SK-N-SH human neuroblastoma cells." Journal of Neurochemistry **77**(3): 804-811.
- Wang, Q., L. Jiang, J. Wang, S. F. Li, Y. Yu, J. You, R. Zeng, X. Gao, L. Y. Rui, W. J. Li and Y. Liu (2009). "Abrogation of Hepatic ATP-Citrate Lyase Protects Against Fatty Liver and Ameliorates Hyperglycemia in Leptin Receptor-Deficient Mice." Hepatology **49**(4): 1166-1175.
- Wasinger, V. C., S. J. Cordwell, A. Cerpapoljak, J. X. Yan, A. A. Gooley, M. R. Wilkins, M. W. Duncan, R. Harris, K. L. Williams and I. Humpherysmith (1995). "Progress with Gene-Product Mapping of the Mollicutes - Mycoplasma-Genitalium." Electrophoresis **16**(7): 1090-1094.
- Weber, C., W. Erl, K. S. C. Weber and P. C. Weber (1997). "HMG-CoA reductase inhibitors decrease CD11b expression and CD11b-dependent adhesion of monocytes to endothelium and reduce increased adhesiveness of monocytes isolated from patients with hypercholesterolemia." Journal of the American College of Cardiology **30**(5): 1212-1217.

- Wheelock, A. M. and A. R. Buckpitt (2005). "Software-induced variance in two-dimensional gel electrophoresis image analysis." Electrophoresis **26**(23): 4508-4520.
- Wieckowski, M. R. and L. Wojtczak (1997). "Involvement of the dicarboxylate carrier in the protonophoric action of long-chain fatty acids in mitochondria." Biochemical and Biophysical Research Communications **232**(2): 414-417.
- Wiese, S. (2007). "Protein labeling by iTRAQ: A new tool for quantitative mass spectrometry in proteome research (vol 7, pg 340, 2007)." Proteomics **7**(6): 1004-1004.
- Wissler, R. W. (1991). "Update on the Pathogenesis of Atherosclerosis." American Journal of Medicine **91**: S3-S9.
- Woerner, M. (2006). 2D Gelelektrophorese von Leberproteinen. Biochemistry. Saarbrücken, Saarland University: 100.
- Woerner, M., K. Melchior, N. Delmotte, K. H. Hwang, K. Monostory, C. G. Huber and R. Bernhardt (2009). "Shotgun proteomic analysis of the microsomal fraction of eukaryotic cells using a two-dimensional reversed-phase x ion-pair reversed-phase HPLC setup." Journal of Separation Science **32**(8): 1165-1174.
- Yan, L., F. Lan, Z. G. Wang and Y. P. Li (2003). "Statins and myotoxicity." Trends in Pharmacological Sciences **24**(3): 113-114.
- Yeagle, P. L., A. D. Albert, K. Boeszebattaglia, J. Young and J. Frye (1990). "Cholesterol Dynamics in Membranes." Biophysical Journal **57**(3): 413-424.
- Yu, Z. F., H. Luo, W. M. Fu and M. P. Mattson (1999). "The endoplasmic reticulum stress-responsive protein GRP78 protects neurons against excitotoxicity and apoptosis: Suppression of oxidative stress and stabilization of calcium homeostasis." Experimental Neurology **155**(2): 302-314.
- Zgoda, V., O. Tikhonova, A. Lisitsa and A. Archakov (2006). "Proteomic profiles of induced hepatotoxicity at the subcellular level." Molecular & Cellular Proteomics **5**(10): S145-S145.
- Zhong, Q., D. A. Putt, F. Xu and L. H. Lash (2008). "Hepatic mitochondrial transport of glutathione: Studies in isolated rat liver mitochondria and H4IIE rat hepatoma cells." Archives of Biochemistry and Biophysics **474**(1): 119-127.
- Zhou, M., A. Jacob, N. Ho, M. Miksa, R. Q. Wu, S. R. Maitra and P. Wang (2008). "Downregulation of protein disulfide isomerase in sepsis and its role in tumor necrosis factor-alpha release." Critical Care **12**(4).

Appendix

Appendix I: Publications resulting from this work

Contributions to international meetings

August 2006: 3rd Summerschool in proteomics basics, Bressanone, Italy
2D Analysis of different protein expression in primary human hepatocytes – a jigsaw
particle of the drug-cholesterol crosstalk analysis – (Poster presentation)
M.Wörner, K.Monostory, R.Bernhardt

March 2007 Status meeting of the STEROLTALK project, Basel, Switzerland
M.Wörner, K.H.Hwang, S.Böhmer, R.Bernhardt

July 2008 17th international symposium on microsomes and drug oxidation, Saratoga
Springs, NY, USA
Cholesterol crosstalk: A proteomic point of view – (Poster presentation)
M.Wörner, K.Monostory, R.Bernhardt

August 2008 Final meeting of the STEROLTALK project, Ljubljana, Slovenia
M.Wörner, R.Bernhardt

Manuscripts

Shotgun proteomic analysis of the microsomal fraction of eukaryotic cells using a two-
dimensional reversed-phase x ion-pair reversed-phase HPLC setup
M.Wörner, K.Melchior, N.Delmotte, K.H.Hwang, K.Monostory, C.G.Huber, R.Bernhardt
Journal of Separation Sciences, Volume 32, Issue 8, pp. 1165-1174, (2009)

The effects of rosuvastatin and the CYP51A1 inhibitor LEK-935 on the proteome of
primary human hepatocytes
M.Wörner, K.Melchior, K.Monostory, J.M.Pascussi, C.G. Huber, R.Bernhardt
In preparation

Sample freezing prior to proteome analysis - Does the samples origin influence the effects ?

M.Wörner, K.Monostory, R.Bernhardt

In preparation

The influence of the quantitation software on the results of gel-free semi-quantitative proteome analysis using the iTRAQ™ labelling.

M.Wörner, R.Bernhardt

In preparation

Appendix II: Details of the proteins found to be regulated

Information about the function and cellular localisation of the proteins, described here was collected from the Expasy/Uniprot database, available at www.expasy.org.

Sample 1 2D spot details

Spot 2 / Proteasome subunit alpha -type5-

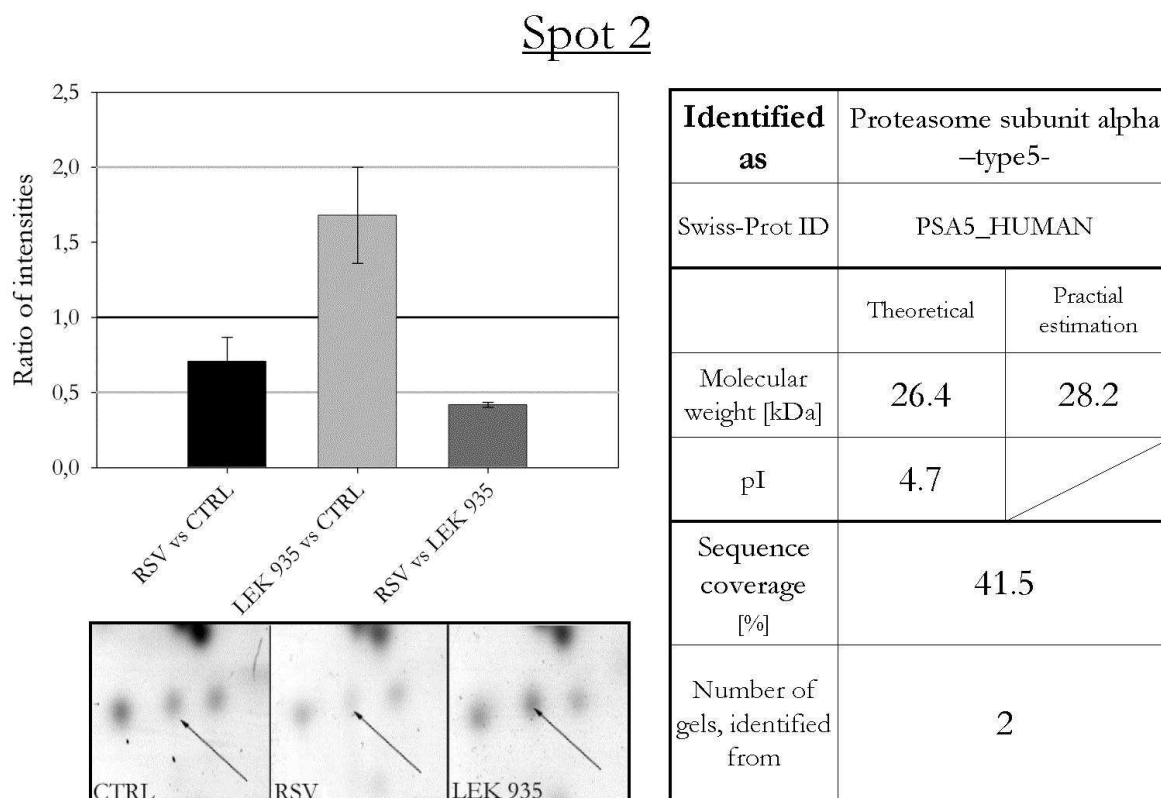


Figure 0-1 Spot 2 found to be regulated in sample 1. The ratio of intensities is depicted in the left upper corner, followed by examples of the spot appearance on the analysed 2D gels. The parameters of identification as well as a comparison of theoretical to experimental data about the molecular weight and the isoelectric point are summarised on the right.

For spot 2 no significant regulation compared to the control sample was detected, but it was found to be down-regulated in the RSV treated samples compared to the samples treated with LEK-935 (see Figure 0-1). The underlying protein was identified in two individual gels leading to a final sequence coverage of 41.5 %. It was regarded as a true positive hit.

Proteasome subunit alpha type 5 directly interacts with an protein complex, which promotes the assembly of the 20S proteasome subunit. It is thereby involved in protein degradation by the proteasome. The observed molecular weight of the protein

correlates well with the theoretically examined one. The pI could not be determined experimentally.

Spot 3 / Annexin A5

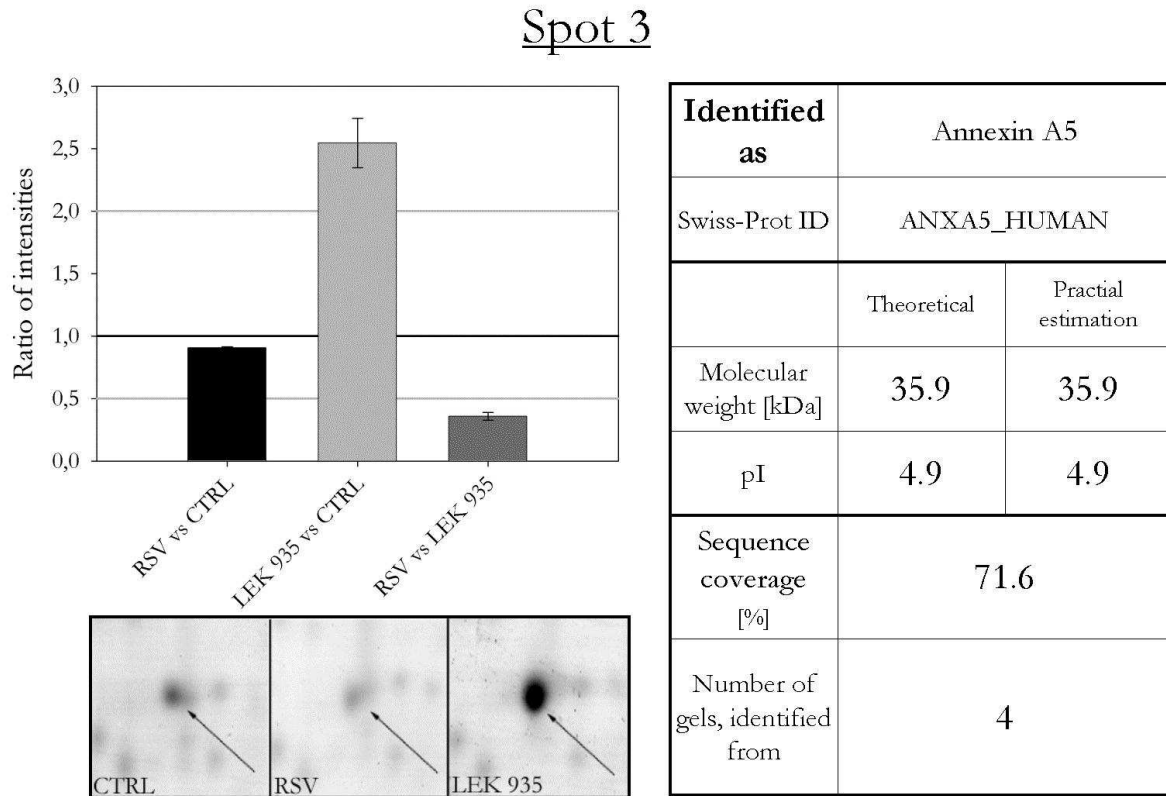


Figure 0-2 Spot 3 found to be regulated in sample 1. The ratio of intensities is depicted in the left upper corner, followed by examples of the spot appearance on the analysed 2D gels. The parameters of identification as well as a comparison of theoretical to experimental data about the molecular weight and the isoelectric point are summarised on the right.

Spot 3 was found to be significantly up-regulated by LEK treatment. As RSV treatment lead to no detectable regulation, the ratio of intensities was also significantly different in the RSV samples compared to LEK samples. According to the up-regulation by LEK, it was regarded as a true positive hit. Mass spectrometry followed by database search lead to the identification of Annexin A5, out of four individual gels, with a final sequence coverage of 71.6 %. Nothing can be said about the molecular weight and the pI as the protein was used as reference for the practical estimations.

Annexin A5 is an anti-coagulant protein, serving as an indirect inhibitor of the thromboplastin-specific complex.

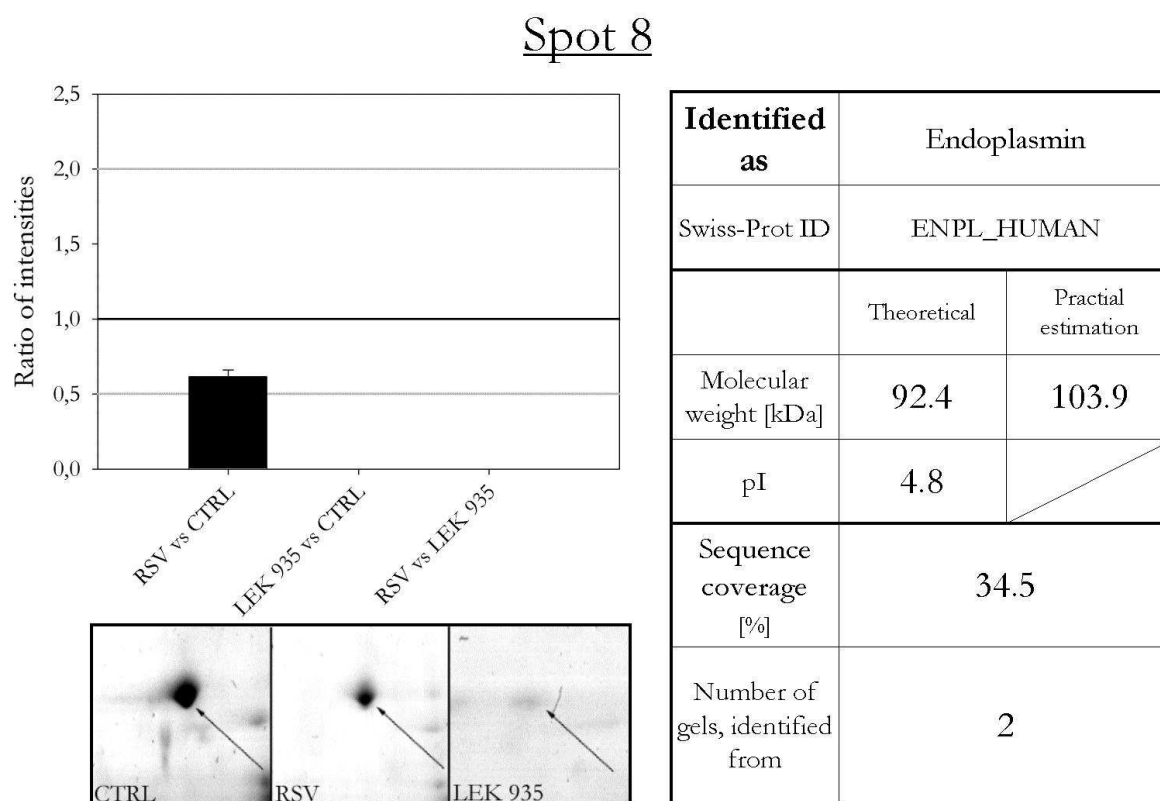
Spot 8 / Endoplasmin

Figure 0-3 Spot 8 found to be regulated in sample 1. The ratio of intensities is depicted in the left upper corner, followed by examples of the spot appearance on the analysed 2D gels. The parameters of identification as well as a comparison of theoretical to experimental data about the molecular weight and the isoelectric point are summarised on the right.

In the gels derived from samples treated with LEK-935, spot 8 was not detectable by the software, although a light shadow was visible on some of the gels (see Figure 0-3). In RSV treated samples no significant regulation could be shown, but looking at Figure 0-3 one can see a tendency to down-regulation. As the spot disappears after LEK treatment, it was regarded as a true positive hit. The estimated molecular weight is a bit higher than theoretically examined. The pI could not be estimated. The protein in spot 8 was identified as endoplasmin by mass spectrometry. Identification was possible out of two gels with a final sequence coverage of 34.5 %. Endoplasmin belongs to the family of heatshock proteins. It serves as a chaperone during protein folding of, mainly, secreted proteins.

Spot 20 / HMG-CoA synthase

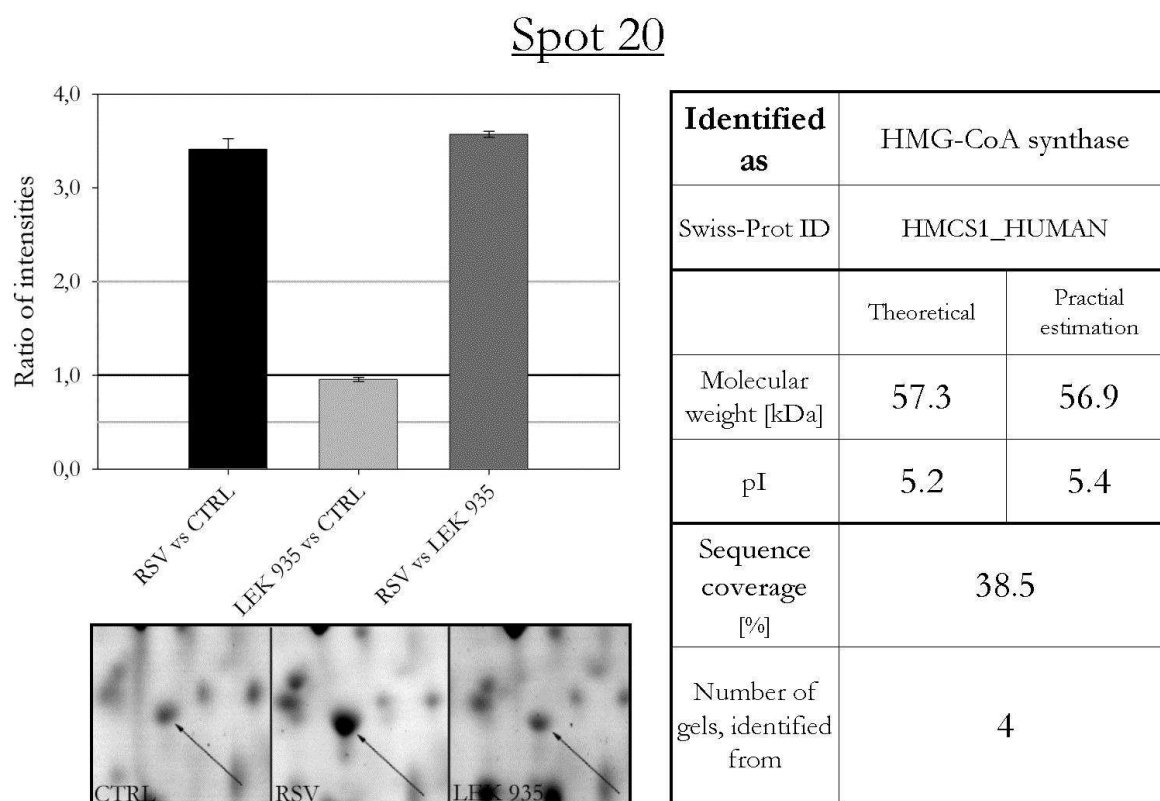


Figure 0-4 Spot 20 found to be regulated in sample 1. The ratio of intensities is depicted in the left upper corner, followed by examples of the spot appearance on the analysed 2D gels. The parameters of identification as well as a comparison of theoretical to experimental data about the molecular weight and the isoelectric point are summarised on the right.

For spot 20, about 3.5 times up-regulation was detected in the RSV sample. The LEK-935 sample showed no significantly different intensities for this spot. So, the ratio intensities for the comparison of RSV and LEK-935 samples remains the same as for the RSV – control comparison. This spot was regarded as a true positive hit, as it was up-regulated by RSV and no down-regulation was detectable at all. The practically estimated pI and molecular weight correlate well with the theoretically examined values.

The protein in this spot was identified as HMG-Co A synthase. Identification succeeded out of four individual gels, with a final sequence coverage of 38.5 %.

HMG-Co A synthase is an important protein for cholesterol-, steroid- and sterol-biosynthesis. It catalyses the formation of hydroxy-methyl-glutaryl-CoA, which is the substrate of the HMG-CoA reductase, the enzyme inhibited by rosuvastatin.

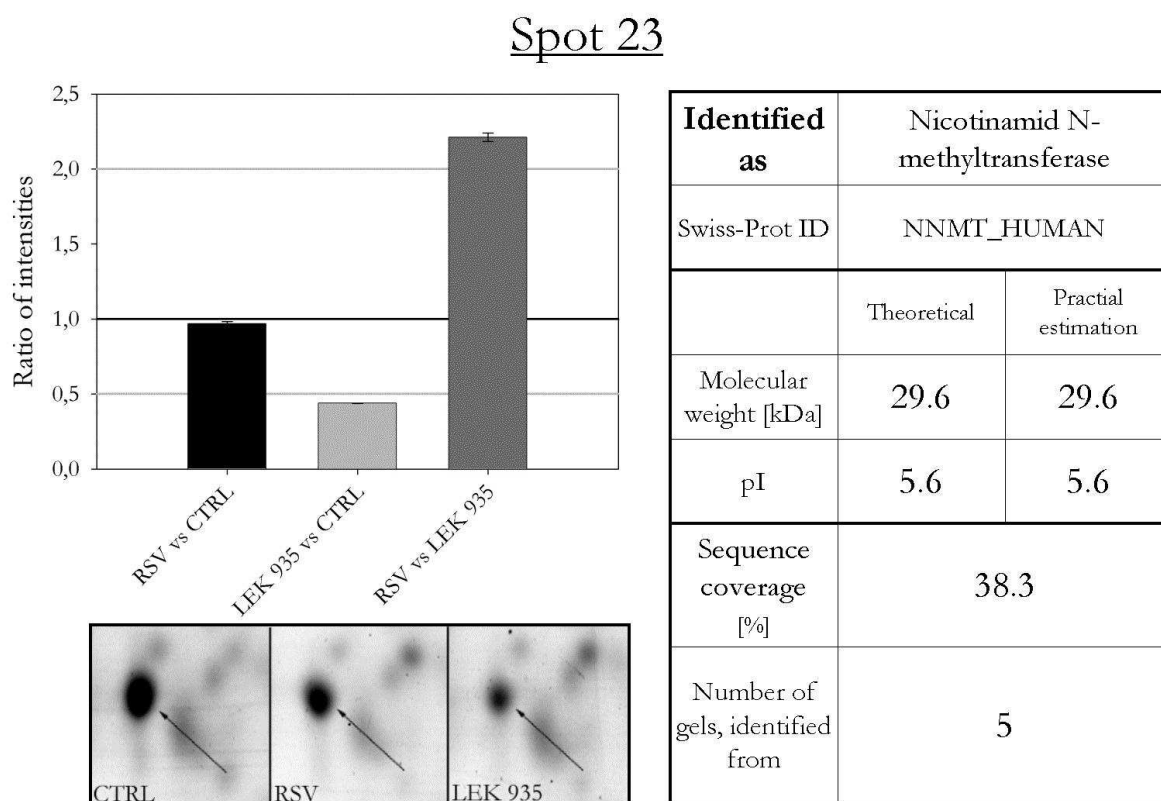
Spot 23 / Nicotinamid N-methyltransferase

Figure 0-5 Spot 23 found to be regulated in sample 1. The ratio of intensities is depicted in the left upper corner, followed by examples of the spot appearance on the analysed 2D gels. The parameters of identification as well as a comparison of theoretical to experimental data about the molecular weight and the isoelectric point are summarised on the right.

LEK samples showed significant down-regulation of spot 23, while it was not changed by RSV treatment, at all. As the spot is down-regulated in LEK-935 sample, it is regarded as a true positive hit. It was identified as nicotinamid N-methyltransferase out of five individual gels, with a final sequence coverage of 38.3 %. Nothing can be said about the pI and MW as this protein was used as a reference for the estimations. Nicotinamid N-methyltransferase catalyses the formation of pyridinium ions, important for the biotransformation of drugs and xenobiotics.

Spot 35 / Heat – shock protein

Spot 35

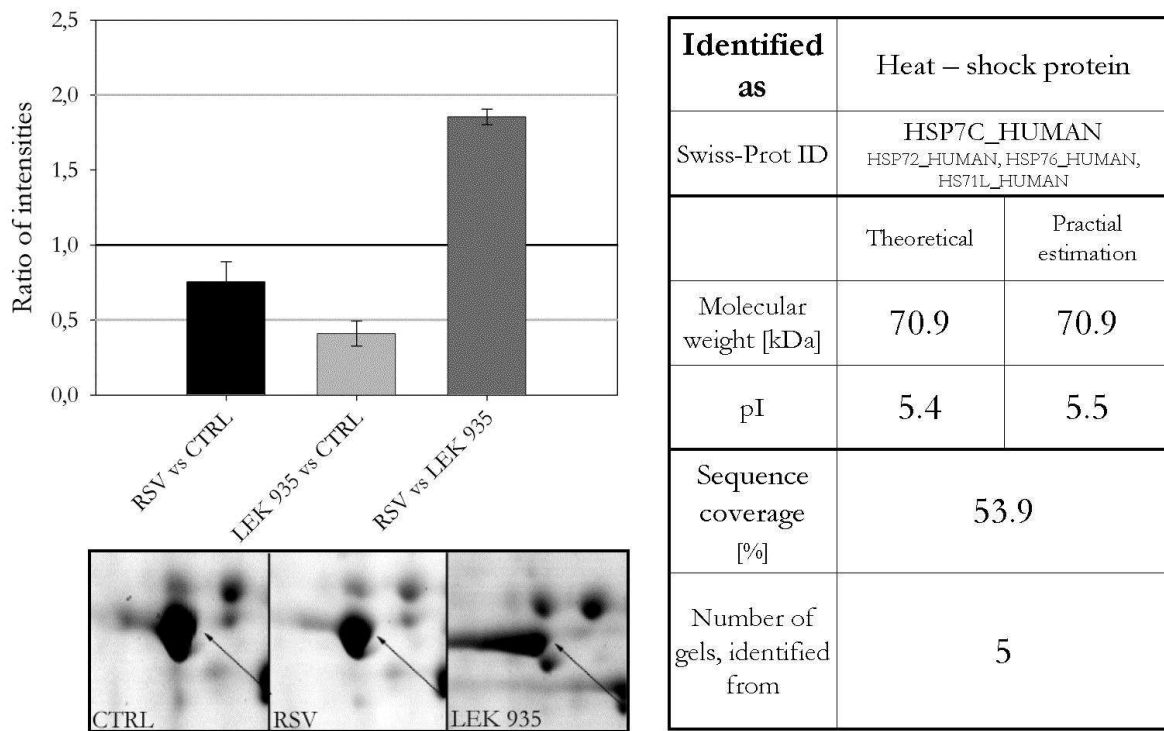


Figure 0-6 Spot 35 found to be regulated in sample 1. The ratio of intensities is depicted in the left upper corner, followed by examples of the spot appearance on the analysed 2D gels. The parameters of identification as well as a comparison of theoretical to experimental data about the molecular weight and the isoelectric point are summarised on the right.

For spot 35, a down-regulation was observed, caused by LEK-935 treatment. This spot was identified as a heat-shock protein. The identification of an individual protein was not possible as the proteins identified share a lot of peptides. HSP7C was the most prominent hit, with an sequence coverage of 53.9 %. Identification of HSP7C succeeded out of five gels. The functionality of all four proteins is similar, they are involved in stress response and mainly the reaction to unfolded proteins. They serve as chaperones for protein-folding. Nevertheless, the regulation is nearby the cut-off of two and it was not possible to identify the “real” protein underlying the spot. So this spot was excluded from further investigations. The practically estimated values for pI and molecular weight correlate well with the theoretical values.

Spot 49 / Isocitrate dehydrogenase [NADP], mitochondrialSpot 49

Identified as	Isocitrate dehydrogenase [NADP], mitochondrial	
Swiss-Prot ID	IDHP_HUMAN	
	Theoretical	Practical estimation
Molecular weight [kDa]	50.9	49.3
pI	8.9	5.7
Sequence coverage [%]	33.0	
Number of gels, identified from	1	

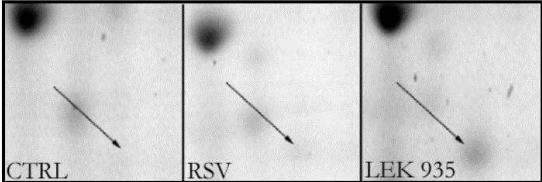


Figure 0-7 Spot 49 found to be regulated in sample 1. The ratio of intensities could not be as the spot was not present in the control and RSV treated samples. Examples of the spot appearance on the analysed 2D gels are shown in the left lower corner. The parameters of identification as well as a comparison of theoretical to experimental data about the molecular weight and the isoelectric point are summarised on the right.

Spot 49 appeared in the LEK samples. It was identified with 33.0 % sequence coverage out of one gel.

Its theoretical pH is quite high (8.9) compared with the pIs of the other proteins identified and does not correlate well with the estimated pI. The strange pI together with the comparatively low sequence coverage (33.0 % compared to averaged 49.5 %) intends to handle this result with care. Nevertheless, it was included in further studies, as it cannot be influenced by the *E.coli* contamination and a low correlation of theoretical pIs and those observed during 2D gel electrophoresis is well known. Isocitrate dehydrogenase is involved in energy metabolism, namely the glyoxylate bypass and the tricarboxylic acid cycle.

Spot 71, Spot 86 / Serum albumin

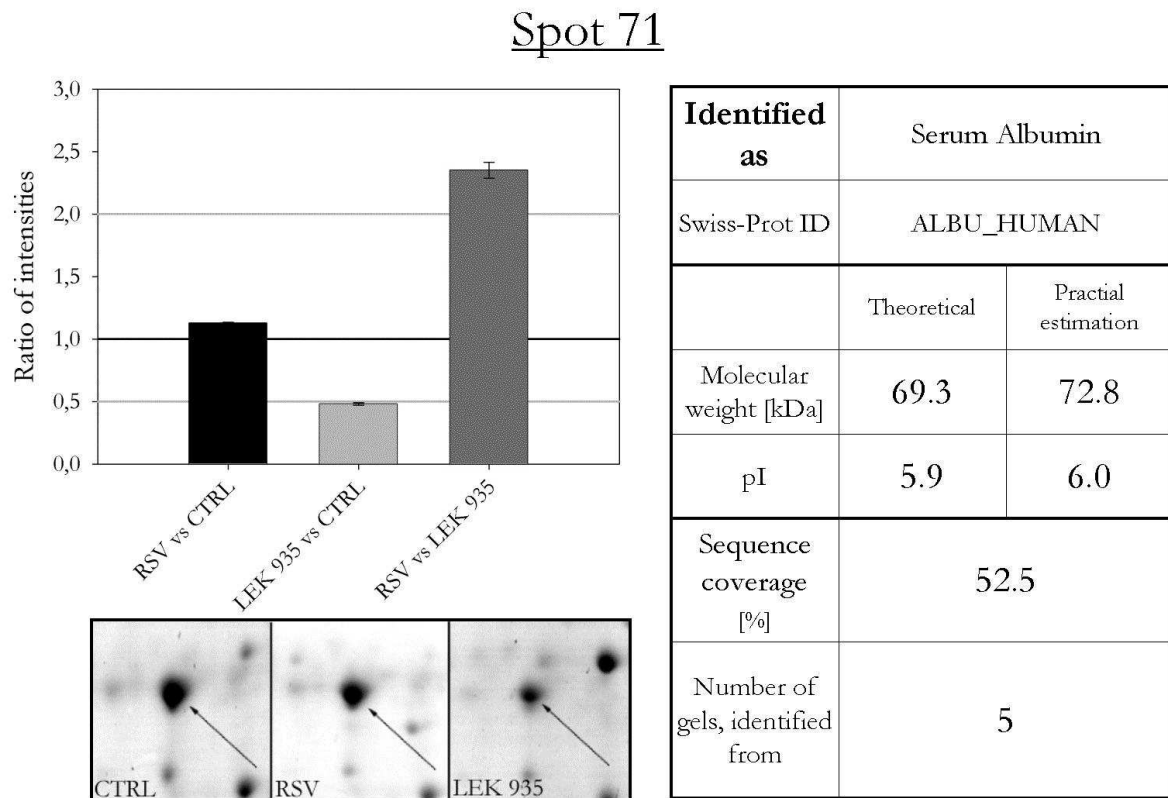


Figure 0-8 Spot 71 found to be regulated in sample 1. The ratio of intensities is depicted in the left upper corner, followed by examples of the spot appearance on the analysed 2D gels. The parameters of identification as well as a comparison of theoretical to experimental data about the molecular weight and the isoelectric point are summarised on the right.

For spot 71 a down-regulation by LEK-935 compared to the control as well as the RSV treated samples was observed. It was identified as serum albumin, out of five individual gels, with a sequence coverage of 52.5 %.

Serum albumin is the major protein found in human plasma. It has a high binding capacity for mono- and divalent anions like Ca^{2+} and Na^+ for example, but also for other molecules like hormones, fatty acids and so on.

Spot 86

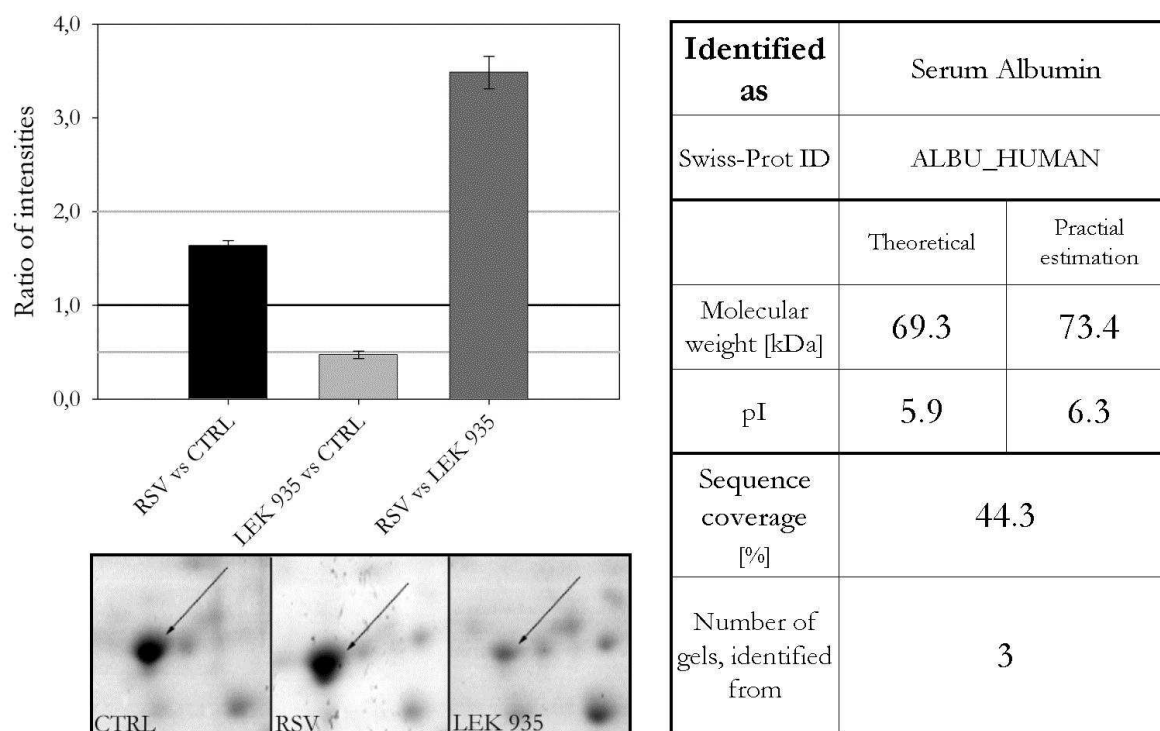


Figure 0-9 Spot 86 found to be regulated in sample 1. The ratio of intensities is depicted in the left upper corner, followed by examples of the spot appearance on the analysed 2D gels. The parameters of identification as well as a comparison of theoretical to experimental data about the molecular weight and the isoelectric point are summarised on the right.

Regulation of spot 86 was similar to the regulation of spot 71. After identification it turned out, that here again serum albumin is the protein present in the spot. It was identified out of three individual gels, with a sequence coverage of 44.3 %. For further information see spot 71. In both cases the practically estimated values for pI and molecular weight correlate well with the theoretical ones.

Spot 83, Spot 88 / Phosphoglucomutase 1

Spot 83

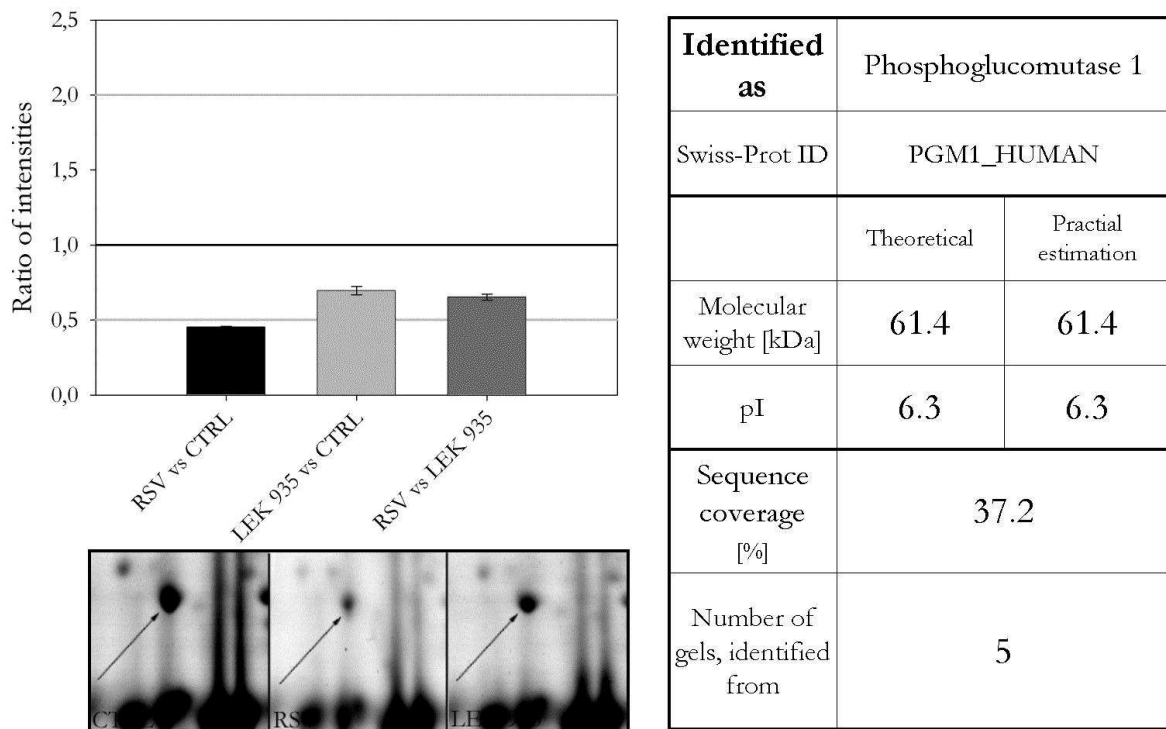


Figure 0-10 Spot 83 found to be regulated in sample 1. The ratio of intensities is depicted in the left upper corner, followed by examples of the spot appearance on the analysed 2D gels. The parameters of identification as well as a comparison of theoretical to experimental data about the molecular weight and the isoelectric point are summarised on the right.

Spot 83 was significantly down-regulated by RSV and some decreasing tendencies were observed in the LEK samples. It was identified as phosphoglucomutase 1. The regulations were regarded as a true positive hit because similar values were also found in spot 88, identified as phosphoglucomutase 1, too. Identification for spot 83 was performed out of five individual gels, with a final sequence coverage of 37.2 %.

Phosphoglucomutase 1 is highly involved in the breakdown as well as the synthesis of glucose. It catalyses the conversion of alpha-D-glucose-1-phosphate to alpha-D-glucose-6-phosphate and back. So it plays a central role in the general energetic metabolism of cells. The practically estimated pI and molecular weight correlate very well with the theoretical values. Differentiating between two isoforms expressed, coming from alternative splicing, is not possible, due to the high similarities between their molecular weights and pIs.

Spot 88

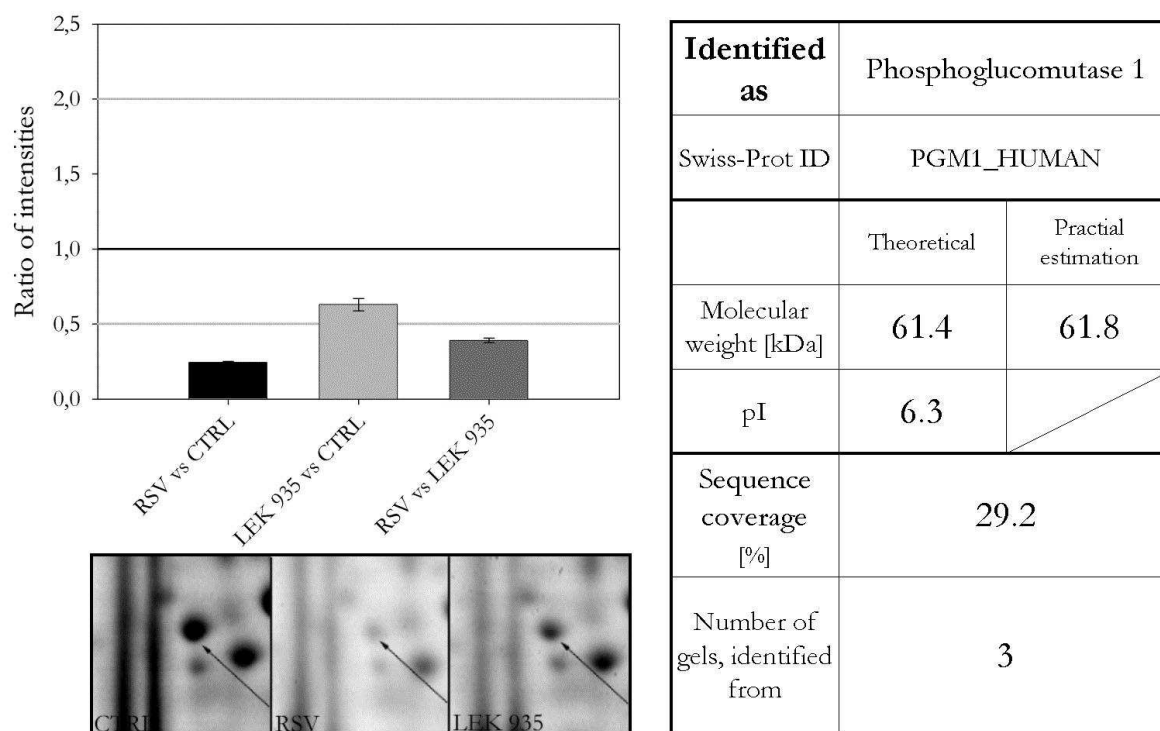


Figure 0-11 Spot 88 found to be regulated in sample 1. The ratio of intensities is depicted in the left upper corner, followed by examples of the spot appearance on the analysed 2D gels. The parameters of identification as well as a comparison of theoretical to experimental data about the molecular weight and the isoelectric point are summarised on the right.

Spot 88 was down-regulated by RSV treatment in comparison to the control as well as the LEK-935 treated sample. It was identified as phosphoglucomutase 1, with a sequence coverage of 29.2 %. Identification was performed out of three individual gels.

Spot 89 / Radixin, Ezrin or Moesin

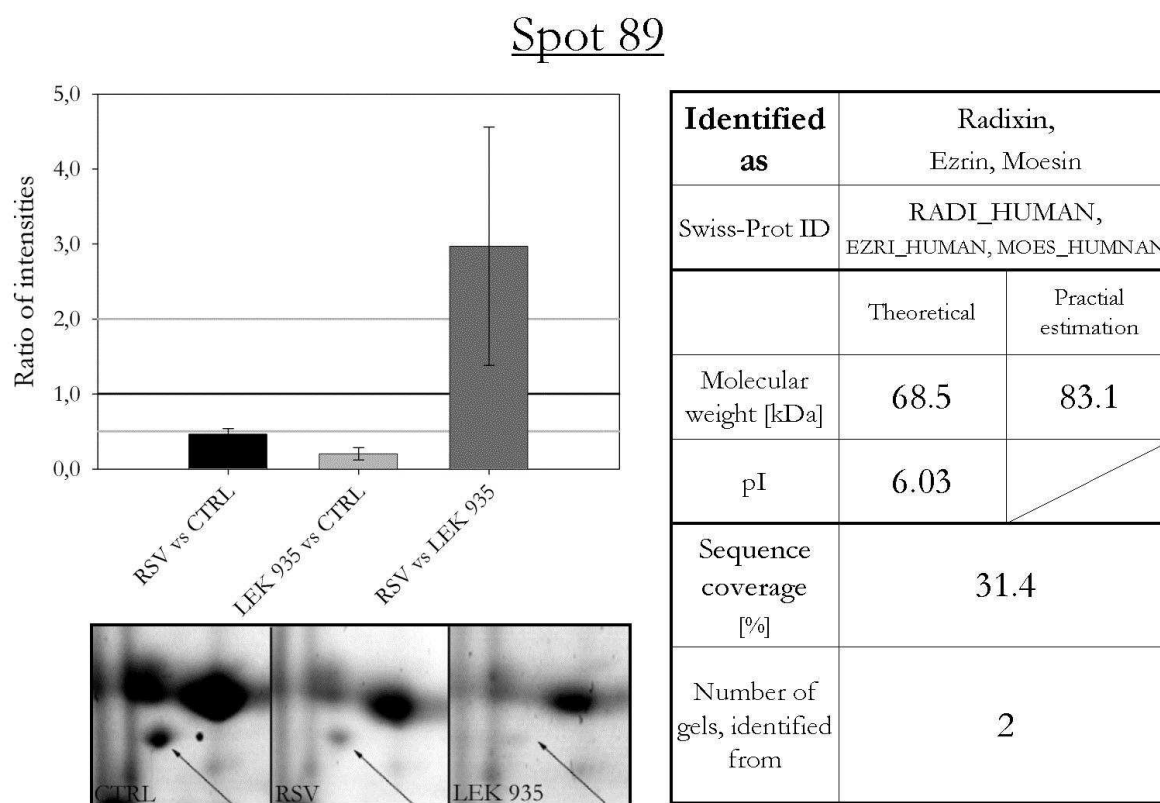


Figure 0-12 Spot 89 found to be regulated in sample 1. The ratio of intensities is depicted in the left upper corner, followed by examples of the spot appearance on the analysed 2D gels. The parameters of identification as well as a comparison of theoretical to experimental data about the molecular weight and the isoelectric point are summarised on the right.

Spot 89 was down-regulated by LEK-935 treatment and showed a strong tendency to down-regulation by RSV treatment. Therefore it was regarded as a true positive hit and further investigated. Identification lead to three possibilities for the protein inside the spot, whereby radixin showed the highest probability. For radixin a sequence coverage of 31.4 % was achieved, by identification out of two individual gels. The three proteins are highly homologous in their amino acid sequence. All are involved in binding of cytoskeletal structures to the cell membrane. According to the ExPASy database, ezrin can be excluded from the hit list because it is specifically expressed in neuronal tissues. As they have quite similar functions and radixin showed a higher sequence coverage than moesin, radixin was chosen for further investigations.

The estimated molecular weight is significantly higher than the theoretically examined value. The pI could not be determined.

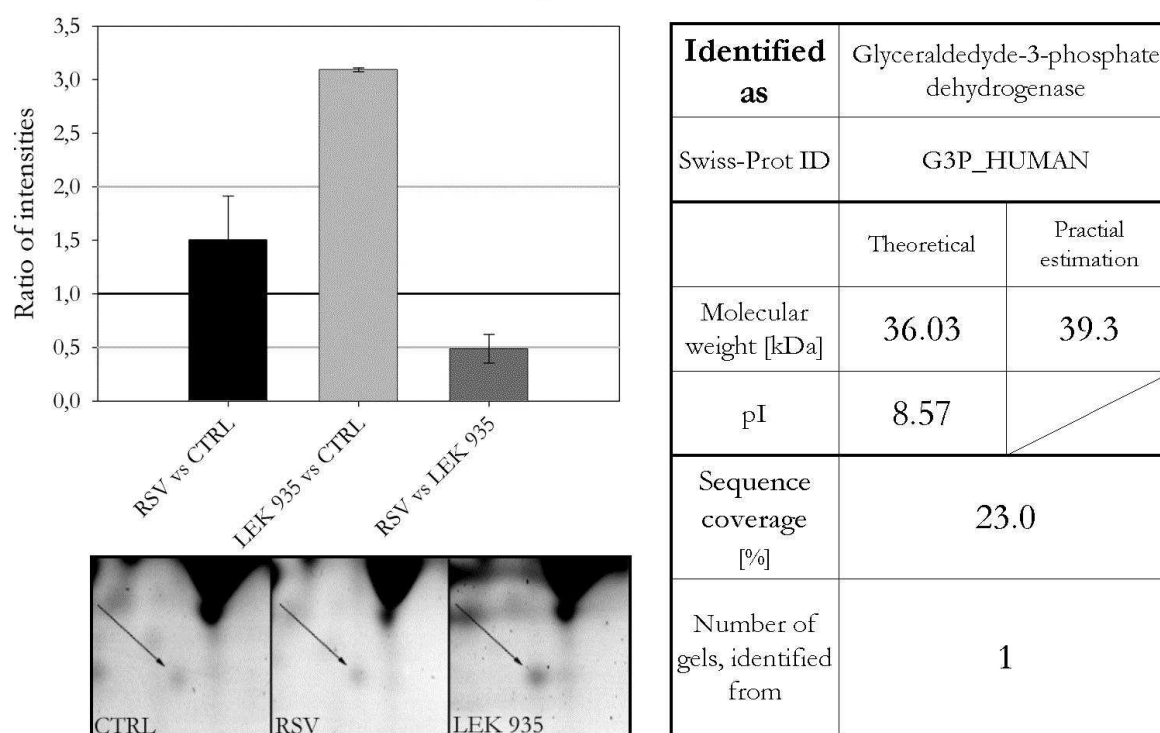
Spot 93 / Glyceraldehyde-3-phosphate dehydrogenaseSpot 93

Figure 0-13 Spot 93 found to be regulated in sample 1. The ratio of intensities is depicted in the left upper corner, followed by examples of the spot appearance on the analysed 2D gels. The parameters of identification as well as a comparison of theoretical to experimental data about the molecular weight and the isoelectric point are summarised on the right.

Treatment with LEK-935 lead to 3.1 times higher intensity of spot 93 than that observed in the control samples. Mass spectrometry followed by database search revealed glyceraldehyde-3-phosphate dehydrogenase as the protein underlying this spot. Identification was possible out of one gel, with a final sequence coverage of 23.0 %.

Glyceraldehyde-3-phosphate dehydrogenase catalyses the rate-determining step in glycolysis and is further involved in membrane trafficking during the early steps of the secretory pathway. It shows a quite high theoretical pI, which does not correlate well with its position on the gels. It is located at the basic side of the spot pattern but other spots located in the same region were identified as proteins with lower pIs. The molecular weight correlates well with the theoretical value.

Spot 94 / Serotransferrin

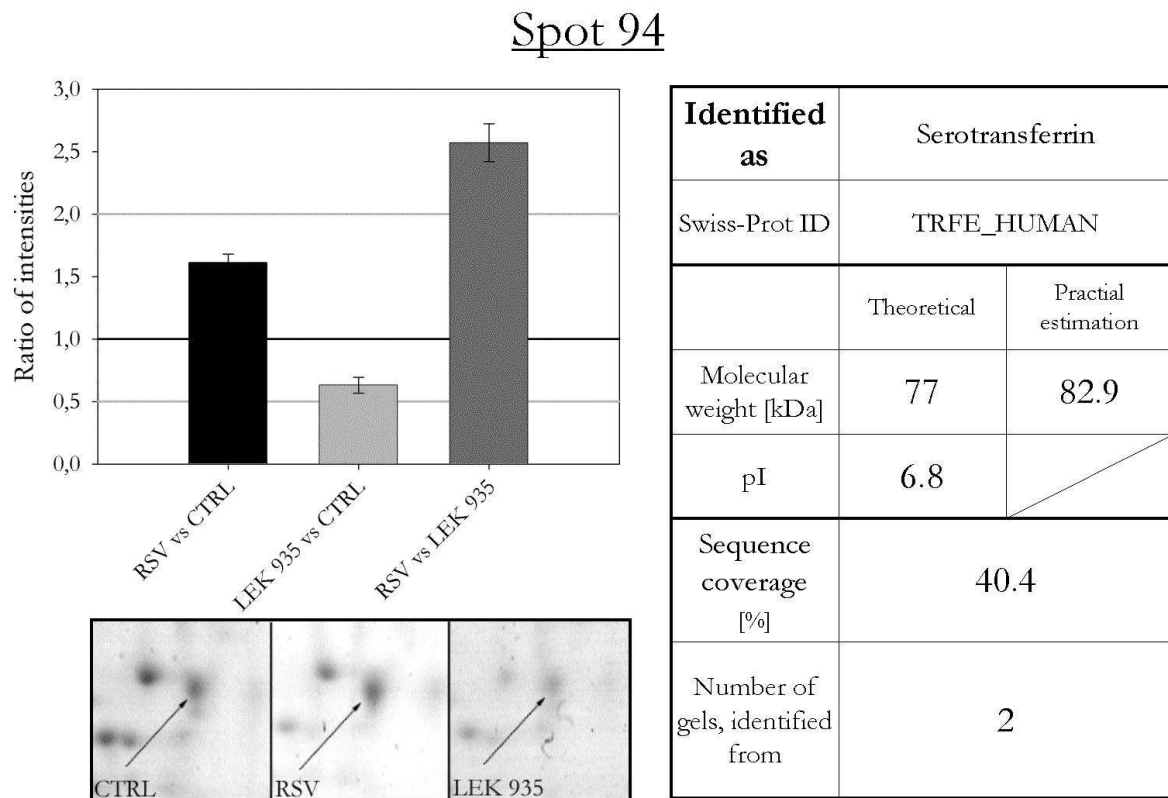


Figure 0-14 Spot 94 found to be regulated in sample 1. The ratio of intensities is depicted in the left upper corner, followed by examples of the spot appearance on the analysed 2D gels. The parameters of identification as well as a comparison of theoretical to experimental data about the molecular weight and the isoelectric point are summarised on the right.

Spot 94 was significantly up-regulated in RSV treated sample compared to LEK-935 treated sample. It was regarded as a true positive hit and identified out of two individual gels, with a sequences coverage of 40.4 %. The pI could not be estimated practically. The estimated molecular weight correlates well with the theoretical value. Serotransferrin is a secreted protein involved in iron transport processes. Beside this function it's suggested to play a role in stimulating cell proliferation. Its expression is liver specific, followed by expression to the plasma.

Sample 1 nLC-MS results

UP

Long chain fatty acid CoA ligase

(ACSL3_HUMAN or ACSL4_HUMAN)

The same set of peptides was identified for either long-chain-fatty-acid CoA ligase 3 or 4.

They are integral membrane proteins, located in the microsomal, peroxisomal or inner mitochondrial membrane. As the name says, they are involved in fatty acid metabolism, either their activation for lipid synthesis or degradation via beta-oxidation. They catalyse the ligation of CoA to a fatty acid under ATP consumption.

They differ in preferation of distinct fatty acids for ligation, while form 3 prefers myristate, laurate, arachidonate and eicosapentaenoate as substrates, only the latter twos are the favourites of form 4.

Form 3 was used for further bioinformatical analysis, as they have quite similar behaviours and functions in the cells.

Apolipoprotein C1

(APOC1_HUMAN)

Apolipoprotein C1 is a secreted protein, involved in the VLDL (up to 10 % of its protein) and HDL (up to 2 % of its protein) cholesterol transport through the body. The protein seems to modulate the interaction of APOE with beta-migrating VLDL and inhibit binding of beta-VLDL to the LDL receptor-related protein.

Apolipoprotein C3

(APOC3_HUMAN)

The Apolipoprotein C3 is a secreted protein, too. It is part of the VLDL (50 %) and HDL (2 %). It inhibits lipoprotein lipase and hepatic lipase and decreased the uptake of lymph chylomicrons.

Succinate dehydrogenase cytochrome b560 subunit, mitochondrial

(C560_HUMAN)

The succinate dehydrogenase cytochrome b560 subunit is a multi-pass membrane protein, located at the inner mitochondrial membrane. It is a mono-heme cytochrome

b, involved in system II of the mitochondrial electron transport chain, responsible for transferring electrons from succinate to ubiquinone.

Lanosterol 14-alpha demethylase

(CP51A_HUMAN)

The lanosterol 14-alpha demethylase, also known as cytochrome P450 51A1, is an integral membrane protein located in the microsomes. It catalyses the C14 demethylation of lanosterol, transforming it into 4,4'-dimethyl cholesta-8,14,24-triene-3-beta-ol. Therefore it plays an important role in cholesterol biosynthetic pathways.

Estradiol 17-beta-dehydrogenase 12

(DHB12_HUMAN)

The estradiol 17-beta-dehydrogenase 12 is a multi-pass membrane protein, located in the membrane of the endoplasmic reticulum. It catalyses the conversion of estrone into estradiol. Thereby it plays a major role in the synthesis of estrogens.

Transmembrane protein 56

(TMM56_HUMAN)

The transmembrane protein 56 is a potential multi-pass membrane protein about which no deeper information is available yet.

ATP-citrate synthase

(ACLY_HUMAN)

The ATP-citrate synthase is a soluble protein, located in the cytoplasm. It is the primary enzyme responsible for synthesis of cytosolic acetyl-CoA and plays a central role in de novo lipid-biosynthesis.

Squalene synthetase

(FDFT_HUMAN)

The squalene synthetase is a multi-pass membrane protein located in the endoplasmic reticulum membrane. It catalyses the two-step formation of squalene from two farnesyl diphosphates and thereby plays a central role in lanosterol and cholesterol synthesis.

Mannose-P-dolichol utilization defect 1 protein

(MPU1_HUMAN)

The mannose-P-dolichol utilisation defect 4 protein is a potential multi-pass membrane protein. Only suggestions are available about its cellular functions.

DOWN

Actin

(ACTS_HUMAN, ACTA_HUMAN, ACTH_HUMAN)

Nearly the same set of peptides was identified for the three sub-forms of actin. All of them are soluble and play a role in cell structure and motion. ACTA seems to be improbable cause its normally located in aortic muscle cells and ACTS is found in skeletal muscle cells, while ACTH plays a role in nearly all cells in the cytoskeleton formation. Nevertheless, no real differentiation was possible due tot the high similarity between these subforms. As, there seems to be an effect on cytoskelectal structures, in general considerations reflected by all three, ACTH, was chosen as a representative of this group in further bioinformatical analysis.

60S ribosomal protein L9

(RL9_HUMAN)

The 60S ribosomal protein L9 is a soluble protein, involved in the ribosomal complex during translation. No detailed information about this protein was available.

Sample 2 2D spot details

Spot 2 / Tubulin beta chain

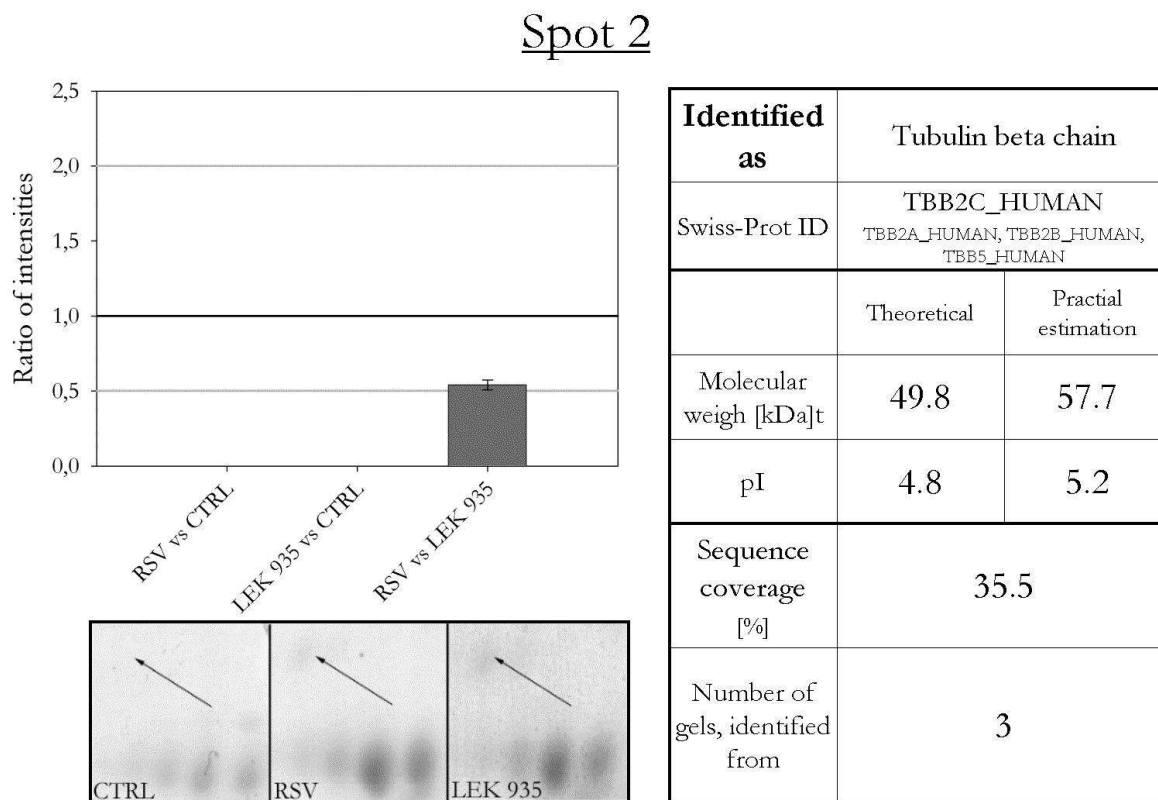


Figure 0-15 Spot 2 found to be regulated in sample 2. The ratio of intensities is depicted in the left upper corner, followed by examples of the spot appearance on the analysed 2D gels. The parameters of identification as well as a comparison of theoretical to experimental data about the molecular weight and the isoelectric point are summarised on the right.

Spot 2 was found to appear in the treated samples, while not being present in the control sample. The spot intensity in LEK treated samples was nearly double to that observed in RSV treated samples.

With a sequence coverage of 35.5 % spot 2 was identified as tubulin beta chain out of three individual gels. Differentiation between beta chain alpha, beta or gamma was not possible. As the three subunits build the microtubules of the cytoskeleton and have thereby similar abilities. The gamma chain was chosen as a representative for further investigations of the regulated proteins regarding their cellular function.

Spot 3 / 78 kDa glucose regulated protein precursorSpot 3

Identified as	78kDa-glucose regulated protein precursor	
Swiss-Prot ID	GRP78_HUMAN	
	Theoretical	Practical estimation
Molecular weigh [kDa]t	72.3	72.3
pI	5.1	5.1
Sequence coverage [%]	37.9	
Number of gels, identified from	1	

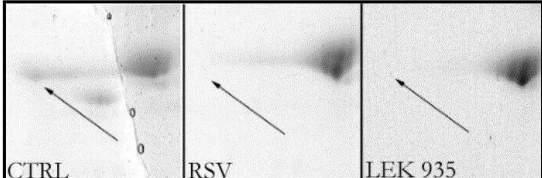


Figure 0-16 Spot 3 found to be regulated in sample 2. The ratio of intensities could not be depicted as the spot was not present in both treated samples. Examples of the spot appearance on the analysed 2D gels are shown in the left lower corner. The parameters of identification as well as a comparison of theoretical to experimental data about the molecular weight and the isoelectric point are summarised on the right.

For spot 3, disappearance was observed after RSV and LEK treatment. The spot was identified as 78 kDa-glucose regulated protein precursor. Identification was performed out of one gel, with a sequence coverage of 37.9 %.

This protein belongs to the group of heat-shock proteins and is involved in the assembly of multimeric protein complexes inside the ER lumen.

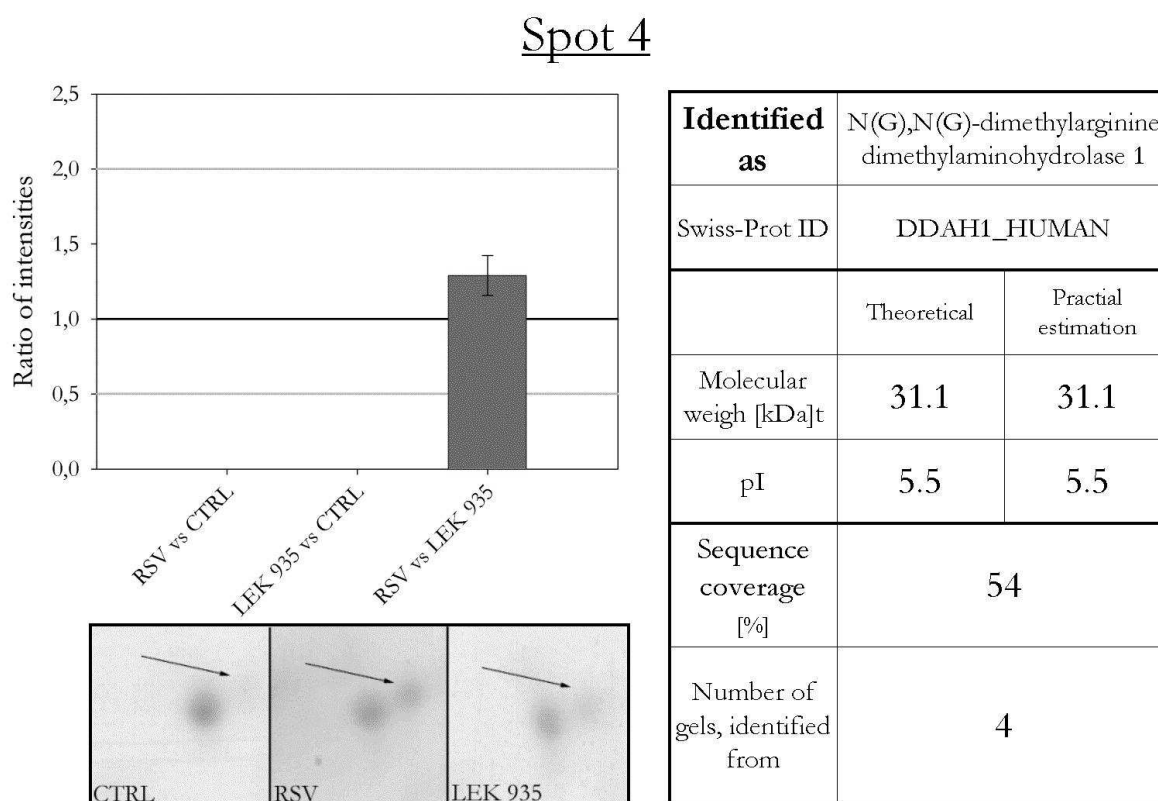
Spot 4 / N(G),N(G)-dimethylarginine dimethylaminohydrolase 1

Figure 0-17 Spot 4 found to be regulated in sample 2. The ratio of intensities is depicted in the left upper corner, followed by examples of the spot appearance on the analysed 2D gels. The parameters of identification as well as a comparison of theoretical to experimental data about the molecular weight and the isoelectric point are summarised on the right.

In the samples treated with RSV as well as those treated with LEK-935, the appearance of spot 4 was observed. It was identified as N(G),N(G)-dimethylarginine dimethylaminohydrolase 1, out of four gels, leading to a final sequence coverage of 54.0 %.

This enzyme plays a role in nitic oxide generation by hydrolysing N(G),N(G)-dimethyl-L-arginine and N(G)-monomethyl-L-arginine, acting as inhibitors of NOS.

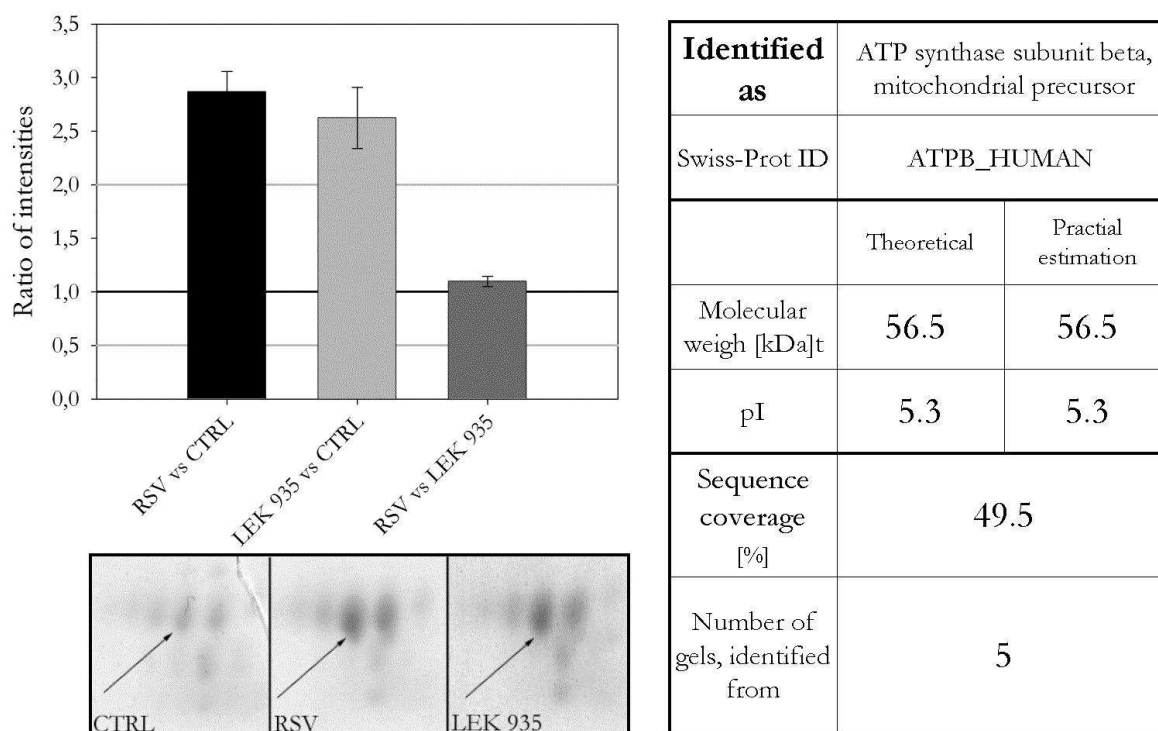
Spot 7, Spot 8 / ATP synthase subunit beta, mitochondrial precursorSpot 7

Figure 0-18 Spot 7 found to be regulated in sample 2. The ratio of intensities is depicted in the left upper corner, followed by examples of the spot appearance on the analysed 2D gels. The parameters of identification as well as a comparison of theoretical to experimental data about the molecular weight and the isoelectric point are summarised on the right.

Spot 7 as well as spot 8 were found to be up-regulated by RSV treatment, while LEK treatment lead to a significant up-regulation of spot 7 but a borderline up-regulation of spot 8. Both spots were identified as ATP synthase subunit beta with a sequence coverage above 44.0 %.

ATP synthase is located at the mitochondrial membrane, catalysing the synthesis of ATP from ADP driven by a proton gradient across the membrane. These spots were chosen as reference for the molecular weight and pI.

Spot 8

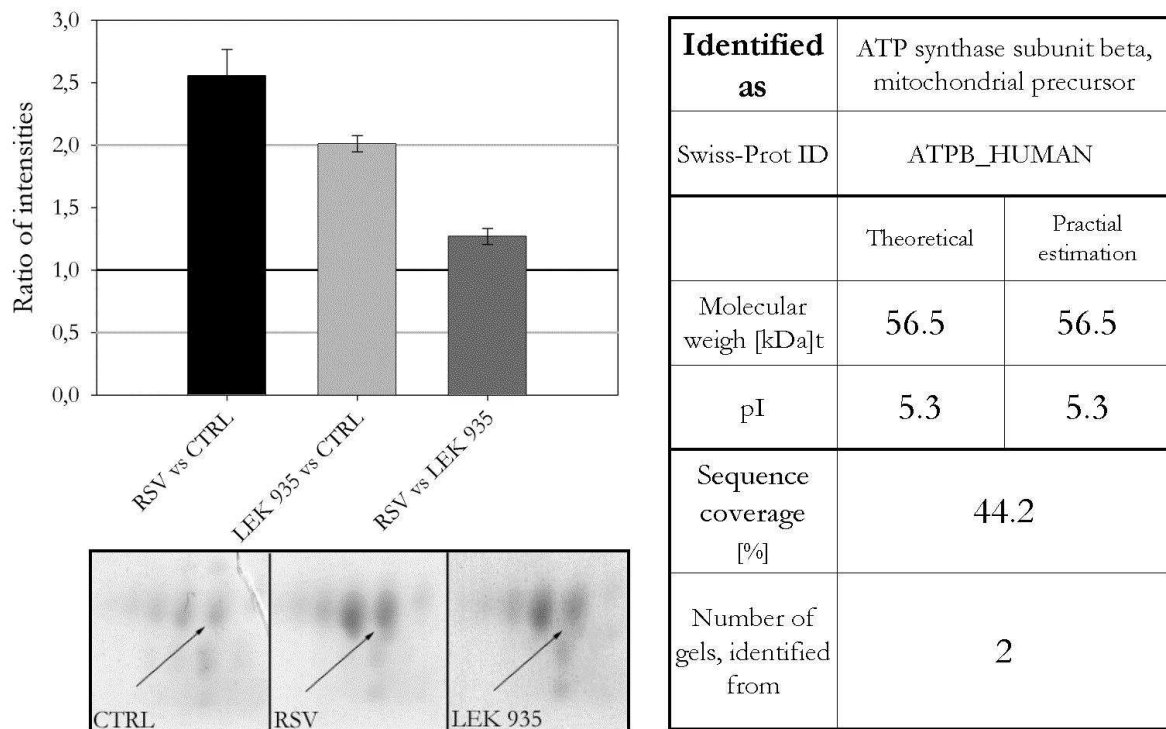


Figure 0-19 Spot 8 found to be regulated in sample 2. The ratio of intensities is depicted in the left upper corner, followed by examples of the spot appearance on the analysed 2D gels. The parameters of identification as well as a comparison of theoretical to experimental data about the molecular weight and the isoelectric point are summarised on the right.

Spot 11 / Actin

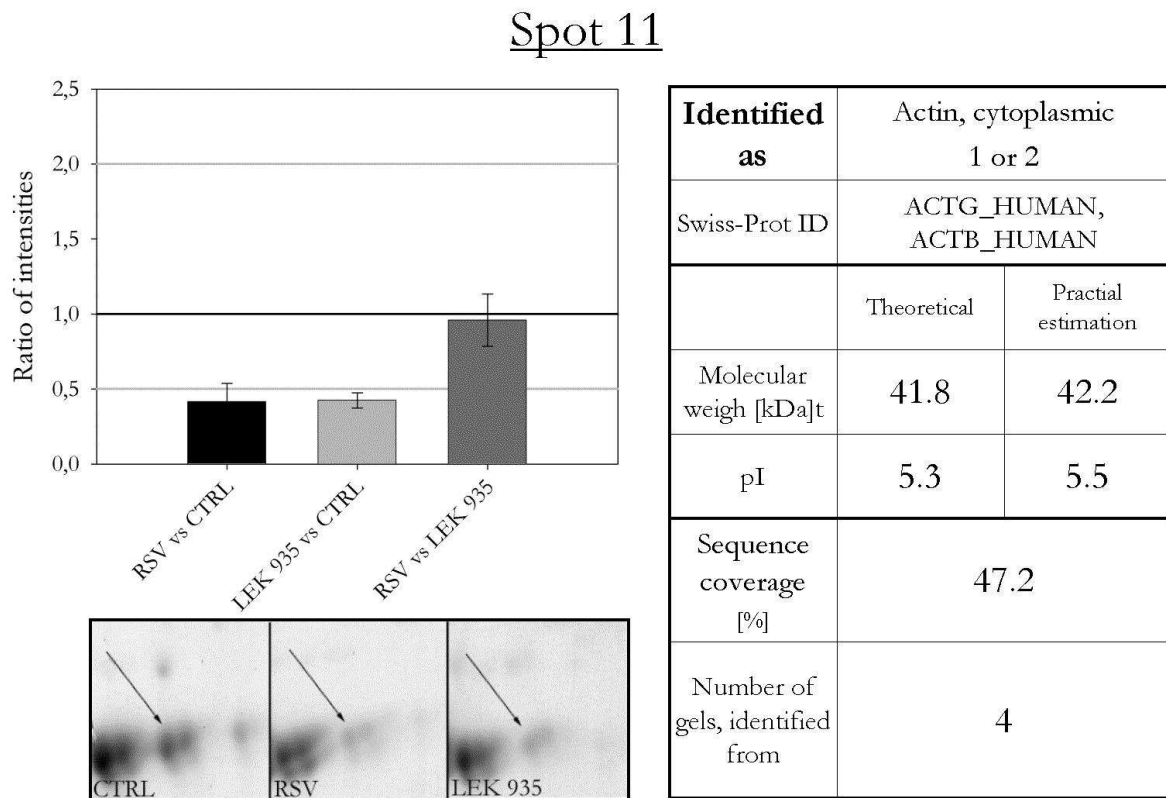


Figure 0-20 Spot 11 found to be regulated in sample 2. The ratio of intensities is depicted in the left upper corner, followed by examples of the spot appearance on the analysed 2D gels. The parameters of identification as well as a comparison of theoretical to experimental data about the molecular weight and the isoelectric point are summarised on the right.

Spot 11 was found to be significantly down-regulated after LEK treatment, while down-regulation observed after RSV treatment is a borderline event as the standard deviation of the ratio of intensities crosses the threshold line. Out of four individual gels, the spot was identified as a cytoplasmic form of actin, with a sequence coverage of 47.2 %. Differentiation between form one or two was not possible.

They behave similar but not identical in the cellular context, serving as structural proteins involved in the cytoskeleton and cell motion.

The cytoplasmic 1 form was chosen for further analysis.

Spot 12 / Eukaryotic initiation factor 4A-1

Spot 12

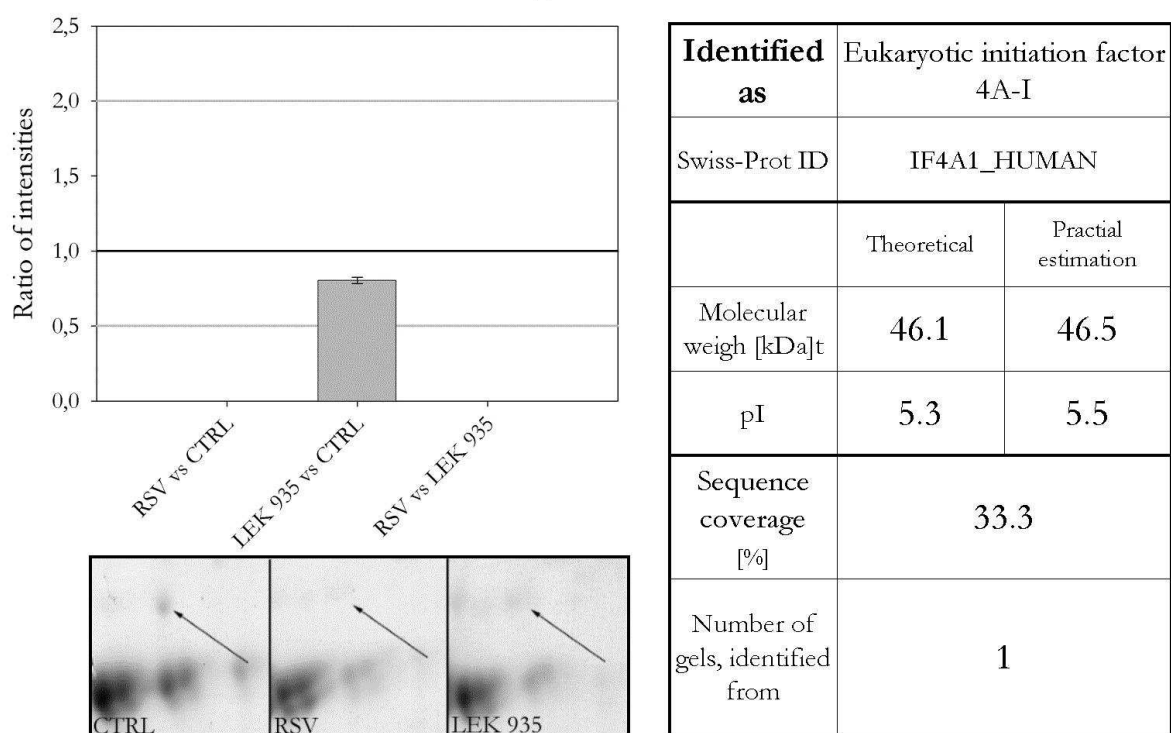
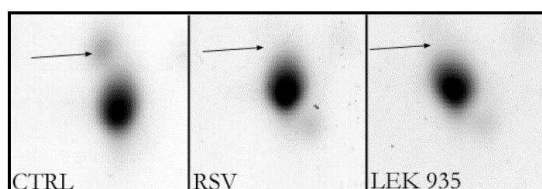


Figure 0-21 Spot 12 found to be regulated in sample 2. The ratio of intensities is depicted in the left upper corner, followed by examples of the spot appearance on the analysed 2D gels. The parameters of identification as well as a comparison of theoretical to experimental data about the molecular weight and the isoelectric point are summarised on the right.

Spot 12 was found to disappear after treating the cells with rosuvastatin. The spot was identified out of one gel with a sequence coverage of 33.3 %- Eukaryotic initiation factor 4A-I was found to be the protein inside the spot.

Its practically estimated pI and molecular weight correlate well with the theoretical values. It is a RNA helicase and part of a protein complex, necessary for mRNA binding to the small ribosomal subunit.

Spot 13 / Superoxide dismutase [Cu-Zn]Spot 13

Identified as	Superoxide dismutase [Cu-Zn]	
Swiss-Prot ID	SODC_HUMAN	
	Theoretical	Practical estimation
Molecular weight [kDa]	15.9	15.9
pI	5.7	5.7
Sequence coverage [%]	44.2	
Number of gels, identified from	1	

Figure 0-22 Spot 13 found to be regulated in sample 2. The ratio of intensities could not be depicted as the spot was not present in both treated samples. Examples of the spot appearance on the analysed 2D gels are shown in the left lower corner. The parameters of identification as well as a comparison of theoretical to experimental data about the molecular weight and the isoelectric point are summarised on the right.

Spot 13 disappeared after both treatments. It was identified as superoxide dismutase [Cu-Zn], out of one gel, with a sequence coverage of 44.2 %

In general, the superoxide dismutase removes radicals produced during biological processes inside the cell. But it is also known to be involved in a negative regulation of cholesterol biosynthetic processes.

Spot 14 / Heat shock protein beta 1, 3-Hydroxyisobutyrat-dehydrogenase, 3-hydroxyanthranilate 3,4-dioxygenase

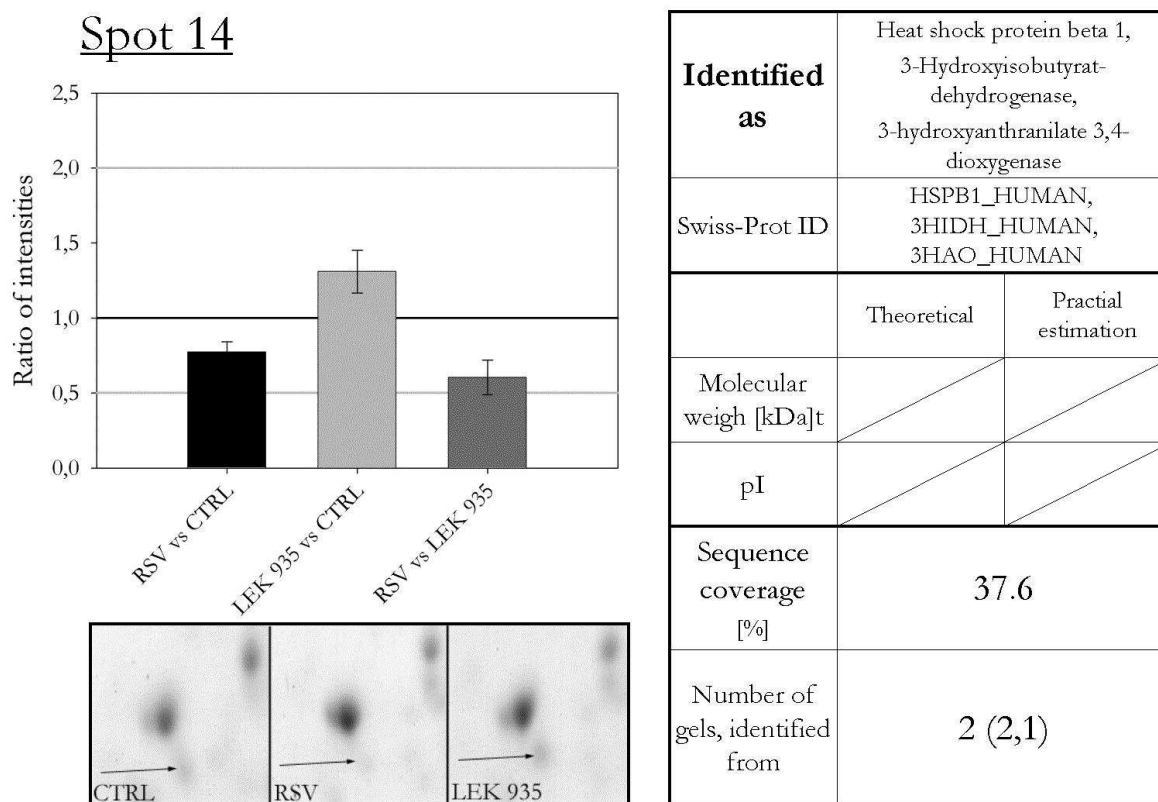


Figure 0-23 Spot 14 found to be regulated in sample 2. The ratio of intensities is depicted in the left upper corner, followed by examples of the spot appearance on the analysed 2D gels. The parameters of identification as well as a comparison of theoretical to experimental data about the molecular weight and the isoelectric point are summarised on the right.

Spot 14 was found to be borderline down-regulated by RSV compared to the LEK-935 treated samples. As this was a borederline regulation and identification revealed three different proteins, this spot was excluded from further investigations.

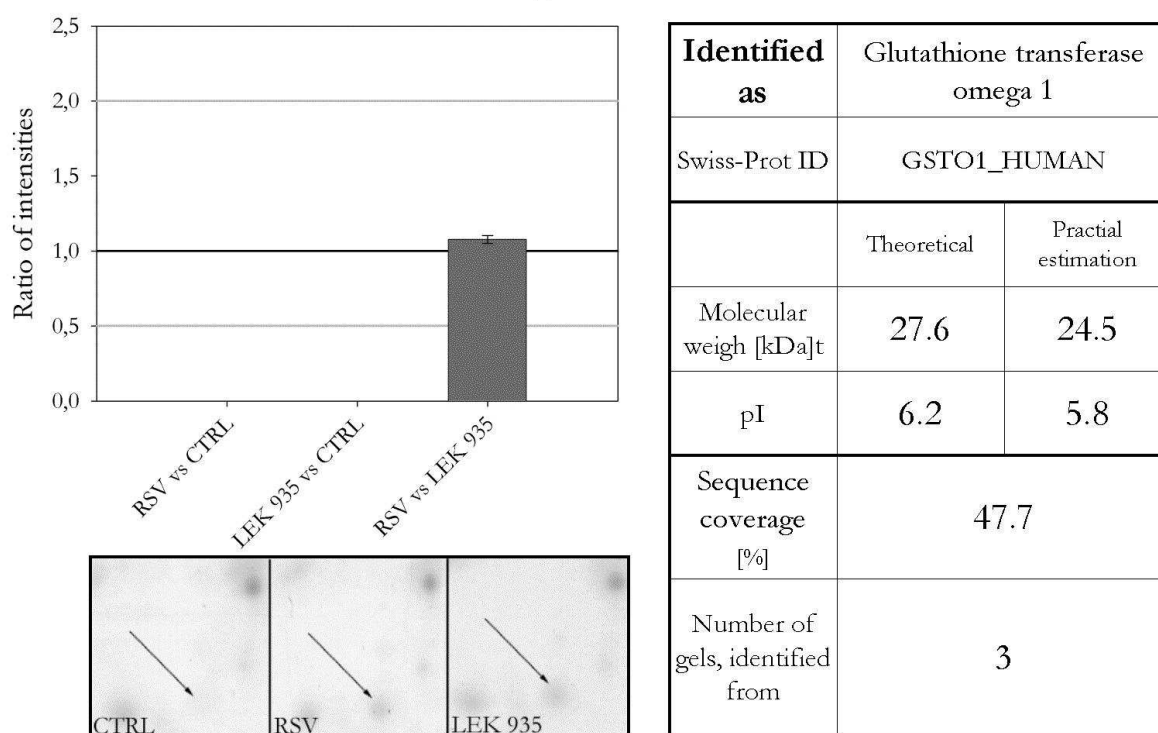
Spot 15, spot 25 / Glutathione transferase omega 1Spot 15

Figure 0-24 Spot 15 found to be regulated in sample 2. The ratio of intensities is depicted in the left upper corner, followed by examples of the spot appearance on the analysed 2D gels. The parameters of identification as well as a comparison of theoretical to experimental data about the molecular weight and the isoelectric point are summarised on the right.

Spot 15 as well as spot 25 appeared after LEK and RSV treatment. They were identified as glutathione-S-transferase omega 1, with a sequence coverage of 47.7 and 45.6 % for spots 15 and 25, respectively. Identification succeeded out of three and four different gels. The theoretical values for pI and molecular weight correlate with the estimated ones.

It transfers glutathione to acceptor molecules, thereby forcing, like other GSTs, the detoxification of endogenous and exogenous substances.

Spot 25

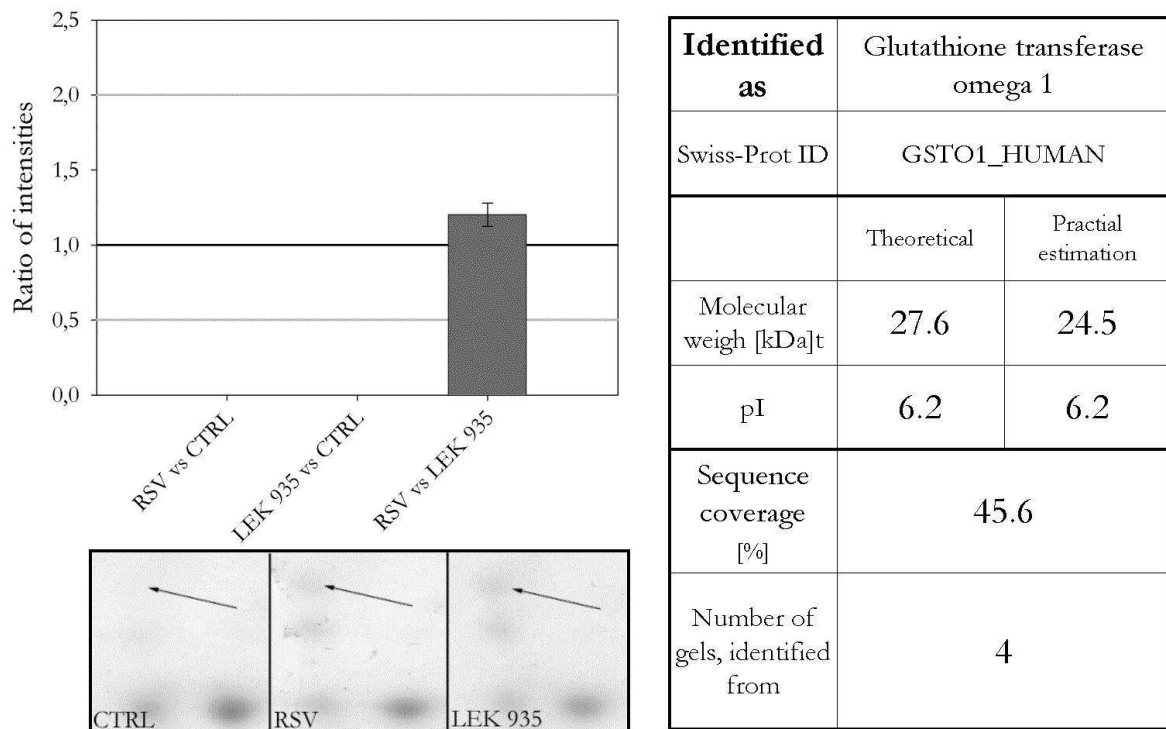


Figure 0-25 Spot 25 found to be regulated in sample 2. The ratio of intensities is depicted in the left upper corner, followed by examples of the spot appearance on the analysed 2D gels. The parameters of identification as well as a comparison of theoretical to experimental data about the molecular weight and the isoelectric point are summarised on the right.

Spot 16 / Retinal-dehydrogenase 1Spot 16

Identified as	Retinal-dehydrogenase 1	
Swiss-Prot ID	AL1A1_HUMAN	
	Theoretical	Practical estimation
Molecular weight [kDa]	54.9	58.0
pI	6.3	6.0
Sequence coverage [%]	29.7	
Number of gels, identified from	2 (no ZipTip)	

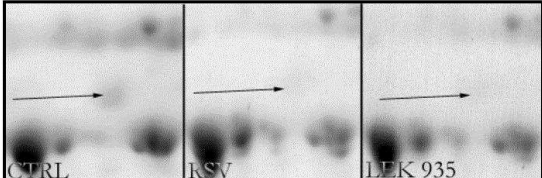


Figure 0-26 Spot 16 found to be regulated in sample 2. The ratio of intensities could not be depicted as the spot was not present in both treated samples. Examples of the spot appearance on the analysed 2D gels are shown in the left lower corner. The parameters of identification as well as a comparison of theoretical to experimental data about the molecular weight and the isoelectric point are summarised on the right.

After LEK as well as RSV treatment, spot 16 could not be observed anymore on the gels. It was identified as retinal-dehydrogenase 1, out of two different gels. Its practically estimated pI and molecular weight correlate well with the theoretical values. The retinal-dehydrogenase 1 is involved in cellular aldehyde metabolic processes and catalyses the conversion of retinal to retinoic acid.

Spot 17 / Selenium binding protein 1, Aldehyd-dehydrogenase

Spot 17

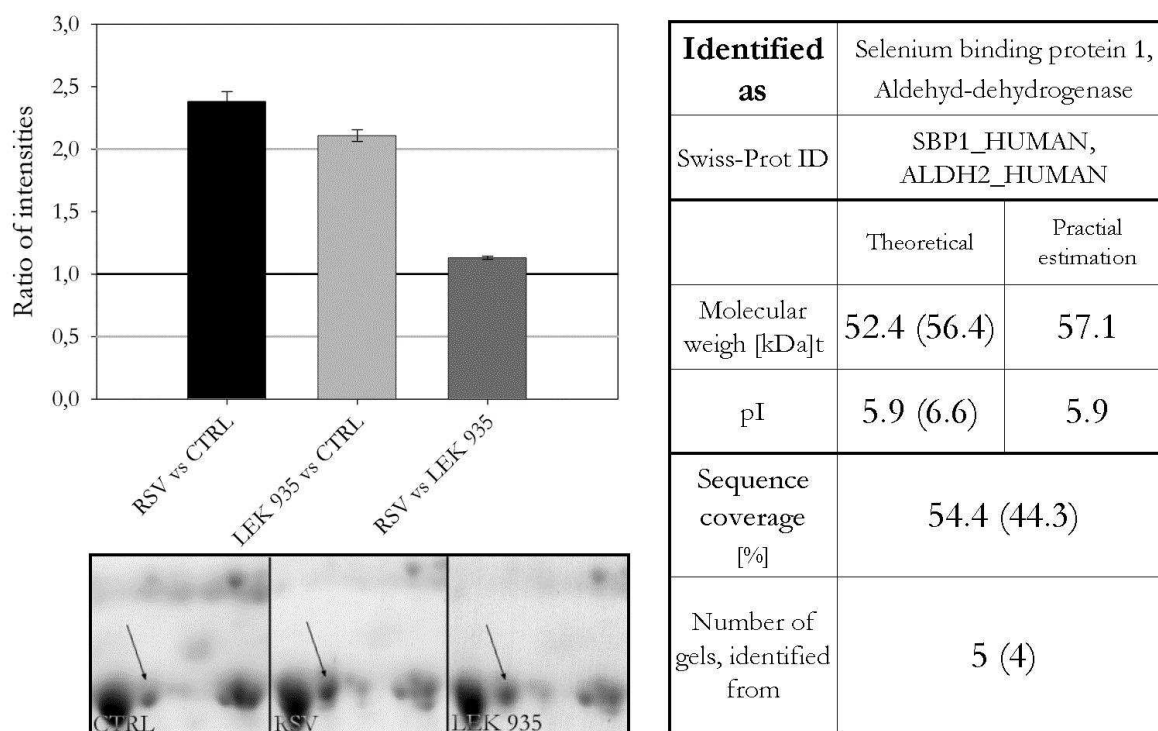


Figure 0-27 Spot 17 found to be regulated in sample 2. The ratio of intensities is depicted in the left upper corner, followed by examples of the spot appearance on the analysed 2D gels. The parameters of identification as well as a comparison of theoretical to experimental data about the molecular weight and the isoelectric point are summarised on the right.

For spot 17 up-regulation was observed after LEK-935 as well as RSV treatment. In nearly all the cases two proteins were identified out of spot 17, Selenium binding protein 1 and Aldehyde dehydrogenase. A differentiation between the two proteins was not possible, as either their molecular weight or their pI correlate with the theoretical values and. Furthermore they exhibit different cellular functions, like xenobiotic sensing and intracellular transport processes for selenium binding protein 1 and alcohol metabolic processes for aldehyde dehydrogenase. Therefore, spot 17 was excluded from further studies.

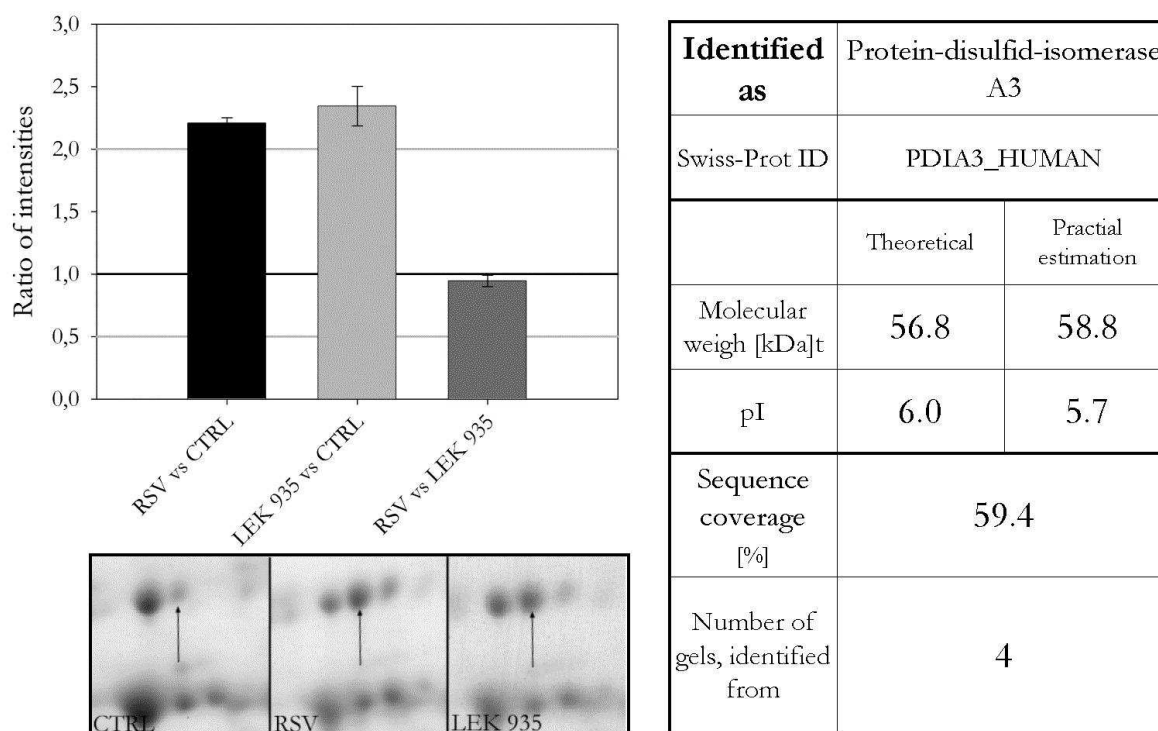
Spot 18, Spot 19 / Protein-disulfid-isomerase A3Spot 18

Figure 0-28 Spot 18 found to be regulated in sample 2. The ratio of intensities is depicted in the left upper corner, followed by examples of the spot appearance on the analysed 2D gels. The parameters of identification as well as a comparison of theoretical to experimental data about the molecular weight and the isoelectric point are summarised on the right.

Spot 18 was found to be significantly up-regulated after both treatments, while spot 19 was not present in the control sample. Appearance as well as up-regulation appeared in a similar manner in both RSV and LEK-935 treated samples.

The spots were identified as protein-disulfide isomerase A3, with sequence coverages of 59.4 and 44.0 % for spots 18 and 19, respectively.

The experimentally determined values for pI and molecular weight correlate well with the theoretical values.

The protein disulfide isomerase catalyses the rearrangement of disulfide bonds in proteins. According to the GO ontologies in the category biological process it is involved in signalling processes as well as the retention of proteins in the ER lumen and their localisation to the nucleus.

Spot 19

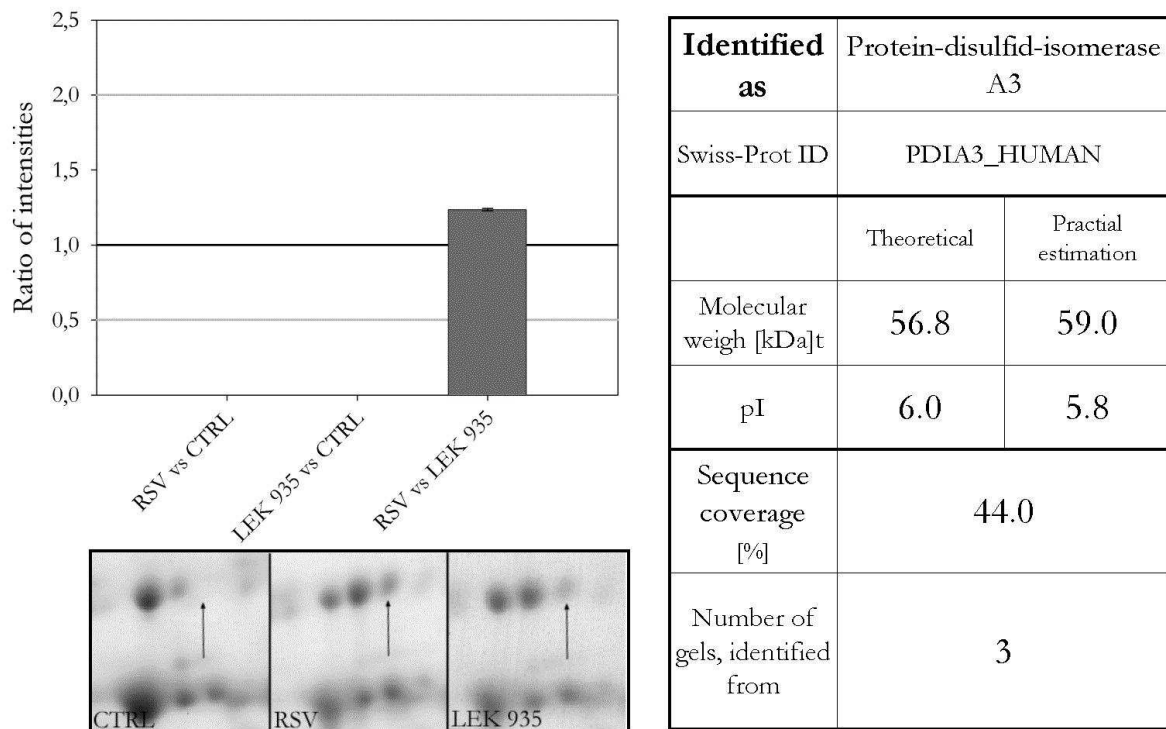


Figure 0-29 Spot 19 found to be regulated in sample 2. The ratio of intensities is depicted in the left upper corner, followed by examples of the spot appearance on the analysed 2D gels. The parameters of identification as well as a comparison of theoretical to experimental data about the molecular weight and the isoelectric point are summarised on the right.

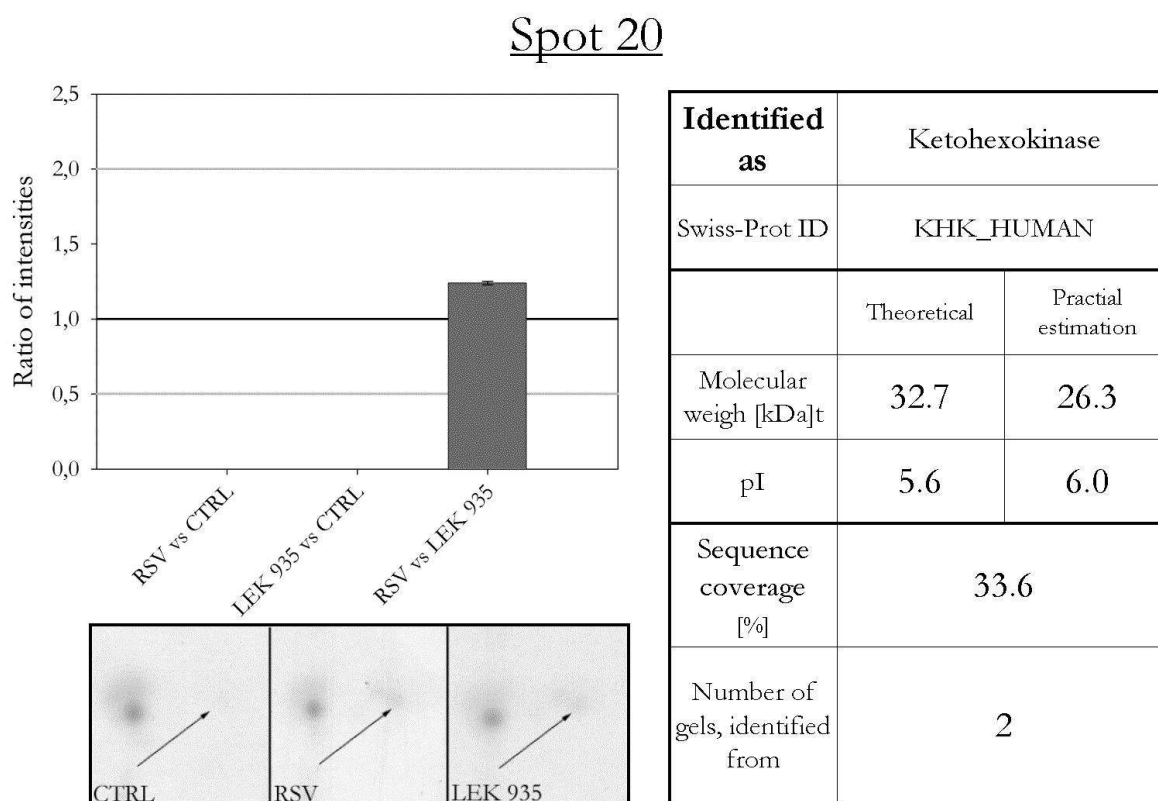
Spot 20 / Ketoheokinase

Figure 0-30 Spot 20 found to be regulated in sample 2. The ratio of intensities is depicted in the left upper corner, followed by examples of the spot appearance on the analysed 2D gels. The parameters of identification as well as a comparison of theoretical to experimental data about the molecular weight and the isoelectric point are summarised on the right.

Spot 20 was found to appear after RSV and LEK-935 treatment. It was identified as ketoheokinase with a sequence coverage of 33.6 %. Its theoretical values for the molecular weight and pI correlate more or less with the experimentally observed data. It phosphorylates D-fructose to D-fructose 1-phosphate by using ATP. So, it is part of the energy metabolism of the cells.

Spot 22 / 3,2-trans-enoyl-CoA isomerase

Spot 22

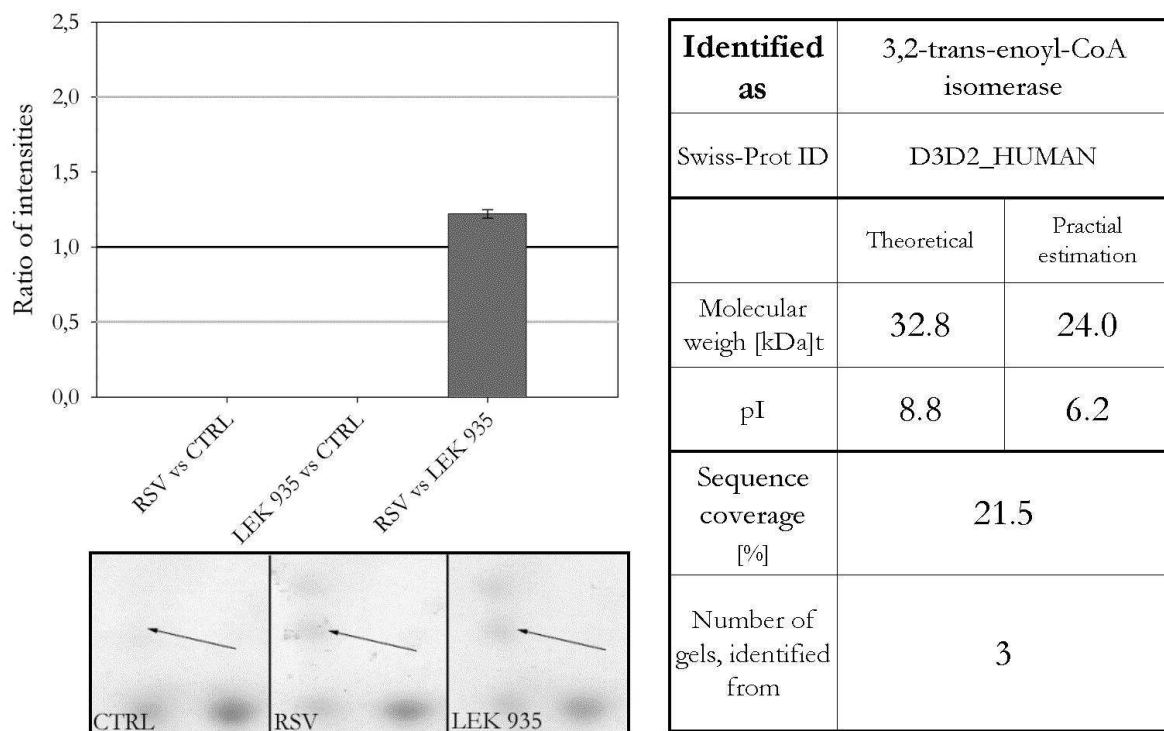


Figure 0-31 Spot 22 found to be regulated in sample 2. The ratio of intensities is depicted in the left upper corner, followed by examples of the spot appearance on the analysed 2D gels. The parameters of identification as well as a comparison of theoretical to experimental data about the molecular weight and the isoelectric point are summarised on the right.

Spot 22 was also shown to appear after treating the cells. It was identified as 3,2-trans-enoyl-CoA isomerase. Identification succeeded out of three individual gels with a final sequence coverage of 21.5 %. The theoretical values for its pI and molecular weight do not correlate with the experimentally gained values.

The enzyme is able to isomerise 3-cis as well as 3-trans double bounds into the 2-trans form in a variety of enoyl-CoA species. So it is involved in fatty acid and thereby lipid metabolic processes. As GO ontology in the category biological process at first fatty acid beta-oxidation is listed.

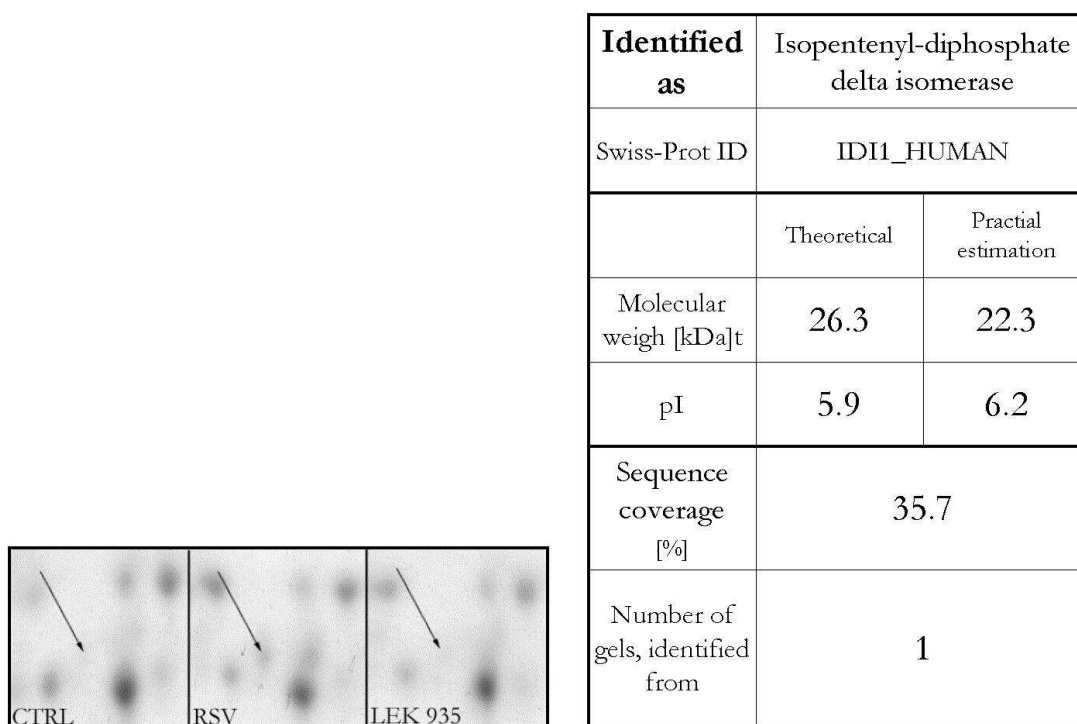
Spot 23 / Isopentenyl-diphosphate delta isomeraseSpot 23

Figure 0-32 Spot 23 found to be regulated in sample 2. The ratio of intensities could not be depicted as the spot was not present in the control and LEK-935 treated samples. Examples of the spot appearance on the analysed 2D gels are shown in the left lower corner. The parameters of identification as well as a comparison of theoretical to experimental data about the molecular weight and the isoelectric point are summarised on the right.

Spot 23 was not present in the control samples but appeared after RSV treatment. It was identified as isopentenyl-diphosphate delta isomerase, with a sequence coverage of 35.7 %. The experimentally values for pI and MW correlate well with the theoretical ones. Because no MS/MS data could be used to support the identification, the protein score of identification was quite low (GPS protein score 54). Therefore, the protein was excluded from further considerations.

The isopentenyl-diphosphate delta isomerase catalyses the 1,3-allylic rearrangement of isopentenyl to its isomer, dimethylallyl diphosphate. So it is involved in cholesterol biosynthesis as well as lipid synthesis.

Spot 24 / Beta-ureidopropionase / Aminoacylase 1

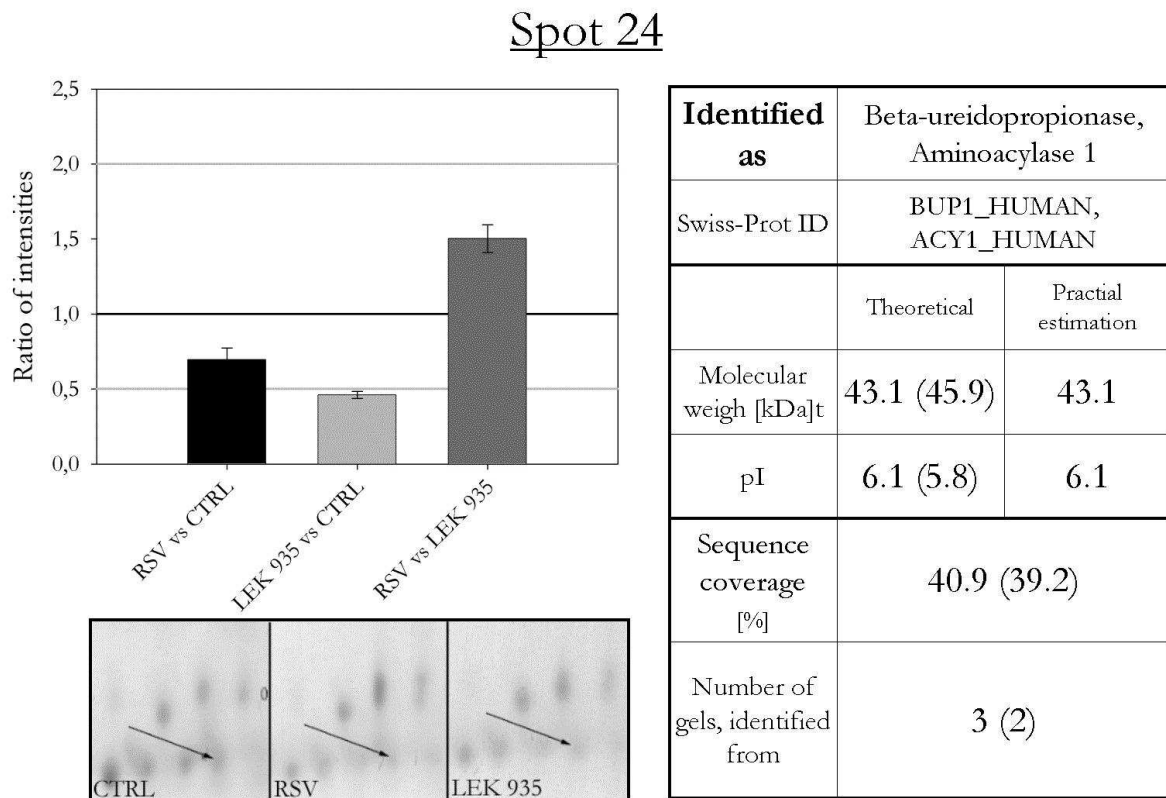


Figure 0-33 Spot 24 found to be regulated in sample 2. The ratio of intensities is depicted in the left upper corner, followed by examples of the spot appearance on the analysed 2D gels. The parameters of identification as well as a comparison of theoretical to experimental data about the molecular weight and the isoelectric point are summarised on the right.

Spot 24 is down-regulated by LEK-935 treatment. During identification in two of three cases two proteins were found in the spot. The pI as well as the molecular weight of both correlate with the experimental data. The sequence coverage during identification is also similar.

Both are able to bind zinc ions and somehow involved in metabolic processes related to amino acids.

As there was no possibility to differentiate between these two enzymes, they were excluded from further investigations.

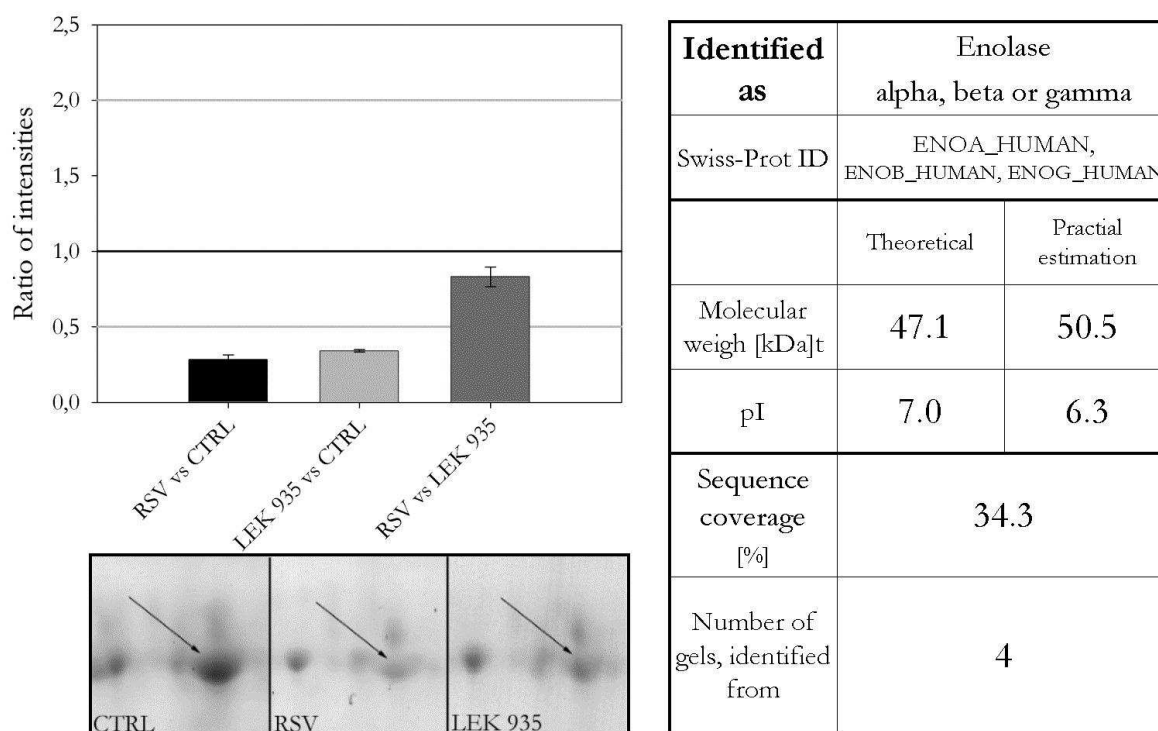
Spot 26 / EnolaseSpot 26

Figure 0-34 Spot 26 found to be regulated in sample 2. The ratio of intensities is depicted in the left upper corner, followed by examples of the spot appearance on the analysed 2D gels. The parameters of identification as well as a comparison of theoretical to experimental data about the molecular weight and the isoelectric point are summarised on the right.

A significant down-regulation was observed for spot 26 after both RSV as well as LEK-935 treatment. This spot could be identified out of four different gels. Identification lead to enolase as underlying protein, with a sequence coverage of 34.3 %. As, in adult tissues, all forms of homo- or heterodimers are observable a differentiation between the isoforms alpha, beta and gamma was not possible. They are of the same size and may also be present at the same time.

As they show different behaviours according to their dimerisation status, this spot was excluded from further studies. Nevertheless, their impact in energy metabolism by their function in glycolysis has to be kept in mind.

Spot 27 / Isocitrate dehydrogenase

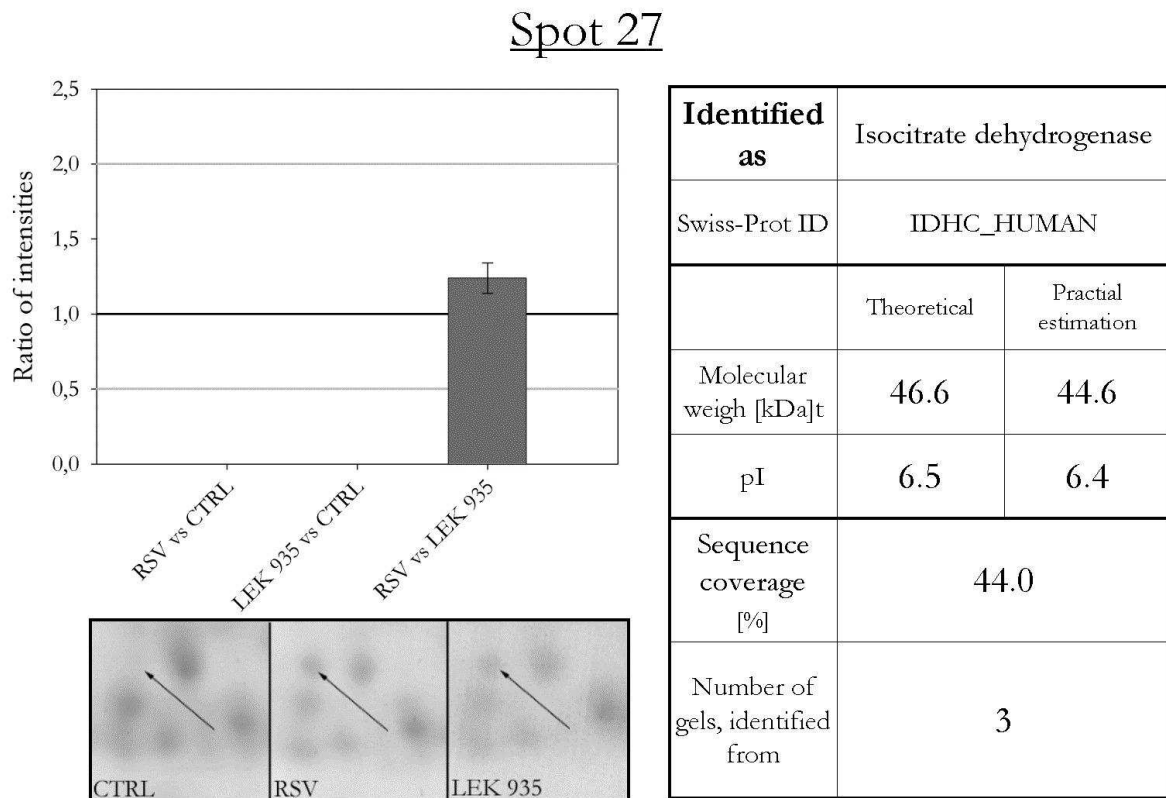


Figure 0-35 Spot 27 found to be regulated in sample 2. The ratio of intensities is depicted in the left upper corner, followed by examples of the spot appearance on the analysed 2D gels. The parameters of identification as well as a comparison of theoretical to experimental data about the molecular weight and the isoelectric point are summarised on the right.

For spot 27 again, appearance was observed after treating the cells. The underlying protein was identified as isocitrate dehydrogenase, with a sequence coverage of 44.0 %.

This enzyme plays a key role in the tricarboxyc acid cycle as well as the Glyoxylate bypass. Its precursor molecule was also found to appear after LEK treatment in sample 1. The precursor molecule showed much higher pI (8.9) not correlating with its position on the gel, while for spot 27, the values correlate very well.

Spot 29, Spot 32 / Catalase

Spot 29

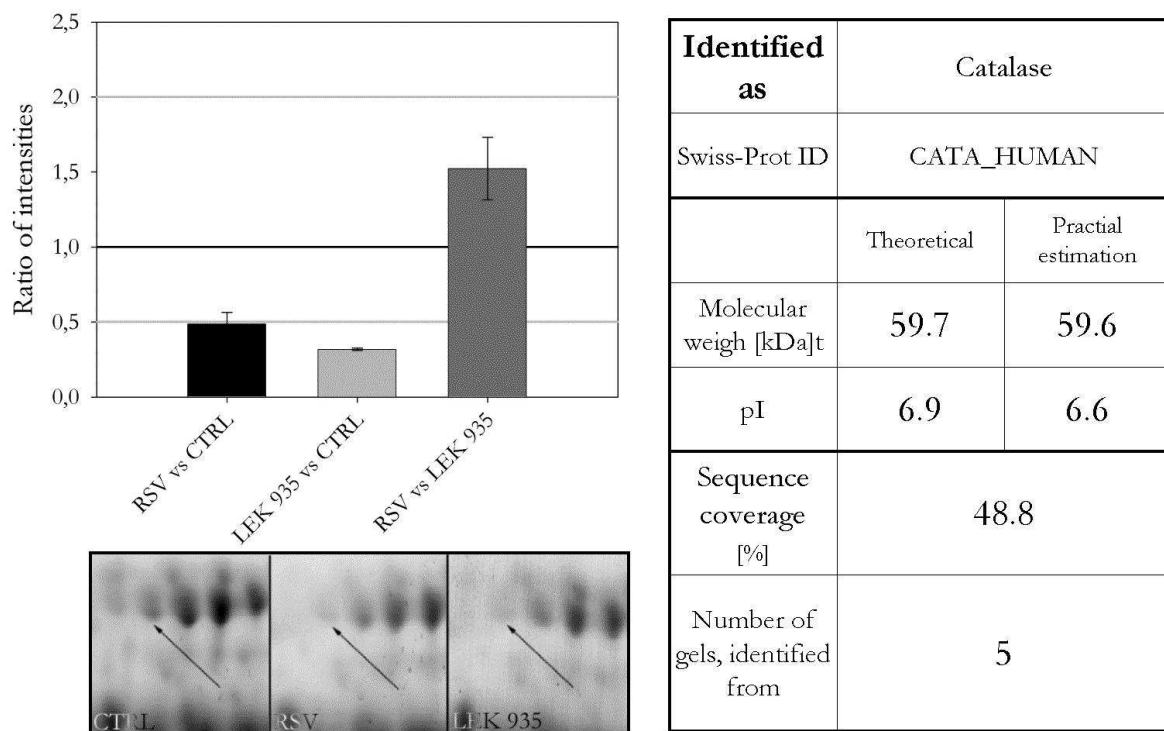


Figure 0-36 Spot 29 found to be regulated in sample 2. The ratio of intensities is depicted in the left upper corner, followed by examples of the spot appearance on the analysed 2D gels. The parameters of identification as well as a comparison of theoretical to experimental data about the molecular weight and the isoelectric point are summarised on the right.

For spot 29 and 32, opposed regulations were observed. While spot 29 was down-regulated by treating the cells, spot 32 was up-regulated. Nevertheless, both lay in one horizontal string of spots and were identified as Catalase. Identification succeeded out of 5 and 6 gels, leading to sequence coverages of 48.8 and 59.4 % for spots 29 and 32, respectively.

Catalase protects the cells of the toxic effect of hydrogen peroxide. As up- as well as down-regulation was observed, in a horizontal string of spots, which may also be caused by freeze-thawing cycles of the sample these hits were excluded from further analysis.

Spot 32

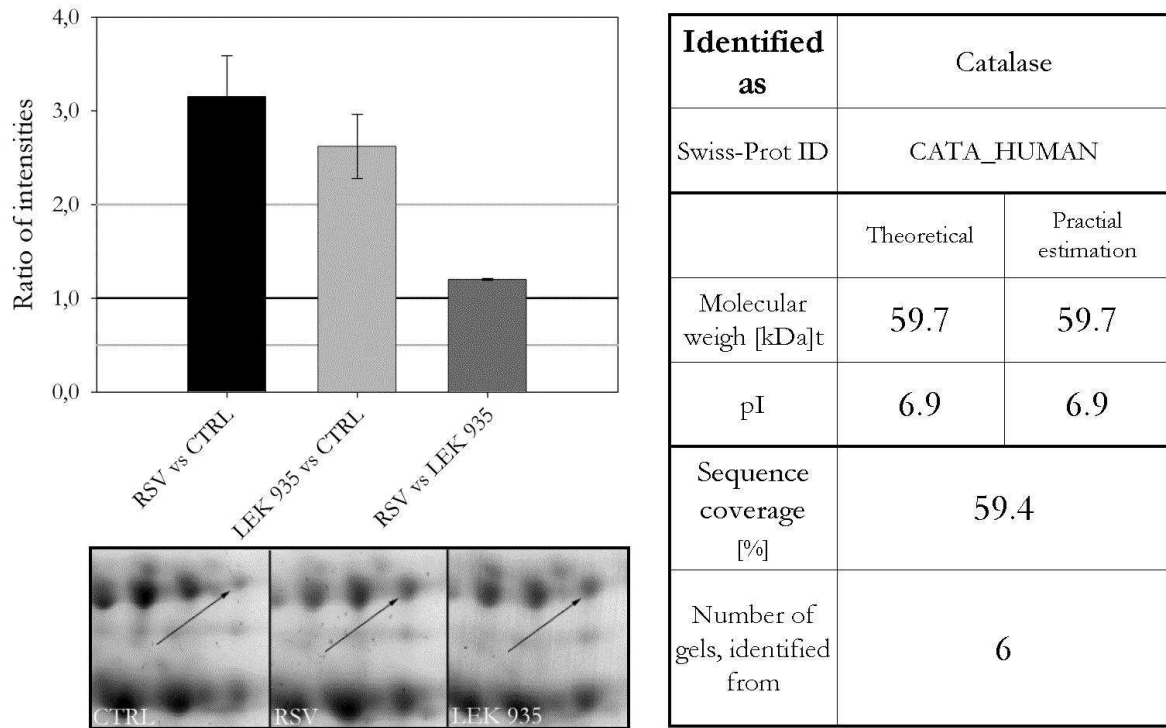


Figure 0-37 Spot 32 found to be regulated in sample 2. The ratio of intensities is depicted in the left upper corner, followed by examples of the spot appearance on the analysed 2D gels. The parameters of identification as well as a comparison of theoretical to experimental data about the molecular weight and the isoelectric point are summarised on the right.

Spot 30 / Carbonic anhydrase

Spot 30

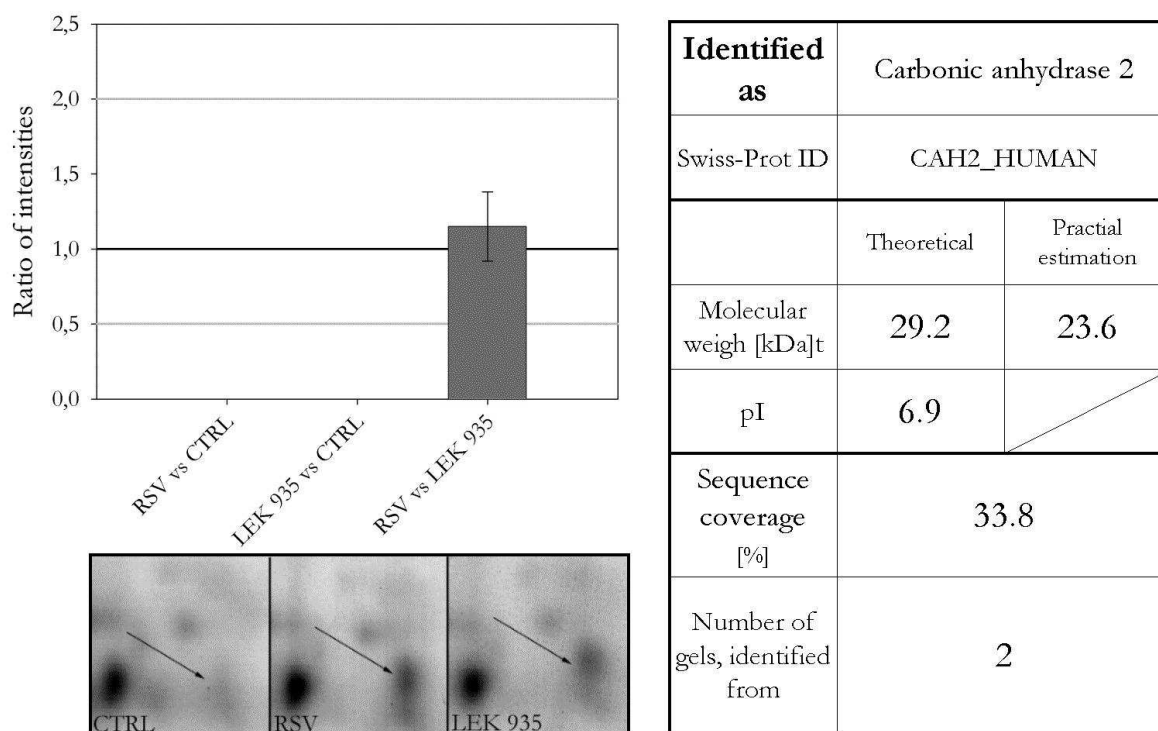


Figure 0-38 Spot 30 found to be regulated in sample 2. The ratio of intensities is depicted in the left upper corner, followed by examples of the spot appearance on the analysed 2D gels. The parameters of identification as well as a comparison of theoretical to experimental data about the molecular weight and the isoelectric point are summarised on the right.

For spot 30, appearance after treatment was observed, even if a shadow of a spot was also visible in some of the control gels (see Figure 0-38). It was identified as carbonic anhydrase, with a sequence coverage of 33.8 %. Experimental estimation of the pI was not possible as it lay outside the range of the reference spots.

The carbonic anhydrase catalyses the reversible hydration of carbon dioxide and is thereby involved in one-carbon metabolic processes.

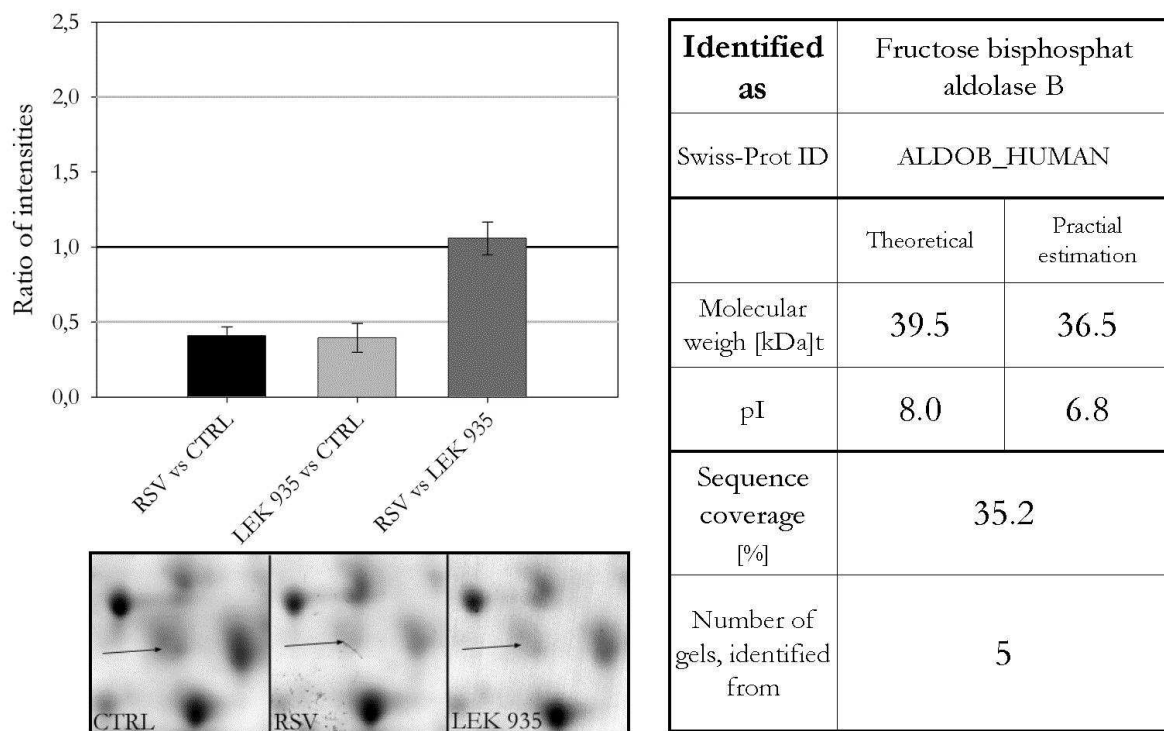
Spot 31 / Fructose-bisphosphat-aldolase BSpot 31

Figure 0-39 Spot 31 found to be regulated in sample 2. The ratio of intensities is depicted in the left upper corner, followed by examples of the spot appearance on the analysed 2D gels. The parameters of identification as well as a comparison of theoretical to experimental data about the molecular weight and the isoelectric point are summarised on the right.

Spot 31 was significantly down-regulated by RSV and LEK-935 treatment. It was identified as fructose bisphosphate aldolase B. Sequence coverage was 35.2 % and identification succeeded out of five different gels. Its theoretical pI value is much higher (8.0) than the observed value of 6.8 while the values for the molecular weight correlate well.

It catalyses one of the steps in glycolysis and is thereby involved in energy metabolism of the cell.

Sample 2 nLC-MS details

UP

Mitochondrial dicarboxylate carrier

(DIC_HUMAN)

The mitochondrial dicarboxylate carrier is a multi-pass membrane protein, located in the inner mitochondrial membrane. It is involved in the translocation of malate, malonate and succinate in exchange for phosphate, sulfate, sulfite or thiosulfate. Among others, it thereby plays a role in gluconeogenesis.

Glyceraldehyde-3-phosphate dehydrogenase

(G3P_HUMAN)

The glyceraldehydes-3-phosphate dehydrogenase is located in the cytoplasm as well as nearby the membrane. It is highly involved in glycolysis but plays also a role membrane trafficking in the early steps of secretion pathway.

Hydroxy-methyl-glutaryl-CoA synthase, cytoplasmic

(HMCS1_HUMAN)

The hydroxy-methyl-glutaryl-CoA synthase is a soluble protein, located in the cytoplasm. It synthesises HMG-CoA from acetyl-CoA and acetoacetyl-CoA, thereby catalysing one of the major preliminary steps to cholesterol-biosynthesis.

Peroxiredoxin 6

(PRDX6_HUMAN)

The peroxiredoxin 6 is a soluble protein found in the cytoplasm, cytoplasmic vesicles and the lysosome. It is involved in the redox regulation of the cell and can reduce H₂O₂. Furthermore it is also able to reduce short chain organi, fatty acid and phospholipid hydroperoxides and therefore plays as role in phospholipid turnover and lipid degradation.

Radixin

(RADI_HUMAN)

Radixin is an peripheral membrane protein, located at the cytoplasmic side of the cell membrane. It probably plays a crucial role by anchoring the actin filaments of the cytoskeleton to the membrane. It is found in high concentration at the sites of cell-cell adherens.

GTP-binding protein SAR1b

(SAR1B_HUMAN)

The GTP-binding protein SAR1b is a peripheral membrane protein, located at the membranes of the endoplasmic reticulum and the Golgi-apparatus. It is involved in the transport processes from the ER to the Golgi.

Defects in the SAR1B are the base for the chylomicron retention disease, suggesting a role in cholesterol transport processes.

Voltage-dependent anion-selective channel protein 2

(VDAC2_HUMAN)

The voltage-dependent anion-selective channel protein 2 is an integral membrane protein located at the outer mitochondrial membrane. It allows the diffusion of small hydrophilic molecules and its open-close status depends on the electric potential across the membrane.

Fibrinogen

(FIBA_HUMAN, FIBB_HUMAN)

The fibrinogen chains are secreted proteins, involved in platelet activation and building fibrin fibers by polymerisation. Both forms the alpha chain as well as the beta chain were independently found to be up-regulated.

Appendix III: Spot identifications from 2D gels**Sample 1**

Spot Number	Spot number Exp I (SSP PDQuest)	Spot Number Exp II (SSP PDQuest)	identified as	Originating from		SwissProt - ID	MW [kDa]	pI	Sequence coverage [%]	Number of individual gels
				Human	E.coli					
1	SSP 0014	SSP 1010	Thiol peroxidase		x					1
2	SSP 0110	SSP 0109	Proteasome subunit alpha type 5	x		PSA5_HUMAN	26.394	4.74	41.5	2
3	SSP 0208	SSP 1201	Annexin A5	x		ANXA5_HUMAN	35.914	4.94	71.6	4
4	SSP 0406	SSP 1417	6-phosphogluconate dehydrogenase; decarboxylating		x					1
5	SSP 0605	SSP 0606	60kDa chaperonin		x					2
6	SSP 0706	SSP 0703	Chaperone proteine Dnak		x					5
7	SSP 0707	SSP 0705	30 S ribosomal protein		x					1
8	SSP 0803	SSP 0807	Endoplasmin	x		ENPL_HUMAN	92.411	4.76	34.5	2
9	SSP 1002	SSP 1002	Alkylhydroperoxid reduktase		x					2
11	SSP 1209	SSP 1205	Elongation factor Ts		x					3
13	SSP 1306	SSP 1307	Phosphoglycerate kinase		x					5
14	SSP 1308	SSP 1309	Glycerophosphoryl diester phosphodiesterase		x					2

Spot Number	Spot number Exp I (SSP PDQuest)	Spot Number Exp II (SSP PDQuest)	identified as	Originating from Human	E.coli	SwissProt - ID	MW [kDa]	pI	Sequence coverage [%]	Number of individual gels
16	SSP 1405	SSP 1406	6-phosphogluconate dehydrogenase; decarboxylating		x					2
18	SSP 1416	SSP 1414	Isocitrate dehydrogenase		x					1
19	SSP 1506	SSP 1512	Aspartate ammonia-lyase		x					3
20	SSP 1511	SSP 1615	HMG-CoA synthase	x		HMCS1_HUMAN	57.257	5.22	38.5	3
21	SSP 2009	SSP 2110	Purine nucleoside phosphorylase deoD-type		x					3
23	SSP 2105	SSP 2103	Nicotinamid N-methyltransferase	x		NNMT_HUMAN	29.555	5.56	38.3	5
25	SSP 2303	SSP 2405	Elongation Factor Tu		x					5
26	SSP 2307	SSP 2310	Mannonate dehydratase		x					1
29	SSP 2403	SSP 2402	Adenoylsuccinate - synthase		x					3
30	SSP 2408	SSP 2407	Enolase		x					4
32	SSP 2501	SSP 1516	Glutamate decarboxylase beta		x					1
33	SSP 2508	SSP 1517	Aminoacyl-histidine dipeptidase		x					1
35	SSP 2718	SSP 2701	Heatshock cognate 71kDa protein	x		HSP7C_HUMAN	70.854	5.37	53.9	5
35						HSP72_HUMAN				
35						HSP76_HUMAN				

Spot Number	Spot number Exp I (SSP PDQuest)	Spot Number Exp II (SSP PDQuest)	identified as	Originating from Human	E.coli	SwissProt - ID	MW [kDa]	pI	Sequence coverage [%]	Number of individual gels
35						HS71L_HUMAN				
36	SSP 3003	SSP 3002	Superoxid-dismutase		x					4
37	SSP 3004	SSP 3107	Triosephosphate isomerase		x					3
41	SSP 3212	SSP 3206	L-asparaginase 2		x					1
42	SSP 3216	SSP 3221	Malat dehydrogenase		x					4
44	SSP 3306	SSP 3302	Fructose bisphosphate aldolase		x					4
45	SSP 3312	SSP 3406	Peptidase B		x					2
49	SSP 3408	SSP 2413	Isocitrate dehydrogenase [NADP]; mitochondrial	x		IDHP_HUMAN	50.877	8.88	33.0	1
50	SSP 3504	SSP 2512	Putative tagatose 6-phosphate kinase gatZ		x					4
54	SSP 3602	SSP 2610	Phosphoenolpyruvate carboxykinase [ATP]		x					4
58	SSP 3701	SSP 2715	Transketolase 1		x					3
59	SSP 3706	SSP 3818	Formate acetyltransferase 1		x					2
60	SSP 3709	SSP 3807	Formate acetyltransferase 1		x					1
61	SSP 3814	SSP 3813	Aconitate hydratase 1		x					1
62	SSP 4108	SSP 4104	Uridine phosphorylase		x					3
64	SSP 4112	SSP 3116	NADP-dependent L-serine/L-allo-threonine dehydrogenase ydfG		x					1

Spot Number	Spot number Exp I (SSP PDQuest)	Spot Number Exp II (SSP PDQuest)	identified as	Originating from		SwissProt - ID	MW [kDa]	pI	Sequence coverage [%]	Number of individual gels
				Human	E.coli					
65	SSP 4210	SSP 4204	Cysteine synthase A		x					1
66	SSP 4310	SSP 4404	Acetate kinase		x					2
67	SSP 4409	SSP 4410	Tryptophanase		x					1
68	SSP 4509	SSP 4507	Dihydrolipoyl dehydrogenase		x					1
70	SSP 4605	SSP 4602	Pyruvate Kinase I		x					3
71	SSP 4702	SSP 3706	Serum Albumin	x		ALBU_HUMAN	69.321	5.92	52.5	5
72	SSP 4705	SSP 4703	Fumarate reductase		x					2
76	SSP 5104	SSP 5102	D-ribose binding protein		x					5
77	SSP 5112	SSP 5114	Tagatose-1;6-bisphosphate aldolase gatY		x					1
78	SSP 5113	SSP 5112	D-ribose binding protein		x					1
81	SSP 5511	SSP 5615	Inosine-5'-monophosphate dehydrogenase		x					2
83	SSP 5610	SSP 5707	Phosphoglucomutase 1	x		PGM1_HUMAN	61.411	6.3	37.2	5
86	SSP 5701	SSP 4710	Serum Albumin	x		ALBU_HUMAN	69.321	5.92	44.3	3
88	SSP 6606	SSP 6702	Phosphoglucomutase 1	x		PGM1_HUMAN	61.411	6.3	29.2	3
89	SSP 6707	SSP 6821	Radixin	x		RADI_HUMAN	68.521	6.03	31.4	2
89			Ezrin	x		EZRI_HUMAN	69.37	5.94	21.3	2
89			Moesin	x		MOES_HUMAN	67.778	6.08	14.9	2
90	SSP 7012	SSP 7011	Superoxide dismutase [Mn]		x					1

Spot Number	Spot number Exp I (SSP PDQuest)	Spot Number Exp II (SSP PDQuest)	identified as	Originating from		SwissProt - ID	MW [kDa]	pI	Sequence coverage [%]	Number of individual gels
				Human	E.coli					
91	SSP 7217	SSP 7211	2-dehydro-3-deoxyphosphooctonate aldolase		x					1
92	SSP 8202	SSP 7312	Aldo-ketoreductase family 1 member	x						2
92			Glyceraldehyde-3 dehydrogenase Salmonella		x					3
93	SSP 8210	SSP 8216	Glyceraldehyde-3 dehydrogenase	x		G3P_HUMAN	36.03	8.57	23.0	1
94	SSP 8706	SSP 8803	Serotransferrin	x		TRFE_HUMAN	77	6.81	40.4	2

Sample 2

Spot No	Spot number Exp I	Spot Number Exp II	identified as	Swiss-Prot ID	MW [kDa]	pI	Sequence coverage [%]	Number of individual gels. identified from
2	SSP 0504	SSP 604	Tubulin beta chain	TBB2C_HUMAN TBB2A_HUMAN TBB2B_HUMAN TBB5_HUMAN	49.799	4.79	35.5	3
3	SSP 0702	SSP 0702	78kDa-glucose regulated protein precursor	GRP78_HUMAN	72.288	5.07	37.9	1
4	SSP 1201	SSP 2203R	N(G);N(G)-dimethylarginine dimethylaminohydrolase 1	DDAH1_HUMAN	31.102	5.53	54	4
7	SSP 1502R	SSP 1502R	ATP synthase subunit beta; mitochondrial precursor	ATPB_HUMAN	56.525	5.26	49.5	5
8	SSP 1505R	SSP 506	ATP synthase subunit beta; mitochondrial precursor	ATPB_HUMAN	56.525	5.26	44.2	4
11	SSP 2307R	SSP 1406	Actin; cytoplasmic 2 Actin; cytoplasmic 1	ACTG_HUMAN ACTB_HUMAN	41.766	5.31	47.2	3
12	SSP 2403R	SSP 1310	Eukaryotic initiation factor 4A-I	IF4A1_HUMAN	46.125	5.32	33.3	1
13	SSP 3005R	SSP 2004	Superoxide dismutase [Cu-Zn]	SODC_HUMAN	15.926	5.7	44.2	1

Spot No	Spot number		identified as	Swiss-Prot ID	MW [kDa]	pI	Sequence coverage [%]	Number of individual gels. identified from
	Exp I	Exp II						
14	SSP 3101	SSP 3101	Heat shock protein beta 1	HSPB1_HUMAN	22.768	5.98	37.6	1
	SSP 3101	SSP 3101	3-Hydroxyisobutyrate-dehydrogenase; mitochondrial precursor	3HIDH_HUMAN	35.306	8.38	32.1	2
	SSP 3101	SSP 3101	3-hydroxyanthranilate 3;4-dioxygenase	3HAO_HUMAN	32.522	5.62	38.1	1
15	SSP 3115R	SSP 3115R	Glutathione transferase omega 1	GSTO1_HUMAN	27.548	6.23	47.7	3
16	SSP 3501	SSP 3604	Retinal-dehydrogenase 1	AL1A1_HUMAN	54.862	6.3	29.7	
17	SSP 3513R	SSP 3513R	Selenium binding protein 1	SBP1_HUMAN	52.358	5.93	54.4	5
			Aldehyd-dehydrogenase; mitochondrial	ALDH2_HUMAN	56.346	6.63	44.3	4
18	SSP 3608R	SSP 3608R	Protein-disulfid-isomerase A3	PDIA3_HUMAN	56.747	5.98	59.4	3
19	SSP 3610R	SSP 3610R	Protein-disulfid-isomerase A3	PDIA3_HUMAN	56.747	5.98	44	3
20	SSP 4102R	SSP 3103	Ketohexokinase	KHK_HUMAN	32.71	5.64	33.6	2
22	SSP 4109	SSP 5105	3;2-trans-enoyl-CoA isomerase	D3D2_HUMAN	32.795	8.8	21.5	3
23	SSP 4112	SSP 4006R	Isopentenyl-diphosphate delta isomerase	IDI1_HUMAN	26.319	5.93	35.4	
24	SSP 4401	SSP 4301	Beta-ureidopropionase	BUP1_HUMAN	43.139	6.09	40.9	3
	SSP 4401	SSP 4301	Aminoacylase 1	ACY1_HUMAN	45.856	5.77	39.2	2
25	SSP 5101R	SSP 5101R	Glutathione transferase omega 1	GSTO1_HUMAN	27.548	6.23	45.6	4
26	SSP 5406R	SSP 5406R	Alpha-enolase	ENOA_HUMAN	47.139	7.01	34.3	4
			Beta-enolase	ENOB_HUMAN				
			Gamma-enolase	ENOG_HUMAN				
27	SSP 5410	SSP 5413	Isocitrate dehydrogenase	IDHC_HUMAN	46.63	6.53	44	3

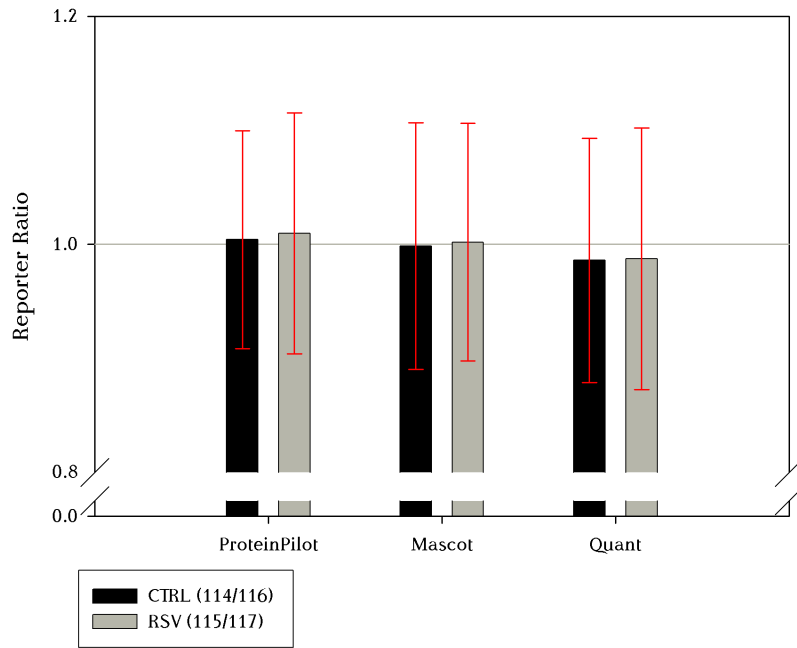
Spot No	Spot number Exp I	Spot Number Exp II	identified as	Swiss-Prot ID	MW [kDa]	pI	Sequence coverage [%]	Number of individual gels. identified from
29	SSP 7618R	SSP 7603	Catalase	CATA_HUMAN	59.719	6.9	48.8	5
30	SSP 8106	SSP 9102	Carbonic anhydrase 2	CAH2_HUMAN	29.228	6.87	33.8	2
31	SSP 8302R	SSP 8302R	Fructose-bisphosphat-aldolase B	ALDOB_HUMAN	39.448	8	35.2	5
32	SSP 8603	SSP 9504	Catalase	CATA_HUMAN	59.719	6.9	59.4	6

Appendix IV: iTRAQ™ evaluation

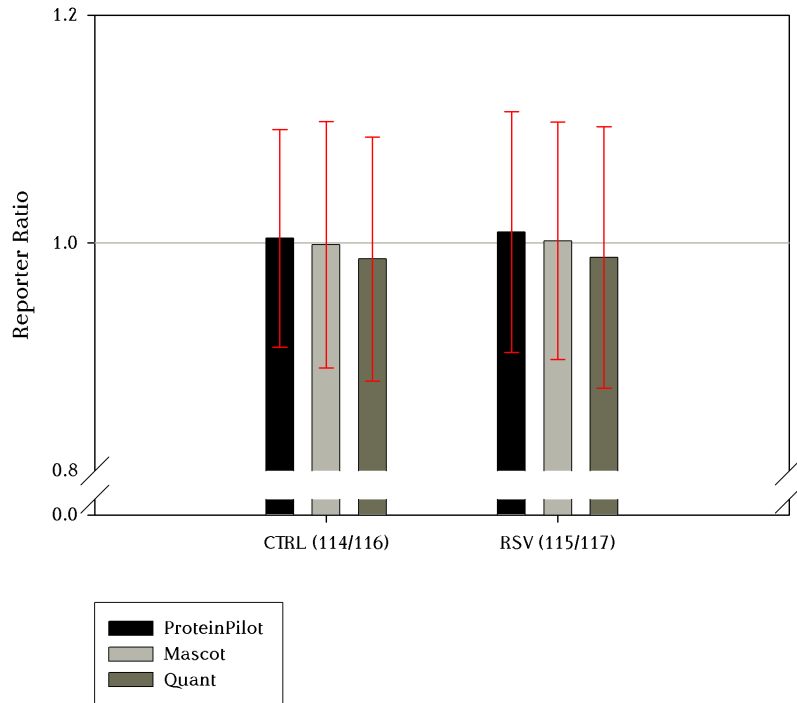
Accurate quantitative measurements are only possible if the labelling procedure for the control and the treated samples does not cause huge differences. The quality of the procedure was examined by labelling the control and the RSV treated samples with two different iTRAQ™ reporter labels each. The control samples were divided and labelled with the reporter 114 and 116 while the RSV samples were divided and labelled with the reporter 115 and 117. Finally, the samples were mixed in a ratio of 1:1:1:1. Below, the averaged internal controls as well as the factor/divisor distributions of the internal controls and the treatment vs control comparisons are depicted as found by the three different software packages used.

The data were not examined as ratios but converted into a factor/divisor form. So, a ratio of 2.0 is regarded as a factor 2.0 as well as a ratio of 0.5 is regarded as a divisor of 2.0, reflecting the factors of up- or down-regulation of the underlying proteins. The factor/divisor should ideally be one for the internal controls (114/116 and 115/117), as the samples were mixed in a ratio of one to one. Sample 1 is HH-129 and Sample 2 is HH-114.

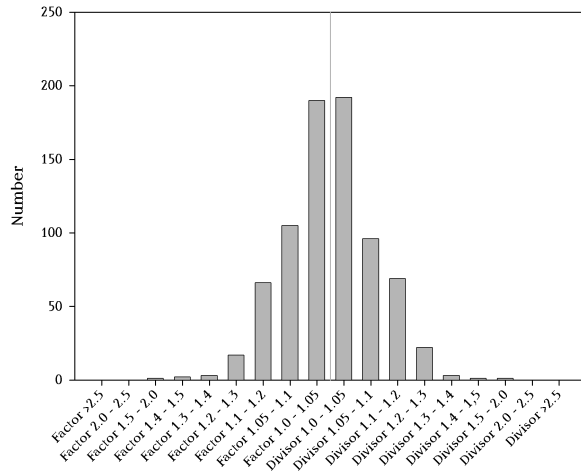
HH-129 Comparison ProteinPilot - Mascot - Quant
Internalcontrols



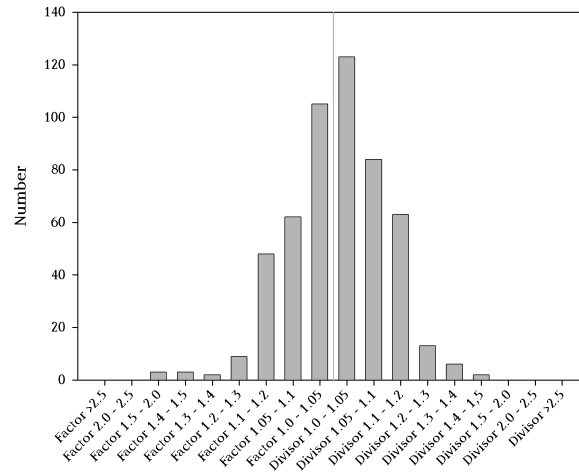
HH-129 Comparison ProteinPilot - Mascot -Quant
Internalcontrols



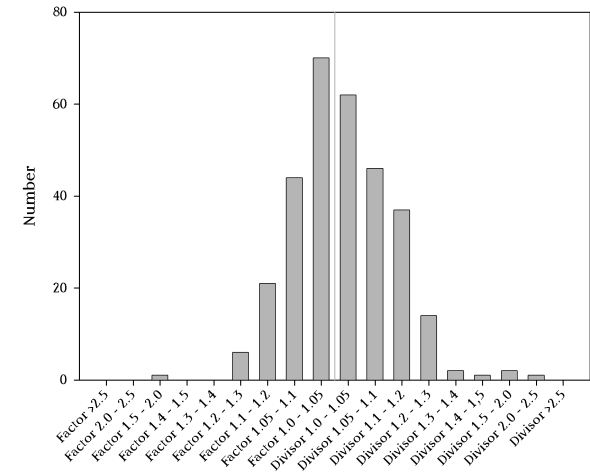
HH-129 Analysis ProteinPilot
Internalcontrol CTRL (114/116)



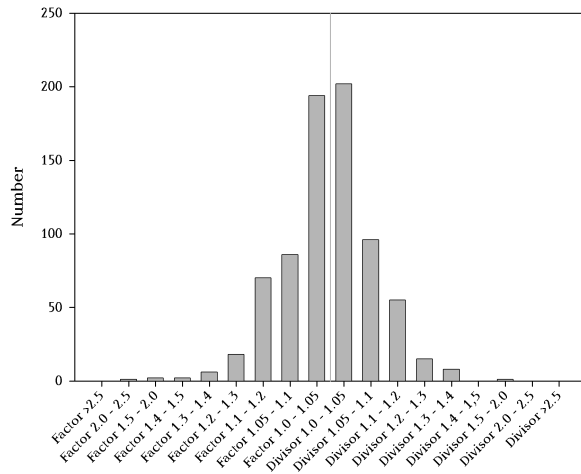
HH-129 Analysis Mascot
Internalcontrol CTRL (114/116)



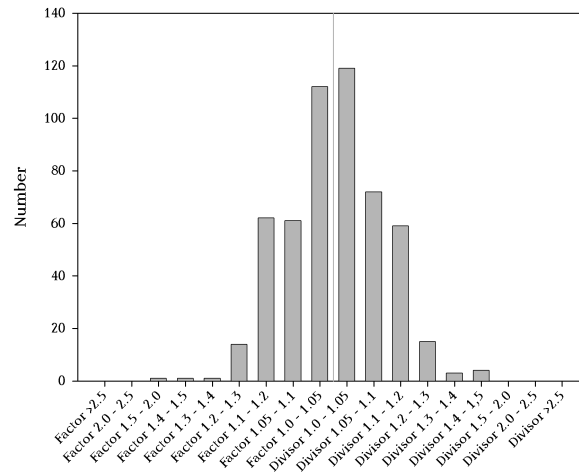
HH-129 Analysis Quant
Internalcontrol CTRL (114/116)



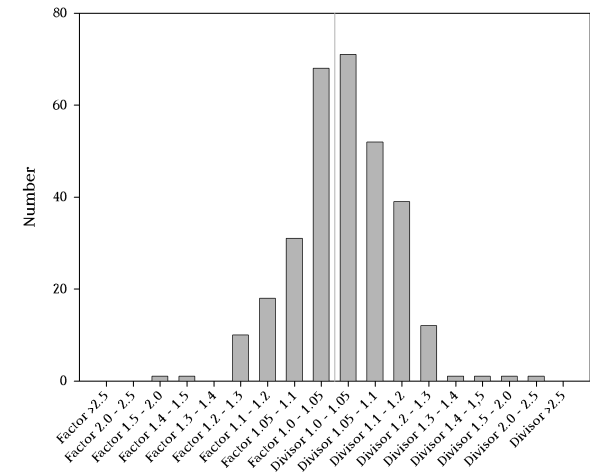
HH-129 Analysis ProteinPilot
Internalcontrol RSV (115/117)



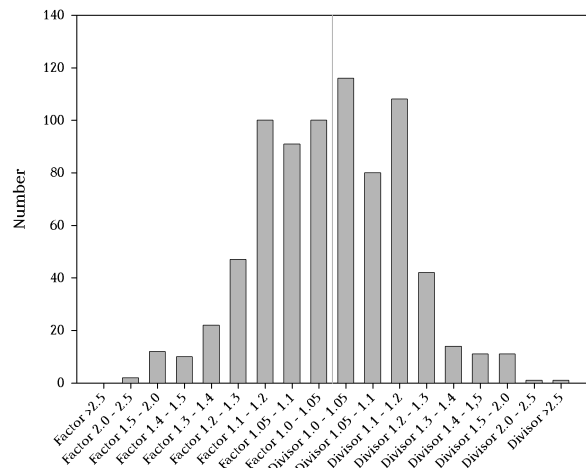
HH-129 Analysis Mascot
Internalcontrol RSV (115/117)



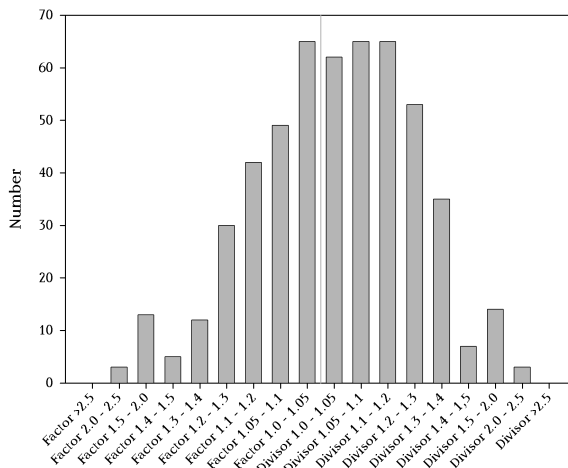
HH-129 Analysis Quant
Internalcontrol RSV (115/117)



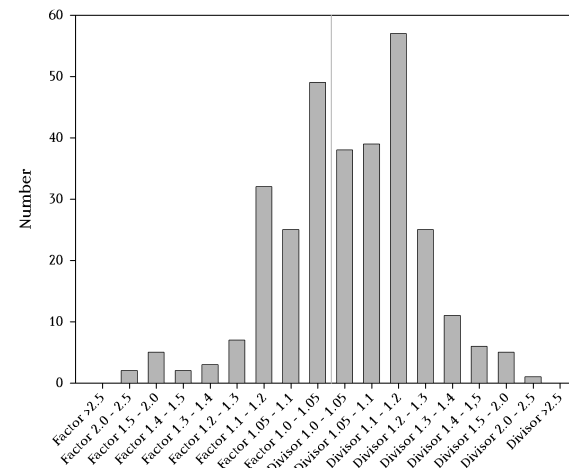
HH-129 Analysis ProteinPilot
RSV vs CTRL (115/114)



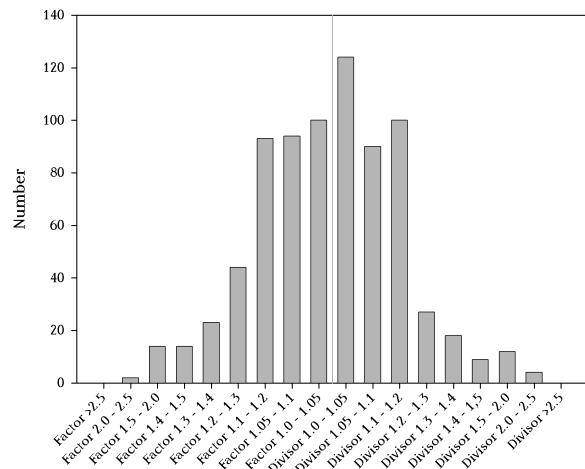
HH-129 Analysis Mascot
RSV vs CTRL (115/114)



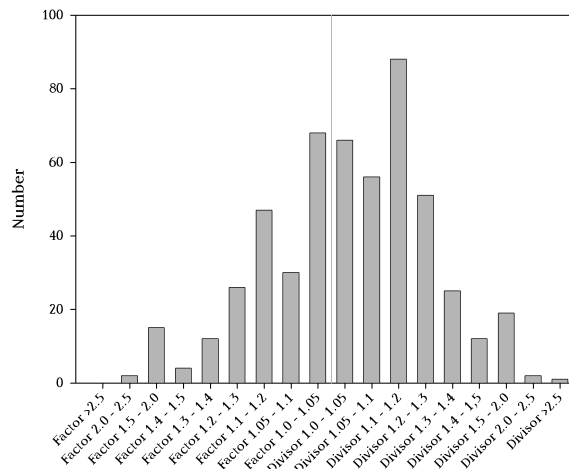
HH-129 Analysis Quant
RSV vs CTRL (115/114)



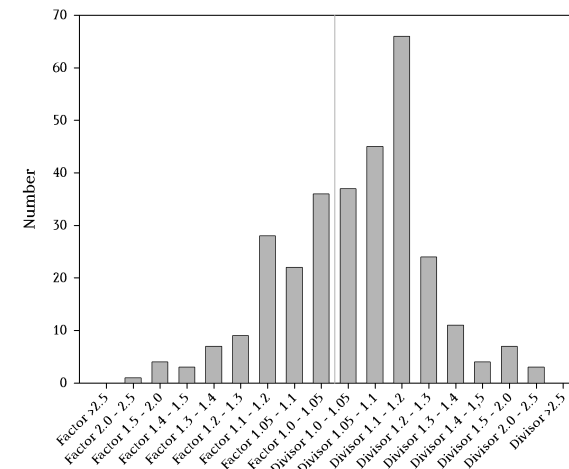
HH-129 Analysis ProteinPilot
RSV vs CTRL (115/116)



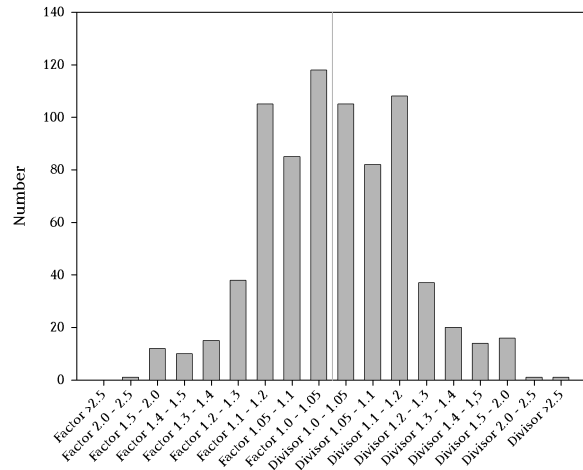
HH-129 Analysis Mascot
RSV vs CTRL (115/116)



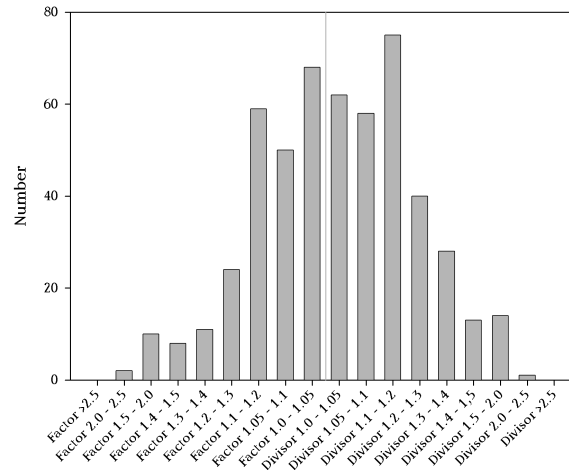
HH-129 Analysis Quant
RSV vs CTRL (115/116)



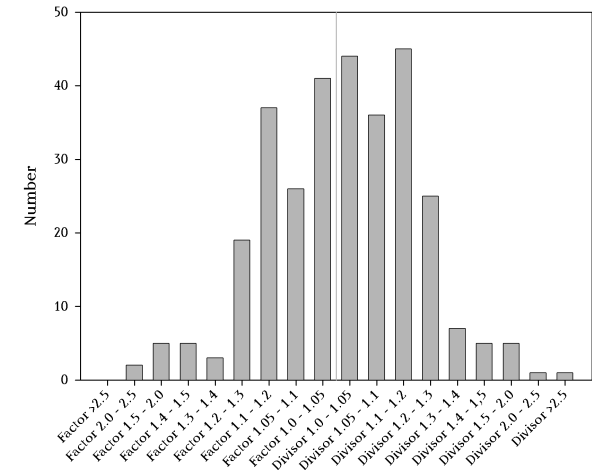
HH-129 Analysis ProteinPilot
RSV vs CTRL (117/114)



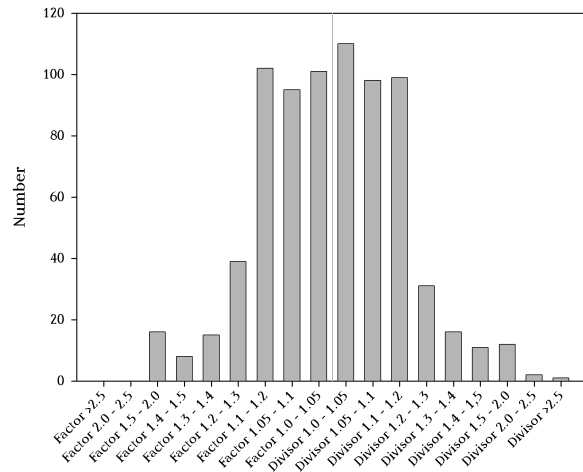
HH-129 Analysis Mascot
RSV vs CTRL (117/114)



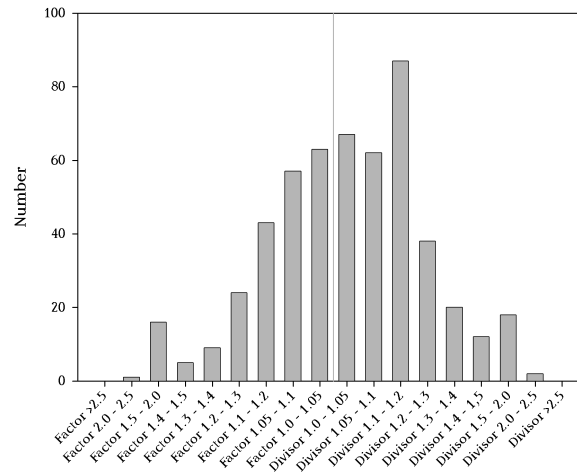
HH-129 Analysis Quant
RSV vs CTRL (117/114)



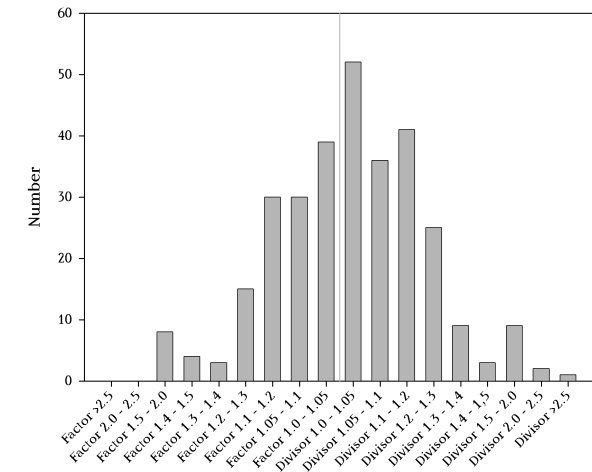
HH-129 Analysis ProteinPilot
RSV vs CTRL (117/116)



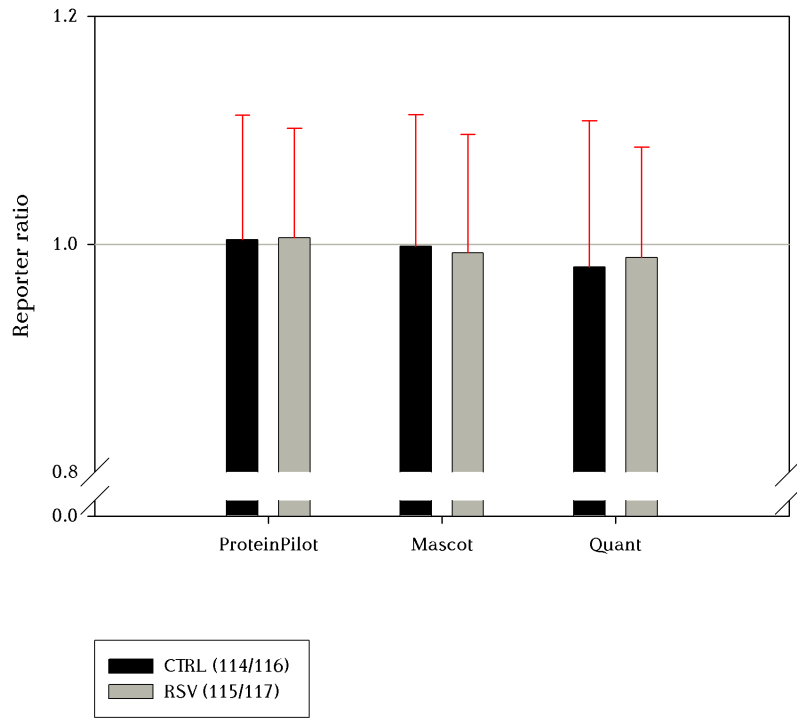
HH-129 Analysis Mascot
RSV vs CTRL (117/116)



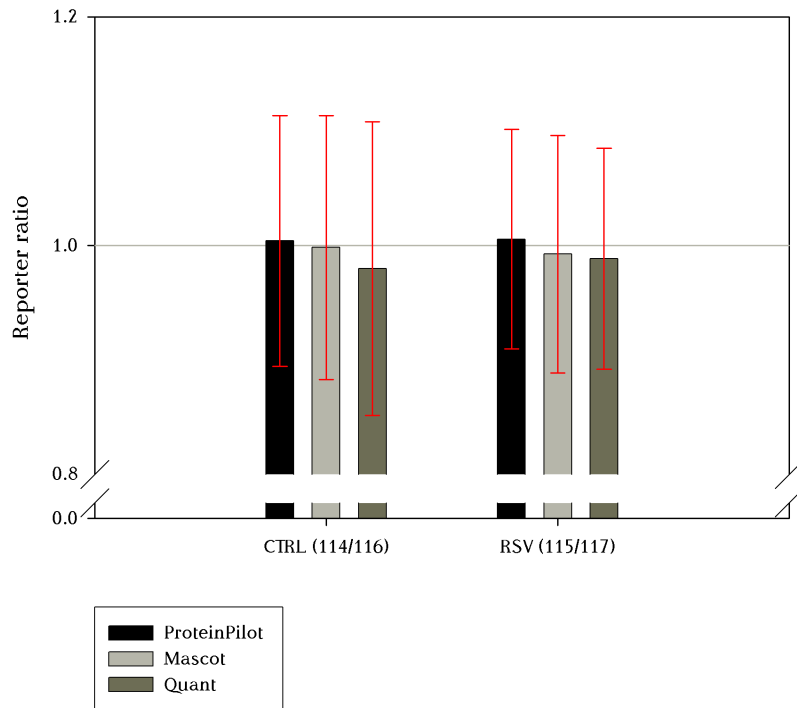
HH-129 Analysis Quant
RSV vs CTRL (117/116)



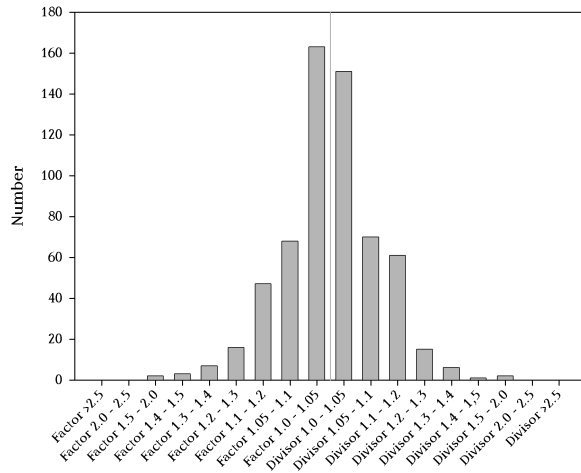
HH-114 Comparison ProteinPilot - Mascot - Quant
Internalcontrols



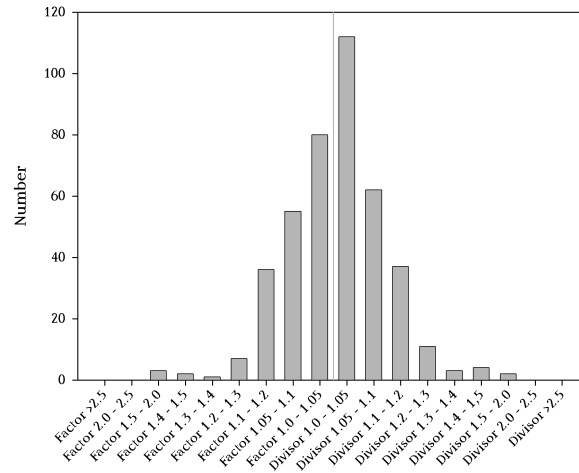
HH-114 Comparison ProteinPilot - Mascot - Quant
Internalcontrols



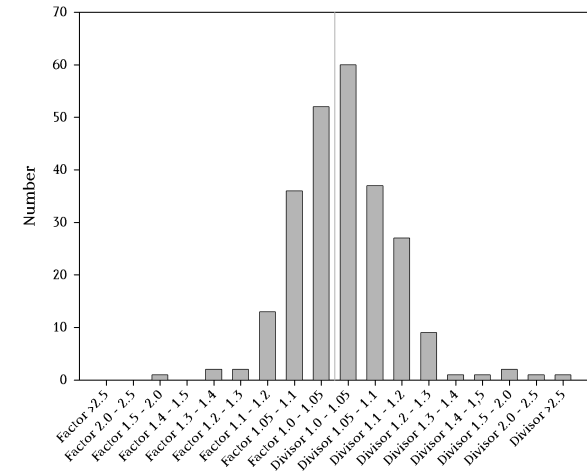
HH-114 Analysis ProteinPilot
Internalcontrol CTRL (114/116)



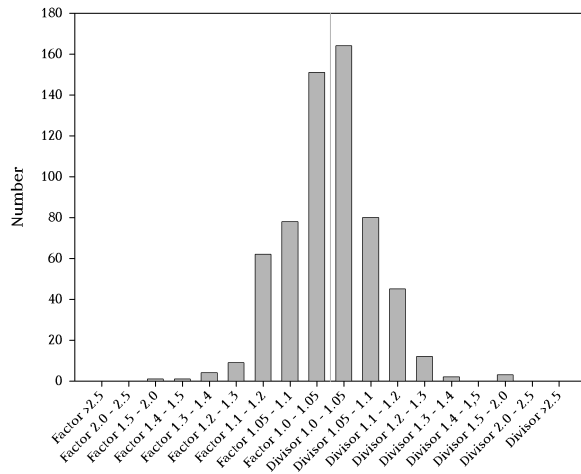
HH-114 Analysis Mascot
Internalcontrol CTRL (114/116)



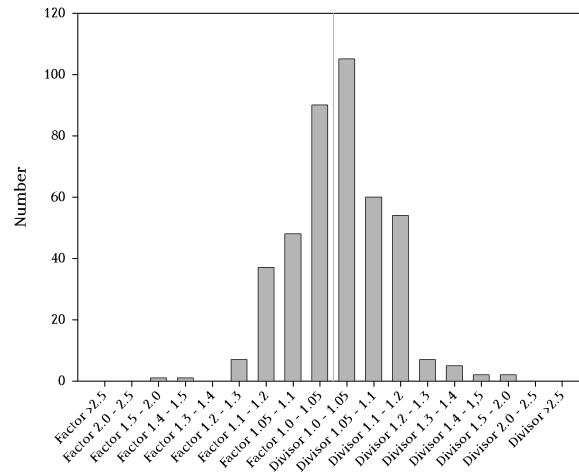
HH-114 Analysis Quant
Internalcontrol CTRL (114/116)



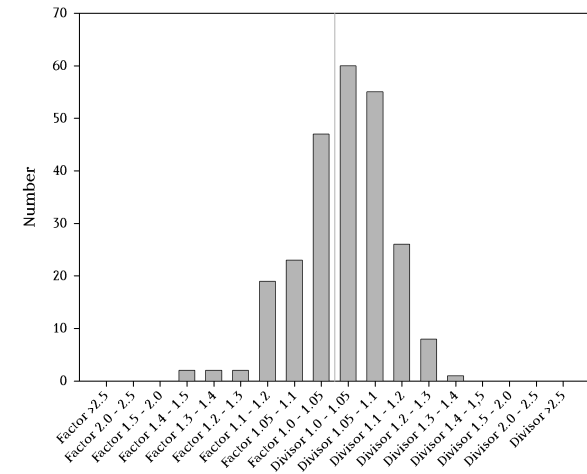
HH-114 Analysis ProteinPilot
Internalcontrol RSV (115/117)



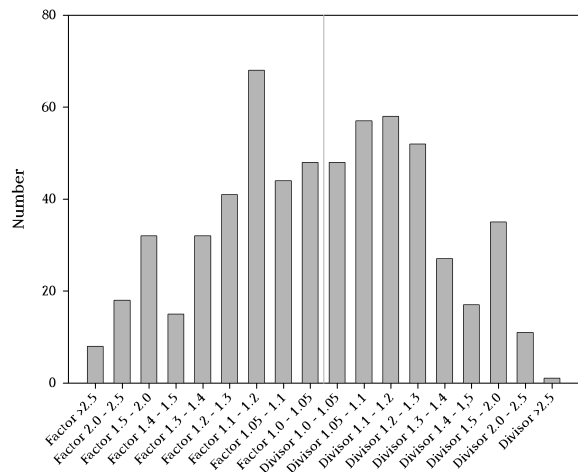
HH-114 Analysis Mascot
Internalcontrol RSV (115/117)



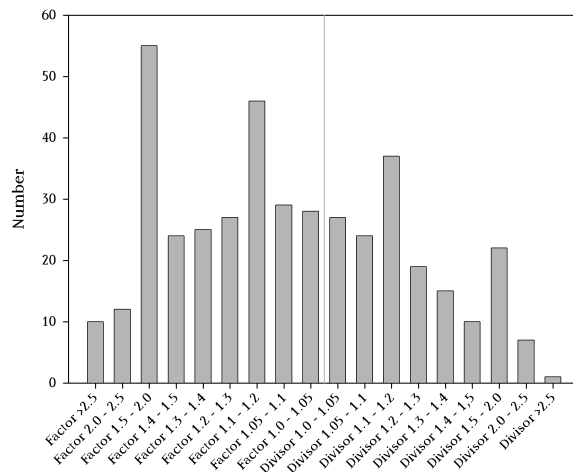
HH-114 Analysis Quant
Internalcontrol RSV (115/117)



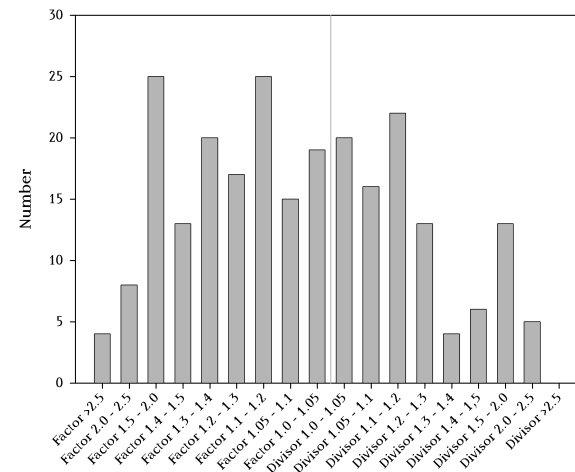
HH-114 Analysis ProteinPilot
RSV vs CTRL (115/114)



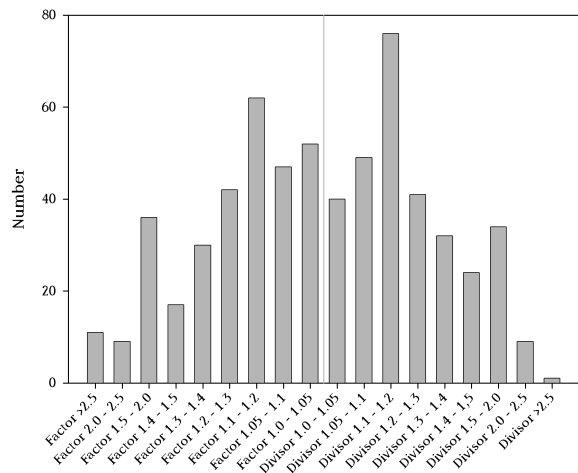
HH-114 Analysis Mascot
RSV vs CTRL (115/114)



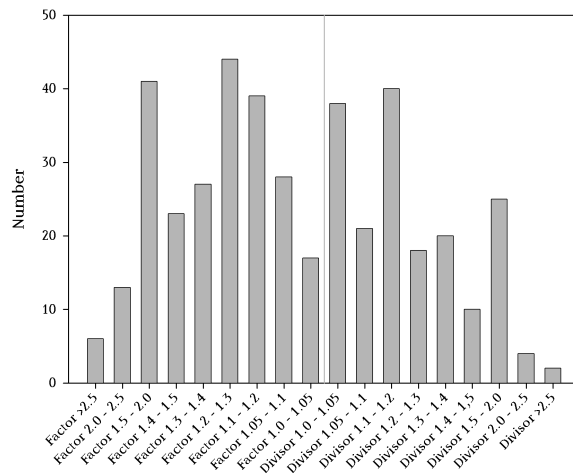
HH-114 Analysis Quant
RSV vs CTRL (115/114)



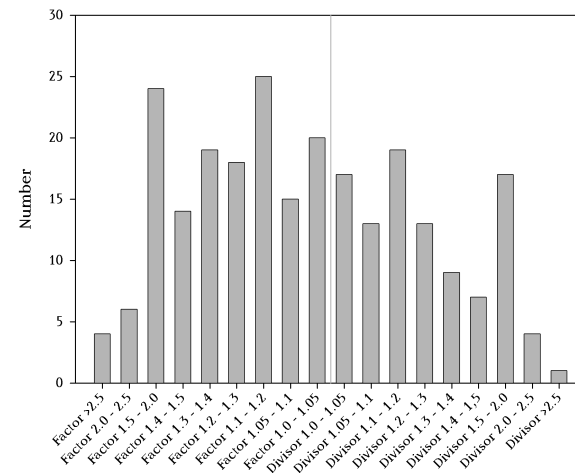
HH-114 Analysis ProteinPilot
RSV vs CTRL (115/116)



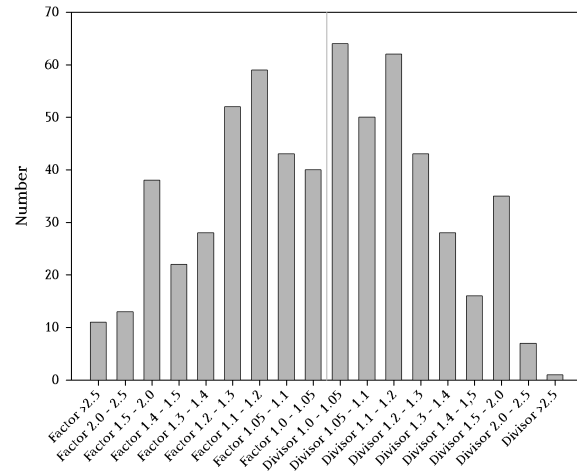
HH-114 Analysis Mascot
RSV vs CTRL (115/116)



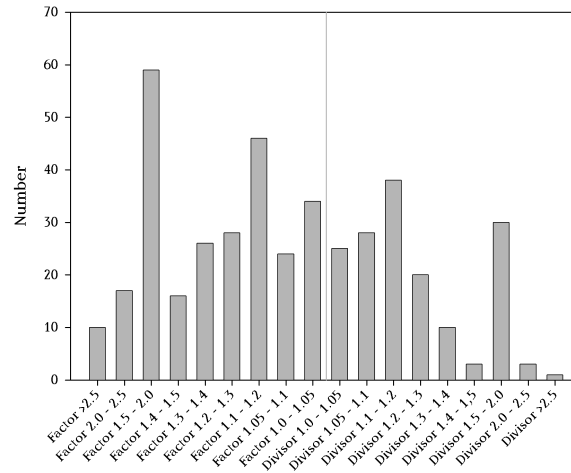
HH-114 Analysis Quant
RSV vs CTRL (115/116)



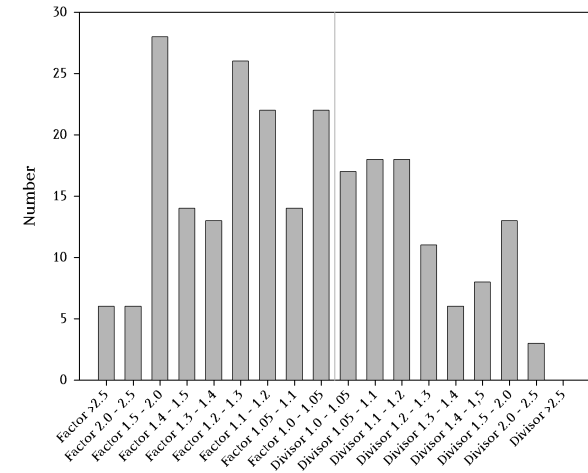
HH-114 Analysis ProteinPilot
RSV vs CTRL (117/114)



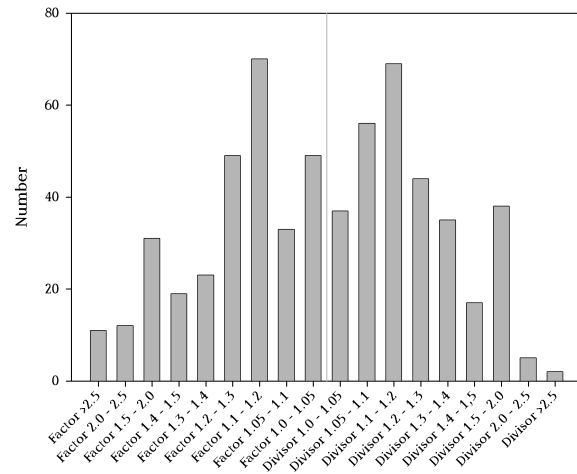
HH-114 Analysis Mascot
RSV vs CTRL (117/114)



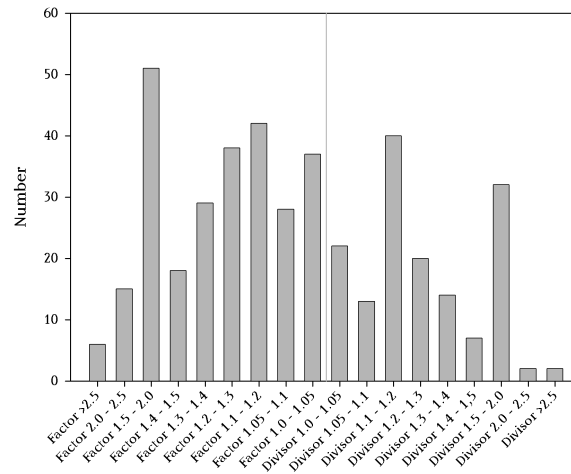
HH-114 Analysis Quant
RSV vs CTRL (117/114)



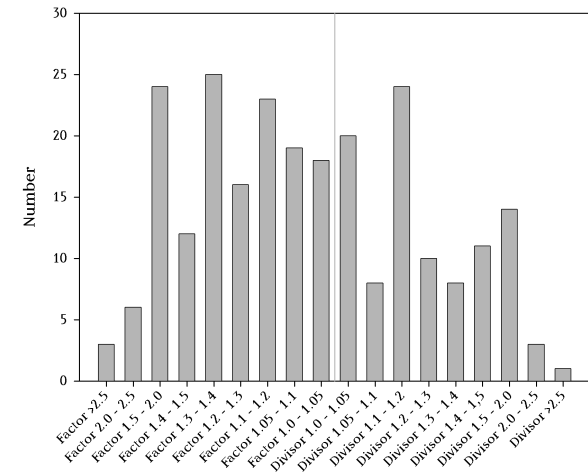
HH-114 Analysis ProteinPilot
RSV vs CTRL (117/116)



HH-114 Analysis Mascot
RSV vs CTRL (117/116)



HH-114 Analysis Quant
RSV vs CTRL (117/116)



Appendix V Complete list of proteins identified by nLC-MS

Sample 1 proteins identified by nLC-MS using MASCOT and the launch peaks to mascot export function			
Number	SwissProt accession	Protein name	Protein score
1	CPSM_HUMAN	Carbamoyl-phosphate synthase [ammonial, mitochondrial precursor	3846
1	PYR1_HUMAN	CAD protein [Includes: Glutamine-dependent carbamoyl-phosphate synthase	118
2	ECHA_HUMAN	Trifunctional enzyme subunit alpha, mitochondrial precursor	3392
3	ATPB_HUMAN	ATP synthase subunit beta, mitochondrial precursor	3022
4	MYH10_HUMAN	Myosin-10	143
4	MYH11_HUMAN	Myosin-11	498
4	MYH9_HUMAN	Myosin-9	2911
5	TBA1B_HUMAN	Tubulin alpha-1B chain	2769
6	ACTB_HUMAN	Actin, cytoplasmic 1	2672
6	ACTG_HUMAN	Actin, cytoplasmic 2	2672
6	ACTK_HUMAN	Kappa-actin	676
6	POTAC_HUMAN		
6	(A26CB_HUMAN - expasy)	Chimeric POIE-actin protein	1263
7	TBA1A_HUMAN	Tubulin alpha-1A chain	2590
7	TBA1C_HUMAN	Tubulin alpha-1C chain	2642
7	TBA3C_HUMAN	Tubulin alpha-3C/D chain	2071
7	TBA3E_HUMAN	Tubulin alpha-3E chain	2045
8	ACSL1_HUMAN	Long-chain-fatty-acid--CoA ligase 1	2413
9	NNIM_HUMAN	NAD(P) transhydrogenase, mitochondrial precursor	2345
10	TBB1_HUMAN	Tubulin beta-1 chain	270
10	TBB2A_HUMAN	Tubulin beta-2A chain	2179
10	TBB2B_HUMAN	Tubulin beta-2B chain	2179
10	TBB3_HUMAN	Tubulin beta-3 chain	2056
10	TBB6_HUMAN	Tubulin beta-6 chain	442
11	TBB5_HUMAN	Tubulin beta chain	2131
12	CH60_HUMAN	60 kDa heat shock protein, mitochondrial precursor	2056
13	TBB2C_HUMAN	Tubulin beta-2C chain	2040
13	TBB4_HUMAN	Tubulin beta-4 chain	1096
13	TBB4Q_HUMAN	Tubulin beta-4q chain	401
14	ATPA_HUMAN	ATP synthase subunit alpha, mitochondrial precursor	2037
15	GFAP_HUMAN	Glial fibrillary acidic protein	52
15	K22O_HUMAN	Keratin, type II cytoskeletal 2 oral	157
15	K2C1B_HUMAN	Keratin, type II cytoskeletal 1b	133
15	K2C3_HUMAN	Keratin, type II cytoskeletal 3	157
15	K2C4_HUMAN	Keratin, type II cytoskeletal 4	133
15	K2C5_HUMAN	Keratin, type II cytoskeletal 5	157
15	K2C6A_HUMAN	Keratin, type II cytoskeletal 6A	157
15	K2C6B_HUMAN	Keratin, type II cytoskeletal 6B	157
15	K2C6C_HUMAN	Keratin, type II cytoskeletal 6C	157
15	K2C7_HUMAN	Keratin, type II cytoskeletal 7	157
15	K2C71_HUMAN	Keratin, type II cytoskeletal 71	133
15	K2C72_HUMAN	Keratin, type II cytoskeletal 72	133
15	K2C73_HUMAN	Keratin, type II cytoskeletal 73	133
15	K2C74_HUMAN	Keratin, type II cytoskeletal 74	133
15	K2C75_HUMAN	Keratin, type II cytoskeletal 75	157
15	K2C78_HUMAN	Keratin, type II cytoskeletal 78	52
15	K2C8_HUMAN	Keratin, type II cytoskeletal 8	2023
15	KRT81_HUMAN	Keratin type II cuticular Hb1	52
15	KRT83_HUMAN	Keratin type II cuticular Hb3	52
15	KRT84_HUMAN	Keratin type II cuticular Hb4	157
15	KRT85_HUMAN	Keratin type II cuticular Hb5	52
15	KRT86_HUMAN	Keratin type II cuticular Hb6	52
15	VIME_HUMAN	Vimentin	52
16	ENPL_HUMAN	Endoplasmic precursor	1977
17	GRP78_HUMAN	78 kDa glucose-regulated protein precursor	1887
18	ETFD_HUMAN	Electron transfer flavoprotein-ubiquinone oxidoreductase, mitochondrial precursor	1774
19	ACTN3_HUMAN	Alpha-actinin-3	271
19	ACTN4_HUMAN	Alpha-actinin-4	1762
20	TBA4A_HUMAN	Tubulin alpha-4A chain	1722
21	CMC2_HUMAN	Calcium-binding mitochondrial carrier protein Aralar2	1689
22	AT12A_HUMAN	Potassium-transporting ATPase alpha chain 2	281
22	AT1A1_HUMAN	Sodium/potassium-transporting ATPase subunit alpha-1 precursor	1676
22	AT1A2_HUMAN	Sodium/potassium-transporting ATPase subunit alpha-2 precursor	903
22	AT1A3_HUMAN	Sodium/potassium-transporting ATPase subunit alpha-3	1086
22	AT1A4_HUMAN	Sodium/potassium-transporting ATPase subunit alpha-4	821
22	ATP4A_HUMAN	Potassium-transporting ATPase alpha chain 1	281
23	ACADV_HUMAN	Very long-chain specific acyl-CoA dehydrogenase, mitochondrial precursor	1655
24	FAS_HUMAN	Fatty acid synthase	1624
25	FLNA_HUMAN	Filamin-A	364
25	FLNB_HUMAN	Filamin-B	1424
25	FLNC_HUMAN	Filamin-C	140
26	IQGA1_HUMAN	Ras GTPase-activating-like protein IQGAP1	101
26	IQGA2_HUMAN	Ras GTPase-activating-like protein IQGAP2	1406
26	IQGA3_HUMAN	Ras GTPase-activating-like protein IQGAP3	101
27	HS90A_HUMAN	Heat shock protein HSP 90-alpha	1339
28	DHB4_HUMAN	Peroxisomal multifunctional enzyme type 2	1334
29	ACTA_HUMAN	Actin, aortic smooth muscle	1224
29	ACTC_HUMAN	Actin, alpha cardiac muscle 1	1326
29	ACTH_HUMAN	Actin, gamma-enteric smooth muscle	1224
29	ACTS_HUMAN	Actin, alpha skeletal muscle	1326
30	ACTN1_HUMAN	Alpha-actinin-1	1291
31	ADH1A_HUMAN	Alcohol dehydrogenase 1A	997
31	ADH1B_HUMAN	Alcohol dehydrogenase 1B	1283
31	ADH1G_HUMAN	Alcohol dehydrogenase 1C	730

Sample 1 proteins identified by nLC-MS using MASCOT and the launch peaks to mascot export function			
Number	SwissProt accession	Protein name	Protein score
32	AOFB_HUMAN	Amine oxidase [flavin-containing] B	1276
33	CLH1_HUMAN	Clathrin heavy chain 1	1221
33	CLH2_HUMAN	Clathrin heavy chain 2	160
34	HS90B_HUMAN	Heat shock protein HSP 90-beta	1215
35	AOFA_HUMAN	Amine oxidase [flavin-containing] A	1184
36	BDH_HUMAN	D-beta-hydroxybutyrate dehydrogenase, mitochondrial precursor	1173
37	CALX_HUMAN	Calnexin precursor	1145
38	K1C18_HUMAN	Keratin, type I cytoskeletal 18	1110
38	K1C19_HUMAN	Keratin, type I cytoskeletal 19	62
39	GDE_HUMAN	Glycogen debranching enzyme	1012
40	QCR2_HUMAN	Cytochrome b-c1 complex subunit 2, mitochondrial precursor	1004
41	DAK_HUMAN (DHAK_HUMAN expasy)	Dihydroxyacetone kinase	994
42	RIB1_HUMAN (RPN1_HUMAN expasy)	Dolichyl-diphosphooligosaccharide--protein glycosyltransferase 67 kDa subunit precursor	954
43	ADH4_HUMAN	Alcohol dehydrogenase 4	950
44	AL1L2_HUMAN	Probable 10-formyltetrahydrofolate dehydrogenase ALDH1L2	119
44	FIHFD_HUMAN	10-formyltetrahydrofolate dehydrogenase	939
45	UD110_HUMAN	UDP-glucuronosyltransferase 1-10 precursor	435
45	UD14_HUMAN	UDP-glucuronosyltransferase 1-4 precursor	925
46	ECHB_HUMAN	Trifunctional enzyme subunit beta, mitochondrial precursor	920
47	ROA2_HUMAN	Heterogeneous nuclear ribonucleoproteins A2/B1	919
48	HYPEP_HUMAN	Epoxide hydrolase 1	910
49	AIFM1_HUMAN	Apoptosis-inducing factor 1, mitochondrial precursor	888
50	VDAC1_HUMAN	Voltage-dependent anion-selective channel protein 1	869
51	DHE3_HUMAN	Glutamate dehydrogenase 1, mitochondrial precursor	862
51	DHE4_HUMAN	Glutamate dehydrogenase 2, mitochondrial precursor	109
52	UD2B7_HUMAN	UDP-glucuronosyltransferase 2B7 precursor	843
53	DHSA_HUMAN	Succinate dehydrogenase [ubiquinone] flavoprotein subunit, mitochondrial precursor	825
54	SQRD_HUMAN	Sulfide:quinone oxidoreductase, mitochondrial precursor	814
55	HMC52_HUMAN	Hydroxymethylglutaryl-CoA synthase, mitochondrial precursor	806
56	FMO3_HUMAN	Dimethylaniline monoxygenase [N-oxide-forming] 3	795
56	FMO4_HUMAN	Dimethylaniline monoxygenase [N-oxide-forming] 4	109
57	ATPO_HUMAN	ATP synthase subunit O, mitochondrial precursor	767
58	NB5R3_HUMAN	NADH-cytochrome b5 reductase 3	765
59	PDIA1_HUMAN	Protein disulfide-isomerase precursor	731
60	FIBA_HUMAN	Fibrinogen alpha chain precursor [Contains: Fibrinopeptide A]	725
61	FIBB_HUMAN	Fibrinogen beta chain precursor [Contains: Fibrinopeptide B]	722
62	1A01_HUMAN	HLA class I histocompatibility antigen, A-1 alpha chain precursor	244
62	1A02_HUMAN	HLA class I histocompatibility antigen, A-2 alpha chain precursor	192
62	1A03_HUMAN	HLA class I histocompatibility antigen, A-3 alpha chain precursor	244
62	1A11_HUMAN	HLA class I histocompatibility antigen, A-11 alpha chain precursor	244
62	1A23_HUMAN	HLA class I histocompatibility antigen, A-23 alpha chain precursor	414
62	1A24_HUMAN	HLA class I histocompatibility antigen, A-24 alpha chain precursor	192
62	1A29_HUMAN	HLA class I histocompatibility antigen, A-29 alpha chain precursor	668
62	1A30_HUMAN	HLA class I histocompatibility antigen, A-30 alpha chain precursor	414
62	1A31_HUMAN	HLA class I histocompatibility antigen, A-31 alpha chain precursor	668
62	1A32_HUMAN	HLA class I histocompatibility antigen, A-32 alpha chain precursor	721
62	1A36_HUMAN	HLA class I histocompatibility antigen, A-36 alpha chain precursor	244
62	1A43_HUMAN	HLA class I histocompatibility antigen, A-43 alpha chain precursor	668
62	1A74_HUMAN	HLA class I histocompatibility antigen, A-74 alpha chain precursor	721
62	1A80_HUMAN	HLA class I histocompatibility antigen, A-80 alpha chain precursor	29
62	1B54_HUMAN	HLA class I histocompatibility antigen, B-54 alpha chain precursor	189
62	1B57_HUMAN	HLA class I histocompatibility antigen, B-57 alpha chain precursor	189
62	1B58_HUMAN	HLA class I histocompatibility antigen, B-58 alpha chain precursor	189
62	1C02_HUMAN	HLA class I histocompatibility antigen, Cw-2 alpha chain precursor	29
62	1C04_HUMAN	HLA class I histocompatibility antigen, Cw-4 alpha chain precursor	189
62	1C05_HUMAN	HLA class I histocompatibility antigen, Cw-5 alpha chain precursor	29
62	1C08_HUMAN	HLA class I histocompatibility antigen, Cw-8 alpha chain precursor	29
62	1C12_HUMAN	HLA class I histocompatibility antigen, Cw-12 alpha chain precursor	192
62	1C14_HUMAN	HLA class I histocompatibility antigen, Cw-14 alpha chain precursor	189
62	1C15_HUMAN	HLA class I histocompatibility antigen, Cw-15 alpha chain precursor	29
62	1C16_HUMAN	HLA class I histocompatibility antigen, Cw-16 alpha chain precursor	192
62	1C17_HUMAN	HLA class I histocompatibility antigen, Cw-17 alpha chain precursor	192
63	ADT2_HUMAN	ADP/ATP translocase 2	703
63	ADT3_HUMAN	ADP/ATP translocase 3	335
63	ADT4_HUMAN	ADP/ATP translocase 4	80
64	ATP5H_HUMAN	ATP synthase subunit d, mitochondrial	701
65	1A25_HUMAN	HLA class I histocompatibility antigen, A-25 alpha chain precursor	685
65	1A26_HUMAN	HLA class I histocompatibility antigen, A-26 alpha chain precursor	685
65	1A33_HUMAN	HLA class I histocompatibility antigen, A-33 alpha chain precursor	685
65	1A34_HUMAN	HLA class I histocompatibility antigen, A-34 alpha chain precursor	685
65	1A66_HUMAN	HLA class I histocompatibility antigen, A-66 alpha chain precursor	685
65	1A68_HUMAN	HLA class I histocompatibility antigen, A-68 alpha chain precursor	208
65	1A69_HUMAN	HLA class I histocompatibility antigen, A-69 alpha chain	208
65	1B13_HUMAN	HLA class I histocompatibility antigen, B-13 alpha chain precursor	39
65	1B15_HUMAN	HLA class I histocompatibility antigen, B-15 alpha chain precursor	206
65	1B18_HUMAN	HLA class I histocompatibility antigen, B-18 alpha chain precursor	39
65	1B27_HUMAN	HLA class I histocompatibility antigen, B-27 alpha chain precursor	39
65	1B35_HUMAN	HLA class I histocompatibility antigen, B-35 alpha chain precursor	206
65	1B40_HUMAN	HLA class I histocompatibility antigen, B-40 alpha chain precursor	39
65	1B41_HUMAN	HLA class I histocompatibility antigen, B-41 alpha chain precursor	39
65	1B44_HUMAN	HLA class I histocompatibility antigen, B-44 alpha chain precursor	39
65	1B45_HUMAN	HLA class I histocompatibility antigen, B-45 alpha chain precursor	39
65	1B46_HUMAN	HLA class I histocompatibility antigen, B-46 alpha chain precursor	206
65	1B47_HUMAN	HLA class I histocompatibility antigen, B-47 alpha chain precursor	39
65	1B49_HUMAN	HLA class I histocompatibility antigen, B-49 alpha chain precursor	39
65	1B50_HUMAN	HLA class I histocompatibility antigen, B-50 alpha chain precursor	39
65	1B51_HUMAN	HLA class I histocompatibility antigen, B-51 alpha chain precursor	206
65	1B52_HUMAN	HLA class I histocompatibility antigen, B-52 alpha chain precursor	206
65	1B53_HUMAN	HLA class I histocompatibility antigen, B-53 alpha chain precursor	206
65	1B55_HUMAN	HLA class I histocompatibility antigen, B-55 alpha chain precursor	206
65	1B56_HUMAN	HLA class I histocompatibility antigen, B-56 alpha chain precursor	206
65	1B59_HUMAN	HLA class I histocompatibility antigen, B-59 alpha chain precursor	206

Sample 1 proteins identified by nLC-MS using MASCOT and the launch peaks to mascot export function			
Number	SwissProt accession	Protein name	Protein score
65	1B73_HUMAN	HLA class I histocompatibility antigen, B-73 alpha chain precursor	43
65	1B78_HUMAN	HLA class I histocompatibility antigen, B-78 alpha chain precursor	206
66	CYB5_HUMAN	Cytochrome b5	680
67	ST2A1_HUMAN	Bile salt sulfotransferase	671
68	UD11_HUMAN	UDP-glucuronosyltransferase 1-1 precursor	661
69	PHB2_HUMAN	Prohibitin-2	656
70	RTN4_HUMAN	Reticulon-4	654
71	PDIA6_HUMAN	Protein disulfide-isomerase A6 precursor	647
72	QCRI_HUMAN	Cytochrome b-c1 complex subunit 1, mitochondrial precursor	644
73	ANXA6_HUMAN	Anexin A6	640
74	FRIL_HUMAN	Ferritin light chain	610
75	UD18_HUMAN	UDP-glucuronosyltransferase 1-8 precursor	554
75	UD19_HUMAN	UDP-glucuronosyltransferase 1-9 precursor	607
76	SPTB1_HUMAN	Spectrin beta chain, erythrocyte	66
76	SPTB2_HUMAN	Spectrin beta chain, brain 1	607
76	SPTN2_HUMAN	Spectrin beta chain, brain 2	66
76	SPTN4_HUMAN	Spectrin beta chain, brain 3	30
77	RIB2_HUMAN (RPN2_HUMAN expasy)	Dolichyl-diphosphooligosaccharide--protein glycosyltransferase 63 kDa subunit precursor	601
78	DCXR_HUMAN	L-xylulose reductase	597
79	ALDOB_HUMAN	Fructose-bisphosphate aldolase B	584
80	NCPB_HUMAN	NADPH--cytochrome P450 reductase	582
81	EF1A1_HUMAN	Elongation factor 1-alpha 1	582
81	EF1A2_HUMAN	Elongation factor 1-alpha 2	285
82	TMED4_HUMAN	Transmembrane emp24 domain-containing protein 4 precursor	384
82	TMED9_HUMAN	Transmembrane emp24 domain-containing protein 9 precursor	579
83	FIBG_HUMAN	Fibrinogen gamma chain precursor	579
84	MTP_HUMAN	Microsomal triglyceride transfer protein large subunit precursor	570
85	ADP1_HUMAN	ADP/ATP translocase 1	568
86	MVP_HUMAN	Major vault protein	562
87	AL1A2_HUMAN	Retinal dehydrogenase 2	35
87	ALDH2_HUMAN	Aldehyde dehydrogenase, mitochondrial precursor	558
88	S27A2_HUMAN	Very long-chain acyl-CoA synthetase	556
89	SAA_HUMAN	Serum amyloid A protein precursor	547
89	SAA3_HUMAN	Putative serum amyloid A-3 protein	31
90	ATPG_HUMAN	ATP synthase subunit gamma, mitochondrial precursor	546
91	IMMT_HUMAN	Mitochondrial inner membrane protein	546
92	PDIA3_HUMAN	Protein disulfide-isomerase A3 precursor	544
93	UD13_HUMAN	UDP-glucuronosyltransferase 1-3 precursor	536
93	UD15_HUMAN	UDP-glucuronosyltransferase 1-5 precursor	463
94	COX2_HUMAN	Cytochrome c oxidase subunit 2	534
95	CPT2_HUMAN	Carnitine O-palmitoyltransferase 2, mitochondrial precursor	528
96	SURF4_HUMAN	Surfeit locus protein 4	513
97	UD16_HUMAN	UDP-glucuronosyltransferase 1-6 precursor	503
98	UDB10_HUMAN	UDP-glucuronosyltransferase 2B10 precursor	501
98	UDB11_HUMAN	UDP-glucuronosyltransferase 2B11 precursor	233
98	UDB28_HUMAN	UDP-glucuronosyltransferase 2B28 precursor	173
99	MEI7A_HUMAN	Methyltransferase-like protein 7A precursor	493
100	UGPA_HUMAN	UTP--glucose-1-phosphate uridylyltransferase	490
101	G3P_HUMAN	Glycerinaldehyde-3-phosphate dehydrogenase	489
102	RS4X_HUMAN	40S ribosomal protein S4, X isoform	486
102	RS4Y2_HUMAN	40S ribosomal protein S4, Y isoform 2	136
103	ROA1_HUMAN	Heterogeneous nuclear ribonucleoprotein A1	473
104	PCBP1_HUMAN	Poly(rC)-binding protein 1	468
105	HNRPM_HUMAN	Heterogeneous nuclear ribonucleoprotein M	456
106	H2A1_HUMAN	Histone H2A type 1	454
106	H2A1A_HUMAN	Histone H2A type 1-A	168
106	H2A1B_HUMAN	Histone H2A type 1-B	454
106	H2A1C_HUMAN	Histone H2A type 1-C	454
106	H2A1D_HUMAN	Histone H2A type 1-D	454
106	H2A1E_HUMAN	Histone H2A type 1-E	454
106	H2A1H_HUMAN	Histone H2A type 1-H	454
106	H2A1J_HUMAN	Histone H2A type 1-J	454
106	H2A2A_HUMAN	Histone H2A type 2-A	454
106	H2A2B_HUMAN	Histone H2A type 2-B	104
106	H2A2C_HUMAN	Histone H2A type 2-C	454
106	H2A3_HUMAN	Histone H2A type 3	454
106	H2AV_HUMAN	Histone H2AV	168
106	H2AX_HUMAN	Histone H2A.x	168
106	H2AZ_HUMAN	Histone H2A.Z	168
107	RL10A_HUMAN	60S ribosomal protein L10a	452
108	DIC_HUMAN	Mitochondrial dicarboxylate carrier	452
109	K6PL_HUMAN	6-phosphofructokinase, liver type	448
110	RL6_HUMAN	60S ribosomal protein L6	442
111	FTCD_HUMAN	Formimidoyltransferase-cyclodeaminase	440
112	PHB_HUMAN	Prohibitin	439
113	NDUS1_HUMAN	NADH-ubiquinone oxidoreductase 75 kDa subunit, mitochondrial precursor	434
114	EF2_HUMAN	Elongation factor 2	433
115	PPCKC_HUMAN	Phosphoenolpyruvate carboxykinase, cytosolic [GTP]	83
115	PPCKM_HUMAN	Phosphoenolpyruvate carboxykinase [GTP], mitochondrial precursor	431
116	AMPN_HUMAN	Aminopeptidase N	431
117	ICPB_HUMAN	T-complex protein 1 subunit beta	430
118	CP4F2_HUMAN	Cytochrome P450 4F2	424
118	CP4F3_HUMAN	Cytochrome P450 4F3	371
118	CP4F8_HUMAN	Cytochrome P450 4F8	174
118	CP4FC_HUMAN	Cytochrome P450 4F12	118
119	MPCP_HUMAN	Phosphate carrier protein, mitochondrial precursor	422
120	RL17_HUMAN	60S ribosomal protein L17	420
121	THTR_HUMAN	Thiosulfate sulfurtransferase	419
122	RS5_HUMAN	40S ribosomal protein S5	417
123	RS19_HUMAN	40S ribosomal protein S19	417
124	SSRA_HUMAN	Translocon-associated protein subunit alpha precursor	416
125	EF1G_HUMAN	Elongation factor 1-gamma	415
126	TERA_HUMAN	Transitional endoplasmic reticulum ATPase	414

Sample 1 proteins identified by nLC-MS using MASCOT and the launch peaks to mascot export function			
Number	SwissProt accession	Protein name	Protein score
127	ILN1_HUMAN	Talin-1	413
127	ILN2_HUMAN	Talin-2	61
128	RS3A_HUMAN	40S ribosomal protein S3a	411
129	CP2E1_HUMAN	Cytochrome P450 2E1	410
130	RS2_HUMAN	40S ribosomal protein S2	406
131	HSP72_HUMAN	Heat shock-related 70 kDa protein 2	86
131	HSP7C_HUMAN	Heat shock cognate 71 kDa protein	401
132	AT5F1_HUMAN	ATP synthase subunit b, mitochondrial precursor	399
133	SERA_HUMAN	D-3-phosphoglycerate dehydrogenase	395
134	VDAC2_HUMAN	Voltage-dependent anion-selective channel protein 2	395
135	FINC_HUMAN	Fibronectin precursor	388
136	CY1_HUMAN	Cytochrome c1, heme protein, mitochondrial precursor	385
137	DHB13_HUMAN	17-beta hydroxysteroid dehydrogenase 13 precursor	385
138	LMAN2_HUMAN	Vesicular integral-membrane protein VIP36 precursor	377
139	SFXN1_HUMAN	Sideroflexin-1	374
140	PSME2_HUMAN	Proteasome activator complex subunit 2	372
141	CLUS_HUMAN	Clusterin precursor	364
142	ASSY_HUMAN	Argininosuccinate synthase	362
143	ABCD3_HUMAN	ATP-binding cassette sub-family D member 3	361
143	GEN_HUMAN	Flap endonuclease GEN homolog 1	61
144	GABT_HUMAN	4-aminobutyrate aminotransferase, mitochondrial precursor	360
145	RL15_HUMAN	60S ribosomal protein L15	356
146	RL3_HUMAN	60S ribosomal protein L3	356
146	RL3L_HUMAN	60S ribosomal protein L3-like	105
147	HNRPK_HUMAN	Heterogeneous nuclear ribonucleoprotein K	354
148	UBIQ_HUMAN	Ubiquitin	353
149	RS7_HUMAN	40S ribosomal protein S7	353
150	AL3A2_HUMAN	Fatty aldehyde dehydrogenase	350
151	DHB11_HUMAN	Estradiol 17-beta-dehydrogenase 11 precursor	348
152	RDH16_HUMAN	Retinol dehydrogenase 16	345
153	RL18A_HUMAN	60S ribosomal protein L18a	343
154	FABPL_HUMAN	Fatty acid-binding protein, liver	342
155	HNRCL_HUMAN	Heterogeneous nuclear ribonucleoprotein C-like 1	167
155	HNRPC_HUMAN	Heterogeneous nuclear ribonucleoproteins C1/C2	340
156	VDAC3_HUMAN	Voltage-dependent anion-selective channel protein 3	337
157	APOA1_HUMAN	Apolipoprotein A-1 precursor	333
158	RL4_HUMAN	60S ribosomal protein L4	328
159	COPG_HUMAN	Coatomer subunit gamma	324
160	ECHM_HUMAN	Enoyl-CoA hydratase, mitochondrial precursor	324
161	GRP75_HUMAN	Stress-70 protein, mitochondrial precursor	320
162	TOM70_HUMAN	Mitochondrial precursor proteins import receptor	316
163	AT2A1_HUMAN	Sarcoplasmic/endoplasmic reticulum calcium ATPase 1	185
163	AT2A2_HUMAN	Sarcoplasmic/endoplasmic reticulum calcium ATPase 2	316
164	MGST1_HUMAN	Microsomal glutathione S-transferase 1	307
165	RL23_HUMAN	60S ribosomal protein L23	307
166	VAPA_HUMAN	Vesicle-associated membrane protein-associated protein A	160
166	VAPB_HUMAN	Vesicle-associated membrane protein-associated protein B/C	305
167	RL21_HUMAN	60S ribosomal protein L21	293
168	AT1B1_HUMAN	Sodium/potassium-transporting ATPase subunit beta-1	292
169	RL7A_HUMAN	60S ribosomal protein L7a	292
170	FRIH_HUMAN	Ferritin heavy chain	291
171	TMPSD_HUMAN	Transmembrane protease, serine 13	90
171	TRY1_HUMAN	Trypsin-1 precursor	287
172	ERG7_HUMAN	Lanosterol synthase	286
173	C1TC_HUMAN	C-1-tetrahydrofolate synthase, cytoplasmic	284
174	MYO1A_HUMAN	Myosin-1a	37
174	MYO1B_HUMAN	Myosin-1b	277
175	RL11_HUMAN	60S ribosomal protein L11	273
176	TGM2_HUMAN	Protein-glutamine gamma-glutamyltransferase 2	271
177	MTC2_HUMAN	Mitochondrial carrier homolog 2	270
178	PAIRB_HUMAN	Plasminogen activator inhibitor 1 RNA-binding protein	270
179	SW_HUMAN (SWC_HUMAN expasy)	Valyl-tRNA synthetase	266
180	ACSL5_HUMAN	Long-chain-fatty-acid-CoA ligase 5	266
181	PON3_HUMAN	Serum paraoxonase/lactonase 3	265
182	RL19_HUMAN	60S ribosomal protein L19	264
183	PYC_HUMAN	Pyruvate carboxylase, mitochondrial precursor	261
184	IXTP_HUMAN	Tricarboxylate transport protein, mitochondrial precursor	259
185	ASGR1_HUMAN	Asialoglycoprotein receptor 1	259
186	RSSA_HUMAN	40S ribosomal protein SA	258
187	RL18_HUMAN	60S ribosomal protein L18	255
188	MLRM_HUMAN	Myosin regulatory light chain 2, nonsarcomeric	255
188	MLRN_HUMAN	Myosin regulatory light chain 2, smooth muscle isoform	46
189	ACPM_HUMAN	Acyl carrier protein, mitochondrial precursor	250
190	RLA0_HUMAN	60S acidic ribosomal protein P0	250
191	S10AA_HUMAN	Protein S100-A10	249
192	KPYR_HUMAN	Pyruvate kinase isozymes R/L	249
193	PECR_HUMAN	Peroxisomal trans-2-enoyl-CoA reductase	249
194	ROA3_HUMAN	Heterogeneous nuclear ribonucleoprotein A3	248
195	CISD1_HUMAN	CDGSH iron sulfur domain-containing protein 1	244
196	FDFT_HUMAN	Squalene synthetase	241
197	GSTA1_HUMAN	Glutathione S-transferase A1	239
197	GSTA2_HUMAN	Glutathione S-transferase A2	239
197	GSTA3_HUMAN	Glutathione S-transferase A3	239
197	GSTA5_HUMAN	Glutathione S-transferase A5	45
198	RL13_HUMAN	60S ribosomal protein L13	238
199	H4_HUMAN	Histone H4	238
200	ATP5J_HUMAN	ATP synthase-coupling factor 6, mitochondrial precursor	237
201	UD2A1_HUMAN	UDP-glucuronosyltransferase 2A1 precursor	28
201	UD2A3_HUMAN	UDP-glucuronosyltransferase 2A3 precursor	28
201	UD2B4_HUMAN	UDP-glucuronosyltransferase 2B4 precursor	237
202	KAD4_HUMAN	Adenylate kinase isoenzyme 4, mitochondrial	232
203	NDUS8_HUMAN	NADH dehydrogenase [ubiquinone] iron-sulfur protein 8, mitochondrial precursor	228
204	HYOU1_HUMAN	Hypoxia up-regulated protein 1 precursor	227

Sample 1 proteins identified by nLC-MS using MASCOT and the launch peaks to mascot export function			
Number	SwissProt accession	Protein name	Protein score
205	IF4G1_HUMAN	Eukaryotic translation initiation factor 4 gamma 1	226
206	COPA_HUMAN	Coatamer subunit alpha	226
207	PSME1_HUMAN	Proteasome activator complex subunit 1	220
208	PLEC1_HUMAN	Plectin-1	220
209	CJ058_HUMAN	Uncharacterized protein C10orf58 precursor	220
210	DYHC_HUMAN (DYHC1_HUMAN expasy)	Dynein heavy chain, cytosolic	219
211	RS4Y1_HUMAN	40S ribosomal protein S4, Y isoform 1	218
212	TIM50_HUMAN	Import inner membrane translocase subunit TIM50, mitochondrial precursor	216
213	AAAD_HUMAN	Arylacetamide deacetylase	214
214	MMAB_HUMAN	Cob(II)yrinic acid a,c-diamide adenosyltransferase, mitochondrial precursor	210
215	RL27A_HUMAN	60S ribosomal protein L27a	210
216	NDUAC_HUMAN	NADH dehydrogenase [ubiquinone] 1 alpha subcomplex subunit 12	209
217	OST48_HUMAN	Dolichyl-diphosphooligosaccharide--protein glycosyltransferase 48 kDa subunit precursor	209
218	MMP19_HUMAN	Matrix metalloproteinase-19 precursor	56
218	VINC_HUMAN	Vitronectin precursor	208
219	CIND1_HUMAN	Catenin delta-1	208
220	HNRPO_HUMAN	Heterogeneous nuclear ribonucleoprotein Q	208
221	NDUA9_HUMAN	NADH dehydrogenase [ubiquinone] 1 alpha subcomplex subunit 9, mitochondrial precursor	207
222	APOC3_HUMAN	Apolipoprotein C-III precursor	206
223	DHB2_HUMAN	Estradiol 17-beta-dehydrogenase 2	202
224	NUCL_HUMAN	Nucleolin	201
225	QCR7_HUMAN	Cytochrome b-c1 complex subunit 7	200
226	RL14_HUMAN	60S ribosomal protein L14	200
227	IF4A1_HUMAN	Eukaryotic initiation factor 4A-I	197
227	IF4A2_HUMAN	Eukaryotic initiation factor 4A-II	142
228	THIL_HUMAN	Acetyl-CoA acetyltransferase, mitochondrial precursor	197
229	HZB1A_HUMAN	Histone H2B type 1-A	76
229	HZB1B_HUMAN	Histone H2B type 1-B	197
229	HZB1C_HUMAN	Histone H2B type 1-C/E/F/G/I	197
229	HZB1D_HUMAN	Histone H2B type 1-D	197
229	HZB1H_HUMAN	Histone H2B type 1-H	197
229	HZB1J_HUMAN	Histone H2B type 1-J	197
229	HZB1K_HUMAN	Histone H2B type 1-K	197
229	HZB1L_HUMAN	Histone H2B type 1-L	197
229	HZB1M_HUMAN	Histone H2B type 1-M	197
229	HZB1N_HUMAN	Histone H2B type 1-N	197
229	HZB1O_HUMAN	Histone H2B type 1-O	197
229	HZB2E_HUMAN	Histone H2B type 2-E	197
229	HZB2F_HUMAN	Histone H2B type 2-F	197
229	HZB3B_HUMAN	Histone H2B type 3-B	197
229	HZBFS_HUMAN	Histone H2B type F-S	197
230	HSP71_HUMAN	Heat shock 70 kDa protein 1	195
230	HSP76_HUMAN	Heat shock 70 kDa protein 6	88
230	HSP77_HUMAN	Putative heat shock 70 kDa protein 7	88
231	COPD_HUMAN	Coatamer subunit delta	195
232	SYMC_HUMAN	Methionyl-tRNA synthetase, cytoplasmic	194
233	RL29_HUMAN	60S ribosomal protein L29	194
234	HNRPD_HUMAN	Heterogeneous nuclear ribonucleoprotein D0	193
235	NNMT_HUMAN	Nicotinamide N-methyltransferase	193
236	ECHP_HUMAN	Peroxisomal bifunctional enzyme	192
237	SFRS3_HUMAN	Splicing factor, arginine/serine-rich 3	192
237	SFRS7_HUMAN	Splicing factor, arginine/serine-rich 7	192
238	ICAM1_HUMAN	Intercellular adhesion molecule 1 precursor	190
239	NDKA_HUMAN	Nucleoside diphosphate kinase A	189
239	NDKB_HUMAN	Nucleoside diphosphate kinase B	189
240	RS6_HUMAN	40S ribosomal protein S6	187
241	UGDH_HUMAN	UDP-glucose 6-dehydrogenase	186
242	TR150_HUMAN	Thyroid hormone receptor-associated protein 3	186
243	DECR_HUMAN	2,4-dienoyl-CoA reductase, mitochondrial precursor	184
244	EST1_HUMAN	Liver carboxylesterase 1 precursor	184
245	K22E_HUMAN	Keratin, type II cytoskeletal 2 epidermal	183
245	K2C1_HUMAN	Keratin, type II cytoskeletal 1	79
246	RL31_HUMAN	60S ribosomal protein L31	183
247	NSDHL_HUMAN	Sterol-4-alpha-carboxylate 3-dehydrogenase, decarboxylating	182
248	NPM_HUMAN	Nucleophosmin	181
249	RAB7A_HUMAN	Ras-related protein Rab-7a	181
250	QCR6_HUMAN	Cytochrome b-c1 complex subunit 6, mitochondrial precursor	180
251	RS30_HUMAN	40S ribosomal protein S30	179
252	S27A5_HUMAN	Bile acyl-CoA synthetase	179
253	MET7B_HUMAN	Methyltransferase-like protein 7B precursor	178
254	KMO_HUMAN	Kynurenine 3-monoxygenase	177
255	RS18_HUMAN	40S ribosomal protein S18	176
256	UDB15_HUMAN	UDP-glucuronosyltransferase 2B15 precursor	176
257	RL12_HUMAN	60S ribosomal protein L12	176
258	MYL6_HUMAN	Myosin light polypeptide 6	175
259	RS9_HUMAN	40S ribosomal protein S9	175
260	PRS7_HUMAN	26S protease regulatory subunit 7	174
261	BHMT1_HUMAN	Betaine-homocysteine S-methyltransferase 1	174
262	GNAI1_HUMAN	Guanine nucleotide-binding protein G(i), alpha-1 subunit	144
262	GNAI3_HUMAN	Guanine nucleotide-binding protein G(k) subunit alpha	144
262	GNAL_HUMAN	Guanine nucleotide-binding protein G(olf) subunit alpha	144
262	GNAO1_HUMAN	Guanine nucleotide-binding protein G(o) subunit alpha 1	144
262	GNAO2_HUMAN	Guanine nucleotide-binding protein G(o) subunit alpha 2	144
262	GNAS1_HUMAN	Guanine nucleotide-binding protein G(s) subunit alpha isoforms XLas	173
262	GNAS2_HUMAN	Guanine nucleotide-binding protein G(s) subunit alpha isoforms short	173
262	GNA11_HUMAN	Guanine nucleotide-binding protein G(t) subunit alpha-1	144
262	GNA12_HUMAN	Guanine nucleotide-binding protein G(t) subunit alpha-2	144
263	DAD1_HUMAN	Dolichyl-diphosphooligosaccharide--protein glycosyltransferase subunit DAD1	173
264	KU86_HUMAN	ATP-dependent DNA helicase 2 subunit 2	173
265	S39AE_HUMAN	Zinc transporter ZIP14	172
266	GSTK1_HUMAN	Glutathione S-transferase kappa 1	171
267	STOM_HUMAN	Erythrocyte band 7 integral membrane protein	170
268	CATA_HUMAN	Catalase	170

Sample 1 proteins identified by nLC-MS using MASCOT and the launch peaks to mascot export function			
Number	SwissProt accession	Protein name	Protein score
269	RS12_HUMAN	40S ribosomal protein S12	168
270	SND1_HUMAN	Staphylococcal nuclease domain-containing protein 1	168
271	ACLY_HUMAN	ATP-citrate synthase	167
272	DHSO_HUMAN	Sorbitol dehydrogenase	167
273	LRC59_HUMAN	Leucine-rich repeat-containing protein 59	167
274	GNAI2_HUMAN	Guanine nucleotide-binding protein G(i), alpha-2 subunit	167
275	RADI_HUMAN	Radixin	164
276	DHB12_HUMAN	Estradiol 17-beta-dehydrogenase 12	163
277	GALT2_HUMAN	Polypeptide N-acetylgalactosaminyltransferase 2	163
278	TMEDA_HUMAN	Transmembrane emp24 domain-containing protein 10 precursor	162
279	CP4FB_HUMAN	Cytochrome P450 4F11	161
280	MYO1C_HUMAN	Myosin-1c	160
281	DH11_HUMAN	Corticosteroid 11-beta-dehydrogenase isozyme 1	160
282	GBG12_HUMAN	Guanine nucleotide-binding protein G(i)/G(S)/G(O) subunit gamma-12 precursor	160
283	CATD_HUMAN	Cathepsin D precursor	159
284	MZOM_HUMAN	Mitochondrial 2-oxoglutarate/malate carrier protein	158
285	ROAA_HUMAN	Heterogeneous nuclear ribonucleoprotein A/B	158
286	APOE_HUMAN	Apolipoprotein E precursor	158
287	GNA12_HUMAN	Guanine nucleotide-binding protein alpha-12 subunit	144
287	GNA13_HUMAN	Guanine nucleotide-binding protein alpha-13 subunit	158
288	MPU1_HUMAN	Mannose-P-dolichol utilization defect 1 protein	158
289	RS3_HUMAN	40S ribosomal protein S3	157
290	RHOA_HUMAN	Transforming protein RhoA precursor	157
290	RHOB_HUMAN	Rho-related GTP-binding protein RhoB precursor	75
290	RHOC_HUMAN	Rho-related GTP-binding protein RhoC precursor	157
291	RS20_HUMAN	40S ribosomal protein S20	156
292	SVJ2B_HUMAN	Synaptojanin-2-binding protein	156
293	COX41_HUMAN	Cytochrome c oxidase subunit 4 isoform 1, mitochondrial precursor	155
294	TMED7_HUMAN	Transmembrane emp24 domain-containing protein 7 precursor	154
295	RL9_HUMAN	60S ribosomal protein L9	154
296	PRDX6_HUMAN	Peroxiredoxin-6	153
297	AL8A1_HUMAN	Aldehyde dehydrogenase family 8 member A1	152
298	FUMH_HUMAN	Fumarate hydratase, mitochondrial precursor	151
299	ES8L2_HUMAN	Epidermal growth factor receptor kinase substrate 8-like protein 2	150
300	PECL_HUMAN	Peroxisomal 3,2-trans-enoyl-CoA isomerase	150
301	STI3A_HUMAN	Dolichyl-diphosphooligosaccharide--protein glycosyltransferase subunit STI3A	149
302	SFRS1_HUMAN	Splicing factor, arginine/serine-rich 1	148
303	GATM_HUMAN	Glycine amidinotransferase, mitochondrial precursor	147
304	ACSL3_HUMAN	Long-chain-fatty-acid--CoA ligase 3	147
304	ACSL4_HUMAN	Long-chain-fatty-acid--CoA ligase 4	147
305	AR6P1_HUMAN	ADP-ribosylation factor-like protein 6-interacting protein 1	146
306	PRS10_HUMAN	26S protease regulatory subunit S10B	145
307	G6PT1_HUMAN	Glucose-6-phosphate translocase	143
308	RAB12_HUMAN	Putative Ras-related protein Rab-12	75
308	RAB14_HUMAN	Ras-related protein Rab-14	75
308	RAB1A_HUMAN	Ras-related protein Rab-1A	142
308	RAB1B_HUMAN	Ras-related protein Rab-1B	142
308	RAB30_HUMAN	Ras-related protein Rab-30	75
308	RAB35_HUMAN	Ras-related protein Rab-35	75
308	RAB37_HUMAN	Ras-related protein Rab-37	75
308	RAB3A_HUMAN	Ras-related protein Rab-3A	75
308	RAB3B_HUMAN	Ras-related protein Rab-3B	75
308	RAB3C_HUMAN	Ras-related protein Rab-3C	75
308	RAB3D_HUMAN	Ras-related protein Rab-3D	75
308	RAB43_HUMAN	Ras-related protein Rab-43	75
308	RAB4A_HUMAN	Ras-related protein Rab-4A	75
308	RAB4B_HUMAN	Ras-related protein Rab-4B	75
308	RAB8A_HUMAN	Ras-related protein Rab-8A	75
308	RAB8B_HUMAN	Ras-related protein Rab-8B	75
308	RB39B_HUMAN	Ras-related protein Rab-39B	75
309	GANAB_HUMAN	Neutral alpha-glucosidase AB precursor	142
310	RL13A_HUMAN	60S ribosomal protein L13a	141
311	ESY1_HUMAN	Extended-synaptotagmin-1	140
312	PDL15_HUMAN	PDZ and LIM domain protein 5	140
313	APOC1_HUMAN	Apolipoprotein C-1 precursor	139
314	UBE2N_HUMAN	Ubiquitin-conjugating enzyme E2 N	139
314	UE2NL_HUMAN	Putative ubiquitin-conjugating enzyme E2 N-like	48
315	RS23_HUMAN	40S ribosomal protein S23	139
316	ATP5L2_HUMAN	ATP synthase subunit g 2, mitochondrial	24
316	ATP5L_HUMAN	ATP synthase subunit g, mitochondrial	138
317	SAM50_HUMAN	Sorting and assembly machinery component 50 homolog	138
318	PON1_HUMAN	Serum paraoxonase/arylesterase 1	137
319	TMED5_HUMAN	Transmembrane emp24 domain-containing protein 5 precursor	136
320	TM109_HUMAN	Transmembrane protein 109 precursor	136
321	ITA1_HUMAN	Integrin alpha-1 precursor	135
322	CX6B1_HUMAN	Cytochrome c oxidase subunit VIb isoform 1	135
323	NDK8_HUMAN	Putative nucleoside diphosphate kinase	132
324	1B07_HUMAN	HLA class I histocompatibility antigen, B-7 alpha chain precursor	132
324	1B08_HUMAN	HLA class I histocompatibility antigen, B-8 alpha chain precursor	132
324	1B14_HUMAN	HLA class I histocompatibility antigen, B-14 alpha chain precursor	132
324	1B37_HUMAN	HLA class I histocompatibility antigen, B-37 alpha chain precursor	132
324	1B38_HUMAN	HLA class I histocompatibility antigen, B-38 alpha chain precursor	132
324	1B39_HUMAN	HLA class I histocompatibility antigen, B-39 alpha chain precursor	132
324	1B42_HUMAN	HLA class I histocompatibility antigen, B-42 alpha chain precursor	132
324	1B48_HUMAN	HLA class I histocompatibility antigen, B-48 alpha chain precursor	132
324	1B67_HUMAN	HLA class I histocompatibility antigen, B-67 alpha chain precursor	132
324	1B81_HUMAN	HLA class I histocompatibility antigen, B-81 alpha chain precursor	132
324	1B82_HUMAN	HLA class I histocompatibility antigen, B-82 alpha chain precursor	132
324	1C01_HUMAN	HLA class I histocompatibility antigen, Cw-1 alpha chain precursor	116
324	1C18_HUMAN	HLA class I histocompatibility antigen, Cw-18 alpha chain precursor	116
324	HLAE_HUMAN	HLA class I histocompatibility antigen, alpha chain E precursor	116
325	PCBP2_HUMAN	Poly(rC)-binding protein 2	132
325	PCBP3_HUMAN	Poly(rC)-binding protein 3	80
326	DNJA3_HUMAN	DnaJ homolog subfamily A member 3, mitochondrial precursor	131

Sample 1 proteins identified by nLC-MS using MASCOT and the launch peaks to mascot export function			
Number	SwissProt accession	Protein name	Protein score
327	CP51A_HUMAN	Cytochrome P450 51A1	131
328	PRS6A_HUMAN	26S protease regulatory subunit 6A	130
329	TCPO_HUMAN	T-complex protein 1 subunit theta	130
330	NDUB9_HUMAN	NADH dehydrogenase [ubiquinone] 1 beta subcomplex subunit 9	128
331	SNX5_HUMAN	Sorting nexin-5	128
332	RL32_HUMAN	60S ribosomal protein L32	127
333	GBB1_HUMAN	Guanine nucleotide-binding protein G(I)/G(S)/G(D) subunit beta-1	127
333	GBB2_HUMAN	Guanine nucleotide-binding protein G(I)/G(S)/G(T) subunit beta-2	70
334	HYES_HUMAN	Epoxide hydrolase 2	127
335	MDR1_HUMAN	Multidrug resistance protein 1	126
336	NDUS3_HUMAN	NADH dehydrogenase [ubiquinone] iron-sulfur protein 3, mitochondrial precursor	124
337	EST2_HUMAN	Carboxylesterase 2 precursor	124
338	EZRL_HUMAN	Ezrin	123
339	OPA1_HUMAN	Dynamin-like 120 kDa protein, mitochondrial precursor	122
340	SPCS2_HUMAN	Signal peptidase complex subunit 2	121
341	IR3IP_HUMAN	Immediate early response 3-interacting protein 1	120
342	DBPA_HUMAN	DNA-binding protein A	118
342	YBOX1_HUMAN	Nuclease sensitive element-binding protein 1	118
342	YBOX2_HUMAN	Y-box-binding protein 2	118
343	DDX17_HUMAN	Probable ATP-dependent RNA helicase DDX17	118
343	DDX3X_HUMAN	ATP-dependent RNA helicase DDX3X	118
343	DDX3Y_HUMAN	ATP-dependent RNA helicase DDX3Y	118
343	DDX5_HUMAN	Probable ATP-dependent RNA helicase DDX5	118
344	MOES_HUMAN	Moesin	118
345	SRP68_HUMAN	Signal recognition particle 68 kDa protein	118
346	LONM_HUMAN	Lon protease homolog, mitochondrial precursor	117
347	FLIL_HUMAN	Protein flightless-1 homolog	116
348	HSPB1_HUMAN	Heat shock protein beta-1	115
349	AP2M1_HUMAN	AP-2 complex subunit mu-1	114
350	DHX9_HUMAN	ATP-dependent RNA helicase A	114
351	SRPRB_HUMAN	Signal recognition particle receptor subunit beta	114
352	RAB10_HUMAN	Ras-related protein Rab-10	114
353	RS15A_HUMAN	40S ribosomal protein S15a	114
354	H17B6_HUMAN	Hydroxysteroid 17-beta dehydrogenase 6 precursor	113
355	TAGL2_HUMAN	Transgelin-2	113
356	DEOC_HUMAN	Putative deoxyribose-phosphate aldolase	113
357	RL27_HUMAN	60S ribosomal protein L27	112
358	RS17_HUMAN	40S ribosomal protein S17	111
359	REEP6_HUMAN	Receptor expression-enhancing protein 6	111
360	GPSN2_HUMAN	Synaptic glycoprotein SC2	110
361	RDH11_HUMAN	Retinol dehydrogenase 11	110
362	NDUS2_HUMAN	NADH dehydrogenase [ubiquinone] iron-sulfur protein 2, mitochondrial precursor	108
363	TMOD3_HUMAN	Tropomodulin-3	108
364	COX5B_HUMAN	Cytochrome c oxidase subunit 5B, mitochondrial precursor	107
365	TOLIP_HUMAN	Toll-interacting protein	107
366	PPIA_HUMAN	Peptidyl-prolyl cis-trans isomerase A	38
366	PPIB_HUMAN	Peptidyl-prolyl cis-trans isomerase B precursor	106
366	PPIC_HUMAN	Peptidyl-prolyl cis-trans isomerase C	38
366	PPIH_HUMAN	Peptidyl-prolyl cis-trans isomerase H	38
367	SYLC_HUMAN	Leucyl-tRNA synthetase, cytoplasmic	106
368	TCPA_HUMAN	T-complex protein 1 subunit alpha	105
369	RS25_HUMAN	40S ribosomal protein S25	105
370	CS60_HUMAN	Succinate dehydrogenase cytochrome b560 subunit, mitochondrial precursor	105
371	CP2A6_HUMAN	Cytochrome P450 2A6	105
371	CP2A13_HUMAN	Cytochrome P450 2A13	105
372	SYRC_HUMAN	Arginyl-tRNA synthetase, cytoplasmic	105
373	KAD3_HUMAN	GTP:AMP phosphotransferase mitochondrial	104
374	ODO1_HUMAN	2-oxoglutarate dehydrogenase E1 component, mitochondrial precursor	104
375	PSD11_HUMAN	26S proteasome non-ATPase regulatory subunit 11	104
376	LMNA_HUMAN	Lamin-A/C	104
377	ODO2_HUMAN	Dihydropyridyllysine-residue succinyltransferase component of 2-oxoglutarate dehydrogenase complex, mitochondrial precursor	103
378	HGD_HUMAN	Homogentisate 1,2-dioxygenase	103
379	ACDSB_HUMAN	Short/branched chain specific acyl-CoA dehydrogenase, mitochondrial precursor	103
380	LMAN1_HUMAN	Protein ERGIC-53 precursor	102
381	CB047_HUMAN	Uncharacterized protein C2orf47, mitochondrial precursor	101
382	NDUS4_HUMAN	NADH dehydrogenase [ubiquinone] iron-sulfur protein 4, mitochondrial precursor	101
383	IDHP_HUMAN	Isocitrate dehydrogenase [NADP], mitochondrial precursor	101
384	ODPB_HUMAN	Pyruvate dehydrogenase E1 component subunit beta, mitochondrial precursor	100
385	ANXA7_HUMAN	Annexin A7	100
386	SEC63_HUMAN	Translocation protein SEC63 homolog	99
387	ILF2_HUMAN	Interleukin enhancer-binding factor 2	99
388	ERLN1_HUMAN	Erlin-1 precursor	24
388	ERLN2_HUMAN	Erlin-2 precursor	99
389	COX6C_HUMAN	Cytochrome c oxidase polypeptide VIc precursor	98
390	PRDX1_HUMAN	Peroxiredoxin-1	97
391	PRKDC_HUMAN	DNA-dependent protein kinase catalytic subunit	97
392	CD81_HUMAN	CD81 antigen	97
393	RL24_HUMAN	60S ribosomal protein L24	97
394	MOSC2_HUMAN	MOSC domain-containing protein 2, mitochondrial precursor	96
395	HPT_HUMAN	Haptoglobin precursor [Contains: Haptoglobin alpha chain; Haptoglobin beta chain]	96
396	KAD2_HUMAN	Adenylate kinase isoenzyme 2, mitochondrial	95
397	NDUAD_HUMAN	NADH dehydrogenase [ubiquinone] 1 alpha subcomplex subunit 13	95
398	F16P1_HUMAN	Fructose-1,6-bisphosphatase 1	95
399	QOR_HUMAN	Quinone oxidoreductase	94
400	RL30_HUMAN	60S ribosomal protein L30	94
401	TCPG_HUMAN	T-complex protein 1 subunit gamma	94
402	GCS1_HUMAN	Mannosyl-oligosaccharide glucosidase	93
403	NDUA6_HUMAN	NADH dehydrogenase [ubiquinone] 1 alpha subcomplex subunit 6	92
404	AL1B1_HUMAN	Aldehyde dehydrogenase X, mitochondrial precursor	92
405	PTBP1_HUMAN	Polypyrimidine tract-binding protein 1	92
406	NB5R1_HUMAN	NADH-cytochrome b5 reductase 1	91
407	FMO5_HUMAN	Dimethylaniline monooxygenase [N-oxide-forming] 5	91
408	ITAV_HUMAN	Integrin alpha-V precursor	91

Sample 1 proteins identified by nLC-MS using MASCOT and the launch peaks to mascot export function			
Number	SwissProt accession	Protein name	Protein score
409	ENOA_HUMAN	Alpha-enolase	91
409	ENOB_HUMAN	Beta-enolase	91
409	ENOG_HUMAN	Gamma-enolase	91
410	SPEB_HUMAN	Agmatinase, mitochondrial precursor	91
411	GTR2_HUMAN	Solute carrier family 2, facilitated glucose transporter member 2	90
412	NDUA8_HUMAN	NADH dehydrogenase [ubiquinone] 1 alpha subcomplex subunit 8	90
413	RS10_HUMAN	40S ribosomal protein S10	90
414	KU70_HUMAN	ATP-dependent DNA helicase 2 subunit 1	90
415	HCDH_HUMAN	Hydroxyacyl-coenzyme A dehydrogenase, mitochondrial precursor	90
416	MCAT_HUMAN	Mitochondrial carnitine/acylcarnitine carrier protein	89
417	TIM13_HUMAN	Mitochondrial import inner membrane translocase subunit tim13	89
418	ODB2_HUMAN	Lipoamide acyltransferase component of branched-chain alpha-keto acid dehydrogenase complex, mitochondrial precursor	89
419	COX1_HUMAN	Cytochrome c oxidase subunit 1	88
420	SDHL_HUMAN	L-serine dehydratase	88
421	PGM1_HUMAN	Phosphoglucomutase-1	88
422	TXND4_HUMAN	Thioredoxin domain-containing protein 4 precursor	88
423	RS13_HUMAN	40S ribosomal protein S13	88
424	AL1A1_HUMAN	Retinal dehydrogenase 1	87
425	HCD2_HUMAN	3-hydroxyacyl-CoA dehydrogenase type-2	87
426	ILF3_HUMAN	Interleukin enhancer-binding factor 3	86
427	ATLA3_HUMAN	Atlastin-3	86
428	SSRD_HUMAN	Translocon-associated protein subunit delta precursor	85
429	RL10_HUMAN	60S ribosomal protein L10	84
429	RL10L_HUMAN	60S ribosomal protein L10-like	45
430	EHD1_HUMAN	EH domain-containing protein 1	55
430	EHD2_HUMAN	EH domain-containing protein 2	53
430	EHD3_HUMAN	EH domain-containing protein 3	55
430	EHD4_HUMAN	EH domain-containing protein 4	84
431	APOB_HUMAN	Apolipoprotein B-100 precursor	82
432	CX7A2_HUMAN	Cytochrome c oxidase polypeptide VIa-liver/heart, mitochondrial precursor	82
433	LACTB_HUMAN	Serine beta-lactamase-like protein LACTB, mitochondrial precursor	81
434	C1QB_HUMAN	Complement component 1 Q subcomponent-binding protein, mitochondrial precursor	80
435	PCCA_HUMAN	Propionyl-CoA carboxylase alpha chain, mitochondrial precursor	79
436	TRAP1_HUMAN	Heat shock protein 75 kDa, mitochondrial precursor	79
437	DLDH_HUMAN	Dihydrolipoyl dehydrogenase, mitochondrial precursor	79
438	PSD12_HUMAN	26S proteasome non-ATPase regulatory subunit 12	77
439	ATPK_HUMAN	ATP synthase subunit f, mitochondrial	77
440	MGLL_HUMAN	Monoglyceride lipase	77
441	EIF3F_HUMAN	Eukaryotic translation initiation factor 3 subunit F	77
442	PDC6L_HUMAN	Programmed cell death 6-interacting protein	77
443	DHC24_HUMAN	24-dehydrocholesterol reductase precursor	75
444	DHRS1_HUMAN	Dehydrogenase/reductase SDR family member 1	75
445	PRS4_HUMAN	26S protease regulatory subunit 4	75
446	NIPS1_HUMAN	Protein NipSnap1	74
446	NIPS2_HUMAN	Protein NipSnap2	43
447	CAZA1_HUMAN	F-actin-capping protein subunit alpha-1	74
448	HMOX1_HUMAN	Heme oxygenase 1	73
449	IF5A1_HUMAN	Eukaryotic translation initiation factor 5A-1	73
449	IF5A2_HUMAN	Eukaryotic translation initiation factor 5A-2	73
450	LYAG_HUMAN	Lysosomal alpha-glucosidase precursor	73
451	DHRS7_HUMAN	Dehydrogenase/reductase SDR family member 7 precursor	73
452	ORNT1_HUMAN	Mitochondrial ornithine transporter 1	72
453	AATM_HUMAN	Aspartate aminotransferase, mitochondrial precursor	71
454	RRBP1_HUMAN	Ribosome-binding protein 1	71
455	GLYAT_HUMAN	Glycine N-acyltransferase	71
456	MEIK1_HUMAN	S-adenosylmethionine synthetase isoform type-1	71
457	ECH1_HUMAN	Delta(3,5)-Delta(2,4)-dienoyl-CoA isomerase, mitochondrial precursor	71
458	UCRL_HUMAN	Cytochrome b-c1 complex subunit Rieske, mitochondrial precursor	71
459	TR125_HUMAN	Tripartite motif-containing protein 25	70
460	EZIG5_HUMAN	E2-induced gene 5 protein	69
461	RL37_HUMAN	60S ribosomal protein L37	68
462	CHDH_HUMAN	Choline dehydrogenase, mitochondrial precursor	67
463	COPB_HUMAN	Coatamer subunit beta	66
464	LYRIC_HUMAN	Protein LYRIC	66
465	PABP1_HUMAN	Polyadenylate-binding protein 1	66
465	PABP4_HUMAN	Polyadenylate-binding protein 4	66
466	EF1U_HUMAN	Elongation factor 1u, mitochondrial precursor	66
467	PTIG_HUMAN	Pituitary tumor-transforming gene 1 protein-interacting protein precursor	65
468	AP1B1_HUMAN	AP-1 complex subunit beta-1	65
469	PCYOX_HUMAN	Prenylcysteine oxidase 1 precursor	65
470	THIM_HUMAN	3-ketoacyl-CoA thiolase, mitochondrial	65
471	RL34_HUMAN	60S ribosomal protein L34	65
472	TYPH_HUMAN	Thymidine phosphorylase precursor	65
473	ADO_HUMAN	Aldehyde oxidase	65
474	AFAD_HUMAN	Afadin	65
475	STIA1_HUMAN	Sulfotransferase 1A1	65
475	STIA2_HUMAN	Sulfotransferase 1A2	65
476	NDUB8_HUMAN	NADH dehydrogenase [ubiquinone] 1 beta subcomplex subunit 8, mitochondrial precursor	64
477	PRDX4_HUMAN	Peroxiredoxin-4	64
478	CATB_HUMAN	Cathepsin B precursor	64
479	ASPH_HUMAN	Aspartyl/asparaginyl beta-hydroxylase	64
480	RS15_HUMAN	40S ribosomal protein S15	63
481	SPYA_HUMAN	Serine-pyruvate aminotransferase	63
482	CO4A_HUMAN	Complement C4-A precursor	62
482	CO4B_HUMAN	Complement C4-B precursor	62
483	VATA_HUMAN	Vacuolar ATP synthase catalytic subunit A	62
484	GYS2_HUMAN	Glycogen [starch] synthase, liver	62
485	A16A1_HUMAN	Aldehyde dehydrogenase family 16 member A1	62
486	RS16_HUMAN	40S ribosomal protein S16	62
487	FKB11_HUMAN	FK506-binding protein 11 precursor	62
488	NOMO1_HUMAN	Nodal modulator 1 precursor	61
488	NOMO2_HUMAN	Nodal modulator 2 precursor	61
488	NOMO3_HUMAN	Nodal modulator 3 precursor	61

Sample 1 proteins identified by nLC-MS using MASCOT and the launch peaks to mascot export function			
Number	SwissProt accession	Protein name	Protein score
489	CHD9_HUMAN	Chromodomain-helicase-DNA-binding protein 9	61
490	NDUA4_HUMAN	NADH dehydrogenase [ubiquinone] 1 alpha subcomplex subunit 4	61
491	H10_HUMAN	Histone H1.0	61
492	SYIC_HUMAN	Isoleucyl-tRNA synthetase, cytoplasmic	60
493	SC22B_HUMAN	Vesicle-trafficking protein SEC22b	60
494	HMDH_HUMAN	3-hydroxy-3-methylglutaryl-coenzyme A reductase	60
495	MMSA_HUMAN	Methylmalonate-semialdehyde dehydrogenase [acylating], mitochondrial precursor	59
496	CP4AB_HUMAN	Cytochrome P450 4A11 precursor	59
497	MIRO1_HUMAN	Mitochondrial Rho GTPase 1	59
498	EIF3A_HUMAN	Eukaryotic translation initiation factor 3 subunit A	59
499	APMAP_HUMAN	Adipocyte plasma membrane-associated protein	59
500	GSTM4_HUMAN	Glutathione S-transferase Mu 4	59
501	CCD56_HUMAN	Coiled-coil domain-containing protein 56	59
502	VNN1_HUMAN	Pantetheinase precursor	59
503	AFG31_HUMAN	Putative AFG3-like protein 1	27
503	AFG32_HUMAN	AFG3-like protein 2	59
504	AP2B1_HUMAN	AP-2 complex subunit beta-1	58
505	CPT1A_HUMAN	Carnitine O-palmitoyltransferase 1, liver isoform	57
506	BZW1_HUMAN	Basic leucine zipper and WZ domain-containing protein 1	57
506	BZW2_HUMAN	Basic leucine zipper and WZ domain-containing protein 2	57
507	PRAF3_HUMAN	PRA1 family protein 3	56
508	CP3A4_HUMAN	Cytochrome P450 3A4	56
508	CP3A5_HUMAN	Cytochrome P450 3A5	56
508	CP3A7_HUMAN	Cytochrome P450 3A7	56
509	SNX1_HUMAN	Sorting nexin-1	56
509	SNX2_HUMAN	Sorting nexin-2	56
510	SPTA2_HUMAN	Spectrin alpha chain, brain	56
511	SC31A_HUMAN	Protein transport protein Sec31A	56
512	SC23A_HUMAN	Protein transport protein Sec23A	56
512	SC23B_HUMAN	Protein transport protein Sec23B	56
513	IF4E_HUMAN	Eukaryotic translation initiation factor 4E	55
514	SEPT2_HUMAN	Septin-2	55
515	RL22_HUMAN	60S ribosomal protein L22	55
516	FBXL7_HUMAN	F-box/LRR-repeat protein 7	55
517	ZN207_HUMAN	Zinc finger protein 207	55
518	EF1D_HUMAN	Elongation factor 1-delta	55
519	APOO_HUMAN	Apolipoprotein O precursor	55
520	COMT_HUMAN	Catechol O-methyltransferase	54
521	EIF3B_HUMAN	Eukaryotic translation initiation factor 3 subunit B	54
522	VIGLN_HUMAN	Vigilin	54
523	SRP54_HUMAN	Signal recognition particle 54 kDa protein	54
524	RL8_HUMAN	60S ribosomal protein L8	54
525	COA2_HUMAN (ACACB_HUMAN expasy) IREB1_HUMAN (ACOC_HUMAN expasy)	Acetyl-CoA carboxylase 2	54
526	IREB1_HUMAN (ACOC_HUMAN expasy)	Iron-responsive element-binding protein 1	54
527	ATP5L_HUMAN	ATP synthase subunit e, mitochondrial	53
528	IDHC_HUMAN	Isocitrate dehydrogenase [NADP] cytoplasmic	53
529	TF1B_HUMAN	Transcription intermediary factor 1-beta	53
530	CP27A_HUMAN	Cytochrome P450 27, mitochondrial precursor	52
531	RAB2A_HUMAN	Ras-related protein Rab-2A	51
532	ICPH_HUMAN	T-complex protein 1 subunit eta	51
533	HSP74_HUMAN	Heat shock 70 kDa protein 4	51
534	ITB1_HUMAN	Integrin beta-1 precursor	51
535	RSMB_HUMAN	Small nuclear ribonucleoprotein-associated proteins B and B=	51
535	RSMN_HUMAN	Small nuclear ribonucleoprotein-associated protein N	51
536	EIF3L_HUMAN	Eukaryotic translation initiation factor 3 subunit l	50
537	ECM29_HUMAN	Proteasome-associated protein ECM29 homolog	50
538	NDK3_HUMAN	Nucleoside diphosphate kinase 3	50
539	BGLR_HUMAN	Beta-glucuronidase precursor	50
540	NDUB6_HUMAN	NADH dehydrogenase [ubiquinone] 1 beta subcomplex subunit 6	49
541	LIPB2_HUMAN	Liprin-beta-2	49
542	TM167_HUMAN	Transmembrane protein 167 precursor	49
543	DDX1_HUMAN	ATP-dependent RNA helicase DDX1	49
544	ICPZ_HUMAN	T-complex protein 1 subunit zeta	49
545	EIF3C_HUMAN	Eukaryotic translation initiation factor 3 subunit C	49
546	CTNB1_HUMAN	Catenin beta-1	45
546	PLAK_HUMAN	junction plakoglobin	48
547	PRP8_HUMAN	Pre-mRNA-processing-splicing factor 8	48
548	GBLP_HUMAN	Guanine nucleotide-binding protein subunit beta-2-like 1	47
549	RS8_HUMAN	40S ribosomal protein S8	47
550	NDUA5_HUMAN	NADH dehydrogenase [ubiquinone] 1 alpha subcomplex subunit 5	47
551	AK1C1_HUMAN	Aldo-keto reductase family 1 member C1	46
551	AK1C2_HUMAN	Aldo-keto reductase family 1 member C2	46
551	AK1C3_HUMAN	Aldo-keto reductase family 1 member C3	46
551	AK1C4_HUMAN	Aldo-keto reductase family 1 member C4	46
552	BR44_HUMAN	Brain protein 44	46
553	SCR2B_HUMAN	Lysosome membrane protein 2	46
554	CFTR_HUMAN	Cystic fibrosis transmembrane conductance regulator	46
554	PLK2_HUMAN	Serine/threonine-protein kinase PLK2	46
555	RL35A_HUMAN	60S ribosomal protein L35a	45
556	PRS6B_HUMAN	26S protease regulatory subunit 6B	45
557	A1AG1_HUMAN	Alpha-1-acid glycoprotein 1 precursor	45
558	ECHD2_HUMAN	Enoyl-CoA hydratase domain-containing protein 2, mitochondrial precursor	45
559	GHC1_HUMAN	Mitochondrial glutamate carrier 1	44
560	IMM56_HUMAN	Transmembrane protein 56	44
561	AHSA1_HUMAN	Activator of 90 kDa heat shock protein ATPase homolog 1	44
562	CAH12_HUMAN	Carbonic anhydrase 12 precursor	43
563	WBP2_HUMAN	WW domain-binding protein 2	43
564	STAT1_HUMAN	Signal transducer and activator of transcription 1-alpha/beta	43
565	TNPO1_HUMAN	Transportin-1	43
565	TNPO2_HUMAN	Transportin-2	30
566	PGES2_HUMAN	Prostaglandin E synthase 2	43
567	STIM1_HUMAN	Stromal interaction molecule 1 precursor	43

Sample 1 proteins identified by nLC-MS using MASCOT and the launch peaks to mascot export function			
Number	SwissProt accession	Protein name	Protein score
568	STRAP_HUMAN	Serine-threonine kinase receptor-associated protein	43
569	ICPD_HUMAN	T-complex protein 1 subunit delta	43
570	DRG1_HUMAN	Developmentally-regulated GTP-binding protein 1	43
571	HMGCL_HUMAN	Hydroxymethylglutaryl-CoA lyase, mitochondrial precursor	43
572	NSF_HUMAN	Vesicle-fusing ATPase	43
573	PRS8_HUMAN	26S protease regulatory subunit 8	42
574	ACSA_HUMAN	Acyl-coenzyme A synthetase ACSMZA, mitochondrial precursor	42
574	ACS2B_HUMAN	Acyl-coenzyme A synthetase ACSM2B, mitochondrial precursor	42
575	AL7A1_HUMAN	Alpha-aminoadipic semialdehyde dehydrogenase	42
576	4F2_HUMAN	4F2 cell-surface antigen heavy chain	42
577	THIK_HUMAN	3-ketoacyl-CoA thiolase, peroxisomal precursor	42
578	SCPDH_HUMAN	Probable saccharopine dehydrogenase	42
579	SYS5C_HUMAN	Seryl-tRNA synthetase, cytoplasmic	41
580	MCA1_HUMAN	Multisynthetase complex auxiliary component p43 [Contains: Endothelial monocyte-activating polypeptide 2	41
581	OPA3_HUMAN	Optic atrophy 3 protein	41
582	DHSB_HUMAN	Succinate dehydrogenase [ubiquinone] iron-sulfur subunit, mitochondrial precursor	41
583	ATP8_HUMAN	ATP synthase protein 8	41
584	H14_HUMAN	Histone H1.4	40
585	RS11_HUMAN	40S ribosomal protein S11	40
586	RL7_HUMAN	60S ribosomal protein L7	39
587	CEPT1_HUMAN	Choline/ethanolaminephosphotransferase 1	39
588	TIM14_HUMAN	Mitochondrial import inner membrane translocase subunit TIM14	39
589	MIA40_HUMAN	Mitochondrial intermembrane space import and assembly protein 40	38
590	HNRGT_HUMAN	RNA-binding motif protein, X-linked-like-2	38
590	HNRPG_HUMAN	Heterogeneous nuclear ribonucleoprotein G	38
591	TIM44_HUMAN	Import inner membrane translocase subunit TIM44, mitochondrial precursor	38
592	IF2G_HUMAN	Eukaryotic translation initiation factor 2 subunit 3	38
593	GEPH_HUMAN	Gephyrin	38
594	RLA1_HUMAN	60S acidic ribosomal protein P1	37
595	CBPM_HUMAN	Carboxypeptidase M precursor	37
596	PDIA4_HUMAN	Protein disulfide-isomerase A4 precursor	37
597	COPB2_HUMAN	Coatomer subunit beta=	37
598	RRAS2_HUMAN	Ras-related protein R-Ras2 precursor	37
599	PRDX5_HUMAN	Peroxiredoxin-5, mitochondrial precursor	37
600	BAAT_HUMAN	Bile acid-CoA:amino acid N-acyltransferase	37
601	IF2B_HUMAN	Eukaryotic translation initiation factor 2 subunit 2	37
602	S28A1_HUMAN	Sodium/nucleoside cotransporter 1	37
603	PYR5_HUMAN	Uridine 5'-monophosphate synthase	37
604	SNX3_HUMAN	Sorting nexin-3	37
605	EIF3E_HUMAN	Eukaryotic translation initiation factor 3 subunit E	37
606	ANXA2_HUMAN	Annexin A2	37
607	HIP1R_HUMAN	Huntingtin-interacting protein 1-related protein	37
608	NDUS5_HUMAN	NADH dehydrogenase [ubiquinone] iron-sulfur protein 5	37
609	NDUV2_HUMAN	NADH dehydrogenase [ubiquinone] flavoprotein 2, mitochondrial precursor	36
610	K0774_HUMAN	Uncharacterized protein KIAA0774	36
611	AK1BA_HUMAN	Aldo-keto reductase family 1 member B10	36
612	CHP1_HUMAN	Calcium-binding protein p22	36
613	ATD3A_HUMAN	ATPase family AAA domain-containing protein 3A	35
613	ATD3C_HUMAN	ATPase family AAA domain-containing protein 3C	35
614	CE033_HUMAN	UPF0465 protein C5orf33	35
615	COX5A_HUMAN	Cytochrome c oxidase subunit 5A, mitochondrial precursor	35
616	BGAL_HUMAN	Beta-galactosidase precursor	35
617	RAP1A_HUMAN	Ras-related protein Rap-1A precursor	35
617	RAP1B_HUMAN	Ras-related protein Rap-1b precursor	35
618	CPNE2_HUMAN	Copine-2	33
618	CPNE3_HUMAN	Copine-3	33
618	CPNE4_HUMAN	Copine-4	33
618	CPNE5_HUMAN	Copine-5	33
618	CPNE6_HUMAN	Copine-6	33
618	CPNE7_HUMAN	Copine-7	33
618	CPNE8_HUMAN	Copine-8	33
619	INF2_HUMAN	Inverted formin-2	35
620	IF3E1_HUMAN	Eukaryotic translation initiation factor 3 subunit E-interacting protein	35
621	ODBB_HUMAN	2-oxoisovalerate dehydrogenase subunit beta, mitochondrial precursor	35
622	C144A_HUMAN	Coiled-coil domain-containing protein 144A	35
623	ATRX_HUMAN	Transcriptional regulator ATRX	34
624	B2MG_HUMAN	Beta-2-microglobulin precursor [Contains: Beta-2-microglobulin form pl 5.3]	34
625	ERAP2_HUMAN	Endoplasmic reticulum aminopeptidase 2	34
626	LAMP2_HUMAN	Lysosome-associated membrane glycoprotein 2 precursor	34
627	APOOL_HUMAN	Apolipoprotein O-like precursor	34
628	ALG5_HUMAN	Dolichyl-phosphate beta-glucosyltransferase	34
629	PXMP2_HUMAN	Peroxisomal membrane protein 2	34
630	GLRX3_HUMAN	Glutaredoxin-3	34
631	PPAL_HUMAN	Lysosomal acid phosphatase precursor	34
632	PGRC1_HUMAN	Membrane-associated progesterone receptor component 1	33
633	CPIA2_HUMAN	Cytochrome P450 1A2	33
634	RS26_HUMAN	40S ribosomal protein S26	33
634	RS26L_HUMAN	40S ribosomal protein S26-like 1	33
635	ACE_HUMAN	APOBEC1 complementation factor	33
635	RBM46_HUMAN	Probable RNA-binding protein 46	33
635	RBM47_HUMAN	RNA-binding protein 47	33
636	SDF2L_HUMAN	Stromal cell-derived factor 2-like protein 1 precursor	33
637	RS14_HUMAN	40S ribosomal protein S14	33
638	PON2_HUMAN	Serum paraoxonase/arylesterase 2	33
639	MRP3_HUMAN	Canalicular multispecific organic anion transporter 2	33
640	ALBU_HUMAN	Serum albumin precursor	33
641	GHC2_HUMAN	Mitochondrial glutamate carrier 2	33
642	APOA2_HUMAN	Apolipoprotein A-II precursor	32
643	STML2_HUMAN	Stomatin-like protein 2	32
644	KIF5C_HUMAN	Kinesin heavy chain isoform 5C	32
645	NDUAA_HUMAN	NADH dehydrogenase [ubiquinone] 1 alpha subcomplex subunit 10, mitochondrial precursor	32

Sample 1 proteins identified by nLC-MS using MASCOT and the launch peaks to mascot export function			
Number	SwissProt accession	Protein name	Protein score
646	CO3_HUMAN	Complement C3 precursor [Contains: Complement C3 beta chain; Complement C3 alpha chain; C3a anaphylatoxin; Complement C3b alpha- chain; Complement C3c alpha- chain fragment 1; Complement C3dg fragment; Complemen...	32
647	1433B_HUMAN	14-3-3 protein beta/alpha	32
647	1433F_HUMAN	14-3-3 protein eta	32
647	1433G_HUMAN	14-3-3 protein gamma	32
647	1433S_HUMAN	14-3-3 protein sigma	32
647	1433T_HUMAN	14-3-3 protein theta	32
647	1433Z_HUMAN	14-3-3 protein zeta/delta	32
648	ACOX1_HUMAN	Acyl-coenzyme A oxidase 1, peroxisomal	32
649	ASH2L_HUMAN	Set1/Ash2 histone methyltransferase complex subunit ASH2	32
650	ARF6_HUMAN	ADP-ribosylation factor 6	32
651	NDUAB_HUMAN	NADH dehydrogenase [ubiquinone] 1 alpha subcomplex subunit 11	32
652	CHCH3_HUMAN	Coiled-coil-helix-coiled-coil-helix domain-containing protein 3, mitochondrial precursor	31
653	GDC1_HUMAN	Grave disease carrier protein	31
654	PDXD1_HUMAN	Pyridoxal-dependent decarboxylase domain-containing protein 1	31
654	PDXD2_HUMAN	Pyridoxal-dependent decarboxylase domain-containing protein 2	31
655	RL23A_HUMAN	60S ribosomal protein L23a	31
656	ANX11_HUMAN	Annexin A11	31
657	IC1_HUMAN	Plasma protease C1 inhibitor precursor	31
658	MOSC1_HUMAN	MOSC domain-containing protein 1, mitochondrial precursor	30
659	PTH2_HUMAN	Peptidyl-tRNA hydrolase 2, mitochondrial precursor	30
660	SC5A1_HUMAN	Sodium/glucose cotransporter 1	30
660	SC5A4_HUMAN	Low affinity sodium-glucose cotransporter	30
661	TM9S2_HUMAN	Transmembrane 9 superfamily member 2 precursor	30
662	OCAD1_HUMAN	OCIA domain-containing protein 1	30
663	DERL1_HUMAN	Derlin-1	30
664	KHDR1_HUMAN	KH domain-containing, RNA-binding, signal transduction-associated protein 1	30
664	KHDR2_HUMAN	KH domain-containing, RNA-binding, signal transduction-associated protein 2	30
664	KHDR3_HUMAN	KH domain-containing, RNA-binding, signal transduction-associated protein 3	30
665	BID_HUMAN	BH3-interacting domain death agonist	30
666	MET10_HUMAN	Putative methyltransferase MET10D	30
667	EMAL4_HUMAN	Echinoderm microtubule-associated protein-like 4	30
668	RM17_HUMAN	39S ribosomal protein L17, mitochondrial precursor	30
669	HIG1A_HUMAN	HIG1 domain family member 1A	30
670	CP2C9_HUMAN	Cytochrome P450 2C9	29
671	PSMD3_HUMAN	26S proteasome non-ATPase regulatory subunit 3	29
672	LEIM1_HUMAN	Leucine zipper-EF-hand-containing transmembrane protein 1, mitochondrial precursor	29
673	FA98A_HUMAN	Protein FAM98A	29
674	SSRG_HUMAN	Translocon-associated protein subunit gamma	29
675	KCY_HUMAN	UMP-CMP kinase	29
676	RRAGA_HUMAN	Ras-related GTP-binding protein A	29
676	RRAGB_HUMAN	Ras-related GTP-binding protein B	29
677	DEN4C_HUMAN	DENN domain-containing protein 4C	29
678	ATP5E_HUMAN	ATP synthase subunit epsilon, mitochondrial	29
679	MFN1_HUMAN	Mitofusin-1	29
679	MFN2_HUMAN	Mitofusin-2	29
680	DDA1_HUMAN	DET1- and DDB1-associated protein 1	29
681	NATI0_HUMAN	N-acetyltransferase 10	29
682	MYOF_HUMAN	Myoferlin	29
683	SF3B2_HUMAN	Splicing factor 3B subunit 2	28
684	CF066_HUMAN (HRP20_HUMAN expasy)	UPF0240 protein C6orf66	28
685	HNRPU_HUMAN	Heterogeneous nuclear ribonucleoprotein U	28
686	CS015_HUMAN	Uncharacterized protein C19orf15 precursor	28
687	RALA_HUMAN	Ras-related protein Ral-A precursor	28
687	RALB_HUMAN	Ras-related protein Ral-B precursor	28
688	NPIN_HUMAN	Neuroplastin precursor	28
689	SSRP1_HUMAN	FACT complex subunit SSRP1	27
690	GALK1_HUMAN	Galactokinase	27

Sample 2 proteins identified by nLC-MS using MASCOT and the launch peaks to mascot export function			
Number	SwissProt accession	Protein name	Protein score
1	CPSM_HUMAN	Carbamoyl-phosphate synthase [ammonial], mitochondrial precursor	3804
1	PYR1_HUMAN	CAD protein [Includes: Glutamine-dependent carbamoyl-phosphate synthase	142
2	TBA1B_HUMAN	Tubulin alpha-1B chain	2363
3	TBA1A_HUMAN	Tubulin alpha-1A chain	2172
3	TBA1C_HUMAN	Tubulin alpha-1C chain	2172
3	TBA3C_HUMAN	Tubulin alpha-3C/D chain	1886
3	TBA3E_HUMAN	Tubulin alpha-3E chain	1614
3	TBA8_HUMAN	Tubulin alpha-8 chain	1315
4	CH60_HUMAN	60 kDa heat shock protein, mitochondrial precursor	2048
5	TBA4A_HUMAN	Tubulin alpha-4A chain	2013
6	ACSL1_HUMAN	Long-chain-fatty-acid-CoA ligase 1	1825
7	ACTB_HUMAN	Actin, cytoplasmic 1	1822
7	ACTG_HUMAN	Actin, cytoplasmic 2	1822
7	ACTK_HUMAN	Kappa-actin	579
7	POTAC_HUMAN (A26CB_HUMAN - expasy)	Chimeric POIE-actin protein	715
8	ECHA_HUMAN	Trifunctional enzyme subunit alpha, mitochondrial precursor	1772
9	ATPB_HUMAN	ATP synthase subunit beta, mitochondrial precursor	1550
10	GFAP_HUMAN	Glial fibrillary acidic protein	63
10	K22O_HUMAN	Keratin, type II cytoskeletal 2 oral	83
10	K2C1B_HUMAN	Keratin, type II cytoskeletal 1b	48
10	K2C3_HUMAN	Keratin, type II cytoskeletal 3	83
10	K2C4_HUMAN	Keratin, type II cytoskeletal 4	48
10	K2C7_HUMAN	Keratin, type II cytoskeletal 7	83
10	K2C71_HUMAN	Keratin, type II cytoskeletal 71	48
10	K2C72_HUMAN	Keratin, type II cytoskeletal 72	48
10	K2C73_HUMAN	Keratin, type II cytoskeletal 73	48
10	K2C74_HUMAN	Keratin, type II cytoskeletal 74	48
10	K2C78_HUMAN	Keratin, type II cytoskeletal 78	63
10	K2C8_HUMAN	Keratin, type II cytoskeletal 8	1548
10	KRT1_HUMAN	Keratin type II cuticular Hb1	63
10	KRT83_HUMAN	Keratin type II cuticular Hb3	63
10	KRT84_HUMAN	Keratin type II cuticular Hb4	83
10	KRT85_HUMAN	Keratin type II cuticular Hb5	63
10	KRT86_HUMAN	Keratin type II cuticular Hb6	63
10	VIME_HUMAN	Vimentin	63
11	GDE_HUMAN	Glycogen debranching enzyme	1536
12	FMO3_HUMAN	Dimethylaniline monooxygenase [N-oxide-forming] 3	1419
13	TBB1_HUMAN	Tubulin beta-1 chain	89
13	TBB5_HUMAN	Tubulin beta chain	1402
14	ATPA_HUMAN	ATP synthase subunit alpha, mitochondrial precursor	1364
15	TBB2A_HUMAN	Tubulin beta-2A chain	1309
15	TBB2B_HUMAN	Tubulin beta-2B chain	1309
16	ACTN3_HUMAN	Alpha-actinin-3	365
16	ACTN4_HUMAN	Alpha-actinin-4	1258
17	TBB2C_HUMAN	Tubulin beta-2C chain	1256
17	TBB4Q_HUMAN	Tubulin beta-4q chain	234
18	NNIM_HUMAN	NAD(P) transhydrogenase, mitochondrial precursor	1219
19	ENPL_HUMAN	Endoplasmic precursor	1150
20	FTHD_HUMAN	10-formyltetrahydrofolate dehydrogenase	1104
21	MYH10_HUMAN	Myosin-10	74
21	MYH11_HUMAN	Myosin-11	208
21	MYH9_HUMAN	Myosin-9	1104
22	AOFA_HUMAN	Amine oxidase [flavin-containing] A	1048
23	CMC2_HUMAN	Calcium-binding mitochondrial carrier protein Aralar2	1023
24	ACTA_HUMAN	Actin, aortic smooth muscle	978
24	ACTC_HUMAN	Actin, alpha cardiac muscle 1	1001
24	ACTH_HUMAN	Actin, gamma-enteric smooth muscle	978
24	ACTS_HUMAN	Actin, alpha skeletal muscle	1001
25	UGPA_HUMAN	UTP-glucose-1-phosphate uridylyltransferase	972
26	HMCS2_HUMAN	Hydroxymethylglutaryl-CoA synthase, mitochondrial precursor	961
27	K1C18_HUMAN	Keratin, type I cytoskeletal 18	947
27	K1C19_HUMAN	Keratin, type I cytoskeletal 19	89
28	CALX_HUMAN	Calnexin precursor	927
29	MET7A_HUMAN	Methyltransferase-like protein 7A precursor	895
30	ADT2_HUMAN	ADP/ATP translocase 2	881
30	ADT4_HUMAN	ADP/ATP translocase 4	33
31	FAS_HUMAN	Fatty acid synthase	804
32	IQGA1_HUMAN	Ras GTPase-activating-like protein IQGAP1	71
32	IQGA2_HUMAN	Ras GTPase-activating-like protein IQGAP2	802
32	IQGA3_HUMAN	Ras GTPase-activating-like protein IQGAP3	71
33	ADH1A_HUMAN	Alcohol dehydrogenase 1A	523
33	ADH1B_HUMAN	Alcohol dehydrogenase 1B	795
33	ADH1G_HUMAN	Alcohol dehydrogenase 1C	707
34	DHB4_HUMAN	Peroxisomal multifunctional enzyme type 2	791
35	FLNA_HUMAN	Filamin-A	64
35	FLNB_HUMAN	Filamin-B	783
36	CA161_HUMAN	Uncharacterized protein C1orf161	28
36	HVEP_HUMAN	Epoxide hydrolase 1	780
37	HS90B_HUMAN	Heat shock protein HSP 90-beta	756
38	UD11_HUMAN	UDP-glucuronosyltransferase 1-1 precursor	274
38	UD110_HUMAN	UDP-glucuronosyltransferase 1-10 precursor	274
38	UD14_HUMAN	UDP-glucuronosyltransferase 1-4 precursor	739
38	UD17_HUMAN	UDP-glucuronosyltransferase 1-7 precursor	274
38	UD18_HUMAN	UDP-glucuronosyltransferase 1-8 precursor	274
38	UD19_HUMAN	UDP-glucuronosyltransferase 1-9 precursor	274
39	AOFB_HUMAN	Amine oxidase [flavin-containing] B	737
40	HS90A_HUMAN	Heat shock protein HSP 90-alpha	725
41	NB5B3_HUMAN	NADH-cytochrome b5 reductase 3	710
42	UD2B7_HUMAN	UDP-glucuronosyltransferase 2B7 precursor	697

Sample 2 proteins identified by nLC-MS using MASCOT and the launch peaks to mascot export function			
Number	SwissProt accession	Protein name	Protein score
43	PYGL_HUMAN	Glycogen phosphorylase, liver form	679
43	PYGM_HUMAN	Glycogen phosphorylase, muscle form	63
44	QCR2_HUMAN	Cytochrome b-c1 complex subunit 2, mitochondrial precursor	678
45	ETFD_HUMAN	Electron transfer flavoprotein-ubiquinone oxidoreductase, mitochondrial precursor	677
46	AT12A_HUMAN	Potassium-transporting ATPase alpha chain 2	185
46	AT1A1_HUMAN	Sodium/potassium-transporting ATPase subunit alpha-1 precursor	667
46	AT1A2_HUMAN	Sodium/potassium-transporting ATPase subunit alpha-2 precursor	406
46	AT1A3_HUMAN	Sodium/potassium-transporting ATPase subunit alpha-3	490
46	AT1A4_HUMAN	Sodium/potassium-transporting ATPase subunit alpha-4	235
46	ATP4A_HUMAN	Potassium-transporting ATPase alpha chain 1	185
47	ACTN1_HUMAN	Alpha-actinin-1	666
48	GSTK1_HUMAN	Glutathione S-transferase kappa 1	654
49	RL3_HUMAN	60S ribosomal protein L3	635
49	RL3L_HUMAN	60S ribosomal protein L3-like	84
50	ECHB_HUMAN	Trifunctional enzyme subunit beta, mitochondrial precursor	628
51	ROA2_HUMAN	Heterogeneous nuclear ribonucleoproteins A2/B1	627
52	VDAC1_HUMAN	Voltage-dependent anion-selective channel protein 1	613
53	RL10A_HUMAN	60S ribosomal protein L10a	613
54	MVP_HUMAN	Major vault protein	603
55	ADH4_HUMAN	Alcohol dehydrogenase 4	600
56	ATPG_HUMAN	ATP synthase subunit gamma, mitochondrial precursor	598
57	AT5F1_HUMAN	ATP synthase subunit b, mitochondrial precursor	598
58	UDB10_HUMAN	UDP-glucuronosyltransferase 2B10 precursor	585
58	UDB11_HUMAN	UDP-glucuronosyltransferase 2B11 precursor	484
58	UDB28_HUMAN	UDP-glucuronosyltransferase 2B28 precursor	286
59	QCR1_HUMAN	Cytochrome b-c1 complex subunit 1, mitochondrial precursor	578
60	COX2_HUMAN	Cytochrome c oxidase subunit 2	551
61	PHB2_HUMAN	Prohibitin-2	522
62	RDH16_HUMAN	Retinol dehydrogenase 16	522
63	FTCD_HUMAN	Formimidoyltransferase-cyclodeaminase	519
64	EF1A1_HUMAN	Elongation factor 1-alpha 1	519
64	EF1A2_HUMAN	Elongation factor 1-alpha 2	246
65	UD2A1_HUMAN	UDP-glucuronosyltransferase 2A1 precursor	64
65	UD2B4_HUMAN	UDP-glucuronosyltransferase 2B4 precursor	516
66	NCPR_HUMAN	NADPH-cytochrome P450 reductase	508
67	1A02_HUMAN	HLA class I histocompatibility antigen, A-2 alpha chain precursor	504
67	1A23_HUMAN	HLA class I histocompatibility antigen, A-23 alpha chain precursor	228
67	1A24_HUMAN	HLA class I histocompatibility antigen, A-24 alpha chain precursor	228
67	1A68_HUMAN	HLA class I histocompatibility antigen, A-68 alpha chain precursor	338
67	1A69_HUMAN	HLA class I histocompatibility antigen, A-69 alpha chain	414
67	1B15_HUMAN	HLA class I histocompatibility antigen, B-15 alpha chain precursor	228
67	1B35_HUMAN	HLA class I histocompatibility antigen, B-35 alpha chain precursor	228
67	1B46_HUMAN	HLA class I histocompatibility antigen, B-46 alpha chain precursor	228
67	1B51_HUMAN	HLA class I histocompatibility antigen, B-51 alpha chain precursor	228
67	1B52_HUMAN	HLA class I histocompatibility antigen, B-52 alpha chain precursor	228
67	1B53_HUMAN	HLA class I histocompatibility antigen, B-53 alpha chain precursor	228
67	1B54_HUMAN	HLA class I histocompatibility antigen, B-54 alpha chain precursor	228
67	1B55_HUMAN	HLA class I histocompatibility antigen, B-55 alpha chain precursor	228
67	1B56_HUMAN	HLA class I histocompatibility antigen, B-56 alpha chain precursor	228
67	1B57_HUMAN	HLA class I histocompatibility antigen, B-57 alpha chain precursor	317
67	1B58_HUMAN	HLA class I histocompatibility antigen, B-58 alpha chain precursor	317
67	1B59_HUMAN	HLA class I histocompatibility antigen, B-59 alpha chain precursor	228
67	1B78_HUMAN	HLA class I histocompatibility antigen, B-78 alpha chain precursor	228
67	1C16_HUMAN	HLA class I histocompatibility antigen, Cw-16 alpha chain precursor	228
68	BDH_HUMAN	D-beta-hydroxybutyrate dehydrogenase, mitochondrial precursor	498
69	CYB5_HUMAN	Cytochrome b5	497
70	GRP78_HUMAN	78 kDa glucose-regulated protein precursor	492
71	PDIA6_HUMAN	Protein disulfide-isomerase A6 precursor	487
72	UD13_HUMAN	UDP-glucuronosyltransferase 1-3 precursor	483
72	UD15_HUMAN	UDP-glucuronosyltransferase 1-5 precursor	362
73	NDUS3_HUMAN	NADH dehydrogenase [ubiquinone] iron-sulfur protein 3, mitochondrial precursor	475
74	ADT1_HUMAN	ADP/ATP translocase 1	470
75	DHE3_HUMAN	Glutamate dehydrogenase 1, mitochondrial precursor	465
75	DHE4_HUMAN	Glutamate dehydrogenase 2, mitochondrial precursor	100
76	ADT3_HUMAN	ADP/ATP translocase 3	465
77	FIBA_HUMAN	Fibrinogen alpha chain precursor [Contains: Fibrinopeptide A]	464
78	RIB1_HUMAN (RPN1_HUMAN expsy)	Dolichyl-diphosphooligosaccharide--protein glycosyltransferase 67 kDa subunit precursor	463
79	ROA1_HUMAN	Heterogeneous nuclear ribonucleoprotein A1	460
80	SAA_HUMAN	Serum amyloid A protein precursor	460
80	SAA3_HUMAN	Putative serum amyloid A-3 protein	45
81	TMPSD_HUMAN	Transmembrane protease, serine 13	242
81	TRY1_HUMAN	Trypsin-1 precursor	455
82	CP2E1_HUMAN	Cytochrome P450 2E1	449
83	CLH1_HUMAN	Clathrin heavy chain 1	440
83	CLH2_HUMAN	Clathrin heavy chain 2	59
84	SQRD_HUMAN	Sulfide:quinone oxidoreductase, mitochondrial precursor	433
85	K2C1_HUMAN	Keratin, type II cytoskeletal 1	430
86	H2A1_HUMAN	Histone H2A type 1	420
86	H2A1A_HUMAN	Histone H2A type 1-A	160
86	H2A1B_HUMAN	Histone H2A type 1-B	420
86	H2A1C_HUMAN	Histone H2A type 1-C	420
86	H2A1D_HUMAN	Histone H2A type 1-D	420
86	H2A1E_HUMAN	Histone H2A type 1-E	420
86	H2A1H_HUMAN	Histone H2A type 1-H	420
86	H2A1J_HUMAN	Histone H2A type 1-J	420
86	H2A2A_HUMAN	Histone H2A type 2-A	420
86	H2A2B_HUMAN	Histone H2A type 2-B	84
86	H2A2C_HUMAN	Histone H2A type 2-C	420
86	H2A3_HUMAN	Histone H2A type 3	420
86	H2AV_HUMAN	Histone H2AV	160
86	H2AX_HUMAN	Histone H2A.x	160

Sample 2 proteins identified by nLC-MS using MASCOT and the launch peaks to mascot export function			
Number	SwissProt accession	Protein name	Protein score
86	H2AZ_HUMAN	Histone H2A.Z	160
87	RS4X_HUMAN	40S ribosomal protein S4, X isoform	412
87	RS4Y1_HUMAN	40S ribosomal protein S4, Y isoform 1	163
87	RS4Y2_HUMAN	40S ribosomal protein S4, Y isoform 2	83
88	ROA3_HUMAN	Heterogeneous nuclear ribonucleoprotein A3	409
89	AIPO_HUMAN	ATP synthase subunit O, mitochondrial precursor	408
90	ECHM_HUMAN	Enoyl-CoA hydratase, mitochondrial precursor	405
91	IF4A1_HUMAN	Eukaryotic initiation factor 4A-1	402
91	IF4A2_HUMAN	Eukaryotic initiation factor 4A-II	305
92	DECR_HUMAN	2,4-dienoyl-CoA reductase, mitochondrial precursor	398
93	ACADV_HUMAN	Very long-chain specific acyl-CoA dehydrogenase, mitochondrial precursor	398
94	PCBP1_HUMAN	Poly(rC)-binding protein 1	392
95	S27A2_HUMAN	Very long-chain acyl-CoA synthetase	388
96	MMP19_HUMAN	Matrix metalloproteinase-19 precursor	54
96	VINC_HUMAN	Vitronectin precursor	380
97	RS2_HUMAN	40S ribosomal protein S2	379
98	RIN4_HUMAN	Reticulon-4	378
99	CP4F2_HUMAN	Cytochrome P450 4F2	378
99	CP4F3_HUMAN	Cytochrome P450 4F3	312
99	CP4F8_HUMAN	Cytochrome P450 4F8	101
99	CP4FB_HUMAN	Cytochrome P450 4F11	86
99	CP4FC_HUMAN	Cytochrome P450 4F12	86
100	ALDH2_HUMAN	Aldehyde dehydrogenase, mitochondrial precursor	377
101	H17B6_HUMAN	Hydroxysteroid 17-beta dehydrogenase 6 precursor	376
102	RS3A_HUMAN	40S ribosomal protein S3a	373
103	RS5_HUMAN	40S ribosomal protein S5	372
104	CP2C9_HUMAN	Cytochrome P450 2C9	369
104	CP2CJ_HUMAN	Cytochrome P450 2C19	100
105	RL14_HUMAN	60S ribosomal protein L14	367
106	ACSL5_HUMAN	Long-chain-fatty-acid-CoA ligase 5	361
107	ATP5H_HUMAN	ATP synthase subunit d, mitochondrial	357
108	RS7_HUMAN	40S ribosomal protein S7	356
109	NUCL_HUMAN	Nucleolin	356
110	UDB15_HUMAN	UDP-glucuronosyltransferase 2B15 precursor	355
111	UD16_HUMAN	UDP-glucuronosyltransferase 1-6 precursor	348
112	COX41_HUMAN	Cytochrome c oxidase subunit 4 isoform 1, mitochondrial precursor	344
113	RL7A_HUMAN	60S ribosomal protein L7a	343
114	AIFM1_HUMAN	Apoptosis-inducing factor 1, mitochondrial precursor	332
115	KTN1_HUMAN	Kinectin	23
115	PRDX6_HUMAN	Peroxiredoxin-6	332
116	DHSA_HUMAN	Succinate dehydrogenase [ubiquinone] flavoprotein subunit, mitochondrial precursor	332
117	FMO5_HUMAN	Dimethylaniline monooxygenase [N-oxide-forming] 5	330
118	FRIH_HUMAN	Ferritin heavy chain	327
119	S27A5_HUMAN	Bile acyl-CoA synthetase	322
120	TMEDA_HUMAN	Transmembrane emp24 domain-containing protein 10 precursor	317
121	HNRPK_HUMAN	Heterogeneous nuclear ribonucleoprotein K	313
122	FIBG_HUMAN	Fibrinogen gamma chain precursor	310
123	MGST1_HUMAN	Microsomal glutathione S-transferase 1	305
124	RL6_HUMAN	60S ribosomal protein L6	303
125	RL19_HUMAN	60S ribosomal protein L19	300
126	RS3_HUMAN	40S ribosomal protein S3	300
127	H4_HUMAN	Histone H4	298
128	GSTA1_HUMAN	Glutathione S-transferase A1	297
128	GSTA2_HUMAN	Glutathione S-transferase A2	297
128	GSTA3_HUMAN	Glutathione S-transferase A3	255
128	GSTA5_HUMAN	Glutathione S-transferase A5	34
129	AL1A1_HUMAN	Retinal dehydrogenase 1	295
130	MOSC2_HUMAN	MOSC domain-containing protein 2, mitochondrial precursor	295
131	FRIL_HUMAN	Ferritin light chain	294
132	RL9_HUMAN	60S ribosomal protein L9	288
133	RL10_HUMAN	60S ribosomal protein L10	285
133	RL10L_HUMAN	60S ribosomal protein L10-like	98
134	RS6_HUMAN	40S ribosomal protein S6	281
135	UBIQ_HUMAN	Ubiquitin	280
136	AL3A2_HUMAN	Fatty aldehyde dehydrogenase	279
137	VNN1_HUMAN	Pantetheinase precursor	279
137	VNN3_HUMAN	Vascular non-inflammatory molecule 3 precursor	148
138	SPTB1_HUMAN	Spectrin beta chain, erythrocyte	45
138	SPTB2_HUMAN	Spectrin beta chain, brain 1	278
138	SPTB2_HUMAN	Spectrin beta chain, brain 2	45
138	SPTB2_HUMAN	Spectrin beta chain, brain 3	45
139	DHB11_HUMAN	Estradiol 17-beta-dehydrogenase 11 precursor	277
140	MCAT_HUMAN	Mitochondrial carnitine/acylcarnitine carrier protein	274
141	1A01_HUMAN	HLA class I histocompatibility antigen, A-1 alpha chain precursor	270
141	1A03_HUMAN	HLA class I histocompatibility antigen, A-3 alpha chain precursor	270
141	1A11_HUMAN	HLA class I histocompatibility antigen, A-11 alpha chain precursor	270
141	1A25_HUMAN	HLA class I histocompatibility antigen, A-25 alpha chain precursor	237
141	1A26_HUMAN	HLA class I histocompatibility antigen, A-26 alpha chain precursor	237
141	1A29_HUMAN	HLA class I histocompatibility antigen, A-29 alpha chain precursor	237
141	1A30_HUMAN	HLA class I histocompatibility antigen, A-30 alpha chain precursor	237
141	1A31_HUMAN	HLA class I histocompatibility antigen, A-31 alpha chain precursor	237
141	1A32_HUMAN	HLA class I histocompatibility antigen, A-32 alpha chain precursor	270
141	1A33_HUMAN	HLA class I histocompatibility antigen, A-33 alpha chain precursor	237
141	1A34_HUMAN	HLA class I histocompatibility antigen, A-34 alpha chain precursor	237
141	1A36_HUMAN	HLA class I histocompatibility antigen, A-36 alpha chain precursor	270
141	1A43_HUMAN	HLA class I histocompatibility antigen, A-43 alpha chain precursor	237
141	1A66_HUMAN	HLA class I histocompatibility antigen, A-66 alpha chain precursor	237
141	1A74_HUMAN	HLA class I histocompatibility antigen, A-74 alpha chain precursor	270
141	1A80_HUMAN	HLA class I histocompatibility antigen, A-80 alpha chain precursor	29
141	1B07_HUMAN	HLA class I histocompatibility antigen, B-7 alpha chain precursor	29
141	1B08_HUMAN	HLA class I histocompatibility antigen, B-8 alpha chain precursor	29
141	1B40_HUMAN	HLA class I histocompatibility antigen, B-40 alpha chain precursor	29
141	1B41_HUMAN	HLA class I histocompatibility antigen, B-41 alpha chain precursor	29

Sample 2 proteins identified by nLC-MS using MASCOT and the launch peaks to mascot export function			
Number	SwissProt accession	Protein name	Protein score
141	1B42_HUMAN	HLA class I histocompatibility antigen, B-42 alpha chain precursor	29
141	1B48_HUMAN	HLA class I histocompatibility antigen, B-48 alpha chain precursor	29
141	1B73_HUMAN	HLA class I histocompatibility antigen, B-73 alpha chain precursor	29
141	1B81_HUMAN	HLA class I histocompatibility antigen, B-81 alpha chain precursor	29
141	1C01_HUMAN	HLA class I histocompatibility antigen, Cw-1 alpha chain precursor	29
141	1C02_HUMAN	HLA class I histocompatibility antigen, Cw-2 alpha chain precursor	29
141	1C03_HUMAN	HLA class I histocompatibility antigen, Cw-3 alpha chain precursor	29
141	1C04_HUMAN	HLA class I histocompatibility antigen, Cw-4 alpha chain precursor	237
141	1C05_HUMAN	HLA class I histocompatibility antigen, Cw-5 alpha chain precursor	29
141	1C06_HUMAN	HLA class I histocompatibility antigen, Cw-6 alpha chain precursor	29
141	1C07_HUMAN	HLA class I histocompatibility antigen, Cw-7 alpha chain precursor	29
141	1C08_HUMAN	HLA class I histocompatibility antigen, Cw-8 alpha chain precursor	29
141	1C12_HUMAN	HLA class I histocompatibility antigen, Cw-12 alpha chain precursor	237
141	1C14_HUMAN	HLA class I histocompatibility antigen, Cw-14 alpha chain precursor	237
141	1C15_HUMAN	HLA class I histocompatibility antigen, Cw-15 alpha chain precursor	29
141	1C17_HUMAN	HLA class I histocompatibility antigen, Cw-17 alpha chain precursor	237
141	1C18_HUMAN	HLA class I histocompatibility antigen, Cw-18 alpha chain precursor	29
141	HLAH_HUMAN	HLA class I histocompatibility antigen, alpha chain H precursor	29
142	SSRA_HUMAN	Translocan-associated protein subunit alpha precursor	269
143	MCH2_HUMAN	Mitochondrial carrier homolog 2	266
144	TMED4_HUMAN	Transmembrane emp24 domain-containing protein 4 precursor	258
144	TMED9_HUMAN	Transmembrane emp24 domain-containing protein 9 precursor	266
145	ANXA6_HUMAN	Annexin A6	264
146	THTR_HUMAN	Thiosulfate sulfurtransferase	264
147	FIBB_HUMAN	Fibrinogen beta chain precursor [Contains: Fibrinopeptide B]	264
148	RL15_HUMAN	60S ribosomal protein L15	260
149	NDUA9_HUMAN	NADH dehydrogenase [ubiquinone] 1 alpha subcomplex subunit 9, mitochondrial precursor	259
150	EF1G_HUMAN	Elongation factor 1-gamma	258
151	RL23_HUMAN	60S ribosomal protein L23	253
152	RS9_HUMAN	40S ribosomal protein S9	246
153	RS13_HUMAN	40S ribosomal protein S13	243
154	K22E_HUMAN	Keratin, type II cytoskeletal 2 epidermal	239
155	EF2_HUMAN	Elongation factor 2	238
156	LMAN2_HUMAN	Vesicular integral-membrane protein VIP36 precursor	236
157	OST48_HUMAN	Dolichyl-diphosphooligosaccharide--protein glycosyltransferase 48 kDa subunit precursor	235
158	MPCP_HUMAN	Phosphate carrier protein, mitochondrial precursor	235
159	RL17_HUMAN	60S ribosomal protein L17	235
160	NDUV1_HUMAN	NADH dehydrogenase [ubiquinone] flavoprotein 1, mitochondrial precursor	234
161	APOC3_HUMAN	Apolipoprotein C-III precursor	233
162	PDIA1_HUMAN	Protein disulfide-isomerase precursor	233
163	CP3A4_HUMAN	Cytochrome P450 3A4	233
163	CP3A5_HUMAN	Cytochrome P450 3A5	63
163	CP3A7_HUMAN	Cytochrome P450 3A7	233
164	H2B1A_HUMAN	Histone H2B type 1-A	139
164	H2B1B_HUMAN	Histone H2B type 1-B	233
164	H2B1C_HUMAN	Histone H2B type 1-C/E/F/G/I	233
164	H2B1D_HUMAN	Histone H2B type 1-D	233
164	H2B1H_HUMAN	Histone H2B type 1-H	233
164	H2B1J_HUMAN	Histone H2B type 1-J	233
164	H2B1K_HUMAN	Histone H2B type 1-K	233
164	H2B1L_HUMAN	Histone H2B type 1-L	233
164	H2B1M_HUMAN	Histone H2B type 1-M	233
164	H2B1N_HUMAN	Histone H2B type 1-N	233
164	H2B1O_HUMAN	Histone H2B type 1-O	233
164	H2B2E_HUMAN	Histone H2B type 2-E	233
164	H2B2F_HUMAN	Histone H2B type 2-F	233
164	H2B3B_HUMAN	Histone H2B type 3-B	233
164	H2BFS_HUMAN	Histone H2B type F-S	233
165	NDU51_HUMAN	NADH-ubiquinone oxidoreductase 75 kDa subunit, mitochondrial precursor	230
166	PHB_HUMAN	Prohibitin	227
167	RL4_HUMAN	60S ribosomal protein L4	226
168	RL12_HUMAN	60S ribosomal protein L12	226
169	HSP72_HUMAN	Heat shock-related 70 kDa protein 2	43
169	HSP7C_HUMAN	Heat shock cognate 71 kDa protein	225
170	PSME1_HUMAN	Proteasome activator complex subunit 1	222
171	NDUAC_HUMAN	NADH dehydrogenase [ubiquinone] 1 alpha subcomplex subunit 12	217
172	AT1B1_HUMAN	Sodium/potassium-transporting ATPase subunit beta-1	217
173	RL24_HUMAN	60S ribosomal protein L24	216
174	BHMT1_HUMAN	Betaine--homocysteine S-methyltransferase 1	215
175	ALDOA_HUMAN	Fructose-bisphosphate aldolase A	73
175	ALDOB_HUMAN	Fructose-bisphosphate aldolase B	214
175	ALDOC_HUMAN	Fructose-bisphosphate aldolase C	88
176	RL27A_HUMAN	60S ribosomal protein L27a	213
177	APMAP_HUMAN	Adipocyte plasma membrane-associated protein	209
178	RRBP1_HUMAN	Ribosome-binding protein 1	208
179	RS24_HUMAN	40S ribosomal protein S24	205
180	PPCKM_HUMAN	Phosphoenolpyruvate carboxykinase [GTP], mitochondrial precursor	204
181	GRP75_HUMAN	Stress-70 protein, mitochondrial precursor	204
182	RLA1_HUMAN	60S acidic ribosomal protein P1	199
183	RL18_HUMAN	60S ribosomal protein L18	197
184	ATP5L_HUMAN	ATP synthase subunit g, mitochondrial	197
185	CX6B1_HUMAN	Cytochrome c oxidase subunit VIb isoform 1	196
186	HNRPU_HUMAN	Heterogeneous nuclear ribonucleoprotein U	195
187	VDAC3_HUMAN	Voltage-dependent anion-selective channel protein 3	193
188	RL13A_HUMAN	60S ribosomal protein L13a	192
189	ERG7_HUMAN	Lanosterol synthase	188
190	RS15A_HUMAN	40S ribosomal protein S15a	186
191	RSSA_HUMAN	40S ribosomal protein SA	186
192	ASSY_HUMAN	Argininosuccinate synthase	181
193	CP2A6_HUMAN	Cytochrome P450 2A6	180
194	CP4AB_HUMAN	Cytochrome P450 4A11 precursor	179
195	NIP51_HUMAN	Protein NipSnap1	179
195	NIP52_HUMAN	Protein NipSnap2	36

Sample 2 proteins identified by nLC-MS using MASCOT and the launch peaks to mascot export function			
Number	SwissProt accession	Protein name	Protein score
196	RL35_HUMAN	60S ribosomal protein L35	177
197	RL13_HUMAN	60S ribosomal protein L13	177
198	DAK_HUMAN (DHAK_HUMAN expasy)	Dihydroxyacetone kinase	171
199	PAIRB_HUMAN	Plasminogen activator inhibitor 1 RNA-binding protein	171
200	HSPB1_HUMAN	Heat shock protein beta-1	167
201	SERA_HUMAN	D-3-phosphoglycerate dehydrogenase	167
202	ANXA2_HUMAN	Annexin A2	166
203	DHB2_HUMAN	Estradiol 17-beta-dehydrogenase 2	161
204	NDUS4_HUMAN	NADH dehydrogenase [ubiquinone] iron-sulfur protein 4, mitochondrial precursor	160
205	CP51A_HUMAN	Cytochrome P450 51A1	160
206	COPG_HUMAN	Coatamer subunit gamma	159
207	C560_HUMAN	Succinate dehydrogenase cytochrome b560 subunit, mitochondrial precursor	157
208	DH11_HUMAN	Corticosteroid 11-beta-dehydrogenase isozyme 1	156
209	CX7AZ_HUMAN	Cytochrome c oxidase polypeptide VIIa-liver/heart, mitochondrial precursor	155
210	NDKA_HUMAN	Nucleoside diphosphate kinase A	144
210	NDKB_HUMAN	Nucleoside diphosphate kinase B	153
211	EST1_HUMAN	Liver carboxylesterase 1 precursor	151
212	NAT8_HUMAN	Probable N-acetyltransferase 8	151
213	LMAN1_HUMAN	Protein ERGIC-53 precursor	151
214	RL7_HUMAN	60S ribosomal protein L7	150
215	APOE_HUMAN	Apolipoprotein E precursor	150
216	SFXN1_HUMAN	Sideroflexin-1	150
217	RIB2_HUMAN (RPN2_HUMAN expasy)	Dolichyl-diphosphooligosaccharide--protein glycosyltransferase 63 kDa subunit precursor	149
218	AR6P1_HUMAN	ADP-ribosylation factor-like protein 6-interacting protein 1	148
219	PDI3_HUMAN	Protein disulfide-isomerase A3 precursor	147
220	CY1_HUMAN	Cytochrome c1, heme protein, mitochondrial precursor	146
221	RL32_HUMAN	60S ribosomal protein L32	146
222	ST2A1_HUMAN	Bile salt sulfotransferase	145
223	S10AA_HUMAN	Protein S100-A10	145
224	RS30_HUMAN	40S ribosomal protein S30	145
225	RS12_HUMAN	40S ribosomal protein S12	143
226	C1TC_HUMAN	C-1-tetrahydrofolate synthase, cytoplasmic	143
227	OCAD2_HUMAN	OCA domain-containing protein 2	142
228	NLIP_HUMAN	Non-specific lipid-transfer protein	140
229	NPM_HUMAN	Nucleophosmin	139
230	G3P_HUMAN	Glyceraldehyde-3-phosphate dehydrogenase	139
231	RS16_HUMAN	40S ribosomal protein S16	138
232	IMMT_HUMAN	Mitochondrial inner membrane protein	138
233	ICPB_HUMAN	T-complex protein 1 subunit beta	137
234	RL21_HUMAN	60S ribosomal protein L21	137
235	MET7B_HUMAN	Methyltransferase-like protein 7B precursor	137
236	TRAP1_HUMAN	Heat shock protein 75 kDa, mitochondrial precursor	136
237	DHSO_HUMAN	Sorbitol dehydrogenase	136
238	TXIP_HUMAN	Tricarboxylate transport protein, mitochondrial precursor	136
239	FINC_HUMAN	Fibronectin precursor	135
240	GNAI1_HUMAN	Guanine nucleotide-binding protein G(i), alpha-1 subunit	117
240	GNAI2_HUMAN	Guanine nucleotide-binding protein G(i), alpha-2 subunit	117
240	GNAI3_HUMAN	Guanine nucleotide-binding protein G(k) subunit alpha	117
240	GNAL_HUMAN	Guanine nucleotide-binding protein G(olf) subunit alpha	117
240	GNAO1_HUMAN	Guanine nucleotide-binding protein G(o) subunit alpha 1	117
240	GNAO2_HUMAN	Guanine nucleotide-binding protein G(o) subunit alpha 2	117
240	GNAS1_HUMAN	Guanine nucleotide-binding protein G(s) subunit alpha isoforms XLas	135
240	GNAS2_HUMAN	Guanine nucleotide-binding protein G(s) subunit alpha isoforms short	135
240	GNAT1_HUMAN	Guanine nucleotide-binding protein G(t) subunit alpha-1	117
240	GNAT2_HUMAN	Guanine nucleotide-binding protein G(t) subunit alpha-2	117
241	RAP1A_HUMAN	Ras-related protein Rap-1A precursor	133
241	RAP1B_HUMAN	Ras-related protein Rap-1b precursor	133
242	AT2A1_HUMAN	Sarcoplasmic/endoplasmic reticulum calcium ATPase 1	81
242	AT2A2_HUMAN	Sarcoplasmic/endoplasmic reticulum calcium ATPase 2	133
242	AT2A3_HUMAN	Sarcoplasmic/endoplasmic reticulum calcium ATPase 3	81
243	IDHP_HUMAN	Isocitrate dehydrogenase [NADP], mitochondrial precursor	132
244	VAPA_HUMAN	Vesicle-associated membrane protein-associated protein A	131
244	VAPB_HUMAN	Vesicle-associated membrane protein-associated protein B/C	108
245	NDUS5_HUMAN	NADH dehydrogenase [ubiquinone] iron-sulfur protein 5	131
246	EFTU_HUMAN	Elongation factor Tu, mitochondrial precursor	131
247	STT3A_HUMAN	Dolichyl-diphosphooligosaccharide--protein glycosyltransferase subunit STT3A	130
248	DHB13_HUMAN	17-beta hydroxysteroid dehydrogenase 13 precursor	130
249	RL35A_HUMAN	60S ribosomal protein L35a	128
250	RS18_HUMAN	40S ribosomal protein S18	127
251	APOA1_HUMAN	Apolipoprotein A-1 precursor	127
252	RLA0_HUMAN	60S acidic ribosomal protein P0	126
253	DIC_HUMAN	Mitochondrial dicarboxylate carrier	124
254	SFRS1_HUMAN	Splicing factor, arginine/serine-rich 1	124
255	PCYOX_HUMAN	Prenylcysteine oxidase 1 precursor	124
256	PSME2_HUMAN	Proteasome activator complex subunit 2	123
257	HNRPQ_HUMAN	Heterogeneous nuclear ribonucleoprotein Q	123
257	HNRPR_HUMAN	Heterogeneous nuclear ribonucleoprotein R	69
258	PON3_HUMAN	Serum paraoxonase/lactonase 3	122
259	RLA2_HUMAN	60S acidic ribosomal protein P2	122
260	IF4G1_HUMAN	Eukaryotic translation initiation factor 4 gamma 1	120
261	NDUS6_HUMAN	NADH dehydrogenase [ubiquinone] iron-sulfur protein 6, mitochondrial precursor	120
262	DHB12_HUMAN	Estradiol 17-beta-dehydrogenase 12	120
263	RHOA_HUMAN	Transforming protein RhoA precursor	119
263	RHOC_HUMAN	Rho-related GTP-binding protein RhoC precursor	119
264	SURF4_HUMAN	Surfeit locus protein 4	119
265	GANAB_HUMAN	Neutral alpha-glucosidase AB precursor	118
266	PCBP2_HUMAN	Poly(rC)-binding protein 2	116
266	PCBP3_HUMAN	Poly(rC)-binding protein 3	78
267	REEP6_HUMAN	Receptor expression-enhancing protein 6	116

Sample 2 proteins identified by nLC-MS using MASCOT and the launch peaks to mascot export function			
Number	SwissProt accession	Protein name	Protein score
268	CPT2_HUMAN	Carnitine O-palmitoyltransferase 2, mitochondrial precursor	116
269	NDUA4_HUMAN	NADH dehydrogenase [ubiquinone] 1 alpha subcomplex subunit 4	113
270	SC22B_HUMAN	Vesicle-trafficking protein SEC22b	113
271	LMNA_HUMAN	Lamin-A/C	112
272	RS20_HUMAN	40S ribosomal protein S20	112
273	SAR1A_HUMAN	GTP-binding protein SAR1a	112
273	SAR1B_HUMAN	GTP-binding protein SAR1b	112
274	RL27_HUMAN	60S ribosomal protein L27	112
275	ASGR1_HUMAN	Asialoglycoprotein receptor 1	111
276	RS23_HUMAN	40S ribosomal protein S23	110
277	CPT1A_HUMAN	Carnitine O-palmitoyltransferase I, liver isoform	108
278	COPB_HUMAN	Coatomer subunit beta	108
279	RL26_HUMAN	60S ribosomal protein L26	106
279	RL26L_HUMAN	60S ribosomal protein L26-like 1	89
280	HNRPD_HUMAN	Heterogeneous nuclear ribonucleoprotein D0	106
281	NDUA8_HUMAN	NADH dehydrogenase [ubiquinone] 1 alpha subcomplex subunit 8	105
282	CHDH_HUMAN	Choline dehydrogenase, mitochondrial precursor	105
283	SCPDH_HUMAN	Probable saccharopine dehydrogenase	104
284	CP2D6_HUMAN	Cytochrome P450 2D6	104
285	CATB_HUMAN	Cathepsin B precursor	104
286	APOC1_HUMAN	Apolipoprotein C-1 precursor	104
287	JAM1_HUMAN	Junctional adhesion molecule A precursor	102
288	COX6C_HUMAN	Cytochrome c oxidase polypeptide VIc precursor	102
289	HNRPM_HUMAN	Heterogeneous nuclear ribonucleoprotein M	101
290	RS11_HUMAN	40S ribosomal protein S11	100
291	GCS1_HUMAN	Mannosyl-oligosaccharide glucosidase	100
292	ICAM1_HUMAN	Intercellular adhesion molecule 1 precursor	99
293	RL34_HUMAN	60S ribosomal protein L34	99
294	RDH11_HUMAN	Retinol dehydrogenase 11	98
295	CP2CL_HUMAN	Cytochrome P450 2C18	98
296	QCR7_HUMAN	Cytochrome b-c1 complex subunit 7	98
297	RS19_HUMAN	40S ribosomal protein S19	96
298	RS8_HUMAN	40S ribosomal protein S8	96
299	DHX9_HUMAN	ATP-dependent RNA helicase A	93
300	THIO_HUMAN	Thioredoxin	93
301	UBA1_HUMAN	Ubiquitin-like modifier-activating enzyme 1	91
302	SFRS3_HUMAN	Splicing factor, arginine/serine-rich 3	91
302	SFRS7_HUMAN	Splicing factor, arginine/serine-rich 7	91
303	LONM_HUMAN	Lon protease homolog, mitochondrial precursor	90
304	PYC_HUMAN	Pyruvate carboxylase, mitochondrial precursor	90
305	KAD4_HUMAN	Adenylate kinase isoenzyme 4, mitochondrial	90
306	UCRI_HUMAN	Cytochrome b-c1 complex subunit Rieske, mitochondrial precursor	89
307	FKBP8_HUMAN	FK506-binding protein 8	88
308	K6PL_HUMAN	6-phosphofructokinase, liver type	88
309	PONI_HUMAN	Serum paraoxonase/arylesterase 1	88
310	ACF_HUMAN (A1CF_HUMAN expasy)	APOBEC1 complementation factor	87
311	FABPL_HUMAN	Fatty acid-binding protein, liver	86
312	PCCB_HUMAN	Propionyl-CoA carboxylase beta chain, mitochondrial precursor	85
313	GLYAT_HUMAN	Glycine N-acyltransferase	85
314	RL31_HUMAN	60S ribosomal protein L31	85
315	TMED2_HUMAN	Transmembrane emp24 domain-containing protein 2 precursor	84
316	RSMB_HUMAN	Small nuclear ribonucleoprotein-associated proteins B and B=	84
316	RSMN_HUMAN	Small nuclear ribonucleoprotein-associated protein N	84
317	PYGB_HUMAN	Glycogen phosphorylase, brain form	84
318	NDUS2_HUMAN	NADH dehydrogenase [ubiquinone] iron-sulfur protein 2, mitochondrial precursor	84
319	H1O_HUMAN	Histone H1.0	84
320	NDUA6_HUMAN	NADH dehydrogenase [ubiquinone] 1 alpha subcomplex subunit 6	83
321	DDX1_HUMAN	ATP-dependent RNA helicase DDX1	83
322	KAD3_HUMAN	GTP:AMP phosphotransferase mitochondrial	83
323	TMM97_HUMAN	Transmembrane protein 97	82
324	CP1A2_HUMAN	Cytochrome P450 1A2	82
325	KMO_HUMAN	Kynurenine 3-monooxygenase	82
326	SC11A_HUMAN	Signal peptidase complex catalytic subunit SEC11A	81
327	DHRST_HUMAN	Dehydrogenase/reductase SDR family member 7 precursor	81
328	AK1C1_HUMAN	Aldo-keto reductase family 1 member C1	81
328	AK1C2_HUMAN	Aldo-keto reductase family 1 member C2	81
328	AK1C3_HUMAN	Aldo-keto reductase family 1 member C3	29
328	AK1C4_HUMAN	Aldo-keto reductase family 1 member C4	29
329	ATP5L_HUMAN	ATP synthase subunit e, mitochondrial	81
330	AAAD_HUMAN	Arylacetamide deacetylase	80
331	RAB7A_HUMAN	Ras-related protein Rab-7a	80
332	RAB10_HUMAN	Ras-related protein Rab-10	63
332	RAB12_HUMAN	Putative Ras-related protein Rab-12	63
332	RAB14_HUMAN	Ras-related protein Rab-14	63
332	RAB1A_HUMAN	Ras-related protein Rab-1A	80
332	RAB1B_HUMAN	Ras-related protein Rab-1B	80
332	RAB30_HUMAN	Ras-related protein Rab-30	63
332	RAB35_HUMAN	Ras-related protein Rab-35	63
332	RAB37_HUMAN	Ras-related protein Rab-37	63
332	RAB3A_HUMAN	Ras-related protein Rab-3A	63
332	RAB3B_HUMAN	Ras-related protein Rab-3B	63
332	RAB3C_HUMAN	Ras-related protein Rab-3C	63
332	RAB3D_HUMAN	Ras-related protein Rab-3D	63
332	RAB43_HUMAN	Ras-related protein Rab-43	63
332	RAB4A_HUMAN	Ras-related protein Rab-4A	63
332	RAB4B_HUMAN	Ras-related protein Rab-4B	63
332	RAB8A_HUMAN	Ras-related protein Rab-8A	63
332	RAB8B_HUMAN	Ras-related protein Rab-8B	63
332	RB39B_HUMAN	Ras-related protein Rab-39B	63
333	GCSF_HUMAN	Glycine dehydrogenase [decarboxylating], mitochondrial precursor	79
334	STIA1_HUMAN	Sulfotransferase 1A1	78

Sample 2 proteins identified by nLC-MS using MASCOT and the launch peaks to mascot export function			
Number	SwissProt accession	Protein name	Protein score
334	ST1A2_HUMAN	Sulfotransferase 1A2	78
335	NSDHL_HUMAN	Sterol 4-alpha-carboxylate 3-dehydrogenase, decarboxylating	78
336	PRS6B_HUMAN	26S protease regulatory subunit 6B	78
337	ABCD3_HUMAN	ATP-binding cassette sub-family D member 3	77
338	ANXA5_HUMAN	Annexin A5	77
339	RL8_HUMAN	60S ribosomal protein L8	77
340	COX1_HUMAN	Cytochrome c oxidase subunit 1	77
341	SPEB_HUMAN	Agmatinase, mitochondrial precursor	77
342	RS15_HUMAN	40S ribosomal protein S15	76
343	GABT_HUMAN	4-aminobutyrate aminotransferase, mitochondrial precursor	76
344	HMOX1_HUMAN	Heme oxygenase 1	76
345	ACS2A_HUMAN	Acyl-coenzyme A synthetase ACSM2A, mitochondrial precursor	76
345	ACS2B_HUMAN	Acyl-coenzyme A synthetase ACSM2B, mitochondrial precursor	76
346	PECL_HUMAN	Peroxisomal 3,2-trans-enoyl-CoA isomerase	76
347	SAA4_HUMAN	Serum amyloid A-4 protein precursor	75
348	ILF2_HUMAN	Interleukin enhancer-binding factor 2	75
349	GPSN2_HUMAN	Synaptic glycoprotein SC2	75
350	SPYA_HUMAN	Serine--pyruvate aminotransferase	75
351	HGD_HUMAN	Homogentisate 1,2-dioxygenase	75
352	TMED7_HUMAN	Transmembrane emp24 domain-containing protein 7 precursor	75
353	BAS1_HUMAN	Basigin precursor	74
354	DHCR7_HUMAN	7-dehydrocholesterol reductase	74
355	MFN1_HUMAN	Mitofusin-1	73
355	MFN2_HUMAN	Mitofusin-2	73
356	SYDC_HUMAN	Aspartyl-tRNA synthetase, cytoplasmic	73
357	CATA_HUMAN	Catalase	73
358	GATM_HUMAN	Glycine amidotransferase, mitochondrial precursor	73
359	ACSL3_HUMAN	Long-chain-fatty-acid-CoA ligase 3	73
359	ACSL4_HUMAN	Long-chain-fatty-acid-CoA ligase 4	73
360	SSRG_HUMAN	Translocon-associated protein subunit gamma	72
361	VDAC2_HUMAN	Voltage-dependent anion-selective channel protein 2	72
362	GLYG_HUMAN	Glycogenin-1	71
363	TERA_HUMAN	Transitional endoplasmic reticulum ATPase	71
364	PCCA_HUMAN	Propionyl-CoA carboxylase alpha chain, mitochondrial precursor	71
365	PGRC1_HUMAN	Membrane-associated progesterone receptor component 1	71
366	DCXR_HUMAN	L-xylulose reductase	71
367	ATP8_HUMAN	ATP synthase protein 8	71
368	HSP71_HUMAN	Heat shock 70 kDa protein 1	70
368	HSP76_HUMAN	Heat shock 70 kDa protein 6	30
368	HSP77_HUMAN	Putative heat shock 70 kDa protein 7	30
369	UDZ3_HUMAN	UDP-glucuronosyltransferase 2A3 precursor	70
370	KU70_HUMAN	ATP-dependent DNA helicase 2 subunit 1	70
371	E2IG5_HUMAN	E2-induced gene 5 protein	69
372	NDUS8_HUMAN	NADH dehydrogenase [ubiquinone] iron-sulfur protein 8, mitochondrial precursor	68
373	ODO2_HUMAN	Dihydropolyllysine-residue succinyltransferase component of 2-oxoglutarate dehydrogenase complex, mitochondrial precursor	68
374	THIM_HUMAN	3-ketoacyl-CoA thiolase, mitochondrial	68
375	E1FA_HUMAN	Electron transfer flavoprotein subunit alpha, mitochondrial precursor	66
376	C1058_HUMAN	Uncharacterized protein C10orf58 precursor	66
377	PPAL_HUMAN	Lysosomal acid phosphatase precursor	66
378	PLEC1_HUMAN	Plectin-1	66
379	NDUA5_HUMAN	NADH dehydrogenase [ubiquinone] 1 alpha subcomplex subunit 5	65
380	PXMP2_HUMAN	Peroxisomal membrane protein 2	65
381	CATD_HUMAN	Cathepsin D precursor	64
382	AMPN_HUMAN	Aminopeptidase N	64
383	CTND1_HUMAN	Catenin delta-1	64
384	CCD56_HUMAN	Coiled-coil domain-containing protein 56	63
385	EZRI_HUMAN	Ezrin	48
385	MOES_HUMAN	Moesin	48
385	RADL_HUMAN	Radixin	63
386	ICPW_HUMAN	T-complex protein 1 subunit zeta-2	34
386	TCPZ_HUMAN	T-complex protein 1 subunit zeta	63
387	ODP2_HUMAN	Dihydropolyllysine-residue acetyltransferase component of pyruvate dehydrogenase complex, mitochondrial precursor	63
388	PIIB_HUMAN	Peptidyl-prolyl cis-trans isomerase B precursor	63
389	HYOU1_HUMAN	Hypoxia up-regulated protein 1 precursor	62
390	HMCS1_HUMAN	Hydroxymethylglutaryl-CoA synthase, cytoplasmic	62
391	TOLIP_HUMAN	Toll-interacting protein	62
392	NDUB6_HUMAN	NADH dehydrogenase [ubiquinone] 1 beta subcomplex subunit 6	61
393	MGLL_HUMAN	Monoglyceride lipase	61
394	CD59_HUMAN	CD59 glycoprotein precursor	61
395	ODB2_HUMAN	Lipoamide acyltransferase component of branched-chain alpha-keto acid dehydrogenase complex, mitochondrial precursor	61
396	ACPM_HUMAN	Acyl carrier protein, mitochondrial precursor	61
397	PTAD1_HUMAN	Protein tyrosine phosphatase-like protein PTPLAD1	60
398	UBE2N_HUMAN	Ubiquitin-conjugating enzyme E2 N	60
399	EBP_HUMAN	3-beta-hydroxysteroid-Delta(8),Delta(7)-isomerase	60
400	TGM2_HUMAN	Protein-glutamine gamma-glutamyltransferase 2	60
401	RL23A_HUMAN	60S ribosomal protein L23a	60
402	G3BP1_HUMAN	Ras GTPase-activating protein-binding protein 1	59
403	ERLN2_HUMAN	Erlin-2 precursor	59
404	RL36_HUMAN	60S ribosomal protein L36	59
405	AL4A1_HUMAN	Delta-1-pyrroline-5-carboxylate dehydrogenase, mitochondrial precursor	58
406	AP1B1_HUMAN	AP-1 complex subunit beta-1	58
406	AP2B1_HUMAN	AP-2 complex subunit beta-1	58
407	RL40_HUMAN	60S ribosomal protein L40	58
408	SPCS2_HUMAN	Signal peptidase complex subunit 2	58
409	KCY_HUMAN	UMP-CMP kinase	58
410	LPPRC_HUMAN	Leucine-rich PPR motif-containing protein, mitochondrial precursor	58
411	AL8A1_HUMAN	Aldehyde dehydrogenase family 8 member A1	58
412	METK1_HUMAN	S-adenosylmethionine synthetase isoform type-1	57
413	PAPS2_HUMAN	Bifunctional 3-phosphoadenosine 5-phosphosulfate synthetase 2	57
414	RB11A_HUMAN	Ras-related protein Rab-11A	56

Number	SwissProt accession	Protein name	Protein score
414	RB11B_HUMAN	Ras-related protein Rab-11B	56
Sample 2 proteins identified by nLC-MS using MASCOT and the launch peaks to mascot export function			
415	PRS7_HUMAN	26S protease regulatory subunit 7	56
416	PRS6A_HUMAN	26S protease regulatory subunit 6A	56
417	MYL6_HUMAN	Myosin light polypeptide 6	56
418	TIM13_HUMAN	Mitochondrial import inner membrane translocase subunit Tim13	55
419	K1C9_HUMAN	Keratin, type 1 cytoskeletal 9	54
420	DNJA1_HUMAN	Dnaj homolog subfamily A member 1	53
421	SYJ2B_HUMAN	Synaptotagmin-2-binding protein	53
422	PSMD1_HUMAN	26S proteasome non-ATPase regulatory subunit 1	53
423	FDFT_HUMAN	Squalene synthetase	53
424	STRAP_HUMAN	Serine-threonine kinase receptor-associated protein	53
425	RE1ST_HUMAN	All-trans-retinol 13,14-reductase precursor	52
426	S61A1_HUMAN	Protein transport protein Sec61 subunit alpha isoform 1	51
427	ATP5J_HUMAN	ATP synthase-coupling factor 6, mitochondrial precursor	51
428	BAAT1_HUMAN	Bile acid-CoA:amino acid N-acyltransferase	50
429	PURA_HUMAN	Transcriptional activator protein Pur-alpha	50
430	CD81_HUMAN	CD81 antigen	49
431	ARF6_HUMAN	ADP-ribosylation factor 6	49
432	LAMP2_HUMAN	Lysosome-associated membrane glycoprotein 2 precursor	48
433	PGM1_HUMAN	Phosphoglucomutase-1	48
434	PRS10_HUMAN	26S protease regulatory subunit S10B	48
435	PH4H_HUMAN	Phenylalanine-4-hydroxylase	48
436	ARSE_HUMAN	Arylsulfatase E precursor	47
437	IF4E_HUMAN	Eukaryotic translation initiation factor 4E	47
438	SYC_HUMAN	Tyrosyl-tRNA synthetase, cytoplasmic	46
439	CP2C8_HUMAN	Cytochrome P450 2C8	46
440	ARSA1_HUMAN	Arsenical pump-driving ATPase	46
441	CPNE2_HUMAN	Copine-2	46
441	CPNE3_HUMAN	Copine-3	46
441	CPNE4_HUMAN	Copine-4	46
441	CPNE5_HUMAN	Copine-5	46
441	CPNE6_HUMAN	Copine-6	46
441	CPNE7_HUMAN	Copine-7	46
441	CPNE8_HUMAN	Copine-8	46
442	K1C10_HUMAN	Keratin, type 1 cytoskeletal 10	46
443	NDK8_HUMAN	Putative nucleoside diphosphate kinase	45
444	TXND5_HUMAN	Thioredoxin domain-containing protein 5 precursor	45
445	RL30_HUMAN	60S ribosomal protein L30	45
446	H2AY_HUMAN	Core histone macro-H2A.1	44
447	TPSN_HUMAN	Tapasin precursor	44
448	ITB1_HUMAN	Integrin beta-1 precursor	44
449	H14_HUMAN	Histone H1.4	43
450	DDX17_HUMAN	Probable ATP-dependent RNA helicase DDX17	43
450	DDX3X_HUMAN	ATP-dependent RNA helicase DDX3X	43
450	DDX3Y_HUMAN	ATP-dependent RNA helicase DDX3Y	43
450	DDX5_HUMAN	Probable ATP-dependent RNA helicase DDX5	43
451	S14L2_HUMAN	SEC14-like protein 2	42
452	RINL_HUMAN	Ribonuclease inhibitor	42
453	RL11_HUMAN	60S ribosomal protein L11	42
454	COX5B_HUMAN	Cytochrome c oxidase subunit 5B, mitochondrial precursor	42
455	RS10_HUMAN	40S ribosomal protein S10	42
456	XPO1_HUMAN	Exportin-1	41
457	BAP31_HUMAN	B-cell receptor-associated protein 31	41
458	ERLN1_HUMAN	Erlin-1 precursor	41
459	ARF4_HUMAN	ADP-ribosylation factor 4	41
460	NNMT_HUMAN	Nicotinamide N-methyltransferase	41
461	3BHS7_HUMAN	3 beta-hydroxysteroid dehydrogenase type 7	41
462	FADS2_HUMAN	Fatty acid desaturase 2	40
463	K0774_HUMAN	Uncharacterized protein KIAA0774	40
464	CP8B1_HUMAN	Cytochrome P450 8B1	40
465	QCR6_HUMAN	Cytochrome b-c1 complex subunit 6, mitochondrial precursor	40
466	HNRPF_HUMAN	Heterogeneous nuclear ribonucleoprotein F	40
467	CRNL1_HUMAN	Crooked neck-like protein 1	40
468	RS25_HUMAN	40S ribosomal protein S25	39
469	ACLY_HUMAN	ATP-citrate synthase	39
470	RAB2A_HUMAN	Ras-related protein Rab-2A	39
470	RAB2B_HUMAN	Ras-related protein Rab-2B	39
471	M2OM_HUMAN	Mitochondrial 2-oxoglutarate/malate carrier protein	39
472	DPYS_HUMAN	Dihydropyrimidinase	39
473	MGST2_HUMAN	Microsomal glutathione S-transferase 2	38
474	SC23A_HUMAN	Protein transport protein Sec23A	38
475	CLUS_HUMAN	Clusterin precursor	38
476	SYQ_HUMAN	Glutaminyl-tRNA synthetase	38
477	NDUB7_HUMAN	NADH dehydrogenase [ubiquinone] 1 beta subcomplex subunit 7	38
478	ARLY_HUMAN	Argininosuccinate lyase	38
479	COX7C_HUMAN	Cytochrome c oxidase subunit 7C, mitochondrial precursor	38
479	SLK_HUMAN	STE20-like serine/threonine-protein kinase	28
480	PAHX_HUMAN	Phytanoyl-CoA dioxygenase, peroxisomal precursor	37
481	MATR3_HUMAN	Matrin-3	37
482	TOM70_HUMAN	Mitochondrial precursor proteins import receptor	36
483	GYS2_HUMAN	Glycogen [starch] synthase, liver	36
484	CALR_HUMAN	Calreticulin precursor	36
485	LACTB_HUMAN	Serine beta-lactamase-like protein LACTB, mitochondrial precursor	36
486	CY5B_HUMAN	Cytochrome b5 type B precursor	36
487	TCPE_HUMAN	T-complex protein 1 subunit epsilon	36
488	SYRC_HUMAN	Arginyl-tRNA synthetase, cytoplasmic	36
489	CFTR_HUMAN	Cystic fibrosis transmembrane conductance regulator	36
489	PLK2_HUMAN	Serine/threonine-protein kinase PLK2	36
490	SYEP_HUMAN	Bifunctional aminoacyl-tRNA synthetase	36
491	ODBB_HUMAN	2-oxoisovalerate dehydrogenase subunit beta, mitochondrial precursor	36
492	THIK_HUMAN	3-ketoacyl-CoA thiolase, peroxisomal precursor	35
493	GALK1_HUMAN	Galactokinase	35
494	ORNT1_HUMAN	Mitochondrial ornithine transporter 1	35

495	BR44_HUMAN	Brain protein 44	35
Sample 2 proteins identified by nLC-MS using MASCOT and the launch peaks to mascot export function			
Number	SwissProt accession	Protein name	Protein score
496	CBR1_HUMAN	Carbonyl reductase [NADPH] 1	35
496	CBR3_HUMAN	Carbonyl reductase [NADPH] 3	35
497	RL29_HUMAN	60S ribosomal protein L29	35
498	G6PT1_HUMAN	Glucose-6-phosphate translocase	34
499	ECHP_HUMAN	Peroxisomal bifunctional enzyme	34
500	NDUA2_HUMAN	NADH dehydrogenase [ubiquinone] 1 alpha subcomplex subunit 2	34
501	DERL1_HUMAN	Derlin-1	34
502	AP2A2_HUMAN	AP-2 complex subunit alpha-2	34
503	CLC3A_HUMAN	C-type lectin domain family 3 member A precursor	34
504	SDFZL_HUMAN	Stromal cell-derived factor 2-like protein 1 precursor	34
505	EFTS_HUMAN	Elongation factor 1s, mitochondrial precursor	33
505	RGL1_HUMAN	Ral guanine nucleotide dissociation stimulator-like 1	33
506	ARMX2_HUMAN	Armadillo repeat-containing X-linked protein 2	33
507	SWV_HUMAN (SWVC_HUMAN expasy)	Valyl-tRNA synthetase	33
508	UBR4_HUMAN	E3 ubiquitin-protein ligase UBR4	33
509	IMM56_HUMAN	Transmembrane protein 56	33
510	SMD3_HUMAN	Small nuclear ribonucleoprotein Sm D3	32
511	MIA40_HUMAN	Mitochondrial intermembrane space import and assembly protein 40	32
512	APOC2_HUMAN	Apolipoprotein C-II precursor	32
513	DAD1_HUMAN	Dolichyl-diphosphooligosaccharide--protein glycosyltransferase subunit DAD1	32
514	1433B_HUMAN	14-3-3 protein beta/alpha	32
514	1433F_HUMAN	14-3-3 protein eta	32
514	1433G_HUMAN	14-3-3 protein gamma	32
514	1433S_HUMAN	14-3-3 protein sigma	32
514	1433T_HUMAN	14-3-3 protein theta	32
514	1433Z_HUMAN	14-3-3 protein zeta/delta	32
515	C144A_HUMAN	Coiled-coil domain-containing protein 144A	32
516	AASS_HUMAN	Alpha-aminoadipic semialdehyde synthase, mitochondrial precursor	32
517	SFXN2_HUMAN	Sideroflexin-2	32
518	LASS4_HUMAN	LAG1 longevity assurance homolog 4	31
519	NPTN_HUMAN	Neuroplastin precursor	31
520	LEIM1_HUMAN	Leucine zipper-EF-hand-containing transmembrane protein 1, mitochondrial precursor	31
521	SPSY_HUMAN	Spermine synthase	31
522	ADO_HUMAN	Aldehyde oxidase	31
523	TOP2B_HUMAN	DNA topoisomerase 2-beta	31
524	COASY_HUMAN	Bifunctional coenzyme A synthase	31
525	MPU1_HUMAN	Mannose-P-dolichol utilization defect 1 protein	30
526	EHD2_HUMAN	EH domain-containing protein 2	30
526	EHD4_HUMAN	EH domain-containing protein 4	30
527	IMB1_HUMAN	Importin subunit beta-1	30
528	NEMO_HUMAN	NF-kappa-B essential modulator	30
529	AHNAK_HUMAN	Neuroblast differentiation-associated protein AHNAK	30
530	PEX13_HUMAN	Peroxisomal membrane protein PEX13	30
531	MLRM_HUMAN	Myosin regulatory light chain 2, nonsarcomeric	30
532	CP27A_HUMAN	Cytochrome P450 27, mitochondrial precursor	29
533	RL5_HUMAN	60S ribosomal protein L5	29
534	RIOK2_HUMAN	Serine/threonine-protein kinase RIO2	29
535	ANM7_HUMAN	Protein arginine N-methyltransferase 7	29
536	PRS4_HUMAN	26S protease regulatory subunit 4	28
537	RL18A_HUMAN	60S ribosomal protein L18a	28
538	TEC_HUMAN	Tyrosine-protein kinase Tec	28
539	ILF3_HUMAN	Interleukin enhancer-binding factor 3	28
540	SPTA2_HUMAN	Spectrin alpha chain, brain	28
541	AK1B1_HUMAN	Aldo-keto reductase family 1 member B10	28
542	PDS5A_HUMAN	Sister chromatid cohesion protein PDS5 homolog A	28
543	OCAD1_HUMAN	OCIA domain-containing protein 1	27
544	NDUAD_HUMAN	NADH dehydrogenase [ubiquinone] 1 alpha subcomplex subunit 13	27
545	WBP2_HUMAN	WW domain-binding protein 2	27

Appendix VI: KEGG pathways affected

The pathways listed below are affected by the proteins found to be regulated.

Sample 1

RSV treatment

Following object(s) was/were not found hsa:148534 hsa:341 hsa:9526

hsa00020 Citrate cycle (TCA cycle) - Homo sapiens (human) hsa:47 ACLY; ATP citrate lyase (EC:2.3.3.8); K01648 ATP citrate (pro-S)-lyase [EC:2.3.3.8] hsa:6391 SDHC; succinate dehydrogenase complex, subunit C, integral membrane protein, 15kDa; K00236 succinate dehydrogenase (ubiquinone) cytochrome b subunit [EC:1.3.5.1]

* **hsa03320 PPAR signaling pathway** - Homo sapiens (human) hsa:2181 ACSL3; acyl-CoA synthetase long-chain family member 3 (EC:6.2.1.3); K01897 long-chain acyl-CoA synthetase [EC:6.2.1.3] hsa:345 APOC3; apolipoprotein C-III ; K08759 apolipoprotein C-III

* **hsa00100 Biosynthesis of steroids** - Homo sapiens (human) hsa:1595 CYP51A1; cytochrome P450, family 51, subfamily A, polypeptide 1 (EC:1.14.13.70); K05917 cytochrome P450, family 51, subfamily A (sterol 14-demethylase) [EC:1.14.13.70] hsa:2222 FDFT1; farnesyl-diphosphate farnesyltransferase 1 (EC:2.5.1.21); K00801 farnesyl-diphosphate farnesyltransferase [EC:2.5.1.21]

* **hsa05016 Huntington's disease** - Homo sapiens (human) hsa:6391 SDHC; succinate dehydrogenase complex, subunit C, integral membrane protein, 15kDa; K00236 succinate dehydrogenase (ubiquinone) cytochrome b subunit [EC:1.3.5.1]

* **hsa00650 Butanoate metabolism** - Homo sapiens (human) hsa:3157 HMGCS1; 3-hydroxy-3-methylglutaryl-Coenzyme A synthase 1 (soluble) (EC:2.3.3.10); K01641 hydroxymethylglutaryl-CoA synthase [EC:2.3.3.10]

* **hsa00190 Oxidative phosphorylation** - Homo sapiens (human) hsa:6391 SDHC; succinate dehydrogenase complex, subunit C, integral membrane protein, 15kDa; K00236 succinate dehydrogenase (ubiquinone) cytochrome b subunit [EC:1.3.5.1]

* **hsa00052 Galactose metabolism** - Homo sapiens (human) hsa:5236 PGM1; phosphoglucomutase 1 (EC:5.4.2.2); K01835 phosphoglucomutase [EC:5.4.2.2]

* **hsa00150 Androgen and estrogen metabolism** - Homo sapiens (human) hsa:51144 HSD17B12; hydroxysteroid (17-beta) dehydrogenase 12 (EC:1.1.1.62); K00044 estradiol 17beta-dehydrogenase [EC:1.1.1.62]; K10251 beta-keto reductase [EC:1.1.1.-]

* **hsa00500 Starch and sucrose metabolism** - Homo sapiens (human) hsa:5236 PGM1; phosphoglucomutase 1 (EC:5.4.2.2); K01835 phosphoglucomutase [EC:5.4.2.2]

- * **hsa01040 Biosynthesis of unsaturated fatty acids** - Homo sapiens (human) hsa:51144 HSD17B12; hydroxysteroid (17-beta) dehydrogenase 12 (EC:1.1.1.62); K00044 estradiol 17beta-dehydrogenase [EC:1.1.1.62]; K10251 beta-keto reductase [EC:1.1.1.-]
- * **hsa00010 Glycolysis / Gluconeogenesis** - Homo sapiens (human) hsa:5236 PGM1; phosphoglucomutase 1 (EC:5.4.2.2); K01835 phosphoglucomutase [EC:5.4.2.2]
- * **hsa04270 Vascular smooth muscle contraction** - Homo sapiens (human) hsa:72 ACTG2; actin, gamma 2, smooth muscle, enteric ; K12315 actin, gamma-enteric smooth muscle
- * **hsa00072 Synthesis and degradation of ketone bodies** - Homo sapiens (human) hsa:3157 HMGCS1; 3-hydroxy-3-methylglutaryl-Coenzyme A synthase 1 (soluble) (EC:2.3.3.10); K01641 hydroxymethylglutaryl-CoA synthase [EC:2.3.3.10]
- * **hsa04920 Adipocytokine signaling pathway** - Homo sapiens (human) hsa:2181 ACSL3; acyl-CoA synthetase long-chain family member 3 (EC:6.2.1.3); K01897 long-chain acyl-CoA synthetase [EC:6.2.1.3]
- * **hsa00071 Fatty acid metabolism** - Homo sapiens (human) hsa:2181 ACSL3; acyl-CoA synthetase long-chain family member 3 (EC:6.2.1.3); K01897 long-chain acyl-CoA synthetase [EC:6.2.1.3]
- * **hsa05010 Alzheimer's disease** - Homo sapiens (human) hsa:6391 SDHC; succinate dehydrogenase complex, subunit C, integral membrane protein, 15kDa; K00236 succinate dehydrogenase (ubiquinone) cytochrome b subunit [EC:1.3.5.1]
- * **hsa00900 Terpenoid biosynthesis** - Homo sapiens (human) hsa:2222 FDFT1; farnesyl-diphosphate farnesyltransferase 1 (EC:2.5.1.21); K00801 farnesyl-diphosphate farnesyltransferase [EC:2.5.1.21]
- * **hsa05012 Parkinson's disease** - Homo sapiens (human) hsa:6391 SDHC; succinate dehydrogenase complex, subunit C, integral membrane protein, 15kDa; K00236 succinate dehydrogenase (ubiquinone) cytochrome b subunit [EC:1.3.5.1]
- * **hsa00030 Pentose phosphate pathway** - Homo sapiens (human) hsa:5236 PGM1; phosphoglucomutase 1 (EC:5.4.2.2); K01835 phosphoglucomutase [EC:5.4.2.2]
- * **hsa00720 Reductive carboxylate cycle (CO2 fixation)** - Homo sapiens (human) hsa:47 ACLY; ATP citrate lyase (EC:2.3.3.8); K01648 ATP citrate (pro-S)-lyase [EC:2.3.3.8]
- * **hsa03010 Ribosome** - Homo sapiens (human) hsa:6133 RPL9; ribosomal protein L9 ; K02940 large subunit ribosomal protein L9e
- * **hsa00280 Valine, leucine and isoleucine degradation** - Homo sapiens (human) hsa:3157 HMGCS1; 3-hydroxy-3-methylglutaryl-Coenzyme A synthase 1 (soluble) (EC:2.3.3.10); K01641 hydroxymethylglutaryl-CoA synthase [EC:2.3.3.10]

LEK-935 treatment

Following object(s) was/were not found hsa:213 hsa:308 hsa:7018

- * **hsa05010 Alzheimer's disease** - Homo sapiens (human) hsa:2597 GAPDH; glyceraldehyde-3-phosphate dehydrogenase (EC:1.2.1.12); K00134 glyceraldehyde 3-phosphate dehydrogenase [EC:1.2.1.12]

- * * **hsa05215 Prostate cancer** - Homo sapiens (human) hsa:7184 HSP90B1; heat shock protein 90kDa beta (Grp94), member 1 ; K09487 heat shock protein 90kDa beta
- * **hsa00480 Glutathione metabolism** - Homo sapiens (human) hsa:3418 IDH2; isocitrate dehydrogenase 2 (NADP+), mitochondrial (EC:1.1.1.42); K00031 isocitrate dehydrogenase [EC:1.1.1.42]
- * **hsa00010 Glycolysis / Gluconeogenesis** - Homo sapiens (human) hsa:2597 GAPDH; glyceraldehyde-3-phosphate dehydrogenase (EC:1.2.1.12); K00134 glyceraldehyde 3-phosphate dehydrogenase [EC:1.2.1.12]
- * **hsa00020 Citrate cycle (TCA cycle)** - Homo sapiens (human) hsa:3418 IDH2; isocitrate dehydrogenase 2 (NADP+), mitochondrial (EC:1.1.1.42); K00031 isocitrate dehydrogenase [EC:1.1.1.42]
- * **hsa00720 Reductive carboxylate cycle (CO2 fixation)** - Homo sapiens (human) hsa:3418 IDH2; isocitrate dehydrogenase 2 (NADP+), mitochondrial (EC:1.1.1.42); K00031 isocitrate dehydrogenase [EC:1.1.1.42]
- * **hsa05200 Pathways in cancer** - Homo sapiens (human) hsa:7184 HSP90B1; heat shock protein 90kDa beta (Grp94), member 1 ; K09487 heat shock protein 90kDa beta
- * **hsa00760 Nicotinate and nicotinamide metabolism** - Homo sapiens (human) hsa:4837 NNMT; nicotinamide N-methyltransferase (EC:2.1.1.1); K00541 nicotinamide N-methyltransferase [EC:2.1.1.1]

Sample 2

RSV treatment

Following object(s) was/were not found hsa:1468 hsa:1973 hsa:23576 hsa:51128

- hsa05016 Huntington's disease** - Homo sapiens (human) hsa:506 ATP5B; ATP synthase, H⁺ transporting, mitochondrial F1 complex, beta polypeptide (EC:3.6.3.14); K02133 F-type H⁺-transporting ATPase subunit beta [EC:3.6.3.14] hsa:6647 SOD1; superoxide dismutase 1, soluble (EC:1.15.1.1); K04565 Cu/Zn superoxide dismutase [EC:1.15.1.1] hsa:7417 VDAC2; voltage-dependent anion channel 2 ; K05862 voltage-dependent anion channel
- * * **hsa04610 Complement and coagulation cascades** - Homo sapiens (human) hsa:2243 FGA; fibrinogen alpha chain ; K03903 fibrinogen, A alpha polypeptide hsa:2244 FGB; fibrinogen beta chain ; K03904 fibrinogen, B alpha polypeptide
- * **hsa00480 Glutathione metabolism** - Homo sapiens (human) hsa:3417 IDH1; isocitrate dehydrogenase 1 (NADP+), soluble (EC:1.1.1.42); K00031 isocitrate dehydrogenase [EC:1.1.1.42] hsa:9446 GSTO1; glutathione S-transferase omega 1 (EC:2.5.1.18); K00799 glutathione S-transferase [EC:2.5.1.18]
- * **hsa00010 Glycolysis / Gluconeogenesis** - Homo sapiens (human) hsa:229 ALDOB; aldolase B, fructose-bisphosphate (EC:4.1.2.13); K01623 fructose-bisphosphate aldolase, class I [EC:4.1.2.13] hsa:2597 GAPDH; glyceraldehyde-3-phosphate dehydrogenase (EC:1.2.1.12); K00134 glyceraldehyde 3-phosphate dehydrogenase [EC:1.2.1.12]

* **hsa04612 Antigen processing and presentation** - Homo sapiens (human) hsa:2923 PDIA3; protein disulfide isomerase family A, member 3 (EC:5.3.4.1); K08056 protein disulfide isomerase family A, member 3 [EC:5.3.4.1] hsa:3309 HSPA5; heat shock 70kDa protein 5 (glucose-regulated protein, 78kDa) ; K09490 heat shock 70kDa protein 5

* **hsa05010 Alzheimer's disease** - Homo sapiens (human) hsa:2597 GAPDH; glyceraldehyde-3-phosphate dehydrogenase (EC:1.2.1.12); K00134 glyceraldehyde 3-phosphate dehydrogenase [EC:1.2.1.12] hsa:506 ATP5B; ATP synthase, H⁺ transporting, mitochondrial F1 complex, beta polypeptide (EC:3.6.3.14); K02133 F-type H⁺-transporting ATPase subunit beta [EC:3.6.3.14]

* **hsa05012 Parkinson's disease** - Homo sapiens (human) hsa:506 ATP5B; ATP synthase, H⁺ transporting, mitochondrial F1 complex, beta polypeptide (EC:3.6.3.14); K02133 F-type H⁺-transporting ATPase subunit beta [EC:3.6.3.14] hsa:7417 VDAC2; voltage-dependent anion channel 2 ; K05862 voltage-dependent anion channel

* **hsa00051 Fructose and mannose metabolism** - Homo sapiens (human) hsa:229 ALDOB; aldolase B, fructose-bisphosphate (EC:4.1.2.13); K01623 fructose-bisphosphate aldolase, class I [EC:4.1.2.13] hsa:3795 KHK; ketohexokinase (fructokinase) (EC:2.7.1.3); K00846 ketohexokinase [EC:2.7.1.3]

* **hsa00650 Butanoate metabolism** - Homo sapiens (human) hsa:3157 HMGCS1; 3-hydroxy-3-methylglutaryl-Coenzyme A synthase 1 (soluble) (EC:2.3.3.10); K01641 hydroxymethylglutaryl-CoA synthase [EC:2.3.3.10]

* **hsa00190 Oxidative phosphorylation** - Homo sapiens (human) hsa:506 ATP5B; ATP synthase, H⁺ transporting, mitochondrial F1 complex, beta polypeptide (EC:3.6.3.14); K02133 F-type H⁺-transporting ATPase subunit beta [EC:3.6.3.14]

* **hsa04810 Regulation of actin cytoskeleton** - Homo sapiens (human) hsa:5962 RDX; radixin ; K05762 radixin

* **hsa05130 Pathogenic Escherichia coli infection** - Homo sapiens (human) hsa:10383 TUBB2C; tubulin, beta 2C ; K07375 tubulin beta

* **hsa04540 Gap junction** - Homo sapiens (human) hsa:10383 TUBB2C; tubulin, beta 2C ; K07375 tubulin beta

* **hsa00680 Methane metabolism** - Homo sapiens (human) hsa:9588 PRDX6; peroxiredoxin 6 (EC:1.11.1.7 1.11.1.15); K00430 peroxidase [EC:1.11.1.7]; K01066 esterase / lipase [EC:3.1.1.-]; K11188 peroxiredoxin 6, 1-Cys peroxiredoxin [EC:1.11.1.15]

* **hsa00020 Citrate cycle (TCA cycle)** - Homo sapiens (human) hsa:3417 IDH1; isocitrate dehydrogenase 1 (NADP⁺), soluble (EC:1.1.1.42); K00031 isocitrate dehydrogenase [EC:1.1.1.42]

* **hsa00072 Synthesis and degradation of ketone bodies** - Homo sapiens (human) hsa:3157 HMGCS1; 3-hydroxy-3-methylglutaryl-Coenzyme A synthase 1 (soluble) (EC:2.3.3.10); K01641 hydroxymethylglutaryl-CoA synthase [EC:2.3.3.10]

* **hsa00071 Fatty acid metabolism** - Homo sapiens (human) hsa:1632 DCI; dodecenoyl-Coenzyme A delta isomerase (3,2 trans-enoyl-Coenzyme A isomerase) (EC:5.3.3.8); K01825 dodecenoyl-CoA delta-isomerase [EC:5.3.3.8]

* **hsa00960 Alkaloid biosynthesis II** - Homo sapiens (human) hsa:9588 PRDX6; peroxiredoxin 6 (EC:1.11.1.7 1.11.1.15); K00430 peroxidase [EC:1.11.1.7]; K01066 esterase / lipase [EC:3.1.1.-]; K11188 peroxiredoxin 6, 1-Cys peroxiredoxin [EC:1.11.1.15]

- * **hsa04020 Calcium signaling pathway** - Homo sapiens (human) hsa:7417 VDAC2; voltage-dependent anion channel 2 ; K05862 voltage-dependent anion channel
- * **hsa00030 Pentose phosphate pathway** - Homo sapiens (human) hsa:229 ALDOB; aldolase B, fructose-bisphosphate (EC:4.1.2.13); K01623 fructose-bisphosphate aldolase, class I [EC:4.1.2.13]
- * **hsa00830 Retinol metabolism** - Homo sapiens (human) hsa:216 ALDH1A1; aldehyde dehydrogenase 1 family, member A1 (EC:1.2.1.36); K07249 retinal dehydrogenase [EC:1.2.1.36]
- * **hsa00982 Drug metabolism - cytochrome P450** - Homo sapiens (human) hsa:9446 GSTO1; glutathione S-transferase omega 1 (EC:2.5.1.18); K00799 glutathione S-transferase [EC:2.5.1.18]
- * **hsa00980 Metabolism of xenobiotics by cytochrome P450** - Homo sapiens (human) hsa:9446 GSTO1; glutathione S-transferase omega 1 (EC:2.5.1.18); K00799 glutathione S-transferase [EC:2.5.1.18]
- * **hsa00720 Reductive carboxylate cycle (CO₂ fixation)** - Homo sapiens (human) hsa:3417 IDH1; isocitrate dehydrogenase 1 (NADP+), soluble (EC:1.1.1.42); K00031 isocitrate dehydrogenase [EC:1.1.1.42]
- * **hsa05014 Amyotrophic lateral sclerosis (ALS)** - Homo sapiens (human) hsa:6647 SOD1; superoxide dismutase 1, soluble (EC:1.15.1.1); K04565 Cu/Zn superoxide dismutase [EC:1.15.1.1]
- * **hsa00280 Valine, leucine and isoleucine degradation** - Homo sapiens (human) hsa:3157 HMGCS1; 3-hydroxy-3-methylglutaryl-Coenzyme A synthase 1 (soluble) (EC:2.3.3.10); K01641 hydroxymethylglutaryl-CoA synthase [EC:2.3.3.10]
- * **hsa00360 Phenylalanine metabolism** - Homo sapiens (human) hsa:9588 PRDX6; peroxiredoxin 6 (EC:1.11.1.7 1.11.1.15); K00430 peroxidase [EC:1.11.1.7]; K01066 esterase / lipase [EC:3.1.1.-]; K11188 peroxiredoxin 6, 1-Cys peroxiredoxin [EC:1.11.1.15]
- * **hsa00910 Nitrogen metabolism** - Homo sapiens (human) hsa:760 CA2; carbonic anhydrase II (EC:4.2.1.1); K01672 carbonic anhydrase [EC:4.2.1.1]

LEK-935 treatment

Following object(s) was/were not found hsa: hsa:1973 hsa:23576

- * **hsa05016 Huntington's disease** - Homo sapiens (human) hsa:506 ATP5B; ATP synthase, H⁺ transporting, mitochondrial F1 complex, beta polypeptide (EC:3.6.3.14); K02133 F-type H⁺-transporting ATPase subunit beta [EC:3.6.3.14] hsa:6647 SOD1; superoxide dismutase 1, soluble (EC:1.15.1.1); K04565 Cu/Zn superoxide dismutase [EC:1.15.1.1]
- * * **hsa05130 Pathogenic Escherichia coli infection** - Homo sapiens (human) hsa:10383 TUBB2C; tubulin, beta 2C ; K07375 tubulin beta hsa:60 ACTB; actin, beta ; K05692 actin beta/gamma 1
- * **hsa00480 Glutathione metabolism** - Homo sapiens (human) hsa:3417 IDH1; isocitrate dehydrogenase 1 (NADP+), soluble (EC:1.1.1.42); K00031 isocitrate dehydrogenase [EC:1.1.1.42] hsa:9446 GSTO1; glutathione S-transferase omega 1 (EC:2.5.1.18); K00799 glutathione S-transferase [EC:2.5.1.18]
- * **hsa04612 Antigen processing and presentation** - Homo sapiens (human) hsa:2923 PDIA3; protein disulfide isomerase family A, member 3 (EC:5.3.4.1); K08056 protein disulfide isomerase family A,

member 3 [EC:5.3.4.1] hsa:3309 HSPA5; heat shock 70kDa protein 5 (glucose-regulated protein, 78kDa) ; K09490 heat shock 70kDa protein 5

* **hsa00051 Fructose and mannose metabolism** - Homo sapiens (human) hsa:229 ALDOB; aldolase B, fructose-bisphosphate (EC:4.1.2.13); K01623 fructose-bisphosphate aldolase, class I [EC:4.1.2.13] hsa:3795 KHK; ketohexokinase (fructokinase) (EC:2.7.1.3); K00846 ketohexokinase [EC:2.7.1.3]

* **hsa00190 Oxidative phosphorylation** - Homo sapiens (human) hsa:506 ATP5B; ATP synthase, H⁺ transporting, mitochondrial F1 complex, beta polypeptide (EC:3.6.3.14); K02133 F-type H⁺-transporting ATPase subunit beta [EC:3.6.3.14]

* **hsa04810 Regulation of actin cytoskeleton** - Homo sapiens (human) hsa:60 ACTB; actin, beta ; K05692 actin beta/gamma 1

* **hsa04540 Gap junction** - Homo sapiens (human) hsa:10383 TUBB2C; tubulin, beta 2C ; K07375 tubulin beta

* **hsa00010 Glycolysis / Gluconeogenesis** - Homo sapiens (human) hsa:229 ALDOB; aldolase B, fructose-bisphosphate (EC:4.1.2.13); K01623 fructose-bisphosphate aldolase, class I [EC:4.1.2.13]

* **hsa00020 Citrate cycle (TCA cycle)** - Homo sapiens (human) hsa:3417 IDH1; isocitrate dehydrogenase 1 (NADP⁺), soluble (EC:1.1.1.42); K00031 isocitrate dehydrogenase [EC:1.1.1.42]

* **hsa05110 Vibrio cholerae infection** - Homo sapiens (human) hsa:60 ACTB; actin, beta ; K05692 actin beta/gamma 1

* **hsa00071 Fatty acid metabolism** - Homo sapiens (human) hsa:1632 DCI; dodecenoyl-Coenzyme A delta isomerase (3,2 trans-enoyl-Coenzyme A isomerase) (EC:5.3.3.8); K01825 dodecenoyl-CoA delta-isomerase [EC:5.3.3.8]

* **hsa05010 Alzheimer's disease** - Homo sapiens (human) hsa:506 ATP5B; ATP synthase, H⁺ transporting, mitochondrial F1 complex, beta polypeptide (EC:3.6.3.14); K02133 F-type H⁺-transporting ATPase subunit beta [EC:3.6.3.14]

* **hsa04530 Tight junction** - Homo sapiens (human) hsa:60 ACTB; actin, beta ; K05692 actin beta/gamma 1

* **hsa05012 Parkinson's disease** - Homo sapiens (human) hsa:506 ATP5B; ATP synthase, H⁺ transporting, mitochondrial F1 complex, beta polypeptide (EC:3.6.3.14); K02133 F-type H⁺-transporting ATPase subunit beta [EC:3.6.3.14]

* **hsa04520 Adherens junction** - Homo sapiens (human) hsa:60 ACTB; actin, beta ; K05692 actin beta/gamma 1

* **hsa00030 Pentose phosphate pathway** - Homo sapiens (human) hsa:229 ALDOB; aldolase B, fructose-bisphosphate (EC:4.1.2.13); K01623 fructose-bisphosphate aldolase, class I [EC:4.1.2.13]

* **hsa04670 Leukocyte transendothelial migration** - Homo sapiens (human) hsa:60 ACTB; actin, beta ; K05692 actin beta/gamma 1

* **hsa00830 Retinol metabolism** - Homo sapiens (human) hsa:216 ALDH1A1; aldehyde dehydrogenase 1 family, member A1 (EC:1.2.1.36); K07249 retinal dehydrogenase [EC:1.2.1.36]

* **hsa00720 Reductive carboxylate cycle (CO₂ fixation)** - Homo sapiens (human) hsa:3417 IDH1; isocitrate dehydrogenase 1 (NADP⁺), soluble (EC:1.1.1.42); K00031 isocitrate dehydrogenase [EC:1.1.1.42]

- * **hsa00980 Metabolism of xenobiotics by cytochrome P450** - Homo sapiens (human) hsa:9446 GSTO1; glutathione S-transferase omega 1 (EC:2.5.1.18); K00799 glutathione S-transferase [EC:2.5.1.18]
- * **hsa00982 Drug metabolism - cytochrome P450** - Homo sapiens (human) hsa:9446 GSTO1; glutathione S-transferase omega 1 (EC:2.5.1.18); K00799 glutathione S-transferase [EC:2.5.1.18]
- * **hsa04510 Focal adhesion** - Homo sapiens (human) hsa:60 ACTB; actin, beta ; K05692 actin beta/gamma 1
- * **hsa05014 Amyotrophic lateral sclerosis (ALS)** - Homo sapiens (human) hsa:6647 SOD1; superoxide dismutase 1, soluble (EC:1.15.1.1); K04565 Cu/Zn superoxide dismutase [EC:1.15.1.1]
- * **hsa00910 Nitrogen metabolism** - Homo sapiens (human) hsa:760 CA2; carbonic anhydrase II (EC:4.2.1.1); K01672 carbonic anhydrase [EC:4.2.1.1]

Acknowledgements

Im Laufe der letzten Jahre haben mich, im Rahmen dieser Arbeit, mehrere Menschen über unterschiedlich lange Zeiträume begleitet ohne die die vorliegende Arbeit nicht so geworden wäre, wie sie es ist. Ihnen allen gebührt ein Dankeschön für die geleisteten Hilfestellungen, das Lob aber auch die Kritik an der richtigen Stelle. Ich hoffe im Folgenden den gebührenden Dank aussprechen zu können.

Zuerst möchte ich Frau Prof. Dr. Rita Bernhardt danken, für die Möglichkeit in ihrer Arbeitsgruppe diese Arbeit durchführen zu können, sowie das in mich gesetzte Vertrauen während der letzten drei Jahre. Ich durfte/konnte viel lernen und bin sehr froh über die Einblicke in die Wissenschaftswelt sowie die Möglichkeiten die sie mir eröffnet hat. Herzlichen Dank !

Ich danke Herrn Prof. Dr. Elmar Heinzle für die gute Zusammenarbeit im Rahmen der massenspektrometrischen Messungen sowie für die Bereitschaft als Zweitkorretkor dieser Arbeit zu fungieren.

Ich danke der Europäischen Kommission für die finanzielle Unterstützung des Steroltalk-Projektes, in dessen Rahmen diese Arbeit entstand, sowie Frau Prof. Damiana Rozman und Frau Prof. Rita Bernhardt für die Koordination des Projektes.

Ich bedanke mich bei Herrn Prof. Christian Huber für die ausgezeichnete Zusammenarbeit im Rahmen der nLC-MS-Analysen.

Mein Dank gilt auch Frau Dr. Katalin Monostory ohne deren Arbeiten im Bereich der Zellkultur die hier vorliegende Studie nicht möglich gewesen wäre, sowie Dr. Jean-Marc Pascussi, der die Validierung der Ergebnisse mittels RT-PCR koordinierte.

Ein großes Dankeschön geht an Andreas, Anja, Anna, Antje, Berna, Bernd, Daniela, Elisa, Eva, Gabi, Hektor, Hoang, Jens, Katharina, Kerstin, Norio, Ringle, Sabrina, Simon, Tarek, Thoa, Thuy, Wanda, Wolfgang - ich habe mich während der letzten drei Jahre sehr wohl gefühlt und sehr gerne mit Euch zusammengearbeitet.

Ich möchte mich auch bei Frau Dr. Susanne Böhmer und Herrn Dr. Kyung-Hoon Hwang für die Hilfestellungen bei Fragen bezüglich der 2D-Gelelektrophorese bedanken.

Weiterer Dank geht an Dr. Katja Melchior für die Unterstützung im Bereich der LC-MS Analytik sowie einige sehr hilfreiche Diskussionen. Dank auch an Dr. Klaus Hollemeyer für die Unterstützung im Rahmen der MALDI-Messungen.

Ein spezielles Dankeschön an Dipl.Biol. Barbara Gregorius sowie Dipl.Chem. Thomas Jakoby für die guten Gespräche, exzellenten Hilfestellungen und sowieso eine gute Zeit.

Ein Dank geht an Herrn Dr. Frank Hannemann für die gute Kondition (jedenfalls besser als noch vor 3 Jahren ☺) sowie die sehr hilfreichen fachlichen Diskussionen und das Korrekturlesen der vorliegenden Arbeit.

Ich danke Frau Dipl.Biol. Britta Wilzewski für die Freundschaft, die guten Gespräche sowie die exzellente Zeit in dem 2 (1) Mädchen - 1 Bub - Zimmer die uns für immer verbinden wird.

Special thanks to “Mr. Nepal” - I’m glad to know you as a good friend of mine - I hope we’ll never lose contact. All the best.

Ein herzliches Dankeschön an meine “Sozialkontakte” Tobias, Sandra, Haiko (GREAT FONT - MAN), Coersche (sänks a lot for corräkting di englisch) - ich hoffe ich hab Euch nicht zu sehr vernachlässigt.

Danken möchte ich auch meiner Familie, allen voran meinen Eltern, ohne deren Unterstützung die vorliegende Arbeit, sowie der Weg dorthin niemals möglich gewesen wäre. - DANKE -

At the last but not the least - Danke an Frau Ina Grosse und Herrn Max Wörner für’s Dasein, Aushalten und Mithelfen wo geht. Ohne Euch wär das hier never ever möglich gewesen - ich weiß es war nicht immer (fast nie) einfach - **!!! Lots of LOVE !!!**